frontiers | Research Topics

Key technologies, markets, and policies towards a smart renewables-dominated power system

Edited by
Zhiyi Li, Jiajia Yang, Yang Li and Changsen Feng

Published in
Frontiers in Energy Research

ISSN 1664-8714
ISBN 978-2-83251-379-8
DOI 10.3389/978-2-83251-379-8

About Frontiers

Frontiers is more than just an open access publisher of scholarly articles: it is a pioneering approach to the world of academia, radically improving the way scholarly research is managed. The grand vision of Frontiers is a world where all people have an equal opportunity to seek, share and generate knowledge. Frontiers provides immediate and permanent online open access to all its publications, but this alone is not enough to realize our grand goals.

Frontiers journal series

The Frontiers journal series is a multi-tier and interdisciplinary set of open-access, online journals, promising a paradigm shift from the current review, selection and dissemination processes in academic publishing. All Frontiers journals are driven by researchers for researchers; therefore, they constitute a service to the scholarly community. At the same time, the *Frontiers journal series* operates on a revolutionary invention, the tiered publishing system, initially addressing specific communities of scholars, and gradually climbing up to broader public understanding, thus serving the interests of the lay society, too.

Dedication to quality

Each Frontiers article is a landmark of the highest quality, thanks to genuinely collaborative interactions between authors and review editors, who include some of the world's best academicians. Research must be certified by peers before entering a stream of knowledge that may eventually reach the public - and shape society; therefore, Frontiers only applies the most rigorous and unbiased reviews. Frontiers revolutionizes research publishing by freely delivering the most outstanding research, evaluated with no bias from both the academic and social point of view. By applying the most advanced information technologies, Frontiers is catapulting scholarly publishing into a new generation.

What are Frontiers Research Topics?

Frontiers Research Topics are very popular trademarks of the *Frontiers journals series*: they are collections of at least ten articles, all centered on a particular subject. With their unique mix of varied contributions from Original Research to Review Articles, Frontiers Research Topics unify the most influential researchers, the latest key findings and historical advances in a hot research area.

Find out more on how to host your own Frontiers Research Topic or contribute to one as an author by contacting the Frontiers editorial office: frontiersin.org/about/contact

Key technologies, markets, and policies towards a smart renewables-dominated power system

Topic editors

Zhiyi Li — Zhejiang University, China

Jiajia Yang — University of New South Wales, Australia

Yang Li — Hohai University, China

Changsen Feng — Zhejiang University of Technology, China

Citation

Li, Z., Yang, J., Li, Y., Feng, C., eds. (2023). *Key technologies, markets, and policies towards a smart renewables-dominated power system*. Lausanne: Frontiers Media SA. doi: 10.3389/978-2-83251-379-8

Table of contents

frontiers | Frontiers in Energy Research

OPINION
published: 09 May 2022
doi: 10.3389/fenrg.2022.919001

Viewpoints on Net-Zero Emissions of Agricultural Energy Internet

Xueqian Fu[1,2,3,4]*

[1]College of Information and Electrical Engineering, China Agricultural University, Beijing, China, [2]National Innovation Center for Digital Fishery, Beijing, China, [3]Key Laboratory of Smart Farming Technologies for Aquatic Animal and Livestock, Ministry of Agriculture and Rural Affairs, Beijing, China, [4]Beijing Engineering and Technology Research Center for Internet of Things in Agriculture, Beijing, China

Keywords: agricultural energy internet, net-zero emissions, solar photovoltaic, photosynthesis, low-carbon energy

INTRODUCTION

With the increased concerns about carbon dioxide emissions reduction, China puts forward carbon peak and neutrality goals. In February 2021, State Grid Corporation of China created action plans for carbon dioxide emissions reduction targets. The purpose of the action plans is to promote the upgrading of China's energy system structures to energy Internet, which is an ideal platform for optimal allocation of clean energy. Energy Internet supports the integration of large-scale renewable power generation, energy storage and diversified loads (Zhang, 2022). Accelerated rural electrification project is an effective way to reduce carbon dioxide emissions. Another important way is to develop integrated management system for energy efficiency and carbon reduction. At present, one of the most concerned renew energies is photovoltaic (PV) power generation (Fu, 2022a). Solar PV grid integration has a significant impact on reducing carbon dioxide emissions from burning fossil fuels and other sources, but it also brings power flow uncertainties in modern power systems (Fu et al., 2020). The iron and steel industry is one of the top pillar industries for China's economy but is responsible for the majority of carbon dioxide emissions. Gan et al. carried out several studies which have demonstrated that steel mills can significantly reduce carbon emissions by participating in the demand-side response program without affecting productivity (Gan et al., 2022). From the experiment, Zhang et al. came to realize that wind energy penetration can affect the carbon dioxide emissions reduced by integrating hydrogen-energy storages (Zhang and Yu, 2022). Yadav et al. intended to outline the framework of a market-to-market coordination, which offered a low-carbon trade agreement for PV producers (Yadav et al., 2021). Akbari-Dibavar et al. presented an optimization dispatch framework of power systems with renewable-energy power plants and coal power plants, and the simulation results indicated that carbon capturing and storing systems can significantly reduce carbon dioxide emissions (Akbari-Dibavar et al., 2021). An agricultural energy internet (AEI) can be identified as a smart renewables-dominated power system, and it has been revealed that an AEI has great potential for emission reduction (Fu and Yang, 2022). The preliminary results in (Huang et al., 2020) throw light on the nature of photovoltaic AEI, which provided reliable and affordable energy to agricultural production with PV power generation. Fu initiated experimental investigation to establish a fishery energy internet, which provided a broad space for the installation of PV systems, consisting of modules, inverter, converters, energy storages (Fu, 2022b). Compared with the study on carbon emissions in the field of energy systems, the study on carbon cycle in the field of agriculture is earlier and paid more attention. Agroecosystem has many ways to sequester carbon in soil, and agricultural sequestration has a significant effect on atmospheric net carbon flux (West and Marland, 2002). There are two main differences between AEI and traditional agricultural energy system. The first difference is the physical system. The primary power supply of an AEI is renewable energy, and the agricultural load is electrified. The traditional

OPEN ACCESS

Edited by:
Zhiyi Li,
Zhejiang University, China

Reviewed by:
Limei Zhang,
Hebei Agricultural University, China
Yunhao Zhao,
North China Electric Power University, China

***Correspondence:**
Xueqian Fu
fuxueqian@cau.edu.cn

Specialty section:
This article was submitted to Smart Grids, a section of the journal Frontiers in Energy Research

Received: *13 April 2022*
Accepted: *22 April 2022*
Published: *09 May 2022*

Citation:
Fu X (2022) Viewpoints on Net-Zero Emissions of Agricultural Energy Internet. Front. Energy Res. 10:919001. doi: 10.3389/fenrg.2022.919001

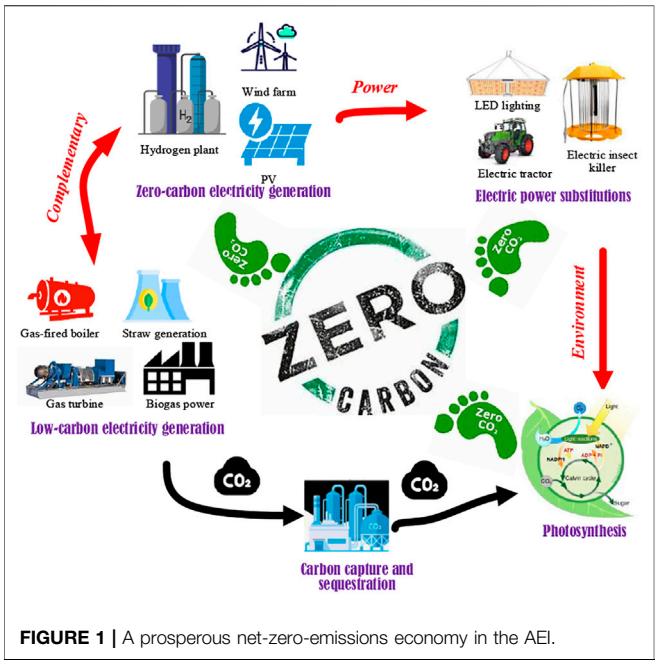

FIGURE 1 | A prosperous net-zero-emissions economy in the AEI.

rural energy system is supplied by the power grid, and the level of agricultural electrification is low. The second difference is the information system. The AEI is based on the combination of smart grid and smart agriculture, while the traditional rural energy system doesn't take full advantage of the Internet of things in agriculture. The research of AEI is still in the primary stage, and renewable energy, agricultural electrification and multi energy complementary technologies have been applied in practical application. However, the carbon cycle between agriculture and energy system is still blank.

The rest of the paper contains three main parts. First, we outline the carbon cycles through energy and agriculture in *Carbon Cycles Through Energy and Agriculture*. Second, we give the paths to net-zero emissions in *Paths to Net-Zero Emissions*. Then, we list math formulas including the formulas related to carbon footprint in energy and agriculture in *Carbon Footprint Calculation Formulas*. Finally, the discussion is presented in *Discussion*, along with the accompanying conclusion section in *Conclusion*.

CARBON CYCLES THROUGH ENERGY AND AGRICULTURE

Agricultural carbon emissions include the following four aspects. 1) Animal husbandry and fisheries produce methane, which accounts for more than a quarter of greenhouse gas emissions from the agricultural sector. 2) Nitrous oxide released in grain production, which involves the production and use of chemical fertilizers, organic fertilizers and pesticides. 3) Agricultural land use reduces the absorption of carbon dioxide. Grassland and forest are transformed into agricultural land, and the annual harvesting activities reduce the absorption of carbon dioxide. 4) Energy consumption in the food supply chain leads to carbon emissions, and the carbon footprint covers food processing, transportation, packaging and retail.

AEI is the best experimental object to realize carbon cycle and net-zero carbon emissions, as shown in **Figure 1**. The carbon footprint forms a closed loop between the energy system and the agricultural system. Whether on the source side or the demand side, the AEI can always find a feasible way to achieve net-zero carbon emissions. In terms of power sources, we develop renewable energies to reduce the carbon emissions from generation. Specifically, we replace coal-fired generation with natural gas-fired power generation and a straw power plant. The main difference between biomass fuel and mineral fuel is that it contains less carbon and can realize low-carbon power generation. We use carbon capture and storage technologies to collect carbon dioxide emitted by low-carbon energy, and the carbon is finally absorbed in the form of carbon rich agriculture. In addition, PV power generation, wind power generation and hydrogen energy are largely integrated to the grid in rural areas. These three energy sources are zero-carbon electricity generations and produce no carbon dioxide. In terms of demand side, an electric farm has become an agricultural production mode net-zero emissions. We promote electric energy substitution (EES) in the AEI *via* replacing oil tractors with electric tractors, replacing pesticides control with electric pesticides. EES not only avoids carbon emissions, but also improves the quality of agricultural products. In addition, the development of agricultural electrification based on EES also provides the basis for the agricultural informatization, which is the basis of smart farming.

PATHS TO NET-ZERO EMISSIONS

The upgrading route to net-zero emissions in an AEI includes carbon capture and sequestration (CCS), electric energy substitution and clean energy. Electric energy substitution and clean energy can be regards as carbon emission reduction technologies. In terms of electric energy substitution, LED lighting, plasma agricultural nitrogen fixation, electric insecticidal and electric agricultural machinery have higher product quality and lower carbon dioxide emission than petroleum agricultural technologies, which are represented by petroleum machinery and chemical fertilizer. Electric farms can significantly reduce the intensity of agricultural greenhouse gas emissions. In terms of renewable energy, rooftop PV, bagasse-based power generation, straw -based power generation and biogas energy generated from livestock manure can not only offset the emission of fossil energy used in agricultural production and rural life, but also reduce the electricity expenditure. In terms of CCS, it is worthwhile mentioning the photosynthesis of farmland and grassland. As a result of agricultural electrification, the carbon sequestration of farmland can be improved, and "net-zero"

carbon emissions can be achieved in an AEI. AEI has two ways to supply the carbon dioxide for a closed greenhouse. The first way is to transmit carbon dioxide from gas-fired power generation to greenhouses. The second way is to use solar energy to power the distributed carbon dioxide capture device to capture carbon dioxide in the air.

CARBON FOOTPRINT CALCULATION FORMULAS

Considering that the carbon emission of AEI has not yet formed a standard, we introduce several important formulas to support the application of carbon emission calculation in China. At present, most of China's agricultural production still uses electricity from the power grid, whose carbon emissions can be calculated according to the government documents of the Ministry of Ecology and Environment of China[1].

$$E_g = AD_g \times EF_g, \tag{1}$$

where E_g, tCO_2, is the emission from the purchased electricity, AD_g, MWh, is the purchased electricity consumption, and EF_g, tCO_2/MWh, is the grid emission factor. In 2021, the Ministry of Ecology and Environment of China set EF_g to 0.5839 tCO_2/MWh.

The carbon emission of natural gas power generation is calculated by the following formula

$$E_{gas} = AD_{gas} \times EF_{gas,} \tag{2}$$

$$AD_{gas} = FC_{gas} \times NCV_{gas,} \tag{3}$$

$$EF_{gas} = CC_{gas} \times OF_{gas} \times \frac{44}{12}, \tag{4}$$

where E_{gas}, tCO_2, is the carbon emissions from natural gas power generation, AD_{gas}, GJ, is the activity data of natural gas, EF_{gas}, tCO_2/GJ, is the emission factor, FC_{gas}, 10^4Nm^3, is consumption of natural gas, NCV_{gas}, GJ/10^4Nm^3, is the low calorific value of natural gas, CC_{gas}, tC/GJ, is the carbon in per unit calorific, and OF_{gas}, %, is the carbon oxidation rate. In 2021, the Ministry of Ecology and Environment of China set NCV_{gas} to 389.31 GJ/10^4Nm^3 and set CC_{gas} to 0.01532 tC/GJ.

DISCUSSION

Major Sticking Points

Net-Zero Emissions of AEI face many challenges and difficulties. The major sticking points can be concluded as follows. 1) Low carbon of rural energy system faces unprecedented economic challenges. It can significantly reduce the carbon emissions of rural energy systems *via* promoting electric energy substitution and renewable energy power generation. However, electricity substitution and renewable energy power generation will significantly increase the cost of agricultural production and rely too much on government subsidy to survive. Poor economy may hinder the promotion of techniques for carbon sequestration and greenhouse gas emission reduction. In addition, China has experimented with emission reduction technologies, but the energy-related production costs and emission reduction effect, need to be demonstrated and verified in the field of engineering. 2) China lacks special policies and standards for agricultural energy system. China has issued a series of policies and measures for green agriculture and renewable energy, and they play a certain role in carbon sequestration and greenhouse gas emission reduction in agricultural energy systems. However, China's carbon peak and neutrality is still blank for the AEI, and there is no technical standard for net-zero emissions of the AEI, resulting in great obstacles to the promotion of a net-zero emissions energy business. 3) We lack a professional research platform for net-zero emissions energy systems in rural areas. As there are no clear requirements for carbon sequestration and greenhouse gas emission reduction in agriculture, there is not only no clear route to carbon peak and carbon neutralization in agricultural energy systems, but also no specialized agency charging for carbon cycle monitoring of agricultural energy systems. The carbon monitoring of the AEI is scattered in different agriculture and energy sectors, which is unable to form a closed-loop monitoring. To carry out the systematic theory of carbon peak and neutrality for AEI, there is an urgent need to establish a professional research platform for net-zero emissions. 4) At present, the development of renewable energy in rural areas lacks top-level design, and the agriculture and energy sectors are uncoordinated. Rural renewable energy planning is difficult to implement and inefficient. Urban-rural dualization is one of the important reasons for the plight of rural renewable energy. To solve the problem of developing renewable energy in rural areas, we should coordinate the urban and rural energy systems. Rural areas should not only establish a clean energy system to replace coal energy systems, but also provide cities with energy products such as biological natural gas and biomass briquette fuel, so as to give full play to the role of renewable energy in reducing carbon.

Advantages

Building renewable energy in rural areas has outstanding advantages and great potential for carbon emission reduction. The vast countryside provides vast space and cheap land for the construction of wind power, PV generation, geothermal energy, etc. Agricultural waste provides a steady stream of fuel for biomass energy. The development and growth of distributed renewable energy has become an important supplement to the rural low-carbon economy growth. Under the background of the vigorous development of rural renewable energy, the low-carbon process of energy system has accelerated. In contrast, the shortage of land and high cost in cities have seriously limited the development of renewable energy. From the perspective of demand side, agricultural production has the

[1]https://www.mee.gov.cn/xxgk2018/xxgk/xxgk06/202112/t20211202_962776.html.

function of CCS, while industrial and commercial production emits carbon dioxide.

CONCLUSION

The construction of AEI is an effective way to serve rural revitalization. This was demonstrated in a number of studies that AEI can not only significantly improve the reliability of energy supply, but also improve energy efficiency and renewable energy in rural areas. AEI relies on agricultural production, renewable energy and electric energy substitution to achieve the goal of zero carbon emissions. The low-carbon of AEI can improve the income level of farmers and improve the human habitat environment. Technical measures for AEI net-zero emissions include the following two aspects: 1) An energy-crop carbon emission model should be established according to the actual agricultural park. 2) A carbon monitoring platform should be built to realize real-time monitoring of carbon emission, carbon sink and carbon credit.

AUTHOR CONTRIBUTIONS

The author confirms being the sole contributor of this work and has approved it for publication.

FUNDING

This study is supported by the National Natural Science Foundation of China under Grant 52007193 and the 2115 Talent Development Program of China Agricultural University.

REFERENCES

Akbari-Dibavar, A., Mohammadi-Ivatloo, B., Zare, K., Khalili, T., and Bidram, A. (2021). Economic-Emission Dispatch Problem in Power Systems with Carbon Capture Power Plants. *IEEE Trans. Ind. Appl.* 57 (4), 3341–3351. July-Aug. 2021. doi:10.1109/TIA.2021.3079329

Fu, X. (2022). Statistical Machine Learning Model for Capacitor Planning Considering Uncertainties in Photovoltaic Power. *Prot. Control Mod. Power Syst.* V (1), 51–63. doi:10.1186/s41601-022-00228-z

Fu, X. (2022). Viewpoints on the Experiences and Challenges of Fishery Energy Internet. *Front. Energy Res.* 10, 884920. doi:10.3389/fenrg.2022.884920

Fu, X., Guo, Q., and Sun, H. (2020). Statistical Machine Learning Model for Stochastic Optimal Planning of Distribution Networks Considering a Dynamic Correlation and Dimension Reduction. *IEEE Trans. Smart Grid* 11 (4), 2904–2917. doi:10.1109/TSG.2020.2974021

Fu, X., and Yang, F. (2022). Viewpoints on the Theory of Agricultural Energy Internet. *Front. Energy Res.* 10, 839108. doi:10.3389/fenrg.2022.871772

Gan, L., Yang, T., Chen, X., Li, G., and Yu, K. (2022). Purchased Power Dispatching Potential Evaluation of Steel Plant with Joint Multienergy System and Production Process Optimization. *IEEE Trans. Ind. Appl.* 58 (2), 1581–1591. March-April 2022. doi:10.1109/TIA.2022.3144652

Huang, K., Shu, L., Li, K., Yang, F., Han, G., Wang, X., et al. (2020). Photovoltaic Agricultural Internet of Things towards Realizing the Next Generation of Smart Farming. *IEEE Access* 8, 76300–76312. doi:10.1109/ACCESS.2020.2988663

West, T., and Marland, G. (2002). Net Carbon Flux from Agricultural Ecosystems: Methodology for Full Carbon Cycle Analyses. *Environ. Pollut.* 116 (Issue 3), 439–444. doi:10.1016/S0269-7491(01)00221-4

Yadav, D., Mekhilef, S., Singh, B., and Rawa, M. (2021). Carbon Trading Analysis and Impacts on Economy in Market-To-Market Coordination with Higher PV Penetration. *IEEE Trans. Ind. Appl.* 57 (6), 5582–5592. Nov.-Dec. 2021. doi:10.1109/TIA.2021.3105495

Zhang, X. (2022). Advanced Wireless Communication Technologies for Energy Internet. *Front. Energy Res.* 10, 889355. doi:10.3389/fenrg.2022.889355

Zhang, Y., and Yu, Y. (2022). Carbon Value Assessment of Hydrogen Energy Connected to the Power Grid. *IEEE Trans. Ind. Appl.* 58 (2), 2803–2811. March-April 2022. doi:10.1109/TIA.2021.3126691

Conflict of Interest: The authors declare that the research was conducted in the absence of any commercial or financial relationships that could be construed as a potential conflict of interest.

Publisher's Note: All claims expressed in this article are solely those of the authors and do not necessarily represent those of their affiliated organizations, or those of the publisher, the editors and the reviewers. Any product that may be evaluated in this article, or claim that may be made by its manufacturer, is not guaranteed or endorsed by the publisher.

frontiers | Frontiers in Energy Research

REVIEW
published: 16 June 2022
doi: 10.3389/fenrg.2022.942450

A Review of Wind Energy Output Simulation for New Power System Planning

Xinmiao Liu[1], *Yuan Yue*[2]*, *Xin Huang*[2], *Wei Xu*[1] *and Xun Lu*[1]

[1]Guangdong Grid Co., Guangzhou, China, [2]School of Electrical Engineering, Xi'an Jiaotong University, Xi'an, China

The uncertain and volatile nature of wind energy have brought huge challenges to power system planning and operation. Therefore, it is necessary to model the wind power output. In this paper simulation models of wind energy output for new power system planning are reviewed. We begin by discussing the characteristics of wind power output, and then introduce the wind power output simulation model based on different application scenarios that are based on probability and time series. Finally, the directions for further research in the future are anticipated.

Keywords: wind energy output, simulation, new power system planning, probability, time series

OPEN ACCESS

Edited by:
Zhiyi Li,
Zhejiang University, China

Reviewed by:
Han Wang,
Shanghai Jiao Tong University, China
Changsen Feng,
Zhejiang University of Technology, China

***Correspondence:**
Yuan Yue
yy1200909@stu.xjtu.edu.cn

Specialty section:
This article was submitted to Smart Grids, a section of the journal Frontiers in Energy Research

Received: *12 May 2022*
Accepted: *01 June 2022*
Published: *16 June 2022*

Citation:
Liu X, Yue Y, Huang X, Xu W and Lu X (2022) A Review of Wind Energy Output Simulation for New Power System Planning. Front. Energy Res. 10:942450. doi: 10.3389/fenrg.2022.942450

1 INTRODUCTION

The energy business is experiencing unprecedented profound changes as a result of the economic development of society and the advancement of science and technology. The operations and planning of power systems are becoming increasingly complicated as new types of energy sources become available (Shortt et al., 2013). In response to the global energy and environmental crisis, governments all over the world have stated that they want to establish a system that uses a large amount of renewable energy (Kroposki et al., 2017). As a result of the revolution in power systems, power system planning studies face new challenges. Increased penetration of renewable energy in power systems, in particular, has resulted in significant uncertainty and fluctuation in power systems (Conejo et al., 2017).

Electricity generated by wind energy differs significantly from that generated by traditional sources. The main distinction is that wind power is uncertain and intermittent (Han et al., 2021). The operation of the power system is made more uncertain by intermittent renewable energy sources. New energy production's growing effect in the power system puts new demands on planning and operation.

Wind energy and other new energy products now play a significant role in the modern power system. Despite the fact that the new energy power generation sector is rapidly expanding, it is difficult to address the issue of new energy power generation planning in the short term due to lack of planning, unstable development, and inadequate associated legislation. Therefore, it is critical to accurately evaluate new energy production efficiency, account for the rational allocation of new energy and conventional energy, increase unified planning and operation scheduling, and promote the industry's overall harmonious growth.

The output of wind farms is an uncontrollable source of energy, and its contribution to the capacity of the power system when it is connected to the grid differs significantly from that of conventional units. As a result, objective evaluation of the wind farm capacity credit is critical for long-term planning, optimal system operation, reliability assessment and other associated concerns.

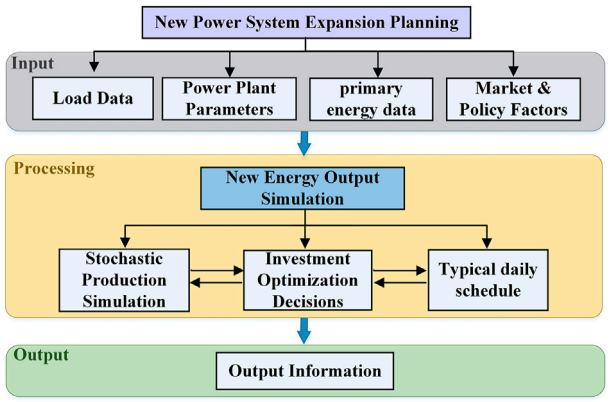

FIGURE 1 | Structure of the new power system planning.

Because of the scarcity of primary energy, wind power have significant seasonal, random, and fluctuating characteristics, necessitating greater use of flexible resources over a variety of time scales, such as cross-seasonal distribution, cross-day adjustment, intraday adjustment, and real-time power and electricity balance. Renewable energy power is increasingly converting the power system into a multi-energy complementary power system (Zhou et al., 2018).

The modeling and processing of stochastic power supply is a key problem in the simulation of renewable energy-led power system production. Wind power output simulation is widely used in power system planning, operation, and reliability assessment. Effective wind energy simulation can boost wind power's grid-connected potential while lowering wind farm operating costs (Zhang et al., 2022).

Figure 1 shows the role of wind power simulation in the expansion planning of the new power system. There are three levels as a whole. The first is to input the basic data required to build the power optimization model, mainly including load data (electricity demand, typical load curve, etc.), power plant data (power plant type, fuel price, average coal consumption, etc.), primary energy data (hydrological information, incoming wind conditions, etc.) and market and policy factors (discount rates, fuel prices, new energy subsidies, etc.). The second layer is the core processing layer of the program, which is responsible for the calculation of power optimization planning. The last layer is the input and output information layer, which includes global information of power supply planning results such as power installation progress, annual investment, annual operating costs, power and electricity balance, and new energy simulation and modeling, stochastic production simulation, typical daily operation simulation, etc. Important results of the module during the iterative computation process.

However, many previous studies on wind power output have focused solely on wind speed forecasting, with little attention paid to wind power simulation.

To focus on addressing the long-term variability and uncertainties of renewables, we particularly limit our discussions to the following areas: 1) Modeling of wind power output without considering time series, primarily based on the long-term characteristics of wind power to carry out modeling based on probability statistics, which is used for power balance, reliability assessment, etc.; 2) Time series modeling of wind power output, mainly used to arrange the operation mode of units under sequential production simulation; 3) Time series and probability modeling, which overcomes the shortcomings of the previous two categories and incorporates both uncertainty and volatility into the model.

The contributions of the paper are listed as follows. First, the characteristics of wind power output are summarized including the uncertainties, peak shaving and correlation. Second, various wind power models based on probability distributions and stochastic scenarios are introduced. Third, wind power output time series modeling, primarily used to arrange the operation mode of units under sequential production simulation, is discussed in this paper.

The remainder of this paper is organized as follows. In **Section 2** the output characteristics of wind power are summarized, including uncertainty, volatility, correlation, peak shaving characteristics. In **Section 3**, the probability-based wind power modeling is summarized, including probability distribution model, capacity confidence, and Copula multi-wind farm correlation. In **Section 4**, time series-based wind power modeling is explained. **Section 5** is about the current concerns and challenges of renewable energy production modeling. Finally, **Section 6** adds a brief summary of the content of the article and a brief outlook. And the structure of this paper is shown in **Figure 2**.

2 WIND POWER OUTPUT CHARACTERISTICS

In this section, the output characteristics of wind power are discussed.

2.1 Uncertainty, Volatility and Ramping Characteristics

The power generation capacity and power generation of wind farms have a strong dependence on wind energy. Unlike fuel and water storage, wind energy cannot be stored on a large scale. The features of wind energy largely impact the output characteristics of wind power. The random and fluctuating characteristics of wind energy result in high unpredictability and volatility in the output and power generation of wind farms. Daily wind power production variations, monthly average power changes, and variances in output characteristics in different seasons all represent the unpredictability and volatility of wind power output.

Uncertainty and volatility are the essential characteristics of new energy power generation such as wind power. Uncertainty makes short-term production arrangements and long-term system planning a certain risk, while volatility has a significant impact on the short-term operation of the power system, requiring the system to be equipped with more many flexible resources.

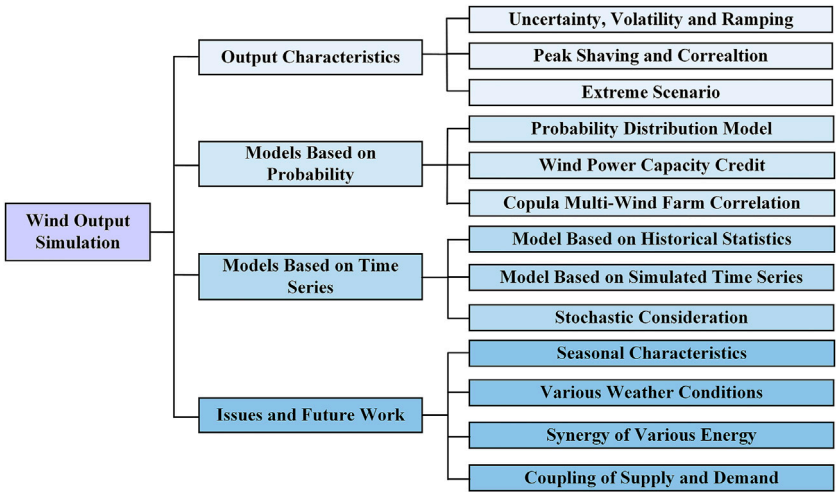

FIGURE 2 | Structure of this paper.

Ramps events are a significant source of uncertainty in wind power generation. Wind power ramps are defined as large variations in wind power production that must adhere to a set of rules, such as a minimum power swing or duration (Sevlian and Rajagopal, 2012; Sevlian and Rajagopal, 2013; Ganger et al., 2014). Extreme wind ramp events need to be closely examined since such a ramp can cause power system security concerns.

2.2 Peak Shaving Characteristics

Wind power's peak shaving characteristics refer to the relationship between wind power and load over the course of a day. Whether wind power can be connected to the grid for power generation mainly depends on whether the system has sufficient peak shaving capacity.

The impact of wind power output power on system peak regulation can be divided into three situations based on the different effects of wind power on the peak-to-valley difference of the system equivalent load: negative peak regulation, positive peak regulation, and over peak regulation. Wind power has obvious anti-peak characteristics, according to statistical analysis (Yang et al., 2014).

2.3 Correlation

2.3.1 Autocorrelation

Autocorrelation is the correlation of a series with itself after applying a given lag (Feijoo and Villanueva, 2016). Autocorrelation can be induced in a series of data by means of autoregressive models, i.e., AR, MA, ARMA, ARIMA (Kashyap, 1982; Zhang, 2003).

2.3.2 Cross-Correlation

Wind resources differ greatly for wind turbines that are far apart in a wind farm or wind farms that are farther apart in different regions, according to studies. Wind resources in different parts of the region show obvious differences due to spatial dispersion. The decoupling or offsetting of each other's fluctuations through the synergistic decoupling effect of each part in the region, thus alleviating the adverse effects on the whole. Grid operation has intermittent fluctuation characteristics. The correlation between multiple output series is used to mathematically express the smoothing effect of wind farm group output.

The following formula can be used to calculate the correlation coefficient between two wind farms:

$$\rho_{ij} = \frac{\sum_{t=1}^{T}\left(p_{it}-\bar{p}_i\right)\left(p_{jt}-\bar{p}_j\right)}{\sqrt{\sum_{t=1}^{T}\left(p_{it}-\bar{p}_i\right)}\sqrt{\sum_{t=1}^{T}\left(p_{jt}-\bar{p}_j\right)}} \tag{1}$$

Among them, $p_{i,t}$, $p_{j,t}$ are the sampling values of output in wind farm i, j , and $\bar{p}_i$, $\bar{p}_j$ are the sampling mean output of wind farm i, j.

If the two output series have a positive correlation, the effect of the volatility superposition will cause the overall output curve to show a trend of large fluctuations, exacerbating the fluctuation of the wind farm group's output. The smoothing effect is influenced by the negative correlation between outputs. The output fluctuations cancel and complement each other, "cutting peaks and filling valleys," as it were. A smooth effect can be seen in the overall output curve and output volatility.

2.4 Extreme Output Scenario

The wind power extreme scenario relates to the situation in which the average net load (load minus renewable energy power) varies the greatest over time. When the downhill event of wind power and the load rise occur at the same time, for example, wind desertion and load shedding may occur, compromising the power system's safety and stability.

In extreme circumstances of wind power production, robust optimization may be employed to discover the best dispatching system. The uncertainty set is primarily utilized to represent the variation range of wind power fluctuations, and even in the

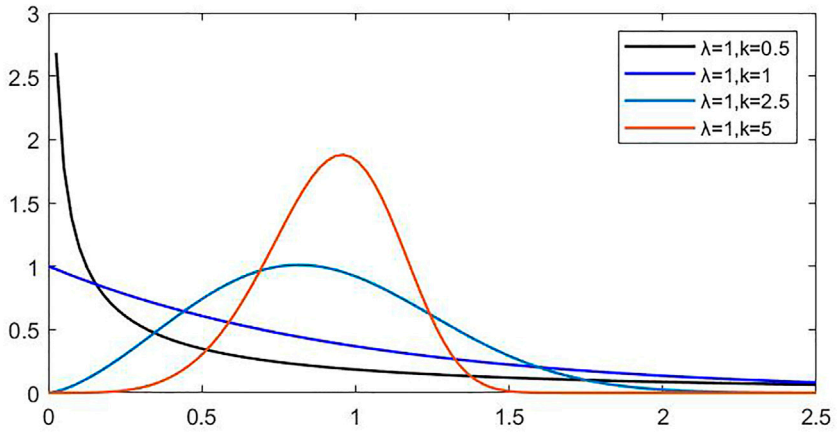

FIGURE 3 | PDF of the Weibull distribution.

worst-case circumstances, a solution with high performance may be found.

3 WIND POWER MODELING BASED ON PROBABILITY

In this section, the probability-based wind power modeling is summarized, including probability distribution model, capacity confidence, and Copula multi-wind farm correlation.

3.1 Probability Distribution Model

Wind power has a range of outputs from 0 to its installed capacity. Therefore, typical two-state models of conventional units cannot be used to establish wind power output models. The long-term characteristics of wind power obey the Weibull distribution, according to research and analysis dating back to the 1980s, and a multi-state unit model was developed as a result (Wang et al., 1984).

From the perspective of probability theory and statistics, Weibull Distribution is a continuous probability distribution, as shown in **Figure 3**, and its probability density is:

$$f(x;\lambda,k) = \begin{cases} \frac{k}{\lambda}\left(\frac{x}{\lambda}\right)^{k-1} e^{-(x/\lambda)^k} & x \geq 0 \\ 0 & x < 0 \end{cases} \tag{2}$$

The PDF of the Weibull distribution, f, has been widely described in the literature, and can be expressed as a function of three parameters, i.e. random variable (x), scale (λ) and shape (k).

The multi-state unit model works by dividing the range of wind power production (output) into numerous periods and calculating the probability that the wind power output falls within each interval (Kim et al., 2012). Wind power is regarded as a multi-state unit whose output may take values at these discrete points, with each interval corresponding to a discrete output value (typically the middle of the period).

$$\begin{cases} p\left(x_i = c_{i,j}\right) = p_{i,j} \\ \sum_j p_{i,j} = 1 \end{cases} \tag{3}$$

where the available capacity and probability of the unit in state j are denoted by $c_{i,j}$ and $p_{i,j}$ respectively.

As can be seen, the continuous output curve of wind power is the basis for the multi-state unit model. The form of the model is consistent with the two-state model of conventional units. On a longer time scale, it can properly capture the randomness of wind power output and reflect the characteristics of wind power replacing traditional power generation. The system reliability of wind farms is directly calculated and considered in the case of reliability calculation models and methods, which is widely used in the research of wind power credit capacity. Also, it is convenient to combine with the stochastic production simulation calculation method based on equivalent continuous load curve and electricity function.

Although the multi-state unit model is introduced in this section on wind farm output modeling, the methods connected with it may be applied to other units as well. Conventional units may have local failures or individual auxiliary equipment failures, but they are not always out of service. Instead, the generator output may not achieve its rated output. The multi-state unit model may also be used to model in this circumstance.

The probability distribution model can depict the long-term power characteristics and power distribution range of renewable energy, but short-term output fluctuation characteristics are difficult to describe (Shao et al., 2021; Feng et al., 2022). The demand for peak shaving and ramping of wind power has also been neglected.

3.2 Wind Power Capacity Credit

Due to the intermittency of wind power output, wind power units of the same capacity have different load-carrying capabilities from conventional thermal power or hydro-power units. Therefore, in the power system sufficiency analysis, wind power capacity cannot be treated the same as conventional units, which is not conducive to the power planning.

The concept of power generation capacity credit was first proposed by Garver (Garver, 1966) in 1966, to measure the load carrying capability of units with different random outage rates in the sense of reliability. And then in the late 1970s, Edward Kahn (Kahn, 1979) and Haslett John (Haslett and Diesendorf, 1981) first applied the concept of capacity credibility to the analysis of wind power, making it possible for uncontrollable, fluctuating and random wind power to participate in traditional power planning analysis and calculation.

The credible capacity of wind power assesses how many conventional units the wind farm can replace in the power balance, or how much creditable capacity the wind farm can produce with a reasonable or acceptable probability of confidence (Voorspools and D'Haeseleer, 2006). Wind power capacity credit is defined as the ratio of capacity that is equivalent to conventional generation to supply the load with the same level of reliability (Zhang et al., 2015).

The concept of wind power capacity credit is usually separated into the following four categories in present research (Amelin, 2009; Graham and Cooper, 2013; Zhang et al., 2015): 1) Equivalent Firm Capacity, EFC; 2) Equivalent Conventional Generation Capacity, ECGC; 3) Equivalent Load-carrying Capability, ELCC; 4) Guaranteed Capacity, GC. From the standpoint of uncertainty analysis, these four categories all specify the fraction of wind power that should be examined under the dimension of conventional unit capacity.

The above four definitions can be grouped into two categories, from the power supply side and the load side, respectively, under the premise of maintaining the reliability unchanged, the conventional unit capacity or additional payload that renewable energy can replace.

These two types of understanding each have their own practical significance: on the power side, how much wind power should be installed to replace conventional units that are about to be retired in order to achieve energy savings and emission reduction targets; on the load side, how much wind power should be planned to meet future load demand increases.

3.3 Copula Multi-Wind Farm Correlation

Multiple wind farms with identical geographical locations in the same wind region are common in places with abundant and concentrated wind energy resources. The output of each wind farm will be highly correlated due to the continuity of wind speed. The impact of integrating wind power into the electricity system will not be correctly evaluated if the correlation between the production of multiple wind farms in the same wind region is overlooked, which would raise the insecurity of system functioning.

Copula function, as a linking function between multiple random variables, is based on Sklar's theorem (Kole et al., 2007). According to Sklar's theorem, when the marginal distribution of multivariate random variables and the appropriate Copula function are determined, the joint probability distribution of these random variables can be obtained, which is the advantage of the Copula function in practical applications.

Copula function connects the marginal distributions of numerous random variables to a joint probability distribution. This function can capture nonlinearity, asymmetry, and tail correlation between variables and theoretically and does not limit the choice of marginal distribution. In (Hong et al., 2010), researchers assess the influence of wind farm connection system reliability when wind speeds are entirely related vs. completely independent. The Copula theory was added into the output modeling of several wind farms in (Li et al., 2013), which described the correlation characteristics across wind farms. In (Cai et al., 2013), Copula function is introduced to systematically model the dependent structure between wind speed and output power of wind farms, and a joint distribution function of wind speed and power of multiple wind farms is established. Scientists utilized the Copula function to model the dependent wind speed and wind power production of several wind farms in (Zhang et al., 2013). Researchers employed the Copula function to characterize the output correlation between neighboring wind farms in space and built a combined probability distribution model for the output of many wind farms in (Wu et al., 2015). On this foundation, a method for assessing multi-wind farm capacity reliability based on output is proposed.

The use of the Copula function can more correctly depict the nonlinear correlation of wind power output (Li et al., 2013; Wang et al., 2013; Ji et al., 2014; Xie et al., 2016), according to (Li et al., 2019). But the modeling approach is difficult, and adaptability is poor when there are a large number of wind farms (Xu et al., 2016). Furthermore (Yang et al., 2018), describes the correlation of the output of several wind farms using an adaptive multivariable nonparametric kernel density function, which can effectively improve the local adaptability problem of the Copula function method.

In (Xu et al., 2021), Wind farms in adjacent locations are affected by similar meteorological factors, and their output shows strong spatial and temporal correlation. Copula function can describe the dependencies between non-normal random variables in detail, and it has become a common method for modeling the joint probability distribution of random variables.

4 WIND POWER OUTPUT SIMULATION BASED ON TIME SERIES

In this section, the time series-based wind power output simulation is summarized, including model based on historical statistics, model based on simulated time series, and model considering both stochastics and variability.

4.1 Model Based on Historical Statistics

In addition to multi-state modeling, the load correction approach, in which the new energy curve is subtracted from the system sequential load curve, is also a widely used method for modeling wind power production. In this way, the system could be spared the effects of random fluctuations in new energy output.

From historical meteorological statistical data, the output curve can be calculated (Hasche et al., 2011). The historical statistics can well reflect the seasonal, diurnal, and autocorrelation characteristics of wind speed, but it is difficult to depict the stochastic characteristics. Especially when the measurement conditions are limited or the wind speed data is scarce, the data may not reflect the annual variation characteristics of wind speed.

In some previous studies, historical meteorological data reanalysis and downscaling techniques have been used to calculate the historical output curve of wind power by restoring the historical wind speed (Hawkins et al., 2011), which solves the data quality problem.

4.2 Simulation Model Based on Time Series

Previous studies have proposed a variety of statistical methods to simulate the sequential output of wind power to compensate for the difficulty of obtaining actual wind power output, with the goal of restoring the stochastic characteristics of wind power output through stochastic simulation.

Auto-Regressive and Moving Average (ARMA) model is the most widely used model in wind power output simulation. First, the autoregressive and moving average model parameters of each order are identified from the historical wind speed data. Then the identified ARMA model is sampled to obtain the time series of wind speed. Finally the wind speed time series is converted into wind power output through the wind output characteristic curve (Billinton et al., 2009; Gao and Billinton, 2009; Chen et al., 2010; Kloeckl and Papaefthymiou, 2010; Qu et al., 2013). ARMA model can accurately describe the volatility of wind speed. However, the wind speed simulated by the ARMA model is frequently normal rather than Weibull distributed, and dealing with the spatial correlation of the output of multiple wind farms is more difficult with the ARMA model. To reflect the spatiotemporal correlation (Lucheroni et al., 2019), employs a multi-dimensional ARMA model. In addition, the ST-ARMA model is used in (Zou et al., 2019) to statistically model the spatiotemporal coupling correlation of multidimensional sequences in a relatively concise form. The ST-ARMA model can generate a large amount of simulated data with the same statistical properties as actual wind output.

The Markov chain model is based on the wind power multi-state unit model, assuming that the state transition of wind power output is only related to the position of the previous state. The state transition matrix of wind power output is established based on historical data, and it is sequentially sampled to obtain the wind power output time series (Leite et al., 2006; Dobakhshari and Fotuhi-Firuzabad, 2009; Salehi-Dobakhshari and Fotuhi-Firuzabad, 2011; Luo et al., 2014). The probability distribution curve of wind power output has no shape constraints. The actual sampling frequency of each state, however, is difficult to stably converge to the expected probability due to the strong autocorrelation of wind power output (Billinton and Huang, 2011).

Furthermore, In (Li et al., 2019) a new method on modeling correlated power time series of multiple wind farms was proposed based on hidden Markov model (HMM). A Markov chain was adopted to model the state of time-varying correlations between wind farms, and wind power outputs at two adjacent moments were set as observations of HMM, which established the mathematical mapping model between wind power correlations and power outputs at two adjacent moments.

(Ning et al., 2010; Olsson et al., 2010) have used the stochastic differential equation model to simulate the wind power output considering the wind speed fluctuation characteristics and the spatial correlation of the output of multiple wind farms.

In general, the time series model of wind power can take into account the time series characteristics of wind power output, but it requires more information on these time series characteristics. In the time series simulation of wind power, it is technically difficult to consider the fluctuation of wind power output, daily characteristics, seasonality, and output correlation of multiple wind farms at the same time.

4.3 Stochastic Consideration

For stochastic factors in power systems, there are two main optimization methods: stochastic optimization and robust optimization. Stochastic optimization requires the use of a random variable probability distribution model, which is incapable of adequately describing the complex variations in real-world uncertainty variables. While robust optimization uses an uncertainty set to determine the changes in an uncertain factor. It is not necessary to assume a probability distribution model in advance, but when considering the optimal solution in the worst-case scenario, the optimal scheduling results may be conservative.

Therefore, stochastic multi-scenario models are described first in this section, followed by robust uncertainty sets. A time series multi-state model based on the Markov chain is further created, and the randomness, volatility, and ramping features are extensively addressed.

4.3.1 Multi-Scenario Model

Researchers suggest a stochastic multi-scenario model for optimal scheduling (Wang et al., 2008). The basic idea of the multi-scenario method is to select and determine multiple typical daily output curves of new energy sources, and then describe the randomness of new energy output using different typical daily curves and their corresponding probabilities.

The data of multiple scenes is generated by sampling based on the input typical new energy data and the normal distribution probability model. The researchers used Monte Carlo sampling (Wang X. et al., 2016) to form the basic scene, and used Latin hypercube sampling to generate the wind power scenario (Li and Zhu, 2016). They may also start with the probability density function of output at a single moment and discretize it using the Wasserstein distance (Wang Q. et al., 2015), with the time series connection generating the basic scene set. The precise probability distribution of wind power production can be established by sampling typical scenarios to represent a large number of complex scenes.

This model is a useful attempt to simultaneously describe the randomness and volatility of energy output. However, it should be noted that the process of creating this type of model is

relatively difficult, and the complexity of related calculations will skyrocket as the number of scenes grows. This makes deciding on the number of scenes difficult. If the number of selected scenes is small, it will be difficult to fully describe the randomness of the output distribution. But if the number of scenes is large, analysis and calculation will be difficult.

4.3.2 Robust Uncertainty Set

Researchers built a robust model (Bertsimas et al., 2013) using an uncertainty set (Dvorkin et al., 2016) to characterize the power prediction error of renewable energy.

Robust optimization (RO) (Zeng and Zhao, 2013) is an common optimization approach to deal with data uncertainty. It is derived to hedge against any perturbation in the input data. Due to the improved modeling capability, two-stage RO has become a popular decision making tool.

Robust optimization is able to cope with any changes in random variables. Traditional robust optimization replaces the probability distribution information of stochastic variables with uncertain sets and determines the best solution that meets all of the requirements. Its solution speed is fast, and its decision-making outcomes are still viable even when numerous unknown parameters are perturbed at the same time.

The budget of the uncertain set was introduced to balance the conservatism and economy of robust optimization. At the same time, the method of reducing the cost of robustness was explored, and a robust optimization model with adjustable conservatism was proposed. Flexible uncertainty sets were first proposed (Zhao et al., 2015), whose upper and lower bounds are optimization variables rather than given values. Flexible uncertainty sets can be applied to economic scheduling, reserve optimization, and unit combination problems (Wang C. et al., 2016; Doostizadeh et al., 2016; Shao et al., 2017).

In (Xu et al., 2020), The suggested method uses kernel density estimation to create an ambiguous set of continuous multivariate probability distributions, and the integrated dispatch optimization model is composed of stochastic and resilient optimization problems.

Furthermore, in (Xu et al., 2022), the researchers propose a data-driven distributed robust optimization method for power system scheduling to deal with the power system operation problem considering wind power uncertainty. The distributed robust optimization method constructed is a combination of stochastic optimization and robust optimization, which can ensure the reliability of the optimization results while making full use of the statistical information of random variables.

4.3.3 Temporal Multi-State Model

Several output curves can retain the fluctuation characteristics of renewable energy output, but cannot fully describe its randomness. Multiple different output states and corresponding probabilities can describe the random characteristics of renewable energy output, but it is difficult to describe its volatility. Simultaneously, the ramping rate and the ramping features of the probability distribution of the ramping rate, as an essential part of the output characteristics of renewable energy, have not been adequately addressed or explained in the aforementioned two kinds of modeling methodologies.

Researchers have proposed a temporal multi-state unit model (Zhaohong et al., 2009), which involves using different multi-state unit models to describe the output characteristics of renewable energy over time in order to account for its randomness and volatility.

In addition, a sequential multi-state unit formation method based on Markov process (王锡凡 et al., 2015) has been proposed to describe the relationship between renewable energy output in adjacent periods while taking into account its ramping characteristics. The multi-state unit model reflects the randomness renewable energy output. The multi-state model of time series further contains the time series fluctuation characteristics of the output of renewable energy. And the Markov state transition matrix intuitively reflects the transition of renewable energy output from a certain state to another state. Compared with the existing methods, the method can more comprehensively describe the output characteristics of renewable energy.

5 ISSUES, CHALLENGES AND FUTURE WORK

Issues and challenges in wind power output modeling research are as follows:

1) Simulation model of wind power output in different seasons: Existing wind power output simulation models frequently use wind power and load data for a whole year, with the calculation results representing wind power's contribution to system reliability throughout the year. However, wind power in some areas has distinct seasonal and daily characteristics. At the same time, in power planning, the calculation of power balance is carried out on a monthly basis, and the peak load on a typical day of each month is used for calculation.
2) Changes in wind power with various weather conditions: Part of the cause for the 2021 Texas blackout was that wind turbines were unable to produce energy owing to equipment freezing, resulting in an inadequate power supply on the power supply side. Under a variety of meteorological conditions, the output power of wind power is unstable and intermittent. Only a scientific power dispatch mode can ensure the stable output of wind power.
3) Synergy of various forms of energy: Compared to traditional power systems, which are primarily based on a single form of energy source and utilization, new power systems realize the transition from one energy source to multiple energy forms on the energy source side. The output modeling of a new energy system must take into account not just a single energy form as the modeling object, but also the coupling and complimentary interactions between the various energy forms. Further research is required in order to realize the complementary coordination of multiple energy sources at various time and space scales.
4) Coupling of the energy supply side and the energy demand side: The new energy power system realizes not only the

transformation from a single energy source to a variety of energy forms on the energy supply side, but also the change from traditional electrical loads to multi-type loads on the energy demand side (such as energy storage, electric vehicles, etc.). As a result, the output modeling of the new energy power system must take into account the information interaction between supply and demand. And a new energy power system output modeling that complements supply and demand must be established.

So for these issues, future work for new power system planning considering variable wind power output will be as follows:

1) It is necessary to research on the simulation model of wind power output in different seasons to better support the power balance.
2) It is an important measure to improve the security of the power system to study the relationship between wind power and meteorological conditions, correctly simulate the wind power output, and improve the emergency support capability.
3) To increase the power system's ability to absorb new energy, it is necessary to investigate the coordinated and complementary properties of numerous energy sources at various time and space scales.
4) To support the overall coordinated control and performance optimization of the system, it is vital to consider the information interaction between the supply side and the demand side as a whole, and to develop a new energy power system model with coupling linkage and complementary supply and demand.

6 CONCLUSION

Simulation models of wind energy output for new power system planning have been reviewed. This paper focuses on addressing the long-term variability and uncertainties of renewables, thus discussing the following parts: 1) Modeling of wind power output without considering time series, primarily based on the long-term characteristics of wind power to carry out modeling based on probability statistics, which is used for power balance, reliability assessment, etc.; 2) Time series modeling of wind power output, mainly used to arrange the operation mode of units under sequential production simulation; 3) Time series and probability modeling, which overcomes the shortcomings of the previous two categories and incorporates both uncertainty and volatility into the model. Finally, this paper highlights issues and challenges in wind power output modeling research, such as considering wind power output in different seasons, wind power output change under various meteorological conditions, coordinating multiple energy sources, and coupling energy supply and demand. And some future work for new power system planning considering variable wind power output is proposed.

AUTHOR CONTRIBUTIONS

XiL: Conceptualization, Writing- Original draft. YY: Methodology, Writing- Original draft. XH: Analysis, Writing- Original draft preparation. WX: Supervision, Writing- Original draft preparation. XuL: Supervision, Writing- Reviewing and Editing.

FUNDING

This research is supported by the Science and Technology Project of China Southern Power Grid Co., Ltd. grant number 030000KK52210022 (GDKJXM20212056).

REFERENCES

Amelin, M. (2009). Comparison of Capacity Credit Calculation Methods for Conventional Power Plants and Wind Power. *IEEE Trans. Power Syst.* 24 (2), 685–691. doi:10.1109/tpwrs.2009.2016493

Bertsimas, D., Litvinov, E., Sun, X. A., Zhao, J., and Zheng, T. (2013). Adaptive Robust Optimization for the Security Constrained Unit Commitment Problem. *IEEE Trans. Power Syst.* 28 (1), 52–63. doi:10.1109/tpwrs.2012.2205021

Billinton, R., and Dange Huang, D. (2011). Incorporating Wind Power in Generating Capacity Reliability Evaluation Using Different Models. *IEEE Trans. Power Syst.* 26 (4), 2509–2517. doi:10.1109/tpwrs.2011.2120633

Billinton, R., Yi Gao, Y., and Karki, R. (2009). Composite System Adequacy Assessment Incorporating Large-Scale Wind Energy Conversion Systems Considering Wind Speed Correlation. *IEEE Trans. Power Syst.* 24 (3), 1375–1382. doi:10.1109/tpwrs.2009.2023263

Cai, F., Yan, Z., Zhao, J., Feng, D., Guo, J., and Hu, D. (2013). Dependence Structure Models for Wind Speed and Wind Power Among Different Wind Farms Based on Copula Theory. *Automation Electr. Power Syst.* 37 (17), 9–16. doi:10.7500/AEPS201207293

Chen, P., Pedersen, T., Bak-Jensen, B., and Chen, Z. (2010). ARIMA-based Time Series Model of Stochastic Wind Power Generation. *IEEE Trans. Power Syst.* 25 (2), 667–676. doi:10.1109/tpwrs.2009.2033277

Conejo, A. J., Cheng, Y., Cheng, Y., Zhang, N., and Kang, C. (2017). Long-term Coordination of Transmission and Storage to Integrate Wind Power. *Csee Jpes* 3 (1), 36–43. doi:10.17775/cseejpes.2017.0006

Dobakhshari, A. S., and Fotuhi-Firuzabad, M. (2009). A Reliability Model of Large Wind Farms for Power System Adequacy Studies. *IEEE Trans. Energy Convers.* 24 (3), 792–801. doi:10.1109/tec.2009.2025332

Doostizadeh, M., Aminifar, F., Ghasemi, H., and Lesani, H. (2016). Energy and Reserve Scheduling under Wind Power Uncertainty: An Adjustable Interval Approach. *IEEE Trans. Smart Grid* 7 (6), 2943–2952. doi:10.1109/tsg.2016.2572639

Dvorkin, Y., Lubin, M., Backhaus, S., and Chertkov, M. (2016). Uncertainty Sets for Wind Power Generation. *IEEE Trans. Power Syst.* 31 (4), 3326–3327. doi:10.1109/tpwrs.2015.2476664

Feijóo, A., and Villanueva, D. (2016). Assessing Wind Speed Simulation Methods. *Renew. Sustain. Energy Rev.* 56, 473–483. doi:10.1016/j.rser.2015.11.094

Feng, C., Liang, B., Li, Z., Liu, W., and Wen, F. (2022). Peer-to-Peer Energy Trading under Network Constraints Based on Generalized Fast Dual Ascent. *IEEE Trans. Smart Grid*, 1. doi:10.1109/TSG.2022.3162876

Ganger, D., Zhang, J., and Vittal, V. (2014). Statistical Characterization of Wind Power Ramps via Extreme Value Analysis. *IEEE Trans. Power Syst.* 29 (6), 3118–3119. doi:10.1109/tpwrs.2014.2315491

Gao, Y., and Billinton, R. (2009). Adequacy Assessment of Generating Systems Containing Wind Power Considering Wind Speed Correlation. *IET Renew. Power Gener.* 3 (2), 217–226. doi:10.1049/iet-rpg:20080036

Garver, L. (1966). EFFECTIVE LOAD CARRYING CAPABILITY OF GENERATING UNITS. *IEEE Trans. Power Apparatus Syst.* PAS-85 (8), 910–919. doi:10.1109/tpas.1966.291652

Graham, W. J., and Cooper, W. H. (2013). Taking Credit. *J. Bus. Ethics* 115 (2), 403–425. doi:10.1007/s10551-012-1406-3

Han, X., Li, T., Zhang, D., and Zhou, X. (2021). New Issues and Key Technologies of New Power System Planning under Double Carbon Goals. *High. Volt. Eng.* 47 (9), 3036–3046. doi:10.13336/j.1003-6520.hve.20210809

Hasche, B., Keane, A., and O'Malley, M. (2011). Capacity Value of Wind Power, Calculation, and Data Requirements: the Irish Power System Case. *IEEE Trans. Power Syst.* 26 (1), 420–430. doi:10.1109/tpwrs.2010.2051341

Haslett, J., and Diesendorf, M. (1981). The Capacity Credit of Wind Power: A Theoretical Analysis. *Sol. Energy* 26 (5), 391–401. doi:10.1016/0038-092x(81)90218-8

Hawkins, S., Eager, D., and Harrison, G. P. (2011). "Characterising the Reliability of Production from Future British Offshore Wind Fleets," in IET Conference on Renewable Power Generation (RPG 2011), 1–6. doi:10.1049/cp.2011.0183

Hong, L., Shi, L., Yao, L., Masoud, B., and Ni, Y. (2010). Fuzzy Modelling and Solution of Load Flow Incorporating Uncertainties of Wind Farm Generation. *Trans. China Electrotech. Soc.* 25 (8), 116–122. 130. doi:10.19595/j.cnki.1000-6753.tces.2010.08.019

Ji, F., Cai, X., and Wang, J. (2014). Wind Power Correlation Analysis Based on Hybrid Copula. *Automation Electr. Power Syst.* 38 (2), 1–5. 32. doi:10.7500/AEPS201208067

Kahn, E. (1979). The Reliability of Distributed Wind Generators. *Electr. Power Syst. Res.* 2 (1), 1–14. doi:10.1016/0378-7796(79)90021-x

Kashyap, R. L. (1982). OPTIMAL CHOICE OF AR AND MA PARTS IN AUTOREGRESSIVE MOVING AVERAGE MODELS. *IEEE Trans. Pattern Anal. Mach. Intell.* PAMI-4 (2), 99–104. doi:10.1109/tpami.1982.4767213

Kim, H., Singh, C., and Sprintson, A. (2012). Simulation and Estimation of Reliability in a Wind Farm Considering the Wake Effect. *IEEE Trans. Sustain. Energy* 3 (2), 274–282. doi:10.1109/tste.2011.2174260

Klöckl, B., and Papaefthymiou, G. (2010). Multivariate Time Series Models for Studies on Stochastic Generators in Power Systems. *Electr. Power Syst. Res.* 80 (3), 265–276. doi:10.1016/j.epsr.2009.09.009

Kole, E., Koedijk, K., and Verbeek, M. (2007). Selecting Copulas for Risk Management. *J. Bank. Finance* 31 (8), 2405–2423. doi:10.1016/j.jbankfin.2006.09.010

Kroposki, B., Johnson, B., Zhang, Y., Gevorgian, V., Denholm, P., Hodge, B.-M., et al. (2017). Achieving a 100% Renewable Grid. *Ieee Power & Energy Mag.* 15 (2), 61–73. doi:10.1109/mpe.2016.2637122

Leite, A. P., Borges, C. L. T., and Falcao, D. M. (2006). Probabilistic Wind Farms Generation Model for Reliability Studies Applied to Brazilian Sites. *IEEE Trans. Power Syst.* 21 (4), 1493–1501. doi:10.1109/tpwrs.2006.881160

Li, J., Wen, J., Cheng, S., and Wei, H. (2013). A Scene Generation Method Considering Copula Correlation Relationship of Multi-Wind Farms Power. *Proc. CSEE* 33 (16), 30–36. doi:10.13334/j.0258-8013.pcsee.2013.16.012

Li, J., and Zhu, D. (2016). Combination of Moment-matching, Cholesky and Clustering Methods to Approximate Discrete Probability Distribution of Multiple Wind Farms. *Iet Renew. Power Gener.* 10 (9), 1450–1458. doi:10.1049/iet-rpg.2015.0568

Li, P., Liu, C., Huang, Y., Wang, W., and Li, Y. (2019). Modeling Correlated Power Time Series of Multiple Wind Farms Based on Hidden Markov Model. *Proc. Chin. Soc. Electr. Eng.* 39 (19), 5683–5691. doi:10.13334/j.0258-8013.pcsee.182412

Lucheroni, C., Boland, J., and Ragno, C. (2019). Scenario Generation and Probabilistic Forecasting Analysis of Spatio-Temporal Wind Speed Series with Multivariate Autoregressive Volatility Models. *Appl. Energy* 239, 1226–1241. doi:10.1016/j.apenergy.2019.02.015

Luo, G., Shi, D., Chen, J., and Wu, X. (2014). A Markov Chain Monte Carlo Method for Simulation of Wind and Solar Power Time Series. *Power Syst. Technol.* 38 (2), 321–327. doi:10.13335/j.1000-3673.pst.2014.02.008

Olsson, M., Perninge, M., and Söder, L. (2010). Modeling Real-Time Balancing Power Demands in Wind Power Systems Using Stochastic Differential Equations. *Electr. Power Syst. Res.* 80 (8), 966–974. doi:10.1016/j.epsr.2010.01.004

Qu, C., Wang, X., Xie, S., and Wu, X. (2013). Impacts of Different Wind Speed Models and Reliability Indices on Capacity Credit Evaluation of Wind Power. *Power Syst. Technol.* 37 (10), 2896–2903. doi:10.13335/j.1000-3673.pst.2013.10.020

Salehi-Dobakhshari, A., and Fotuhi-Firuzabad, M. (2011). Integration of Large-Scale Wind Farm Projects Including System Reliability Analysis. *IET Renew. Power Gener.* 5 (1), 89–98. doi:10.1049/iet-rpg.2008.0110

Sevlian, R., and Rajagopal, R. (2013). Detection and Statistics of Wind Power Ramps. *IEEE Trans. Power Syst.* 28 (4), 3610–3620. doi:10.1109/tpwrs.2013.2266378

Sevlian, R., and Rajagopal, R. (2012). "Wind Power Ramps: Detection and Statistics," in Proceeding of the 2012 IEEE Power and Energy Society General Meeting. doi:10.1109/PESGM.2012.6344969

Shao, C., Feng, C., Fu, X., Yang, P., Wang, X., and Wang, X. (2021). Multi Energy Power System Production Simulation:State of Arts and Challenges. *Proc. Chin. Soc. Electr. Eng.* 41 (6), 2029–2039. doi:10.13334/j.0258-8013.pcsee.200801

Shao, C., Wang, X., Shahidehpour, M., Wang, X., and Wang, B. (2017). Security-Constrained Unit Commitment with Flexible Uncertainty Set for Variable Wind Power. *IEEE Trans. Sustain. Energy* 8 (3), 1237–1246. doi:10.1109/tste.2017.2673120

Shortt, A., Kiviluoma, J., and O'Malley, M. (2013). Accommodating Variability in Generation Planning. *IEEE Trans. Power Syst.* 28 (1), 158–169. doi:10.1109/tpwrs.2012.2202925

Voorspools, K. R., and D'Haeseleer, W. D. (2006). An Analytical Formula for the Capacity Credit of Wind Power. *Renew. Energy* 31 (1), 45–54. doi:10.1016/j.renene.2005.03.017

Wang, C., Liu, F., Wang, J., Wei, W., and Mei, S. (2016a). Risk-Based Admissibility Assessment of Wind Generation Integrated into a Bulk Power System. *IEEE Trans. Sustain. Energy* 7 (1), 325–336. doi:10.1109/tste.2015.2495299

Wang, J., Cai, X., and Ji, F. (2013). Simulation Method of Correlated Random Variables Based on Copula. *Proc. CSEE* 33 (22), 75–82.

Wang, J., Shahidehpour, M., and Li, Z. (2008). Security-constrained Unit Commitment with Volatile Wind Power Generation. *IEEE Trans. Power Syst.* 23 (3), 1319–1327. doi:10.1109/tpwrs.2008.926719

Wang, Q., Dong, W., and Yang, L. (2015a). A Wind Power/Photovoltaic Typical Scenario Set Generation Algorithm Based on Wasserstein Distance Metric and Revised K-Medoids Cluster. *Proc. Chin. Soc. Electr. Eng.* 35 (11), 2654–2661. doi:10.13334/j.0258-8013.pcsee.2015.11.003

Wang, X., Shao, C., Wang, X., Jin, X., and Lu, S. (2015b). *A Renewable Energy Power Modeling Method Based on Markov Process*.

Wang, X., Dai, H.-z., and Thomas, R. (1984). Reliability Modeling of Large Wind Farms and Associateed Electric Utility Interface Systems. *IEEE Trans. Power Apparatus Syst.* PAS-103 (3), 569–575. doi:10.1109/tpas.1984.318746

Wang, X., Hu, Z., Zhang, M., and Hu, M. (2016b). "Two-stage Stochastic Optimization for Unit Commitment Considering Wind Power Based on Scenario Analysis," in Proceeding of the 2016 China International Conference on Electricity Distribution (CICED) (IEEE).

Wu, Y., Zhang, L., Li, H., Lou, S., and Yang, Y. (2015). Wind-power Capacity Credibility Assessment Considering Power Output Correlation of Multiple Wind Farms. *Electr. Power Autom. Equip.* 35 (11), 8–12. doi:10.16081/j.issn.1006-6047.2015.11.002

Xie, M., Xiong, J., Liu, M., and Zhou, S. (2016). Modeling of Multi Wind Farm Output Correlation Based on Copula and its Application in Power System Economic Dispatch. *Power Syst. Technol.* 40 (4), 1100–1106. doi:10.13335/j.1000-3673.pst.2016.04.018

Xu, C., Xu, X., Yan, Z., and Li, H. (2022). Distributionally Robust Optimal Dispatch Method Considering Mining of Wind Power Statistical Characteristics. *Automation Electr. Power Syst.* 46 (2), 33–42. doi:10.7500/AEPS20210413003

Xu, X., Wang, H., Yan, Z., Lu, Z., Kang, C., and Xie, K. (2021). Overview of Power System Uncertainty and its Solutions under Energy Transition. *Automation Electr. Power Syst.* 45 (16), 2–13. doi:10.7500/AEPS20210301003

Xu, X., Yan, Z., Shahidehpour, M., Li, Z., Yan, M., and Kong, X. (2020). Data-Driven Risk-Averse Two-Stage Optimal Stochastic Scheduling of Energy and Reserve with Correlated Wind Power. *IEEE Trans. Sustain. Energy* 11 (1), 436–447. doi:10.1109/tste.2019.2894693

Xu, Y., Chen, K., Li, J., and Nie, Y. (2016). A New Method Analyzing Output Correlation of Multi-Wind Farms Based on Combination of Copula Function and Kernel Estimation Theory. *Trans. China Electrotech. Soc.* 31 (13), 92–100. doi:10.19595/j.cnki.1000-6753.tces.2016.13.011

Yang, D., Zhou, S., and Bao, F. (2014). Analysis on Peak Load Regulation Capability of Power Grid Integrated with Wind Farms in Valley Load Period. *Power Syst. Technol.* 38 (6), 1446–1451. doi:10.13335/j.1000-3673.pst.2014.06.004

Yang, N., Huang, Y., Ye, D., Wang, X., Li, H., Li, S., et al. (2018). Modeling of Output Correlation of Multiple Wind Farms Based on Adaptive Multivariable Nonparametric Kernel Density Estimation. *Proc. Chin. Soc. Electr. Eng.* 38 (13), 3805–3812. doi:10.13334/j.0258-8013.pcsee.171751

Zeng, B., and Zhao, L. (2013). Solving Two-Stage Robust Optimization Problems Using a Column-And-Constraint Generation Method. *Operations Res. Lett.* 41 (5), 457–461. doi:10.1016/j.orl.2013.05.003

Zhang, G. P. (2003). Time Series Forecasting Using a Hybrid ARIMA and Neural Network Model. *Neurocomputing* 50, 159–175. doi:10.1016/s0925-2312(01)00702-0

Zhang, N., Kang, C., Duan, C., Tang, X., Huang, J., Lu, Z., et al. (2010). Simulation Methodology of Multiple Wind Farms Operation Considering Wind Speed Correlation. *Int. J. Power Energy Syst.* 30 (4), 264–273. doi:10.2316/Journal.203.2010.4.203-4843

Zhang, N., Kang, C., Xiao, J., Li, H., Wang, Z., Shi, R., et al. (2015). Review and Prospect of Wind Power Capacity Credit. *Proc. Chin. Soc. Electr. Eng.* 35 (1), 82–94. doi:10.13334/j.0258-8013.pcsee.2015.01.011

Zhang, N., Kang, C., Xu, Q., Jiang, C., Chen, Z., and Liu, J. (2013). Modelling and Simulating the Spatio-Temporal Correlations of Clustered Wind Power Using Copula. *J. Electr. Eng. Technol.* 8 (6), 1615–1625. doi:10.5370/jeet.2013.8.6.1615

Zhang, S., Wang, C., Liao, P., Xiao, L., and Fu, T. (2022). Wind Speed Forecasting Based on Model Selection, Fuzzy Cluster, and Multi-Objective Algorithm and Wind Energy Simulation by Betz's Theory. *Expert Syst. Appl.* 193, 116509. doi:10.1016/j.eswa.2022.116509

Zhao, J., Zheng, T., and Litvinov, E. (2015). Variable Resource Dispatch through Do-Not-Exceed Limit. *IEEE Trans. Power Syst.* 30 (2), 820–828. doi:10.1109/tpwrs.2014.23333f67

Zhaohong, B., Xin, Z., Zijing, W., and Xifan, W. (2009). "Studies on Models and Algorithms of the Power System Probabilistic Production Simulation Integrated with Wind Farm," in Proceeding of the 2009 IEEE Power & Energy Society General Meeting.

Zhou, X., Chen, S., Lu, Z., Huang, Y., Ma, S., and Zhao, Q. (2018). Technology Features of the New Generation Power System in China. *Proc. Chin. Soc. Electr. Eng.* 38 (7), 1893–1904. doi:10.13334/j.0258-8013.pcsee.180067

Zou, J., Zhu, J., Lai, X., Xie, P., and Xuan, P. (2019). Simulation of Wind Power Output Series Based on Space-Time Auto-Regressive Moving Average Model. *Automation Electr. Power Syst.* 43 (3), 101–107. doi:10.7500/AEPS20180328002

Conflict of Interest: XiL, WX, and XuL Were employed by the company Guangdong Power Grid Co., Ltd.

The remaining authors declare that the research was conducted in the absence of any commercial or financial relationships that could be construed as a potential conflict of interest.

frontiers | Frontiers in Energy Research

ORIGINAL RESEARCH
published: 06 July 2022
doi: 10.3389/fenrg.2022.951618

Analysis on Influence of Residents' Response Probability Distribution on Load Aggregation Effect

Weichun Zhang[1], *Qinran Hu*[1,2]* *and Xiaorong Yu*[3]

[1]School of Electrical Engineering, Southeast University, Nanjing, China, [2]Jiangsu Provincial Key Laboratory of Smart Grid Technology and Equipment, Nanjing, China, [3]Taizhou Power Supply Company State Grid Jiangsu Electric Power Co., Ltd, Taizhou, China

Residential loads are essential resources, and they can participate in grid scheduling through aggregation, with great potential. However, inherent uncertainties challenge the realization of accurate load aggregation (LA), leading to the failure to fully play a role in grid operation. In this context, this paper analyzes the influence of the probability of residents participating in LA on the actual aggregation effect. Firstly, the LA problem is modeled, and the optimization objective is equivalently transformed from minimizing the mismatch between the actual load regulation and the target to minimizing the sum of variances of the overall response probabilities. Response probabilities of residents are then simulated based on the β distribution model, and various typical distributions can be generated by modifying only two hyperparameters. In order to evaluate the actual aggregation effect, a multi-armed bandit model that can be used for LA is adopted, and an evaluation framework is designed. The simulation results show that for different probability distributions, the smaller the sum of variances of all residents' response probabilities are, the more accurate aggregation can be achieved.

Keywords: residential load aggregation, response probability, β distribution, multi-armed bandit, error analysis

OPEN ACCESS

Edited by:
Zhiyi Li,
Zhejiang University, China

Reviewed by:
Qingxin Shi,
North China Electric Power University, China
Peishuai Li,
Nanjing University of Science and Technology, China

***Correspondence:**
Qinran Hu
qhu@seu.edu.cn

Specialty section:
This article was submitted to Smart Grids, a section of the journal Frontiers in Energy Research

Received: *24 May 2022*
Accepted: *14 June 2022*
Published: *06 July 2022*

Citation:
Zhang W, Hu Q and Yu X (2022) Analysis on Influence of Residents' Response Probability Distribution on Load Aggregation Effect. Front. Energy Res. 10:951618. doi: 10.3389/fenrg.2022.951618

1 INTRODUCTION

Modern power grids are transitioning to a low-carbon energy system, and traditional coal-fired units are gradually retiring (Zhou et al., 2021). Renewable energy sources (RES) represented by photovoltaics and wind power have gained unprecedented development opportunities. According to IRENA, the total installed capacity of global RES in 2021 is 3064 GW, accounting for 38%, with a year-on-year increase of 257 GW (IRENA, 2022). The widespread access of a high proportion of RES will become the fundamental feature of new power systems in the future. However, the output of RES is random and uncertain, and large-scale grid connections will bring significant challenges to grid scheduling. In recent years, many severe power outages have occurred, such as "2019·8·9" in the United Kingdom (Sun et al., 2019) and "2020·8·14" in California (Hu et al., 2020).

To solve these problems, researchers pay attention to the flexible, controllable loads with increasing proportion, which have great potential to regulate their operating power quickly without affecting users' comfort (Chen et al., 2018; Qi et al., 2020). In this context, load aggregation technology emerged as the times required. Appropriate control strategies aggregate many scattered demand-side resources into a whole managed by load aggregators (Burger et al., 2017). Through specific electricity prices or incentives means, users are urged to regulate their power

consumption patterns to assist grid scheduling (Sun et al., 2017). For residential thermostatically controlled loads (RTCLs) with energy storage properties (Hao et al., 2015), such as air conditioners and water heaters, the power regulation speed is faster than traditional thermal power plants and hydropower plants. Moreover, RTCLs have flexible control methods and low response costs, which are ideal for participating in LA (Gong et al., 2020).

In order to fully utilize the effect of RTCLs on the grid, a vital requirement is to achieve accurate and reliable load aggregation (Saleh et al., 2017). However, this is a challenging problem: the residents' response behavior to the load regulation signal is uncertain (Mathieu et al., 2013), which is affected by many factors, such as incentives (Qi et al., 2020), weather (Kou et al., 2021), electricity usage habits (Baek et al., 2021), and the load aggregator's knowledge of these factors is limited. Accurately estimating these uncertainties is essential. Overestimating will reduce the utilization of RTCLs while underestimating will blindly send load regulation instructions, which will cause the actual aggregation to deviate from the target and bring risks to the power grid (Syrri and Mancarella, 2016).

Much research has been done on the uncertainty of residents' response behavior. Li et al. (2017) derived the relationship between aggregated power and temperature based on the first-order thermal parameter model of RTCLs and established an approximate aggregation model of RTCLs. Luo et al. (2020) established the uncertainty model of the load regulation by analyzing the characteristics of different types of loads and using the probability method and fuzzy theory. Sun et al. (2020) considered the uncertainty of electricity consumption habits to establish a user preference model and obtained a probability estimate of load regulation amount through Bayesian inference. Gong et al. (2020) designed a hierarchical robust control mechanism to achieve precise power tracking by aggregating RTCLs in uncertain time-varying environments.

Load aggregation is a behavior that residents voluntarily participate in. Most of the existing studies only model the regulation power of residents in the LA scenario, ignoring the relevant research on their response probabilities. In addition, in existing pilots, in order to improve the probabilities of users actively participating in LA, blind incentives such as currency are often used, resulting in high costs. Therefore, analyzing the impact of the residents' response probability distribution on the aggregation effect can provide a reference for load aggregators to formulate plans and make more effective use of RTCLs.

In order to fill the above research gap, aiming at the scenario of residential loads aggregation, this paper derives and verifies the mapping relationship between the response probability and the actual aggregation effect. The main contributions of this paper include the following:

1) A response probability generation model based on the β distribution is proposed, which can simulate a variety of typical distributions by modifying only two hyperparameters, and derives the relationship between the aggregation effect and the response probability distribution through theoretical analysis.
2) An evaluation framework of the load aggregation effect based on the multi-armed bandit (MAB) model is designed, which can be utilized to analyze the effect of response probability on the aggregation effect.

The rest of the paper is organized as follows: **Section 2** models the load aggregation problem from a probabilistic perspective and derives a preliminary theory. In **Section 3**, a simulation method of residents' response probability distribution is proposed, and the corresponding analysis is carried out. **Section 4** designs a framework for evaluating the effect of LA, and based on this, a case study is carried out to verify our theory in **Section 5**. **Section 6** concludes this work.

2 LOAD AGGREGATION MODEL

Residents' response to aggregation instructions is uncertain, influenced by various factors, such as age, education, and temperature. The concrete manifestation of this uncertainty is whether the user agrees to regulate the load. This paper abstracts it from the perspective of probability and sets the probability that user i agrees to regulate as p_i, that is, the response probability, and can regulate the load of 1 unit. The binary variable X_i is introduced to characterize the response result. Obviously, X_i obeys the Bernoulli distribution, that is, $X_i \sim \mathrm{Bern}(p_i)$:

$$X_i = \begin{cases} 1 & p_i \\ 0 & 1 - p_i \end{cases} \tag{1}$$

According to the properties of Bernoulli distribution, when the instruction is issued to resident i, the expected value of its load regulation $E(X_i) = p_i$, and the variance $\sigma_i^2 = p_i(1 - p_i)$.

We consider such a scenario: in the t-th event, the power system needs to curtail the load D, and the load aggregator should select a subset $S_t \subseteq [n]$ among all n users in the area A_n to send instructions. The goal is to minimize the deviation $G_t(t)$ between the actual curtailment and D:

$$\min G_t(t) = \left(\sum\nolimits_{i \in S_t} X_{t,i} - D \right)^2 \tag{2}$$

Since $X_{t,i}$ is a random variable, **Eq. 2** should be modified to minimize the mathematical expectation of $G_t(t)$. Moreover, the expectation operator can be removed by rigorous derivation, and the simplified result is as follows:

$$\min_{S_t \subseteq [n]} \mathbb{E}\, G_t(t) \Leftrightarrow \min_{S_t \subseteq [n]} \left(\sum_{i \in S_t} p_i - D \right)^2 + \sum_{i \in S_t} p_i(1 - p_i) \tag{3}$$

Eq. 3 is a combinatorial optimization problem, and the decision variable is the set S_t of selected residents. However, it is NP-hard, and only approximate algorithms can be adopted. Especially when the number of residents n and the target D are large, many residents need to be selected each time, which will produce a "Combinatorial Explosion."

It can be seen from **Eq. 3** that the actual load aggregation deviation $G_t(t)$ at the t-th event is affected by three factors, the target D, the selected set S_t, and the response probability set $\mathbb{P}_t =$

$\{p_i: i \in S_t\}$. These three are not independent of each other because D affects the determination of S_t, and S_t determines $\mathbb{P}_t$. It should be noted that the power grid may be in various working states, such as different levels of frequency fluctuations, which results in a time-varying value of D issued to the load aggregator in A_n rather than a fixed value. Under this background, in order to minimize $G_t(t)$ for any D, two critical aspects should be considered: 1) the determination of S_t, that is, the users' selection algorithm, mainly affects the first term on the right side of **Eq. 3**; 2) the set of response probabilities of all residents in A_n: $\mathbb{P} = \{p_i: \forall\ i \in [n]\}$, affecting the second term.

The core of this paper is not how to solve S_t accurately but mainly focuses on analyzing the effect of $\mathbb{P}$ on the aggregation effect, which is essentially more fundamental than studying the precise selection strategy. For the convenience of analysis, intuition is to approximately transform **Eq. 3** into the following optimization problem and propose our theory:

$$\min \sum_{i \in [n]} p_i (1 - p_i) \Leftrightarrow \min \sum_{i \in [n]} \sigma_i^2 = f(\mathbb{P}) \tag{4}$$

Theorem 1. For M different $\mathbb{P}$ residents groups $\Psi = \{\mathbb{P}_1, \mathbb{P}_2, \ldots, \mathbb{P}_M\}$, the one with the smallest sum of variances can achieve the most accurate load aggregation, defined as the optimal response probability distribution $\mathbb{P}^*$:

$$\mathbb{P}^* = \{\mathbb{P}_u | \forall \mathbb{P}_v \in \mathcal{P}:\ f(\mathbb{P}_u) \le f(\mathbb{P}_v)\} \tag{5}$$

For rigorous analysis, the probability sets $\forall\ \mathbb{P} \in \Psi$ studied in this paper should all have the same mean p_{mean}, $\bar{\mathbb{P}}_1 = \bar{\mathbb{P}}_2 = \ldots = \bar{\mathbb{P}}_M = p_{mean}$, which is an important constraint. For instance, for two probability sets $\bar{\mathbb{P}}_1$ and $\bar{\mathbb{P}}_2$ with mean values of 1 and 0.1, respectively, given the same regulation target D, it is clear that the response of the latter will be poor or even no response, resulting in a high aggregation mismatch. In this case of inequality, it is pointless to analyze still the effect of the probability distribution on the aggregation, so it should be restricted to have the same mean.

From the non-negativeness of the variance σ_i^2, it can be seen that the sum $f(\mathbb{P}) \ge 0$, if and only if p_i is 0 or 1, the equal sign is true, as shown in **Eq. 6**. Therefore, for sets with the mean p_{mean}, the optimal distribution $\mathbb{P}^*$ that can achieve the minimum aggregation mismatch is given by **Eq. 7**.

$$f(\mathbb{P}) = 0 \Leftrightarrow p_i \in \{0, 1\}, \forall p_i \in \mathbb{P} \tag{6}$$

$$\mathbb{P}^* = \left\{\mathbb{P}_u \middle| \mathbb{P}_u^1 = \complement_{\mathbb{P}_u} \mathbb{P}_u^0:\ \left|\mathbb{P}_u^1\right| = \left[n p_{mean}\right], \left|\mathbb{P}_u^0\right| = n - \left|\mathbb{P}_u^1\right|\right\} \tag{7}$$

where the symbol " $\complement$" represents the complement, and Ψ_u^1 and Ψ_u^0 represent the subsets in $\mathbb{P}_u$ whose values are 0 and 1, respectively. "$|\cdot|$" is defined as the cardinality of a finite set, and " $[\cdot]$" means rounding.

3 RESPONSE PROBABILITY SETS GENERATION METHOD

The core of this paper is to analyze the impact of residents' response probabilities set $\mathbb{P}$ on the actual aggregation effect, and a response probability generation model should be designed to simulate $\mathbb{P}$. The shape of the probability distribution is infinitely different, not all cases can be obtained, and it is not necessary. Therefore, this paper adopts the β distribution, which is vital in the field of machine learning, which is a parametric probability distribution model that only contains two parameters, α and $\beta > 0$, usually denoted as $Y \sim \mathrm{Be}(\alpha, \beta)$. By setting the parameters, a variety of typical probability distributions can be simulated, all within the interval (0, 1), and then $M \times n$ random sampling is performed to generate a set Ψ containing M kinds of $\mathbb{P}$. Some properties of the β distribution are as follows:

3.1 Probability Density Function

$$f(Y; \alpha, \beta) = \frac{\Gamma(\alpha + \beta)}{\Gamma(\alpha)\Gamma(\beta)} Y^{\alpha - 1} (1 - Y)^{\beta - 1} \tag{8}$$

where $\Gamma(z)$ is the Γ function.

3.2 Expectation and Variance

$$\mu = E(Y) = \frac{\alpha}{\alpha + \beta} \tag{9}$$

$$Var(Y) = E(Y - \mu)^2 = \frac{\alpha\beta}{(\alpha + \beta)^2 (\alpha + \beta + 1)} \tag{10}$$

Assuming that the elements $\mathbb{P}$ within Ψ have the same mean μ, combined with **Eq. 9**, we can derive the relationship between α and β:

$$\beta = \alpha\left(\frac{1}{\mu} - 1\right) \tag{11}$$

Therefore, a probability set $\mathbb{P}$ is generated based on the β distribution, denoted by $\mathbb{P} \sim \mathrm{Be}[\alpha, \alpha(1/\mu\text{-}1)]$. Only by modifying the parameter α, the set Ψ of M probability distributions can be obtained. In addition, the β distribution has another property: as α increases monotonically, the variance $Var(\mathbb{P})$ of $\forall\ p_i \in \mathbb{P}$ will decrease monotonically according to the trend of the inverse proportional function, which means that p_i gradually approaches the fixed mean μ, and the degree of dispersion decreases. The relationship between the two is as follows:

$$Var(\mathbb{P}) = \frac{\alpha\beta}{(\alpha + \beta)^2 (\alpha + \beta + 1)} = \frac{\mu^2 (1 - \mu)}{\alpha + \mu} \tag{12}$$

Further, when the number of residents n is large enough, we can simplify **Eq. 4** to eliminate the summed symbol Σ and analyze the analytical relationship between **Eqs 4**, **12**. Before that, two assumptions are listed first due to the limited sample size.

Assumption 1. The mean of the probability sample p_i is equal to the expectation of the β distribution, which $\mathbb{P}$ follows:

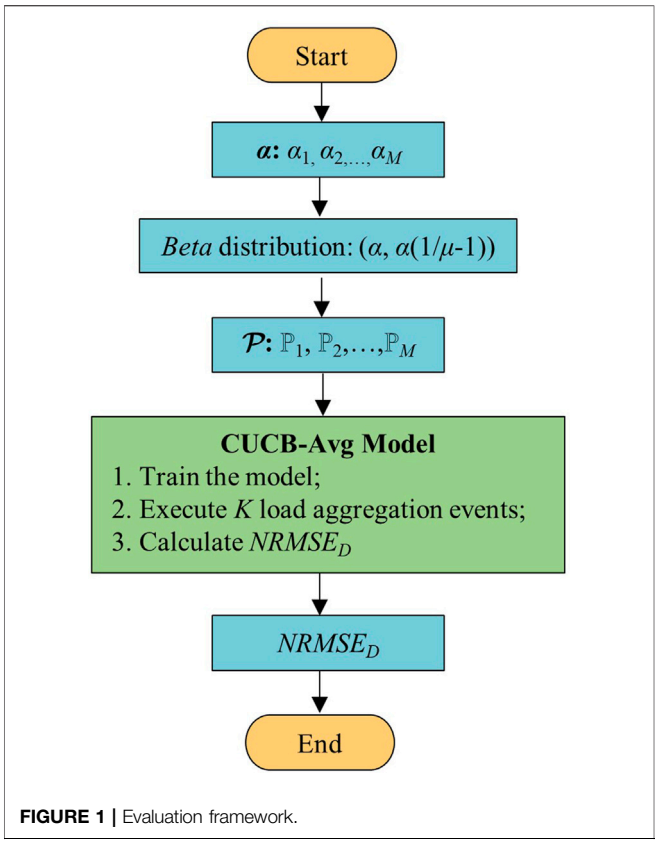

FIGURE 1 | Evaluation framework.

$$\sum_{i\in[n]} p_i \Big/ n = \mu$$

Assumption 2. The sample mean of the probability square p_i^2 is equal to the expectation of the distribution, which follows:

$$\sum_{i\in[n]} p_i^2 \Big/ n = E(p^2)$$

Theorem 2. The relationship between the sum of variances $f(\mathbb{P})$ of the probabilities and the variance $Var(\mathbb{P})$ of the β distribution is:

$$f(\mathbb{P}) = n\left[\mu(1-\mu) - Var(\mathbb{P})\right] = \frac{n\mu(1-\mu)}{1+\frac{\mu}{\alpha}} \tag{13}$$

As can be seen from **Eq. 13**, the trend of change between the two is precisely the opposite. $f(\mathbb{P})$ is a monotonically increasing function of α, which means that the aggregation mismatch becomes larger and less precise as the α increases.

4 EVALUATION FRAMEWORK OF LOAD AGGREGATION EFFECT

In this section, we first introduce a CUCB-Avg algorithm that can be adopted to select user sets in load regulation events, and based on this, we design a framework to evaluate the impact of the residents' response probability set $\mathbb{P}$ on the LA effect.

4.1 Users Selection Algorithm

The response probability set $\mathbb{P}$ of residents is unknown to the load aggregator, and it is a complex problem how to select appropriate users to send the regulation instructions in load regulation events. This is similar to the setting of the classic MAB problem: for a slot machine with multiple arms, after each arm is pulled, it will obtain a payoff that obeys an unknown distribution. How can the gambler obtain the maximum cumulative payoff within a limited number of pulls? If each resident corresponds to an arm, its actual curtailment X_i can be regarded as the reward of this arm. The common denominator is to understand the uncertainty of an arm/user to make a choice. Unlike the MAB problem, the goal of LA is to minimize the mismatch **Eq. 2**.

MAB is an essential framework for dealing with uncertainty problems, and typical sub-methods include CUCB (Chen et al., 2013), UCB1 (Auer et al., 2002), and LinUCB (Li et al., 2010), etc., For the LA scenario, this paper introduces an improved CUCB, the CUCB-Avg algorithm (Li et al., 2020), to select the residents set S_t. This method considers the sample mean $\bar{p}_i$ of p_i and assigns it a confidence interval. From an optimistic point of view, the actual value of p_i is estimated with upper confidence bound and bounded to [0,1],

$$G_i(t) = \min\left(\bar{p}_i(t-1) + \sqrt{\frac{\alpha \ln t}{2T_i(t-1)}}, 1\right) \tag{14}$$

where α is a positive constant used to weigh the sample mean and confidence interval. $T_i(t\text{-}1)$ is the number of times user i has been selected in the past $(t\text{-}1)$ events. Based on **Eq. 14**, the CUCB-Avg algorithm mainly includes three steps to select users: 1) calculating $G_i(t)$ for each user i, 2) selecting the highest m_t users in descending order and sending instructions, 3) updating incrementally according to the actual response feedback. The specific process of the algorithm is as follows:

Algorithm 1. CUCB-Avg

Inputs: D, α>2
Initialization: $T_i(1)$, $\bar{p}_i(1)$:
1: Calculate the ideal maximum regulation target $D_{ide} = n$. Send instructions to all n users;
2: Observe the actual curtailment D_{ac};
3: $\bar{p}_i(1) = D_{ac}/D_{ide}$;
for $t = 2,\ldots,T$, **do**
1: Based on Eq. 14, calculate the upper confidence bound for each i.
2: Rank $G_i(t)$ in descending order, denote the order as idx.
3: Find the smallest m_t such that $\sum_{j=1}^{m_t} \bar{p}_{idx(j)} > D - 1/2$.
4: Play S_t={$idx(1)$, $idx(2)$,…, $idx(m)$} and send instructions.
5: Update $T_i(t)$ and $\bar{p}_i(t)$, $\forall i \in S_t$:
5.1: $\bar{p}_i(t) = [\bar{p}_i(t-1)T_i(t-1) + Z_i]/[T_i(t-1)+1]$;
5.2: $T_i(t) = T_i(t-1) + 1$;
Outputs: Set of users S_t and actual load curtailment $D_{act}(t) = \sum_{j=1}^{m_t} Z_{idx(j)}$.
end for

4.2 Evaluation Framework

In load regulation events, due to the uncertainty and randomness of residents, CUCB-Avg's estimation of the actual probability p_i is not entirely accurate, and there is still a mismatch between the actual aggregation amount and the target D. In this paper, the

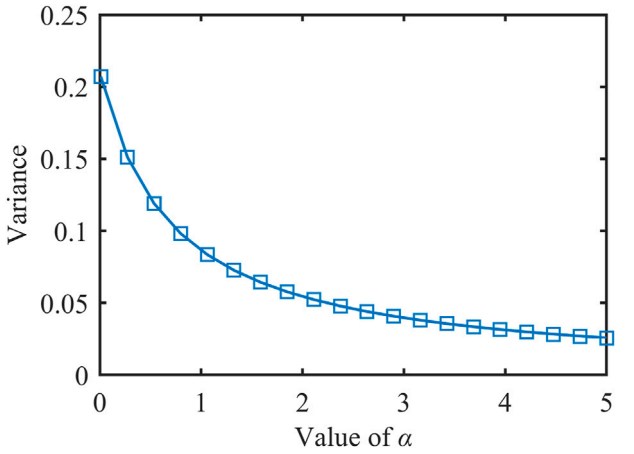

FIGURE 2 | The variance of different β distributions.

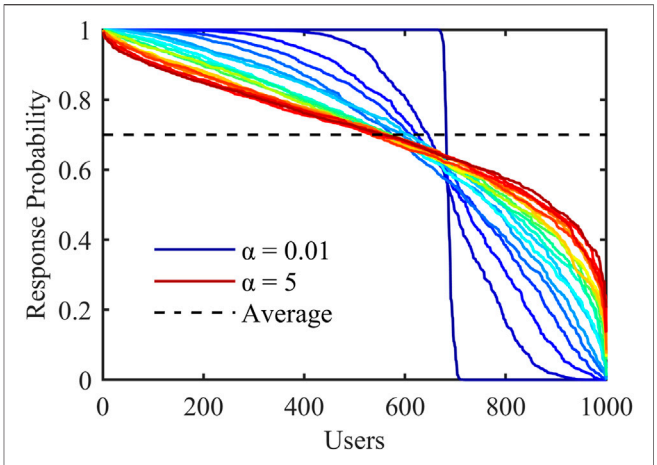

FIGURE 3 | Curve graph.

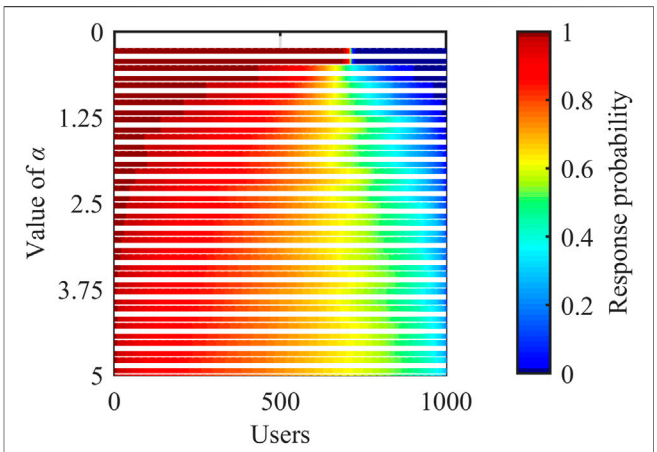

FIGURE 4 | Heat map.

normalized root mean square error ($NRMSE_D$) is adopted to evaluate the effect of aggregation, where $D_{act,k}$ is the actual aggregation amount of K times for the target D.

$$NRMSE_D = \sqrt{\frac{\sum_{k=1}^{K}\left(D_{act,k} - D\right)^2}{K}} \Big/ D \tag{15}$$

Based on this, we propose a framework for evaluating the impact of response probability on the aggregation effect, as shown in **Figure 1**.

Step 1. Set M values $\{\alpha_1, \alpha_2, ..., \alpha_M\}$ of the parameter α, and calculate β according to **Eq. 11**. Generate the corresponding sets of response probabilities for all residents based on the β distribution $\Psi = \{\mathbb{P}_1, \mathbb{P}_2, \ldots, \mathbb{P}_M\}$;

Step 2. Train the CUCB-Avg model with different $\mathbb{P}$ as inputs;

Step 3. Based on the algorithm's understanding of uncertainties, the Monte Carlo method is adopted to perform K events, and $NRMSE_D$ is calculated according to **Eq. 15**;

Step 4. Compare $NRMSE_D$ corresponding to different α, and evaluate the effect of $\mathbb{P}$ on the aggregation effect.

5 CASE STUDY

To verify the theories derived in the previous section, we conduct simulations based on the proposed evaluation framework to analyze the impact of different sets $\mathbb{P}$ of response probabilities on the actual aggregation effect. We focus on the area A_n with $n = 1000$ residents, equipped with intelligent terminals that can participate in LA, and the adjustable capacity contracted with the load aggregator is 2.5 kW, which is equivalent to 1 unit load.

5.1 Setting of Response Probability Sets

Before analysis, Ψ should be generated containing various probability distributions based on the β distribution model. Additionally, we set all distributions with the same mean $p_{mean} = \mu = 0.7$. Specifically, it includes the following steps:

1) Set the parameter α in the interval [0.01, 5], and take $M = 20$ values in equal steps;
2) Calculate β based on **Eq. 11**;
3) Generate n random numbers following the β distribution, which correspond to the response probabilities of n residents, and the set is $\mathbb{P}_j$, $j = 1, 2 \ldots, M$;

As α increases, $Var(\mathbb{P})$ is shown in **Figure 2**. It can be seen from the figure that $Var(\mathbb{P})$ is monotonically decreasing and similar to the hyperbolic function, which is consistent with **Eq. 12**.

Through the above steps, Ψ of M probability distributions with the same mean μ is generated. Due to a large amount of data, it is not clear to visualize the dataset with a histogram. Therefore, we adopt a curve graph and heat map as follows:

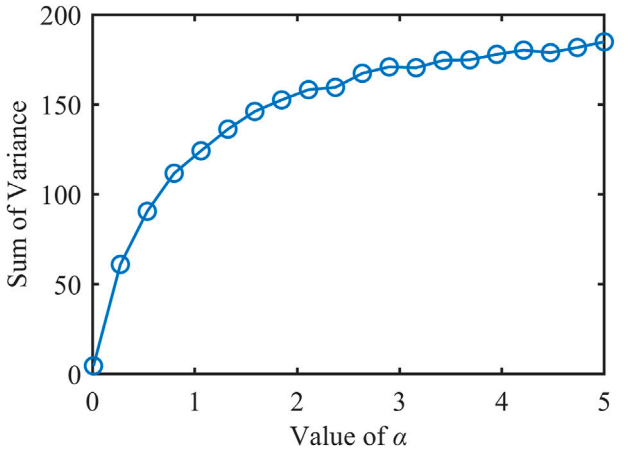

FIGURE 5 | The sum of variances corresponding to different α

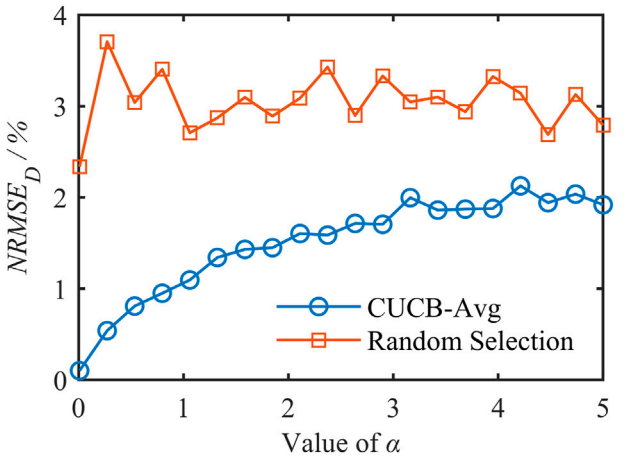

FIGURE 6 | $NRMSE_D$ of D = 0.8 MW.

1) Curve graph. For $\mathbb{P}_j$, sort the response probability p_i in descending order, and draw M curves. The horizontal axis represents the residents, and the vertical axis represents the response probability, as shown in **Figure 3**:

It can be seen that as α increases, the curve gradually slopes and approaches the horizontal dashed line with a mean $\mu = 0.7$. This is because the variance $Var(\mathbb{P})$ gradually decreases, and the value of p_i shrinks to 0.7.

2) Heat map. It is similar to the previous graph but is equivalent to looking down on the X-Y plane on the Z-axis of the three-dimensional coordinate system. M curves are arranged in parallel at equal intervals. Different colors represent the value of p_i. Y-axis represents α, and the corresponding M color bands are drawn, as shown in **Figure 4**:

Figure 4 shows the distribution of each $\mathbb{P}_j$ more intuitively. When $\alpha = 0.01$, $\mathbb{P}_1$ has almost only probability values at both ends of the color band, namely 0 and 1. As α grows, the probabilities corresponding to the color of the middle segment gradually increase and approach 0.7.

In addition, the variation of $f(\mathbb{P})$ with the parameter α should also be supplemented, as shown in **Figure 5**. It should be noted that although **Figures 2, 5** are both about variance, their meanings are entirely different: the former means that α will produce different β distributions, and $Var(\mathbb{P})$ of the distribution is calculated based on **Eq. 10**; the latter is related to the setting that the load regulation follows the Bernoulli distribution, and the sum $f(\mathbb{P})$ of variances is calculated based on **Eq. 4**. The mathematical relationship between the two is shown in **Eq. 13**.

5.2 Load Aggregation Deviation

CUCB-Avg model is trained for $T = 1000$ times and performs $K = 300$ Monte Carlo simulations to calculate $NRMSE_D$. Additionally, to highlight the superiority of CUCB-Avg, here we introduce a conventional random selection (RS) method as the benchmark (Chen et al., 2020). RS only

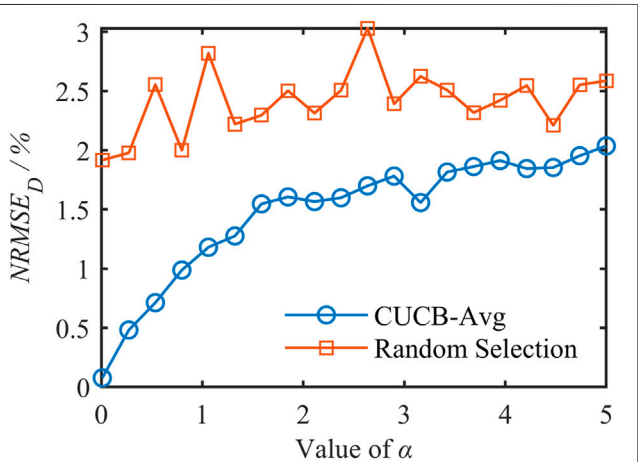

FIGURE 7 | $NRMSE_D$ of D = 1.2 MW.

focuses on the average p_{mean} of $\mathbb{P}$. For a given target D, calculate the number of users N_{RS} to be selected based on **Eq. 16**, and then send instructions randomly.

$$N_{RS} = D/p_{mean} \tag{16}$$

The relative relationship between the target D and the number of residents n (or the maximum adjustable capacity Q) also affects the aggregation mismatch. To eliminate this effect and purely analyze the function of $\mathbb{P}$, we set D to be 0.8, 1.2, and 1.6 MW, respectively. $NRMSE_D$ is calculated based on CUCB-Avg and RS, as shown in **Figures 6–8**.

As can be seen from the three figures,

1) The curve obtained by CUCB-Avg is significantly lower than RS, achieving smaller $NRMSE_D$ and better performance.
2) The curve corresponding to CUCB-Avg rises significantly, consistent with **Theorem 1** and **Theorem 2**: a larger α will lead to a larger $f(\mathbb{P})$ and a worse aggregation accuracy. Especially

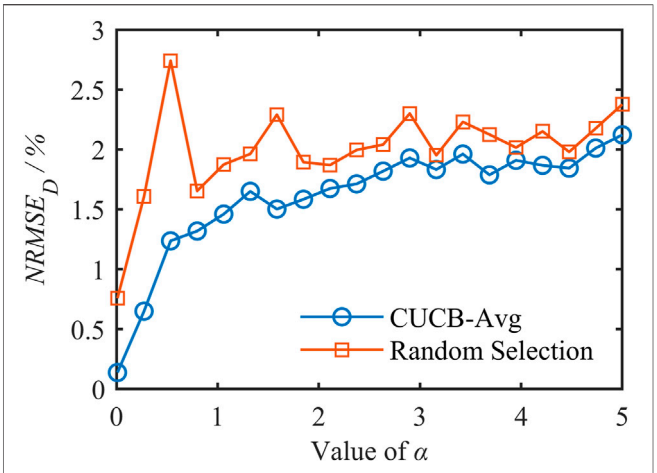

FIGURE 8 | $NRMSE_D$ of D = 1.6 MW.

when α is 0.01, the error achieved by CUCB-Avg is only 0.15%. Moreover, as α increases, the two curves gradually approach because the variance of the β distribution decreases, making all p_i close to μ, and S_t selected by the two methods are similar, resulting in an approximate aggregation effect.

3) The curve corresponding to RS fluctuates wildly, and there is no apparent upward trend when D is small. This does not mean that $\mathbb{P}$ does not affect the aggregation effect. It is because RS has been randomly selected without a strategy, and a different set of users is determined in each Monte Carlo simulation. When D = 1.6 MW is close to the maximum adjustable capacity $Q = 2.5np_{mean}$ kW = 1.75 MW, almost all users are selected to send instructions. Therefore, the effect of $\mathbb{P}$ on the aggregation effect is more prominent, showing a slight upward trend.
4) As D increases, the gap between the two curves gradually narrows. When D is small, only a part of users need to be selected to send instructions, and CUCB-Avg strategically determines S_t, so it has more obvious advantages than RS.

6 CONCLUSION

With the transition from modern power grids to low-carbon energy systems, residential load resources on the demand side play an increasingly important role. Aiming at the uncertainty of residents' response behavior in the LA scenario, this paper first models the problem. In order to facilitate the analysis of the response probabilities, the optimization objective is equivalently transformed from minimizing the mismatch between the actual load regulation amount and the target to minimizing the sum of variances of the overall response probabilities. Then a response probability generation model based on the β distribution is proposed, which can simulate a variety of typical distributions only by modifying two hyperparameters. Moreover, explore the connection between the β distribution and the sum of probabilities variances.

Furtherly, this paper adopts a CUCB-Avg algorithm whose performance is better than the conventional random method, which can be utilized to select appropriate users to send instructions in each event. Based on this, a framework for evaluating the effect of the sum of variances on the aggregation effect is designed. The simulation results show that the smaller the sum of variances for different probability distributions, the more accurate load aggregation can be achieved.

Residents' response probabilities can be improved through incentives. Future work will study incentives allocation strategies for limited costs to improve the probability distribution and further enhance the aggregation effect.

DATA AVAILABILITY STATEMENT

The raw data supporting the conclusions of this article will be made available by the authors, without undue reservation.

AUTHOR CONTRIBUTIONS

WZ: model construction and writing the manuscript. QH: CUCB-Avg algorithm and literature review. XY: literature review.

FUNDING

This research is supported by the National Natural Science Foundation of China (51907026), the Natural Science Foundation of Jiangsu Province (BK20190361), the Key Research and Development Program of Jiangsu Province (BE2020081-2).

REFERENCES

Auer, P., Cesa-Bianchi, N., and Fischer, P. (2002). Finite-time Analysis of the Multiarmed Bandit Problem. *Mach. Learn.* 47, 235–256. doi:10.1023/A:1013689704352

Baek, K., Lee, E., and Kim, J. (2021). Resident Behavior Detection Model for Environment Responsive Demand Response. *IEEE Trans. Smart Grid* 12, 3980–3989. doi:10.1109/TSG.2021.3074955

Burger, S., Chaves-Ávila, J. P., Batlle, C., and Pérez-Arriaga, I. J. (2017). A Review of the Value of Aggregators in Electricity Systems. *Renew. Sustain. Energy Rev.* 77, 395–405. doi:10.1016/j.rser.2017.04.014

Chen, W., Wang, Y., and Yuan, Y. (2013). "Combinatorial Multi-Armed Bandit: General Framework, Results and Applications," in Proceedings of the 30th International Conference on Machine Learning, Atlanta, GA, June 6–21, 2013, 151–159.

Chen, X., Hu, Q., Shi, Q., Quan, X., Wu, Z., and Li, F. (2020). Residential HVAC Aggregation Based on Risk-Averse Multi-Armed Bandit Learning for Secondary Frequency Regulation. *J. Mod. Power Syst. Clean. Energy* 8, 1160–1167. doi:10.35833/MPCE.2020.000573

Chen, X., Wang, J., Xie, J., Xu, S., Yu, K., and Gan, L. (2018). Demand Response Potential Evaluation for Residential Air Conditioning Loads. *IET Gener. Transm. & Distrib.* 12, 4260–4268. doi:10.1049/iet-gtd.2018.5299

Gong, X., Castillo-Guerra, E., Cardenas-Barrera, J. L., Cao, B., Saleh, S. A., and Chang, L. (2021). Robust Hierarchical Control Mechanism for Aggregated Thermostatically Controlled Loads. *IEEE Trans. Smart Grid* 12, 453–467. doi:10.1109/tsg.2020.3009989

Hao, H., Sanandaji, B. M., Poolla, K., and Vincent, T. L. (2015). Aggregate Flexibility of Thermostatically Controlled Loads. *IEEE Trans. Power Syst.* 30, 189–198. doi:10.1109/TPWRS.2014.2328865

Hu, Q., Ding, H., Chen, X., Chen, T., Ding, Y., and Li, Y. (2020). Analysis on Rotating Power Outage in California, USA in 2020 and its Enlightenment to Power Grid of China. *Autom. Electr. Power Syst.* 44, 11–18. doi:10.7500/AEPS20201016002

IRENA (2022). Renewable Capacity Statistics 2022. Available at: https://www.irena.org/publications/2022/Apr/Renewable-Capacity-Statistics-2022 (Accessed May 15, 2022).

Kou, X., Li, F., Dong, J., Olama, M., Starke, M., Chen, Y., et al. (2021). A Comprehensive Scheduling Framework Using SP-ADMM for Residential Demand Response with Weather and Consumer Uncertainties. *IEEE Trans. Power Syst.* 36, 3004–3016. doi:10.1109/TPWRS.2020.3029272

Li, L., Chu, W., Langford, J., and Schapire, R. E. (2010). "A Contextual-Bandit Approach to Personalized News Article Recommendation," in Proceedings of the 19th International Conference on World Wide Web (WWW 2010), Raleigh, NC, April 26–30, 2010, 661–670. doi:10.1145/1772690.1772758

Li, Y., Hu, Q., and Li, N. (2020). A Reliability-Aware Multi-Armed Bandit Approach to Learn and Select Users in Demand Response. *Automatica* 119, 109015. doi:10.1016/j.automatica.2020.109015

Li, Y., Yao, J., Yong, T., Ju, P., Yang, S., and Shi, X. (2017). Estimation Approach to Aggregated Power and Response Potential of Residential Thermostatically Controlled Loads. *Proc. CSEE* 37, 5519–5528. doi:10.13334/j.0258-8013.pcsee.161493

Luo, J., Zhao, S., Feng, Y., Liu, Z., Dong, W., and Yanhong, Y. (2020). Optimal Operation of Integrated Electricity-Gas System Considering Uncertainty of Integrated Demand Response. *Electr. POWER* 53, 119–126.

Mathieu, J. L., Vaya, M. G., and Andersson, G. (2013). "Uncertainty in the Flexibility of Aggregations of Demand Response Resources," in IECON 2013 - 39th Annual Conference of the IEEE Industrial Electronics Society, Vienna, Austria, 10-13 November 2013, 8052–8057. doi:10.1109/IECON.2013.6700479

Qi, N., Cheng, L., Xu, H., Wang, Z., and Zhou, X. (2020). Practical Demand Response Potential Evaluation of Air-Conditioning Loads for Aggregated Customers. *Energy Rep.* 6, 71–81. doi:10.1016/j.egyr.2020.12.019

Saleh, S. A., Pijnenburg, P., and Castillo-Guerra, E. (2017). Load Aggregation from Generation-Follows-Load to Load-Follows-Generation: Residential Loads. *IEEE Trans. Ind. Appl.* 53, 833–842. doi:10.1109/TIA.2016.2626261

Sun, H., Xu, T., Guo, Q., Li, Y., Lin, W., Yi, J., et al. (2019). Analysis on Blackout in Great Britain Power Grid on August 9th, 2019 and its Enlightenment to Power Grid in China. *Proc. CSEE* 39, 6183–6192. doi:10.13334/j.0258-8013.pcsee.191632

Sun, L., Gao, C., Tan, J., and Cui, G. (2017). Load Aggregation Technology and its Applications. *Autom. Electr. Power Syst.* 41, 159–167. doi:10.7500/AEPS20161023001

Sun, W., Liu, X., Xiang, W., and Li, H. (2020). User Preference Learning and Response Optimization Based on Bayesian Inference. *Autom. Electr. Power Syst.* 44, 92–100. doi:10.7500/AEPS20200310002

Syrri, A. L. A., and Mancarella, P. (2016). Reliability and Risk Assessment of Post-contingency Demand Response in Smart Distribution Networks. *Sustain. Energy, Grids Netw.* 7, 1–12. doi:10.1016/j.segan.2016.04.002

Zhou, X., Zhao, Q., Zhang, Y., and Sun, L. (2021). Integrated Energy Production Unit: An Innovative Concept and Design for Energy Transition toward Low-Carbon Development. *CSEE J. Power Energy Syst.* 7, 1133–1139. doi:10.17775/CSEEJPES.2021.05950

Conflict of Interest: XY was employed by the Company Taizhou Power Supply Company State Grid Jiangsu Electric Power Co., Ltd.

The remaining authors declare that the research was conducted in the absence of any commercial or financial relationships that could be construed as a potential conflict of interest.

Publisher's Note: All claims expressed in this article are solely those of the authors and do not necessarily represent those of their affiliated organizations, or those of the publisher, the editors and the reviewers. Any product that may be evaluated in this article, or claim that may be made by its manufacturer, is not guaranteed or endorsed by the publisher.

frontiers | Frontiers in Energy Research

TYPE Original Research
PUBLISHED 22 July 2022
DOI 10.3389/fenrg.2022.963177

OPEN ACCESS

EDITED BY
Yang Li,
Hohai University, China

REVIEWED BY
Farhad Shahnia,
Murdoch University, Australia
Zhengmao Li,
Nanyang Technological University, Singapore

*CORRESPONDENCE
Yidi Zhang,
irisyidiz@163.com

SPECIALTY SECTION
This article was submitted to Smart Grids,
a section of the journal
Frontiers in Energy Research

RECEIVED 07 June 2022
ACCEPTED 30 June 2022
PUBLISHED 22 July 2022

CITATION
Zhang Y, Deng H, Yang J, Xu C, Zhou Z, Wen F and Qi D (2022), Impacts of renewable portfolio standard on carbon emission peaking and tradable green certificate market: A system dynamics analysis method.
Front. Energy Res. 10:963177.
doi: 10.3389/fenrg.2022.963177

Impacts of renewable portfolio standard on carbon emission peaking and tradable green certificate market: A system dynamics analysis method

Yidi Zhang[1]*, Hui Deng[2,3], Jiajia Yang[1], Chengwei Xu[2,3], Ziqing Zhou[2,3], Fushuan Wen[4] and Donglian Qi[4]

[1]College of Electrical Engineering, Zhejiang University, Hangzhou, China, [2]State Grid Zhejiang Electric Power Co, Ltd. Research Institute, Hangzhou, China, [3]State Grid Zhejiang Electric Power Co, Ltd. Power Market Simulation Laboratory, Hangzhou, China, [4]Hainan Institute, Zhejiang University, Sanya, China

With the announcement of the carbon peaking and carbon neutrality target in China as well as the launch of the nationwide green power renewable generation trading, one of the key issues is how to design an effective renewable portfolio standard (RPS) and build an efficient tradable green certificate (TGC) market. The quota that stipulates the share of electricity supplied from qualified renewable energy (RE) sources has substantial impacts on the TGC market, the electricity market, and the occurred time of carbon emission peaking. However, few studies have been reported on effectively quantifying the impacts of quota variation. Given this background, this paper presents an innovative system dynamics (SD) model to evaluate the impacts of quota variation on the trading results of the TGC market and the trend of carbon emissions in China for the next decade. The proposed SD model takes factors such as the accommodating capability by the power system for RE generation, the policy-driven carbon emission reduction target as well as the decreasing fixed feed-in tariff (FIT) for RE generation as constraints for the first time. These factors are quantified in the constraints based on the current RE policies and market trading mechanism in China to improve the evaluation accuracy of the SD model. Using real-world data, simulations under various scenarios are carried out to validate the feasibility and efficiency of the proposed model. The methods for further improving the design of TGC market are also further explored, which are expected to effectively guide China to achieve the carbon peaking target.

KEYWORDS

carbon emission peaking, renewable energy generation, renewable portfolio standard, tradable green certificate, system dynamics

1 Introduction

Climate change is one of the major global challenges currently faced by most countries and governments in the world. In 2020, the Chinese government announced its carbon peaking and carbon neutrality target by the year 2030 and 2060 (the so-called "3,060" target) respectively to achieve a clean and low-carbon energy structure. One of the key measures to achieve the "3,060" target is the restructure of energy mix and the increase of the proportion of renewable energy (RE) generation. Therefore, RE will gradually become the main sources of power supply by replacing traditional fossil fuels. Moreover, the RE generation project in China has no longer been granted the feed-in tariff (FIT) from the central government since 2021 (Shayegh and Sanchez, 2021; Zhou and Solomon, 2021). A new series of policies related to the renewable portfolio standard (RPS) and tradable green certificate (TGC) will be developed for RE generators after ceasing the FIT scheme (Tu et al., 2020; Yang et al., 2021). However, the development of the TGC market and the electricity market is still in its infancy in China, and the RPS policy is still not well defined. The quota in the RPS policy stipulates the share of electricity supplied from qualified RE sources. In practice, the preset quotas in the RPS policy will affect the decision-making of participants in the electricity market and TGC market trading, and then impact the time of reaching carbon peaking in China (Tan et al., 2021). Therefore, setting an appropriate RPS quota and developing a TGC transaction mechanism by studying the dynamic development of RE will be of great significance for achieving the carbon emission target (Feng et al., 2021).

Currently, the TGC market in China is still in the cultivation period (Das et al., 2010; Kreikebaum et al., 2010). Aiming at establishing an effective TGC trading market, several regulations have been proposed by National Development and Reform Commission (NDRC) in China to improve the TGC market and RPS policy, as shown in Table 1. Although relevant policies have been put forward to clearly specify the responsible entities and quota implementation method under the RPS policy, these policies have not established a feasible TGC trading mechanism and an appropriate quota determination technique. Besides, considering China's RPS policy and TGC market are still in their infancy, the lack of effective quota determination methods will reduce the operation efficiency of the TGC market, thus impede the willingness of responsible entities to trade in the TGC market (Li et al., 2019; Feng et al., 2022). All those would bring extra uncertainty for achieving the carbon peaking target. According to the data from the China Green Certificates Subscription Platform, the cumulative TGC transaction volume of wind power and photovoltaic accounts for only 1.1245% and 10.9850% of the total issued volume. In addition, the highest prices of TGC for wind power and photovoltaic are 382.3 yuan/piece and 872.8 yuan/piece respectively, which are much higher than the international average prices. It can be seen that without an effective method for determining the consumption responsibility weights, the current TGC market is inactive with a high TGC price and fails to promote RE consumption in a market-oriented way. As a result, the quota needs to be appropriately determined and the trading mechanism of the TGC market under RPS policy should be optimized to effectively guide the TGC transaction and thus promote low-carbon development.

Meanwhile, existing research on the dynamic development of RE mainly focuses on the following aspects: 1) Investigating RE market systems that are appropriate for national conditions. After studying the incentive policies of RE in various countries, (Jiang et al., 2020), compares these mechanisms, and then puts forward the suggestion that China should promote the RPS in stages; Learning from the successful experience of the RPS policy in Texas, some policy recommendations for China are proposed in (Yang et al., 2011). 2) Studying the relationship between factors such as consumer costs of electricity and electricity price in the

TABLE 1 Issued policies in renewable energy in China.

Year	Authority	Released policy	Main contents	Policy limitations
2017	National Development and Reform Commission	The Rules of Green Electricity Certificate Issuance and Voluntary Subscription (Trial) (National Development and Reform Commission, 2017)	To establish an initial framework for TGC transactions	Lack of market liquidity and a mandatory mechanism
2019	National Development and Reform Commission	Notice on Establishing and Improving the Guarantee Mechanism of Renewable Energy Power Consumption (National Development a nd Reform Commission, 2019)	To build the guarantee mechanism for RPS	Lack of the bond between RPS policy and the TGC market
2020	National Development and Reform Commission	Opinions on Promoting the Healthy Development of Non-Water Renewable Energy Power Generation (National Development and Reform Commission, 2020)	To fully implement the TGC market based on RPS from 2021	Lack of effective quota determination methods
2021	Zhejiang Provincial Development and Reform Commission	Renewable Energy Power Consumption Guarantee Implementation Plan of Zhejiang Province (Trial) (Zhejiang Provincial Development and Reform Commission, 2021)	To define responsible entities and corresponding quota implementation methods	Lack of feasible TGC trading mechanism

electricity market under the RPS. By using the National Energy Modeling System (NEMS), the impact of enforced RPS regulations on the US energy market and the power industry is analyzed in (Kydes, 2007). Studies in (Unger and Ahlgren, 2005) show that the RPS would reduce the prices of wholesale electricity and CO2-emission permits by simulating the electricity markets of Nordic countries. 3) Solving the optimization problem of RPS policy making and trading portfolio: Based on the IOS New England test system, a tri-level optimization model including a state regulator, a power utility, and a wholesale electricity market is proposed in (Kim et al., 2021) and used to analyze the impact of the incentive intensity of the RPS on policy making; A decision-making optimization model of the medium-and long-term electricity market considering the risk cost of RE generation is established in (Feng, 2020), and the best purchase plan of electricity is obtained for organizers.

The development of RE is closely related to a variety of factors such as electricity demand, electricity price, and profit margins that generators can obtain in the electricity industry. Besides, these factors can be further affected by the government's energy policies. Therefore, the well-developed system dynamics (SD) model is applicable for the research. SD is a discipline that analyzes information feedback systems. It will dynamically simulate the changing process of each unit in the system according to the causal feedback of internal and external factors (Na ncy, 2012; Fetene Adane et al., 2019). Applications of the SD method in hydropower station dispatching, fossil fuel consumption, and other research directions are introduced in (Ebert, Freitag, Sperandio), showing the feasibility and diversity of this method in the electrical industry. However, there are few applications of this method in the field of energy at present. In (Koegelenberg and Pillay, 2015), the future power demand of the forestry and logging sector in South Africa is predicted by SD, and the impact of production lines and technical improvement on power demand is studied through sensitivity analysis. Ref. (Yang et al., 2006). employed the SD approach to model the evolution curve of variables in the California electricity market. Taking policies into account, the effects of different economic growth rates on carbon emissions and energy consumption in China are predicted based on SD in (Liu et al., 2015). The SD model of the electricity market and the TGC market are constructed in (Hasani-Marzooni and Hosseini, 2012) and applied to analyze the incentive effect on wind energy investment.

In general, the application of the SD method in existing research mainly focused on the evaluation and sensitivity analysis of RE proportion in the electricity market. However, the study of the TGC market under the RPS is still insufficient. First, the impact of the RPS policy on carbon emissions and the TGC market needs to be evaluated quantitatively. In existing research, the impact of green certificate quota on the dynamic evolution of TGC market and the electricity market has rarely been studied. Second, the constraints of the power systems in accommodating RE generation are not considered in the existing SD models, which may result in an overestimation of the generation capacity of RE. Third, the current policies in China are not studied sufficiently in existing publications, which makes it impossible to simulate the development of RE there accurately. To fill these knowledge gaps, the main significance and contributions of this paper are summarized as follows:

1) An elaborate curve of RPS quota value for the next decade and three policy recommendations are proposed, which can effectively help China construct the TGC market and achieve the carbon peaking targets.
2) A multi-agent SD model considering multiple types of complex factors is established to improve the assessment accuracy, based on the current RE policies and market trading mechanism in China. The formulated multi-agent SD model can evaluate the impact of quota variation on the trading result of the TGC market and the trend of carbon emissions in China comprehensively and concretely for the next decade.
3) Extensive numerical simulations using practical statistics of China are conducted to demonstrate the feasibility and efficiency of the proposed SD model and policy recommendations.

The rest of this paper is organized as follows: Section 2 constructs the causal loop and SD model to show the overall framework of TGC market and electricity market. Section 3 enumerates the precise data needed in the proposed model and discusses the simulation results of this study. Section 4 is the conclusion of the paper.

2 Model construction

Based on the current status of RPS policy and TGC market in China, the formulation of the quota is the key to the effective operation of the RPS policy and corresponding TGC market. Take the Zhejiang Province as an example, under the RPS policy, the government established a series of policies defining responsible entities that are obliged to have quota and corresponding quota implementation methods (Yang et al., 2006). Specifically, the responsible entities are divided into two types. The first type is electricity retailers that supply or sell electricity directly to power end-users. The second type is large scale power users that directly take part in the wholesale electricity market and enterprises with self-provided power plants (Fan et al., 2021; Xu et al., 2021). Each type of the responsible entities can fulfill their demand of RPS quota in three ways: 1) by purchasing or self-providing RE power directly; 2) by subscribing to TGC (a unit of TGC corresponding to 1 MWh of RE consumption); 3) by inter-provincial transaction of excess consumption.

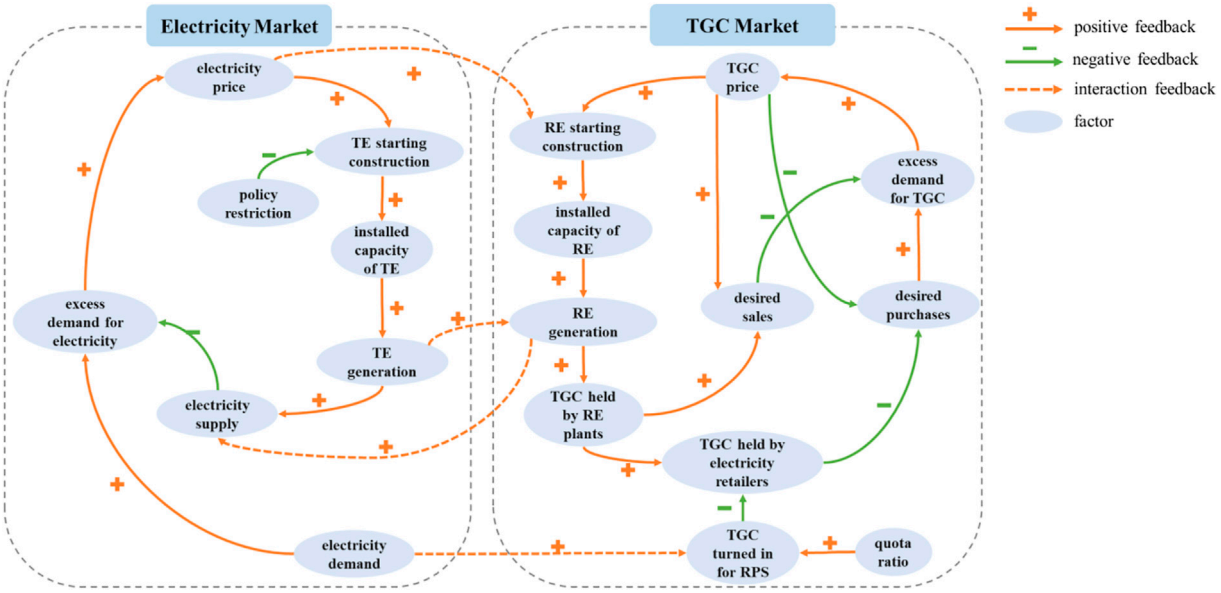

FIGURE 1
Illustration of the constructed causal loops.

As observed from the practice in the Zhejiang Province, the quota will have an impact on the trading behavior and clearing results of the responsible entities in the power and the TGC markets. The quantitative evaluation of impacts needs to be thoroughly analyzed so as to better determine the policy that improves the RPS policy. The TGC market and the electricity market are linked with each other by shared elements existing in both markets, including the electricity price and electricity demand. Therefore, in this section, an electricity and TGC market-coupled trading SD model is developed to simulate the interactions between electricity and TGC markets as well as the impacts of the RPS policy on market trading results and carbon emissions.

2.1 Assumptions

The following assumptions are made when developing the electricity and TGC markets-coupled trading SD model.

1) The subject restricted by the RPS policy in this paper is electricity retailers, which are obliged to purchase a certain percentage of electricity from RE generators.
2) One unit of TGC represents 1000 kWh of electricity generated by RE, and it is the same for all RE generation technologies.
3) Since the subsidized RE projects have already been rewarded for their environmental values by their FIT, the subsidized RE projects are not allowed to participate in the TGC transaction, but they still account for green energy generation.
4) Wind power and photovoltaic generation are selected as the representatives of RE generation technologies.

2.2 Causal loop

According to the analysis of the current RPS policy and TGC market in China as well as the assumptions in section 2.1, the causal loop model of the electricity and TGC market-coupled trading is shown in Figure 1. The causal loop model is a method to iconically describe the information feedback of internal and external factors, and the causal loop is widely adopted in the SD model to evaluate the trend of electricity market.

1)TGC Market

The TGC market is presented on the right side of Figure 1.

a) Loop-1 in the TGC market: RE generation →(+) TGC held by RE plants →(+) desired sales →(-) excess demand for TGC →(+) TGC price →(+) RE starting construction →(+) installed capacity of RE; TGC price →(+) desired sales

In the TGC market, the RPS policy encourages RE generators to compensate for the economic losses caused by FIT reduction via selling the TGC. Specifically, the TGC issued by the government will be sent to the RE generators based on their generating capacity. Then the RE generators will sell the TGC in the TGC market, and thus the TGC's sales volume will be increased. After that, the excess demand for TGC in the

market will decrease, which will have a negative effect on the TGC price based on the typical supply-demand relationship. Consequently, due to the decreased excess demand for TGC, the TGC price will be reduced and the profits that RE generators can obtain from selling TGC will be cut down. Since the investment willingness of RE generators is closely related to the profit margin that these generators can get in the TGC market, the investment of RE generators will be reduced. The above process will gradually reduce the number of newly installed RE generators.

b) Loop-2 in the TGC market: TGC held by RE plants →(+) TGC held by electricity retailers →(-) desired purchases →(+) excess demand for TGC→(+) TGC price →(+) RE starting construction →(+) installed capacity of RE →(+) RE generation; quota ratio →(+) TGC turned in for RPS →(-) TGC held by electricity retailers; TGC price →(-) desired purchases; electricity demand →(+) TGC turned in for RPS

The output of RE generators is positively correlated with the number of TGC available to electricity retailers. In the proposed SD model, the number of TGC owned by electricity retailers is defined as the difference between the number of TGC bought from RE generators and the number of TGC that is required to be submitted based on the predetermined quota. If the submitted TGC is decreased, the TGC owned by the electricity retailers will be lifted. Moreover, the increased TGC owned by electricity retailers will cut down their demand in the TGC market, which will further reduce the TGC price and finally cut down the number of newly installed RE generators.

2)Electricity Market

The electricity market is on the left side of Figure 1.

a) Loop-1 in the electricity market: electricity demand →(+) excess demand for electricity →(+) electricity price →(+) TE starting construction →(+) installed capacity of TE →(+) TE generation →(+) electricity supply →(-) excess demand for electricity

In the electricity market, the excess demand for electricity will be increased due to the economic development. The increase in excess demand for electricity will lead to rising electricity prices and the growth of profits for traditional energy (TE) generators, which will further result in an increase in installed generating capacity and total electricity generation. Finally, the increase in electricity supply will in turn cut down the electricity excess demand.

b) Loop-2 in the electricity market: policy restriction →(-) TE starting construction

For China, in order to achieve the target of carbon peaking in 2030, the growth rate of installed construction of TE generators will gradually slow down in the future, and its construction volume will be determined not only by the profit space of TE generators but also by the policy constraints. Considering the limitation of the carbon peaking target, the carbon emission constraint is added to the installed capacity of TE generators in the proposed SD model.

3)Interaction Between the Two Markets

The interaction between the two markets is highlighted by the dotted line in Figure 1.

Loops of interactions: TE generation →(+) RE generation; RE generation →(+) electricity supply; With the expanded integration scale of RE, the fluctuation and randomness of RE have a significant impact on the safe operation of power system. In this context, the fluctuation of renewable power supply will become the main source of system uncertainty. In practice, the power generation of RE will be constrained by power grid dispatching and planning (Al-Shetwi et al., 2020; Lei et al., 2020). Considering that the power system's capacity to consume RE is limited, the growth of RE generation will be constrained by the system's capability to consume RE. The above constraints are considered in the proposed model.

2.3 SD model of markets

According to the causal loop, the SD model of market-coupled trading can be obtained based on the operation characteristics of electricity market and TGC market, as shown in Figure 2. Factors in Figure 1 is subdivided into several detailed factors, and the corresponding relationship between the causal loop and SD model is shown in Table 2. The function and logical relationships between the subjects are also determined to illustrate the operation mechanism of the market-coupled trading model, as presented in sections 2.3.1, 2.3.2.

2.3.1 TGC market

1) TGC price constraints:

In the TGC market, the TGC price is affected by the excess demand for TGC and obtained from the incentive for TGC price through the smooth function. In detail, the excess demand for TGC is collectively determined by the desired purchases and the desired sales of TGC, which depend on the amount of TGC held by electricity retailers and RE plants respectively. According to Assumption 3, the electricity of subsidized RE generators can be converted into the corresponding quantity of TGC. The quantitative relationships between the mentioned variables are given by Eqs 1–3.

$$P_{inc}^{TGC}(t) = P_0^{TGC} + \int_0^t S_{exc}^{TGC}(t)dt \tag{1}$$

$$S_{exc}^{TGC}(t) = S_{pur}^{TGC}(t) - S_{sale}^{TGC}(t) \tag{2}$$

$$S_{e,real}^{TGC}(t) = S_e^{TGC}(t) + \frac{Q_0^{RE}}{1000} \tag{3}$$

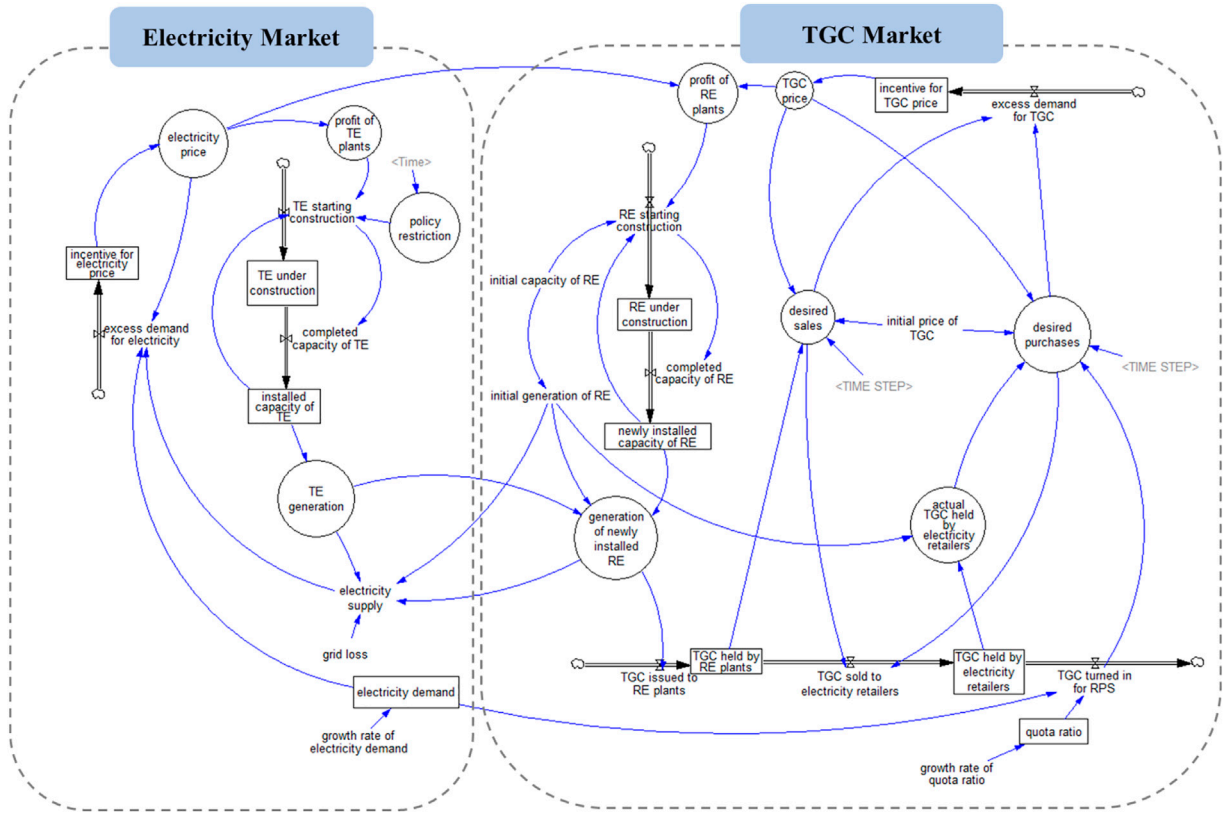

FIGURE 2
Illustration of the developed SD model.

TABLE 2 The corresponding relationship between the causal loop and SD model.

Factors in causal loop	Factors in SD model	Justification
RE generation	1. Initial generation of RE 2. Generation of newly installed RE	Due to FIT, the "initial generation of RE" is rewarded for their environmental values and not allowed to participate in the TGC transaction while the "generation of newly installed RE" is allowed
TGC held by electricity retailers	1. TGC held by electricity retailers 2. Actual TGC held by electricity retailers	The "initial generation of RE" still account for green energy generation. These projects and the "TGC held by electricity retailers" combine the "actual TGC held by electricity retailers"
Excess demand for electricity	1. Excess demand for electricity 2. Incentive for electricity price	The "excess demand for electricity" will have a time-delayed effect on the electricity price. Therefore, the "incentive for electricity price" is introduced
Excess demand for TGC	1. Excess demand for TGC 2. Incentive for TGC price	The "excess demand for TGC" will have a time-delayed effect on the TGC price. Therefore, the "incentive for TGC price" is introduced

where $P_{\text{inc}}^{TGC}(t)$ is the incentive for TGC price, P_0^{TGC} is the initial price of TGC, $S_{exc}^{TGC}(t)$ is the excess demand for TGC, $S_{pur}^{TGC}(t)$ is the desired purchases of TGC, $S_{sale}^{TGC}(t)$ is the desired sales of TGC. $S_{e,real}^{TGC}(t)$ is the actual amount of TGC held by electricity retailers, $S_e^{TGC}(t)$ is the amount of TGC held by electricity retailers.

2) Accommodating RE constraints:

The amount of completed installed capacity of RE is determined by the amount of RE capacity at the beginning of construction through the delay function. Due to the constraints on the ability of the system to integrate RE, the amount of newly

installed RE generation is restricted by the amount of TE generation. The specific equations are shown in Eqs 4–6.

$$K_{new}^{RE}(t) = K_0^{RE} + \int_0^t K_f^{RE}(t)dt \tag{4}$$

$$K_f^{RE}\left(t + T^{RE}\right) = K_s^{RE}(t) \tag{5}$$

$$Q_{new}^{RE}(t) = \begin{cases} Q^{TE}(t) \times \eta - Q_0^{RE}, \ if\ K_{new}^{RE}(t) \times \dfrac{h}{12} + Q_0^{RE} \geq Q^{TE}(t) \times \eta \\ K_{new}^{RE}(t) \times \dfrac{h}{12}, \ if\ K_{new}^{RE}(t) \times \dfrac{h}{12} + Q_0^{RE} \leq Q^{TE}(t) \times \eta \end{cases} \tag{6}$$

where $K_{new}^{RE}(t)$ is the amount of newly installed capacity of RE, K_0^{RE} is the initial value of the newly installed capacity of RE, $K_f^{RE}(t)$ is the amount of completed installed capacity of RE, $K_s^{RE}(t)$ is the amount of RE capacity at the beginning of construction. T^{RE} is the construction duration of RE generators. $Q_{new}^{RE}(t)$ is the amount of newly installed RE generation, Q_0^{RE} is the initial amount of RE generation, h is the annual utilization hours of RE, $Q^{TE}(t)$ is the amount of TE generation, η is the constraint parameter.

3) RPS quota constraints:

The quota of RPS is gradually increasing under the influence of the growth rate, and the growth speed is increasing by degrees. The calculation method is shown in Eq. 7.

$$R^{RPS}(t) = R_0^{RPS} + \int_0^t \left[r \times R^{RPS}(t-1)\right] \tag{7}$$

where $R^{RPS}(t)$ is RPS quota, R_0^{RPS} is the initial value of RPS quota, r is the growth rate of RPS quota.

2.3.2 Electricity market

1) Electricity price constraints:

As for the electricity market, the electricity price is affected by the excess demand for electricity and obtained from the incentive for electricity price through the smooth function, which is shown in Eqs 8, (9).

$$C_{inc}^{E}(t) = C_0^E + \int_0^t Q_{exc}^{E}(t)dt \tag{8}$$

$$Q_{exc}^{E}(t) = Q_{dem}^{E}(t) - Q_{\sup}^{E}(t) \tag{9}$$

where $C_{inc}^{E}(t)$ is the incentive for electricity price, C_0^E is the initial price of electricity, $Q_{exc}^{E}(t)$ is the excess demand for electricity. $Q_{dem}^{E}(t)$ is the demand for electricity, $Q_{\sup}^{E}(t)$ is the amount of electricity supply.

2) Relevant policy constraints:

The amount of completed installed capacity of TE is determined by the amount of TE capacity at the beginning of construction through the delay function. Moreover, in order to achieve the target of carbon peaking, policy will be proposed to constrain the construction of TE. The constraint of policy-driven carbon emission reduction target on the amount of TE capacity at the beginning of construction are shown in Eqs 10–13.

$$K^{TE}(t) = K_0^{TE} + \int_0^t K_f^{TE}(t)dt \tag{10}$$

$$K_f^{TE}\left(t + T^{TE}\right) = K_s^{TE}(t) \tag{11}$$

$$K^{car}(t) = e^{-0.06175t+17.125} \tag{12}$$

$$K_s^{TE}(t) = \min\left(m \times K^{TE}(t), K^{car}(t)\right) \tag{13}$$

where $K^{TE}(t)$ is the amount of installed capacity of TE, K_0^{TE} is initial value of the installed capacity of TE, $K_f^{TE}(t)$ is amount of completed installed capacity of TE. T^{TE} is the construction duration of TE generators. $K^{car}(t)$ is the policy restriction. $K_s^{TE}(t)$ is the amount of TE capacity at the beginning of construction. m is the profit of TE.

3 Numerical results and analysis

3.1 Data configuration

To enhance the accuracy and credibility of the simulation, the key parameters of the model are from the actual power system operation of Zhejiang Province in 2020, as shown in Table 3. Vensim PLE is used to simulate the SD model. Combined with the actual situation of Zhejiang Province, the simulation cycle is assumed from 2021 to 2030, and the step length is 1 month. The growth rate of electricity demand is estimated based on the average annual growth rate of Zhejiang Province. Meanwhile, the initial value of the RPS quota is determined as 20% based on the target of carbon peaking and the actual situations in Zhejiang Province.

3.2 Scenario settings

Determining the appropriate quota is the key to ensure that the TGC market comes into effect under the RPS policy. Furthermore, appropriate quotas will encourage an increase in non-fossil energy consumption (Xin-gang et al., 2020; Yu et al., 2021). In order to research the impact of different quotas on the TGC market and electricity market, three scenarios of high (0.008), medium (0.006), and low (0.004) growth rates are set to simulate the interaction mechanism and development tendency by the SD model. The specific curves of the RPS

TABLE 3 Specification of key parameters in the simulation.

Types	Parameters	Value
Constant	Growth rate of electricity demand (%)	4
	Network loss (%)	6.8
Initial value of variable	Price of green certificates (yuan/piece)	150
	Capacity of renewable energy (MW)	17,030
	Electricity demand (10^8*kWh)	4,830
	RPS quota (%)	20
	Incentive for electricity price (yuan/kWh)	0.4153
	Capacity of traditional energy (MW)	59,940
	Incentive for green certificates price (yuan/piece)	150

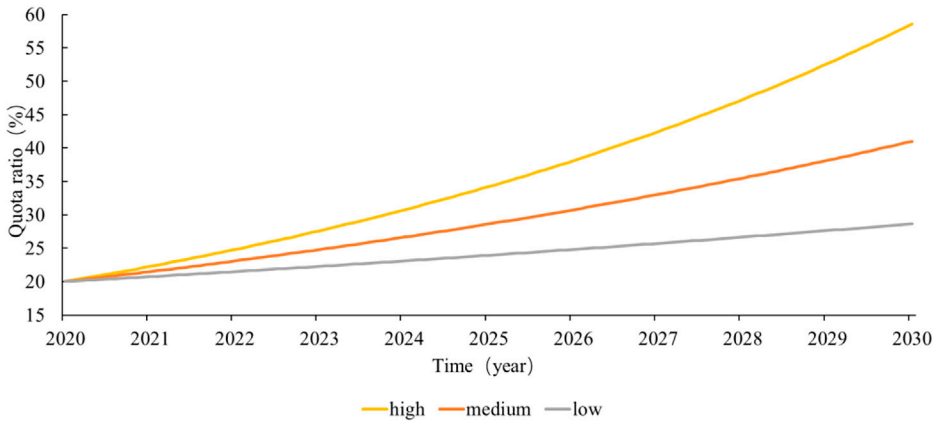

FIGURE 3
RPS quotas under three scenarios.

quota from 2020 to 2030 under three scenarios are shown in Figure 3. Three curves rise at different speeds and reach the highest points of 29%, 41%, and 59% by 2030 respectively.

3.3 Simulation results and analysis

3.3.1 The effectiveness of RPS

Through analyzing the variation trend of energy structure under three different quota curves given in Figure 3, it is found that the quota curve under the medium growth rate best meets the requirements of the energy development plan of Zhejiang Province in 2025 (Zhejiang Provincial Development and Reform Commission, 2021). As a result, the following study is conducted under the medium growth rate quota curve.

1) Impacts of RPS on the energy structure

By comparing the simulation results of energy structure change tendency under different scenarios, a series of RPS quotas of medium growth rate is proposed to meet the requirements of "The 14th Five-Year Plan for Renewable Energy Development in Zhejiang Province" (Zhejiang Provincial Development and Reform Commission, 2021). The growth tendency of the energy structure and power generation of RE and TE from 2021 to 2030 is shown in Figure 4.

Figure 4 shows that the capacity of TE and RE will reach 74.6942 and 34.3033 GW respectively in 2025, which approaches the estimated data of thermal power (74.62 GW) and the capacity of non-water RE (34.30 GW) based on the RE development plan of Zhejiang Province in 2025 (Zhejiang Provincial Development and Reform Commission, 2021). The installed capacity and the power generation of TE will be increased in 2021–2027. However, due to the restriction imposed by the RPS policy, the newly installed capacity of TE will be substantially reduced from 2027. As a result, the total capacity of TE is stable at 91 GW and the

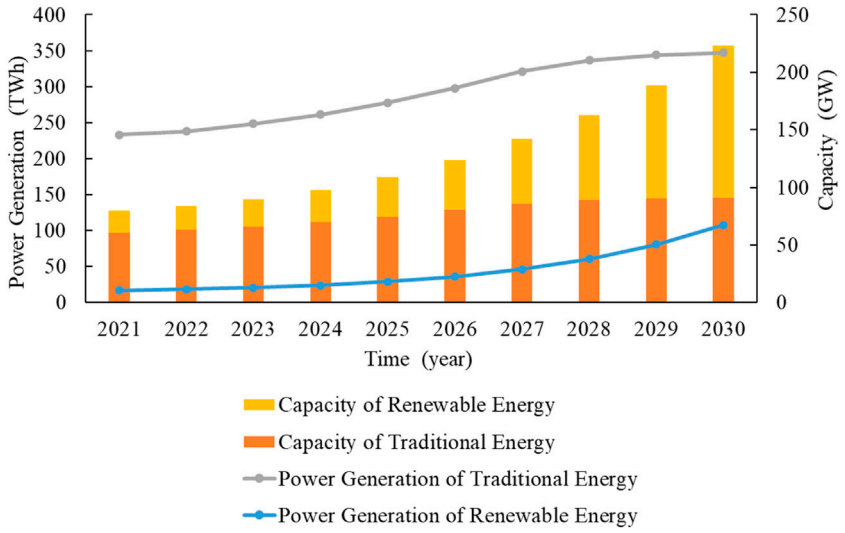

FIGURE 4
Energy structure and power generation.

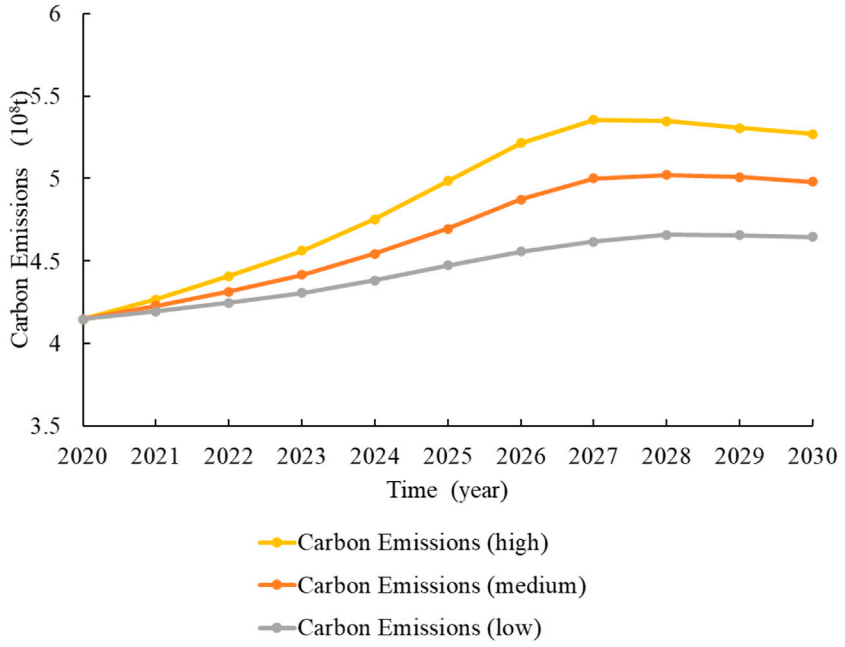

FIGURE 5
Carbon emissions under three scenarios.

annual TE power generation stabilizes at 347 TWh. Meanwhile, the installed capacity of RE is increasing annually, and by 2029 the installed capacity of RE will exceed that of TE. In 2030, the total installed capacity of RE reaches 132 GW and the annual RE power generation reaches 108 TWh. It can be concluded from Figure 4 that the TGC market and RPS policy will promote the optimization of energy structures in Zhejiang Province.

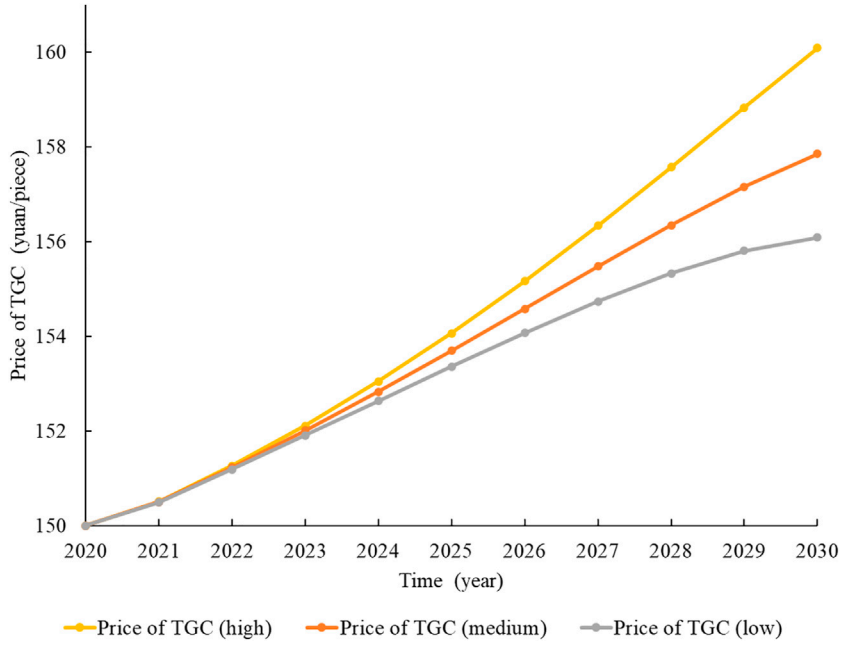

FIGURE 6
TGC prices under three scenarios.

2) Impacts of RPS on carbon emissions

The quota of RPS has an effect on the development of RE and further influences the volume of carbon emissions. In order to analyze the variation of carbon emissions under different growth rates and evaluate the time of carbon peaking, three different scenarios are simulated in this subsection.

According to the data of the China Electricity Council (CEC), in 2020, the amount of carbon dioxide emissions per unit of thermal generation is about 832 g/kWh. Meanwhile, the exploitation and development of RE is a replacement of TE, which brings a decline in carbon dioxide emissions. When the monthly carbon emission of traditional energy is greater than the monthly carbon emission reduction of renewable energy, the carbon emission of the power system is in a growth period, and the carbon dioxide emission gradually increases. The carbon peaking target of the power system will be achieved when the carbon emission of TE equals to the carbon emission reduction of RE. The trends of carbon emissions under different RPS quotas are shown in Figure 5.

In addition to the power generation, carbon emissions also come from steel, cement, chemical industry, crude oil refining and other sources. As a result, the carbon peaking time of the power system obtained from the simulation is earlier than 2030. As shown in Figure 5, the increased growth rate will enhance carbon emission reduction. In addition, it can be seen that the carbon peaking time under different scenarios varies from 2026 to 2028, and the high growth rate will help achieve the carbon peaking target in advance. Meanwhile, in the case of the medium growth rate, the time of carbon peaking is in the first quarter of 2027 when the volume of carbon emissions reaches $5.02*10^8$ t. Figure 5 indicates that the implementation of TGC and RPS could reduce carbon emissions and advance the time of carbon peaking.

3) Impacts of RPS on TGC prices

The tendencies of TGC prices under different scenarios are simulated through the SD model, as shown in Figure 6.

As can be seen from Figure 6, the TGC price keeps on rising from 2020 to 2030. In addition, there is a positive correlation between the quota growth rate and the growth rate of the TGC price. According to the price-demand relationship, an increase in TGC price will reduce the purchase demand of buyers, limiting the transaction scale of the TGC market. However, considering that the TGC market aims to stimulate the development of RE through market-oriented transactions rather than FIT, the limited transaction scale caused by the continuous rise of TGC prices will not be conducive to RE development (Zhao et al., 2019; Li et al., 2020). Considering the current situation in China, the TGC prices in China are much higher than the international average. In addition, for the responsible entities in Chinese enterprises, they still have insufficient understanding of the TGC market and are highly sensitive to the TGC price.

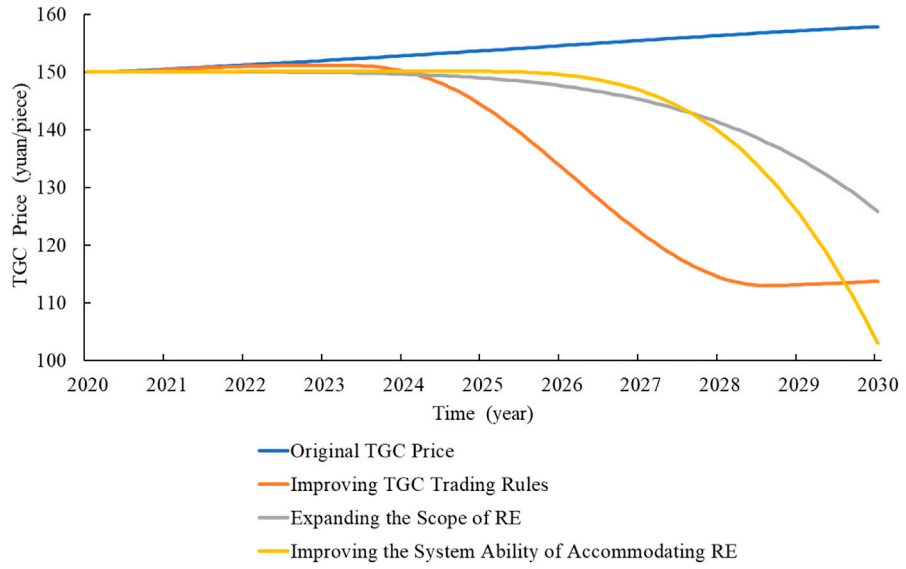

FIGURE 7
TGC prices under different scenarios.

Therefore, reducing the TGC price will promote the TGC trading and activate the TGC market in China, which will further help promote the development of China's RE industry.

3.3.2 Analysis of TGC market

To encourage the efficient use of RE, targeted improvements to the system of TGC transactions are proposed from three aspects (Heimvik and Amundsen, 2021). The TGC prices of the improved system and the original price are shown in Figure 7:

1) Improvement of TGC trading rules

By adjusting the relevant parameters in the process of TGC trading, the changing trend of the TGC price under the improvement of trading rules is simulated. Compared with the original TGC price, the TGC price under the trading rules maintains a similar growth trend during the initial years as shown in Figure 7. However, the price will start to decrease in 2024, and will reach 113 yuan/piece in 2028 and then remain stable. The TGC price reduction brought by the improved trading rules will increase the total TGC trading volume and enhance the transaction efficiency.

In this paper, the improvement of TGC trading rules is realized by the expansion of the desired sales and desired purchases. For the practical TGC market, several suggestions are given to increase the desired sales and desired purchases. Firstly, the secondary market for TGC should be established. According to the existing rules, TGC has no right to conduct a secondary sale after the transaction. Therefore, the secondary TGC market improves the currency of the TGC and reduces the TGC price in a market-oriented way. Besides, a more comprehensive information system should be added to the TGC markets. By displaying detailed transaction information such as TGC trading volume and clearing TGC price in the transaction system, the transparency of the TGC market can be improved. Furthermore, the government can simplify the application and issuance mechanisms of TGC to improve the transaction efficiency of the TGC market.

2) Expanding the scope of RE

As is shown in Figure 7, the TGC price, after expanding the scope of issuance, shows a downward trend annually. Specifically, from 2020 to 2025, the reduction of the TGC price is insignificant. After 2026, the decline of TGC price becomes more and more significant, and it will reach 126 yuan/piece (20% decrease) in 2030. Consequently, expanding the application scope of TGC and increasing the number of traded TGC in the TGC market will decline the TGC prices. Meanwhile, there are few types of RE applicable to TGC in China, including only onshore wind and centralized photovoltaic generation projects that are on the FIT list or sold at regulated prices. With the continuous development of RE, the application scope of TGC should be further expanded to allow more RE projects to participate in TGC trading.

3) Improvement of the system capability of accommodating RE

Since the output of RE has strong uncertainty, the increasing proportion of RE in the power system requires the cooperation of

flexible generators and the participation of demand response to realize the interaction of energy, information, and transaction on both supply and demand sides.

It can be seen from Figure 6 that improving the consumption capacity of the power system can reduce the TGC price. From 2020 to 2026, the prices increase slightly due to the delay effect of the implementation of new policies and engineering construction. From 2026 to 2030, the TGC prices will be significantly reduced due to the improvement in the consumption capacity of the system, and will drop to 103 yuan/piece in 2030. Therefore, in the face of a high RE proportion in the power system, it is necessary to improve the system's capability to consume RE and promote its development.

In the practical power system, the way to improve the system's capability in accommodating RE, such as transmission channel construction and auxiliary service device investment, will have a positive effect on the TGC market's development. However, considering both the cost of the above construction and the benefit brought by the TGC market, the reasonable improvement degree needs to be determined.

4 Conclusion

The implementation of the TGC market based on RPS policy has a significant impact on the development of RE and the achievement of the carbon peaking target. In this paper, a SD model considering multiple types of complex factors is established to construct a market-coupled trading system. Compared with existing algorithms and models, the proposed SD model is innovative by integrating constraints on the system RE integrating capability, the policy-driven carbon emission reduction target, as well as the decreasing fixed FIT for RE. These factors are quantified in the constraints based on the current RE policies and market trading mechanism in China to improve the evaluation accuracy of the SD model. Then, the tendencies of key elements and the volume of carbon emissions from 2021 to 2030 are simulated based on the actual statistics of China. The evolution processes of energy structure, carbon emission and the TGC price are simulated and analyzed under multiple scenarios. Finally, an elaborate curve of RPS quota value for the next decade and policy recommendations on the mechanism of TGC market are proposed from three aspects, which is a useful guideline for China to construct the TGC market and achieve the carbon peaking targets. Based on the proposed model and simulation results, there are still some problems that need to be studied in the future, which are listed as follows: 1) In order to simulate the changing trend of electricity prices more accurately, the electricity market could be further broken down into the spot market and the forward market in the electricity and TGC market-coupled trading SD model. 2) Considering the differences in construction cycles and costs between different types of RE technologies, the unit power generation of different types of RE technologies should be quantified into different numbers of TGCs.

Data availability statement

The original contributions presented in the study are included in the article/supplementary material, further inquiries can be directed to the corresponding author.

Author contributions

YZ, HD, and CX conceptualized the study. HD, JY, and CX performed the analysis. YZ, JY, CX, and DQ performed investigations. HD and ZZ acquired resources. HD, CX, and ZZ acquired funding. YZ wrote the original draft. JY, CX, and FW reviewed and edited the manuscript. All authors agreed to be accountable for the content of the work.

Funding

The authors declare that this study received funding from a Science and Technology Project of State Grid Zhejiang Electric Power Co., Ltd. (No. B311DS21000A). The funder had the following involvement in the study: HD and CX conceptualized the study and performed the analysis. CX performed investigations. HD and ZZ acquired resources. HD, CX, and ZZ acquired funding. CX reviewed and edited the manuscript.

Conflict of interest

Authors HD, CX, and ZZ are employed by State Grid Zhejiang Electric Power Co., Ltd., Research Institute and State Grid Zhejiang Electric Power Co., Ltd., Power Market Simulation Laboratory.

The remaining authors declare that the research was conducted in the absence of any commercial or financial relationships that could be construed as a potential conflict of interest.

Publisher's note

References

Al-Shetwi, A. Q., Hannan, M. A., Jern, K. P., Mansur, M., and Mahlia, T. M. I. (2020). Grid-connected renewable energy sources: Review of the recent integration requirements and control methods. *J. Clean. Prod.* 253, 119831. doi:10.1016/j.jclepro.2019.119831

Das, D., Kreikebaum, F., Divan, D., and Lambert, F. (2010). "Reducing transmission investment to meet renewable portfolio standards using Smart wires," in IEEE PES T&D 2010, New Orleans, LA, 1–7. doi:10.1109/TDC.2010.5484217

Ebert, P., Freitag, S., and Sperandio, M. (2017). "Applications of system dynamics in the electrical sector," in 2017 52nd international universities power engineering conference, Heraklion, Greece, 1–6. doi:10.1109/UPEC.2017.8231899

Fan, J.-L., Wang, J.-X., Hu, J.-W., Yang, Y., and Wang, Y. (2021). Will China achieve its renewable portfolio standard targets? an analysis from the perspective of supply and demand. *Renew. Sustain. Energy Rev.* 138, 110510. doi:10.1016/j.rser.2020.110510

Feng, C., Liang, B., Li, Z., Liu, W., and Wen, F. (2022). "Peer-to-Peer energy trading under network constraints based on generalized fast dual ascent," in IEEE trans. Smart grid, 1–12. doi:10.1109/tsg.2022.3162876

Feng, T.-t., Li, R., Zhang, H.-m., Gong, X.-l., and Yang, Y.-s. (2021). Induction mechanism and optimization of tradable green certificates and carbon emission trading acting on electricity market in China. *Resour. Conservation Recycl.* 169, 105487. doi:10.1016/j.resconrec.2021.105487

Feng, Y., Fan, J., Jiang, Y., Li, X., Li, T., Gao, C., et al. (2020). "Optimal trading strategy of inter-and intra-provincial medium-and long-term power exchange considering renewable portfolio standard." in 2020 12th IEEE PES Asia-Pacific Power and Energy Engineering Conference, Nanjing, China, 1–5. doi:10.1109/APPEEC48164.2020.9220555

Fetene Adane, T., Bianchi, M. F., Archenti, A., and Nicolescu, M. (2019). Application of system dynamics for analysis of performance of manufacturing systems. *J. Manuf. Syst.* 53, 212–233. doi:10.1016/j.jmsy.2019.10.004

Hasani-Marzooni, M., and Hosseini, S. H. (2012). Dynamic interactions of TGC and electricity markets to promote wind capacity investment. *IEEE Syst. J.* 6 (1), 46–57. doi:10.1109/jsyst.2011.2162891

Heimvik, A., and Amundsen, E. S. (2021). Prices vs. percentages: Use of tradable green certificates as an instrument of greenhouse gas mitigation. *Energy Econ.* 99, 105316. doi:10.1016/j.eneco.2021.105316

Jiang, Y., Cao, H., Yang, L., Fei, F., Li, J., and Lin, Z. (2020). Mechanism design and impact analysis of renewable portfolio standard. *Automation Electr. Power Syst.* 44 (07), 187–199. doi:10.7500/AEPS20190602001

Kim, J., Bialek, S., Unel, B., and Dvorkin, Y. (2021). Strategic policymaking for implementing renewable portfolio standards: a tri-level optimization approach. *IEEE Trans. Power Syst.* 36 (6), 4915–4927. doi:10.1109/tpwrs.2021.3078726

Koegelenberg, T., and Pillay, N. S. (2015). A system dynamics approach to simulating the electricity demand for the South African forestry & logging sector," in International Conference on the Industrial and Commercial Use of Energy (ICUE), Cape Town, South Africa, 84–88. doi:10.1109/ICUE.2015.7280251

Kreikebaum, F., Das, D., and Divan, D. (2010). "Reducing transmission investment to meet renewable portfolio standards using controlled energy flows," in *IEEE Innovative Smart grid technologies (ISGT)*, Gaithersburg, MD, 1–8. doi:10.1109/ISGT.2010.5434726

Kydes, A. S. (2007). Impacts of a renewable portfolio generation standard on US energy markets. *Energy Policy* 35 (2), 809–814. doi:10.1016/j.enpol.2006.03.002

Lei, G., Song, H., and Rodriguez, D. (2020). Power generation cost minimization of the grid-connected hybrid renewable energy system through optimal sizing using the modified seagull optimization technique. *Energy Rep.* 6, 3365–3376. doi:10.1016/j.egyr.2020.11.249

Li, X., Wang, W., Wang, H., Wu, J., Fan, X., Xu, Q., et al. (2020). Dynamic environmental economic dispatch of hybrid renewable energy systems based on tradable green certificates. *Energy* 193, 116699. doi:10.1016/j.energy.2019.116699

Li, Z., Wang, C., Ye, X., Li, Y., and Lei, X. (2019). "Evaluation of renewables portfolio standards trading volume and analysis of influencing factors," in *2019 Chinese automation congress (CAC)*, Hangzhou, China, 3897–3900. doi:10.1109/CAC48633.2019.8997379

Liu, X., Mao, G., Ren, J., Li, R. Y. M., Guo, J., and Zhang, L. (2015). How might china achieve its 2020 emissions target? a scenario analysis of energy consumption and CO_2 emissions using the system dynamics model. *J. Clean. Prod.* 103, 401–410. doi:10.1016/j.jclepro.2014.12.080

Nancy, G. L. (2012). "A brief introduction to system dynamics modeling," in *Engineering a safer world: Systems thinking applied to safety* (MIT Press), 517–519.

National Development and Reform Commission (2019). Notice on establishing and improving the guarantee mechanism of renewable energy power consumption. Available online at: http://zfxxgk.nea.gov.cn/auto87/201905/t20190515_3662.htm. (accessed on April 20, 2022).

National Development and Reform Commission (2020). *Opinions on promoting the healthy development of non-water renewable energy power generation*. Available online at: http://www.gov.cn/zhengce/zhengceku/2020-02/03/content_5474144.htm.(accessed on April 20, 2022).

National Development and Reform Commission (2017). *The Rules of green electricity certificate Issuance and voluntary subscription (trial)*. Policy. Available online at: http://www.nea.gov.cn/2017-02/06/c_136035626.htm.(accessed on April 20, 2022).

Shayegh, S., and Sanchez, D. L. (2021). Impact of market design on cost-effectiveness of renewable portfolio standards. *Renew. Sustain. Energy Rev.* 136, 110397. doi:10.1016/j.rser.2020.110397

Tan, Q., Ding, Y., Zheng, J., Dai, M., and Zhang, Y. (2021). The effects of carbon emissions trading and renewable portfolio standards on the integrated wind–photovoltaic–thermal power-dispatching system: real case studies in china. *Energy* 222, 119927. doi:10.1016/j.energy.2021.119927

Tu, Q., Mo, J., Betz, R., Cui, L., Fan, Y., Liu, Y., et al. (2020). Achieving grid parity of solar PV power in China- the role of tradable green certificate. *Energy Policy* 144, 111681. doi:10.1016/j.enpol.2020.111681

Unger, T., and Ahlgren, E. O. (2005). Impacts of a common green certificate market on electricity and CO_2-emission markets in the nordic countries. *Energy Policy* 33 (16), 2152–2163. doi:10.1016/j.enpol.2004.04.013

Xin-gang, Z., Pei-ling, L., and Ying, Z. (2020). Which policy can promote renewable energy to achieve grid parity? feed-in tariff vs. renewable portfolio standards. *Renew. Energy* 162, 322–333. doi:10.1016/j.renene.2020.08.058

Xu, J., Lv, T., Hou, X., Deng, X., and Liu, F. (2021). Provincial allocation of renewable portfolio standard in china based on efficiency and fairness principles. *Renew. Energy* 179, 1233–1245. doi:10.1016/j.renene.2021.07.101

Yang, D.-x., Jing, Y.-q., Wang, C., Nie, P.-y., and Sun, P. (2021). Analysis of renewable energy subsidy in china under uncertainty: feed-in tariff vs. renewable portfolio standard. *Energy Strategy Rev.* 34, 100628. doi:10.1016/j.esr.2021.100628

Yang, H., Wang, G., Zhou, L., and Zhou, R. (2006). "A study of power market dynamics based on system dynamics modeling." in *International conference on power system Technology*, Chongqing, China, 1–6. Available at: https://ieeexplore.ieee.org/document/4116273/. doi:10.1109/ICPST.2006.321448

Yang, J., Zheng, J., Wei, L., and Zhu, S. (2011). "The experience and revelation from renewable portfolio standard in texas for China," in 2011 International Conference on Electrical and Control Engineering, Yichang, China, 3236–3239. doi:10.1109/ICECENG.2011.6056816

Yu, B., Zhao, Z., Zhao, G., An, R., Sun, F., Li, R., et al. (2021). Provincial renewable energy dispatch optimization in line with Renewable portfolio standard policy in china. *Renew. Energy* 174, 236–252. doi:10.1016/j.renene.2021.04.055

Zhao, X.-g., Zhou, Y., Zuo, Y., Meng, J., and Zhang, Y.-z. (2019). Research on optimal benchmark price of tradable green certificate based on system dynamics: a china perspective. *J. Clean. Prod.* 230, 241–252. doi:10.1016/j.jclepro.2019.04.408

Zhejiang Provincial Development and Reform Commission (2021). *Renewable energy power consumption guarantee implementation Plan of Zhejiang Province (trial)*. Policy. Available online at: http://fzggw.zj.gov.cn/art/2021/8/11/art_1599567_58930212.html.(accessed on April 20, 2022).

Zhou, S., and Solomon, B. D. (2021). The interplay between renewable portfolio standards and voluntary green power markets in the united states. *Renew. Energy* 178, 720–729. doi:10.1016/j.renene.2021.06.110

frontiers | Frontiers in Energy Research

ORIGINAL RESEARCH
published: 25 July 2022
doi: 10.3389/fenrg.2022.963062

A Convex–Concave Procedure-Based Method for Optimal Power Flow of Offshore Wind Farms

Yuwei Chen[1,2], Hongke Li[1,2], Qing Chen[1,2], Rui Xie[1,2] and Xiaohe Wang[1,2]*

[1]*Key Laboratory of Far-shore Wind Power Technology of Zhejiang Province, Hangzhou, China,* [2]*PowerChina Huadong Engineering Corporation Limited, Hangzhou, China*

In recent years, offshore wind farms have boomed all over the world. It is essential to manage the energy dispatch of the offshore wind power systems to reduce transmission losses. This article proposes an optimization method for the optimal power flow of offshore wind power systems based on the convex–concave procedure. First, the nonlinear variables in the power flow constraints of the offshore wind power system are relaxed with newly defined variables. Second, the non-convex constraints are reconstructed according to the variables' characteristics so that the optimization method satisfies all constraints at the same time. Meanwhile, by applying the Taylor series expansion, the relaxation variables' gaps are changed dynamically, and the convex relaxation is tightened to ensure the effectiveness of the proposed method. Finally, the feasibility of the relaxation and the optimized solution is verified by the simulation to realize the power optimization in the real offshore wind system.

Keywords: offshore wind systems, optimal power flow, convex optimization, convex–concave procedure, quadratic relaxation

OPEN ACCESS

Edited by:
Zhiyi Li,
Zhejiang University, China

Reviewed by:
Zhengmao Li,
Nanyang Technological University, Singapore
Shiwei Xie,
Fuzhou University, China

****Correspondence:***
Yuwei Chen
chenyuwei@zju.edu.cn

Specialty section:
This article was submitted to Smart Grids, a section of the journal Frontiers in Energy Research

Received: *07 June 2022*
Accepted: *20 June 2022*
Published: *25 July 2022*

Citation:
Chen Y, Li H, Chen Q, Xie R and Wang X (2022) A Convex–Concave Procedure-Based Method for Optimal Power Flow of Offshore Wind Farms. Front. Energy Res. 10:963062. doi: 10.3389/fenrg.2022.963062

1 INTRODUCTION

With the steady progress of energy reforms around the world, the proportion of renewable energy sources, such as wind energy and solar energy, is increasing (Zhang et al., 2017). It is estimated that by 2035, the installed capacity of wind power will reach more than one billion kilowatts, of which the offshore wind power is about 350 million kilowatts. Wind power will become one of the main power sources affecting each country's energy structure and security. At the same time, considering the vigorous development trend of offshore oil and gas platforms, and their complex network format, it is very significant to carry out energy management for offshore wind power systems (Shafiee, 2015).

In energy management, how to reduce system losses is the top priority of optimization (Khan et al., 2016; Li Z. et al., 2020). The loss of offshore wind power is usually caused by line losses of the submarine transmission cable (Apostolaki-Iosifidou et al., 2019). Therefore, it is of great significance to propose an effective solution method to reduce the line losses on the basis of ensuring energy conservation and satisfying the corresponding physical relationship on the basis of how to carry out refined physical modelling for offshore wind power systems.

The offshore wind system is a typical nonlinear system. In the optimization of nonlinear systems, since the problem is non-convex and NP (HardKonar and Sidiropoulos, 2017), the commonly used solution methods are the linear programming method based on the approximate fitting (Bourguignon et al., 2015), gradient (Guirguis et al., 2016; Neftci et al., 2019) and Newton method-based algorithm (Li et al., 2020a), Lagrange multiplier method (Ruan et al., 2020; Xie et al., 2022),

interior point method (Fazlyab et al., 2017), and various heuristic and intelligent algorithms (Rokbani et al., 2021; Goli et al., 2021; Li et al., 2022). In these algorithms, the approximated method has high solving efficiency, but it will lead to some errors in the process of linearization, which affects the feasibility of the optimal solution. Gradient and Newton-based algorithms require a high-quality initial value in the iterative calculation and may fall into the ill condition. Lagrange multiplier and interior point method have certain requirements for the value of obstacle function. Therefore, it is difficult to solve the nonlinear and non-convex problem using the common analytical solution algorithm. When using the heuristic algorithm, it needs a lot of running time and storage space, and it is hard to find the global optimal solution.

In order to find the global optimal solution of the optimization problem, the convex optimization-based methods have gradually entered the field of power system management. This is because if an optimization problem can be written in a standard convex optimization format, the local optimal solution is the global one. In addition, convex optimization can be solved efficiently by many analytical methods (Boyd et al., 2004). Therefore, to apply the convex optimization technique into non-convex and nonlinear problems, some relaxation methods should be imposed to reshape the non-convex solution domain.

According to the mathematical expression form of the relaxation, the convex relaxation methods can be roughly divided into second-order cone relaxations (Abdelouadoud et al., 2015), semi-definite relaxations (Jubril et al., 2014), convex hull relaxations (Li Q et al., 2018), and quadratic relaxations (Hijazi et al., 2017). Among these methods, the method proposed by Li Y et al. (2018) showed that the second-order cone relaxation method is suitable for the network with a radial topology, of which the recovery of the angle information is conditional. Ma et al. (2020) pointed out that semi-definite programming cannot obtain the feasible optimal solution in a special three-node network. Cremers and Kolev (2010) pointed out that the constructions of convex hulls lead to different relaxed regions in the solution domain. Chen et al. (2021) proposed a quadratic relaxation with certain constraints on the angle difference in the network, which can only be applied to the special meshed topology. Therefore, the above methods have some limitations in the application of power optimization, and it is difficult to ensure the accuracy of relaxation.

In the current research on the energy optimization of offshore wind farms, few methods use convex relaxations. The convex relaxation-based methods will enlarge the solution domain through the variable replacement, which may cause the loss of information. Therefore, it is challenging to recover the complete system information after relaxations, and the feasible optimal solution cannot be obtained unless the conditions of exact relaxations are met. The change of topology and system parameters will result in inexact relaxations. So the generality and flexibility of the convex relaxation-based method is poor.

In summary, how to use the convex relaxation method to realize the accurate relaxation is of great significance. To fill the research gap of the above literature, this article proposes a convex–concave procedure-based method for the energy optimization of offshore wind power systems. This method mainly focuses on the problem of wind turbines' output and the energy distribution in the offshore wind power system. This method inherits the advantages of traditional convex optimization methods, which can be efficiently solved with the global optimal solution. In this method, the optimization problem of the offshore wind power system is first modelled mathematically, and the second-order cone relaxation method is used to deal with the non-convex constraints in the optimization. Then, in order to reduce the relaxation gap, a Taylor series expansion-based technique is imposed to contract the relaxation region; that is, the iterative process is imposed with the convex–concave procedure so that the solution domain is close to the one before relaxation. Thus, the efficient energy management of offshore wind power systems can be achieved, and the energy management problem of the offshore wind power system can be solved while maximizing the economic benefits of the system.

2 OPTIMIZATION MODEL

Figure 1 is a schematic diagram of offshore wind power systems. Among them, the wind power system is usually composed of offshore wind farms and electrical collector systems, which interconnects multiple wind farms. In order to transfer the power of the offshore wind power system to the power grid side, the substation is required.

The research of this article focuses on the offshore wind power system, that is, the energy management of the offshore wind farms and collector line systems. The offshore wind power system is a typical nonlinear system, of which the mathematical model is non-convex. It is composed of the objective function, equality constraints, and inequality constraints. The aim of the optimization is to maximize the transmitted power to the grid. The constraints are about the power flow, energy, voltage, load,

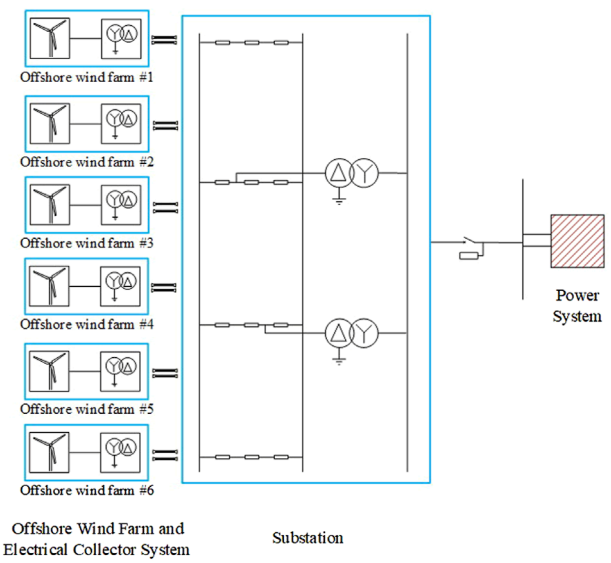

FIGURE 1 | Schematic diagram of offshore wind power systems.

and generators' constraints. In addition, the topology of the system should be considered as well.

In the optimization model of the offshore wind system, define the voltage variable of each node i with the complex variable $U_i = V_i \angle \theta_i$. The generated active and reactive power of node i is P_i^g and Q_i^g. The active and reactive consumption power of node i is P_i^c and Q_i^c. For branch i~j, the current variable is I_{ij}, the admittance is Y_{ij}, the conductance is G_{ij}, and the susceptance is B_{ij}. The transmitted apparent power, active power, and reactive power of the branch i~j are denoted as S_{ij}, P_{ij}, and Q_{ij}, respectively.

2.1 Objective Function

The objective function of the offshore wind farm is to maximize the on-grid electricity, that is, to minimize the transmission loss of the system. The mathematical expression of the power loss is

$$f = \sum P_i^g - \sum P_i^c. \tag{1}$$

P_i^g and P_i^c are the generated power and consumption power of node i, respectively.

2.2 System Constraints

Based on the operating conditions and physical relationships of the offshore wind power system, the constraints are established as follows:

1) The relationship between the transmitted power and current with the node's voltage is

$$S_{ij} = U_i I_{ij}^*. \tag{2}$$

In the abovementioned equation, * is the conjugate operator. Variables S_{ij}, U_i, and I_{ij} are complex variables.

2) The relationship between node's voltage and branch current:

$$I_{ij} = \left(U_i - U_j\right) Y_{ij}. \tag{3}$$

where Y_{ij} is the complex variable.

3) Power balance law of active and reactive power:

$$P_i = \sum P_{ij} = \sum P_i^g - P_i^c. \tag{4}$$

$$Q_i = \sum Q_{ij} = \sum Q_i^g - Q_i^c. \tag{5}$$

Superscripts g and c denote the generator nodes and load nodes, respectively. In the offshore wind farm system, a majority of the nodes are generator nodes.

4) Voltage ranges

$$V_i^{\min} \le V_i \le V_i^{\max}. \tag{6}$$

$$\theta_i^{\min} \le \theta_i \le \theta_i^{\max}. \tag{7}$$

5) Power ranges

$$P_i^{c\min} \le P_i^c \le P_i^{c\max}. \tag{8}$$

$$Q_i^{c\min} \le Q_i^c \le Q_i^{c\max}. \tag{9}$$

$$P_i^{g\min} \le P_i^g \le P_i^{g\max}. \tag{10}$$

$$Q_i^{g\min} \le Q_i^g \le Q_i^{g\max}. \tag{11}$$

Superscripts min and max are the lower and upper bounds, which are constants. For the active power and reactive power of node i, the limited bounds are defined according to the operating constraints of the equipment. The active power and reactive power in the abovementioned formula are real variables.

6) Branch constraints:

$$P_{ij}^{\min} \le P_{ij} \le P_{ij}^{\max}. \tag{12}$$

$$Q_{ij}^{\min} \le Q_{ij} \le Q_{ij}^{\max}. \tag{13}$$

For the active power and reactive power of the transmission line, according to the operating constraints of lines, the bounds are limited.

2.3 Optimization Model

Based on the objective function and constraints modelled earlier, the optimization model can be summarized as

$$\begin{aligned} &\min \quad (1) \\ &\text{s.t.} \quad (2) - (13). \end{aligned} \tag{14}$$

In this optimization problem, because of the constraints in **Eqs 2**, **3**, it is a non-convex, nonlinear, and NP-hard problem.

By adjusting the active and reactive power output of the offshore wind power system, it can provide reactive power support for the offshore collector systems. Thus, the power loss and the reactive power configuration of the substations can be reduced. In view of this, the article proposes a convex relaxation method to optimize the offshore wind power system efficiently.

3 CONVEX RELAXATION-BASED METHOD FOR OFFSHORE WIND SYSTEMS

3.1 Slack Variables' Definition

Six real variables are defined as follows:

$$a_i = V_i^2 \cos \theta_i^2, \tag{15}$$

$$b_i = V_i^2 \sin \theta_i^2, \tag{16}$$

$$a_{ij} = V_i \cos \theta_i V_j \cos \theta_j, \tag{17}$$

$$b_{ij} = V_i \sin\theta_i V_j \sin\theta_j, \tag{18}$$

$$s_{ji} = V_j cos\theta_j V_i \sin\theta_i, \tag{19}$$

$$s_{ij} = V_i \cos\theta_i V_j \sin\theta_j. \tag{20}$$

By substituting **Eq. 3** into **Eq. 2**, we can get the branch power flow of active power and reactive power as

$$P_{ij} = \Re\left(V_i V_i^* Y_{ij}^*\right) - \Re\left(V_i V_j^* Y_{ij}^*\right), \tag{21}$$

$$Q_{ij} = \Im\left(V_i V_i^* Y_{ij}^*\right) - \Im\left(V_i V_j^* Y_{ij}^*\right), \tag{22}$$

where $\Re$ and $\Im$ represent the real and imaginary parts of the complex variables, respectively. By replacing the voltage-related variables with the newly defined variables, the branch power flow of each transmission line from the two directions will become

$$P_{ij} = -\left(a_{ij} + b_{ij}\right) G_{ij} + B_{ij}\left(s_{ji} - s_{ij}\right) + G_{ij}\left(a_i + b_i\right) \tag{23}$$

$$P_{ji} = -\left(a_{ij} + b_{ij}\right) G_{ij} - B_{ij}\left(s_{ji} - s_{ij}\right) + G_{ij}\left(a_j + b_j\right) \tag{24}$$

$$Q_{ij} = -\left(a_{ij} + b_{ij}\right) B_{ij} - G_{ij}\left(s_{ji} - s_{ij}\right) + B_{ij}\left(a_i + b_i\right) \tag{25}$$

$$Q_{ji} = -\left(a_{ij} + b_{ij}\right) B_{ij} + G_{ij}\left(s_{ji} - s_{ij}\right) + B_{ij}\left(a_j + b_j\right) \tag{26}$$

Since we have the voltage constraints in **Eq. 6** and **Eq. 7**, the newly defined six variables have the corresponding ranges as well.

$$\left(V_i^{\min}\right)^2 \le a_i + b_i \le \left(V_i^{\max}\right)^2 \tag{27}$$

$$\min\left\{V_i V_j cos\left(\theta_{ij}\right)\right\} \le a_{ij} + b_{ij} \le \max\left\{V_i V_j cos\left(\theta_{ij}\right)\right\}, \tag{28}$$

$$\min\left\{sin\left(\theta_{ij}\right)\right\} \le s_{ji} - s_{ij} \le \max\left\{sin\left(\theta_{ij}\right)\right\}, \tag{29}$$

where $\theta_{ij} \in [\theta_{ij}^{\min}, \theta_{ij}^{\max}]$. The limits of θ_{ij} can be obtained from the ranges of θ_i and θ_j. Therefore, $\min\{cos(\theta_{ij})\}$, $\max\{cos(\theta_{ij})\}$, $\min\{sin(\theta_{ij})\}$, and $\max\{sin(\theta_{ij})\}$ are known in advance according to the relationship of trigonometric functions. The six variables defined in **Eqs 15–20** have the following four series of equality constraints.

$$s_{ij}^2 = a_i b_j \tag{30}$$

$$s_{ji}^2 = a_j b_i \tag{31}$$

$$a_{ij}^2 = a_i a_j \tag{32}$$

$$b_{ij}^2 = b_i b_j \tag{33}$$

With the slack variables added, the optimization problem in **Eq. 14** can be rewritten as

$$\begin{aligned} &\min \quad (1) \\ &\text{s.t.} \quad (4)-(5), (8)-(13), (23)-(33). \end{aligned} \tag{34}$$

The non-convexity of **Eq. 34** comes from the constraints of **Eqs 30–33**, which are in standard quadratic formats. To deal with this non-convexity, the convex–concave procedure is imposed in the next subsection.

3.2 Convex–Concave Procedure

For the constraints in **Eqs 30–33**, we can reconstruct them with the two groups of inequality constraints as

$$\frac{\left(a_i + a_j\right)^2}{4} - \left[a_{ij}^2 + \frac{\left(a_i - a_j\right)^2}{4}\right] \le 0, \tag{35}$$

$$\frac{\left(b_i + b_j\right)^2}{4} - \left[b_{ij}^2 + \frac{\left(b_i - b_j\right)^2}{4}\right] \le 0, \tag{36}$$

$$\frac{\left(a_i + b_j\right)^2}{4} - \left[s_{ij}^2 + \frac{\left(a_i - b_j\right)^2}{4}\right] \le 0, \tag{37}$$

$$\frac{\left(a_i + b_j\right)^2}{4} - \left[s_{ji}^2 + \frac{\left(a_j - b_i\right)^2}{4}\right] \le 0, \tag{38}$$

$$\frac{\left(a_i + a_j\right)^2}{4} - \left[a_{ij}^2 + \frac{\left(a_i - a_j\right)^2}{4}\right] \ge 0, \tag{39}$$

$$\frac{\left(b_i + b_j\right)^2}{4} - \left[b_{ij}^2 + \frac{\left(b_i - b_j\right)^2}{4}\right] \ge 0, \tag{40}$$

$$\frac{\left(a_i + b_j\right)^2}{4} - \left[s_{ij}^2 + \frac{\left(a_i - b_j\right)^2}{4}\right] \ge 0, \tag{41}$$

$$\frac{\left(a_i + b_j\right)^2}{4} - \left[s_{ji}^2 + \frac{\left(a_j - b_i\right)^2}{4}\right] \ge 0. \tag{42}$$

It can be found that the constraints in **Eqs 39–42** are second-order cone relaxations, which are convex, and the convex optimization problem is defined as

$$\begin{aligned} &\min \quad (1) \\ &\text{s.t.} \quad (4)-(5), (8)-(13), (23)-(29), (39)-(42). \end{aligned} \tag{43}$$

Set the convex solution domain of convex optimization **Eq. 43** with the convex set Ω. In addition, all the variables in **Eq. 43** are defined with the convex set X. Then **Eq. 34** can be equivalently written as

$$\begin{aligned} &\min f_0(X), \\ &\text{s.t.} \quad f_k(X) - g_k(X) \le 0. \quad X \in \Omega. \end{aligned} \tag{44}$$

In **Eq. 44**, $f_k(X)$ refers to the first term in **Eqs 35–38**, and $g_k(X)$ refers to the second term in **Eqs 35–38**. It can be found that both $f_k(X)$ and $g_k(X)$ are convex functions.

Due to the policy of first-order Taylor expansion series at $X(t)$, where t is the index number of the iteration times, $g_k(X)$ in **Eqs 35–38** can be linearized as

$$g_k(X;X^{(t)})^{(a)'} = a_{ij}^2 + \frac{\left(a_i - a_j\right)^2}{4} \overset{\Delta}{=} a_{ij}^{2(t)} + 2a_{ij}^{(t)}\left(a_{ij} - a_{ij}^{(t)}\right) + \frac{\left(a_i^{(t)} - a_j^{(t)}\right)^2}{4} + \frac{a_i^{(t)} - a_j^{(t)}}{2} \times \left(a_i - a_i^{(t)} - a_j + a_j^{(t)}\right) \quad (45)$$

$$g_k(X;X^{(t)})^{(b)'} = b_{ij}^2 + \frac{\left(b_i - b_j\right)^2}{4} \overset{\Delta}{=} b_{ij}^{2(t)} + 2b_{ij}^{(t)}\left(s_{ij} - b_{ij}^{(t)}\right) + \frac{\left(b_i^{(t)} - b_j^{(t)}\right)^2}{4} + \frac{b_i^{(t)} - b_j^{(t)}}{2} \times \left(b_i - b_i^{(t)} - b_j + b_j^{(t)}\right) \quad (46)$$

$$g_k(X;X^{(t)})^{(c)'} = s_{ij}^2 + \frac{\left(a_i - b_j\right)^2}{4} \overset{\Delta}{=} s_{ij}^{2(t)} + 2s_{ij}^{(t)}\left(s_{ij} - s_{ij}^{(t)}\right) + \frac{\left(a_i^{(t)} - b_j^{(t)}\right)^2}{4} + \frac{a_i^{(t)} - b_j^{(t)}}{2} \times \left(a_i - a_i^{(t)} - b_j + b_j^{(t)}\right) \quad (47)$$

$$g_k(X;X^{(t)})^{(d)'} = s_{ji}^2 + \frac{\left(a_j - b_i\right)^2}{4} \overset{\Delta}{=} s_{ji}^{2(t)} + 2s_{ji}^{(t)}\left(s_{ji} - s_{ji}^{(t)}\right) + \frac{\left(a_j^{(t)} - b_i^{(t)}\right)^2}{4} + \frac{a_j^{(t)} - b_i^{(t)}}{2} \times \left(a_j - a_j^{(t)} - b_i + b_i^{(t)}\right). \quad (48)$$

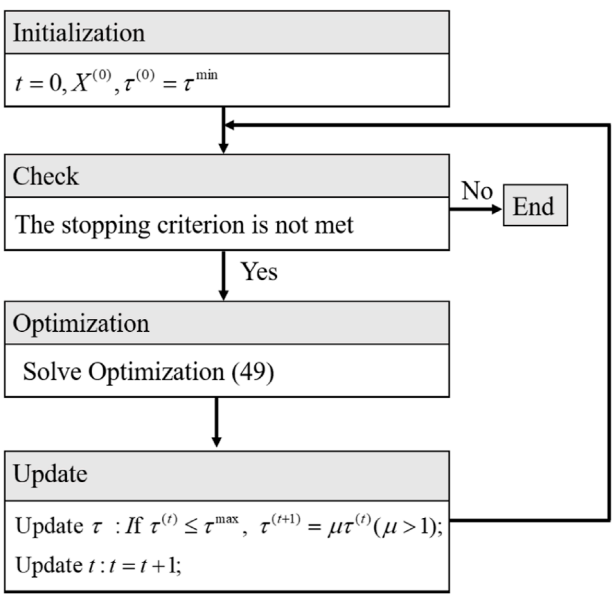

FIGURE 2 | Solving process of the proposed method.

To drive the Taylor expansion series be exactly equal to the equality before the expansion, the penalty term is involved. $R(X) = \tau^{(t)}\sum_{k=1}^{w} d_k$ is defined, where w is the total number of constraints (35)–(38) in the system, and $\tau^{(t)}$ indicates the penalty factor in the tth iteration whose limit is from $\tau^{\min}$ to $\tau^{\max}$. d_k is an introduced non-negative variable, which is intended to be the slack variable for constraints in **Eqs 35–38**. Considering the sum of d_k is $\sum_{k=1}^{w} d_k^{(t+1)}$, which is expected to be around zero, the solution obtained from **Eq. 44** will be exactly the one from **Eq. 34**. Therefore, the penalty term is added into the objective function to drive d_k to be zero.

With $R(X)$ as penalty terms in the objective function, the objective function differences between the tth and the $t+1$-th iteration with $R(X)^{(t)} - R(X)^{(t+1)}$ are recorded. Substituting $g_k(X;X^{(t)})'$ to replace $g_k(X)$, optimization **Eq. 44** will be

$$\begin{aligned} &\min f_0(X) + \tau\sum_{k=1}^{w} d_k, \\ &\text{s.t.} \quad f_k(X) - g_k(X;X^{(t)})' \le d_k, \quad X \in \Omega \\ &\quad d_k \ge 0. \quad k = 1,2\ldots,w \end{aligned} \quad (49)$$

Since the convex–concave procedure method is an iterative algorithm, the stopping criterion will be no more the improvement of the objective function or $\sum_{k=1}^{w} d_k^{(t+1)}$, which tends to be zero. Moreover, τ is set with limited constant τ^{max}, and a step length of 1.5 is set for τ in the iteration. Thus, the algorithm allows a low penalty on violations which in turn permits an enlarged solution region with a lower objective value. Consider a very small positive $\delta \approx 0$ as the stopping signal. Therefore, the total stopping criterion of the convex–concave procedure method will be all of the inequalities. Thus, $\sum_{k=1}^{w} d_k^{(t+1)} > \delta, \tau^{(t)} < \tau^{\max}$ and $|R(X)^{(t)} - R(X)^{(t+1)}| > \delta$ are violated. The whole solving process is shown in **Figure 2**.

Thus, with the convex–concave procedure applied, the non-convex offshore wind system's optimization problem in **Eq. 14** is transferred to **Eq. 49**. In each iteration, the convex optimization is solved efficiently and the sum of gaps is considered. Thus, when the iteration is stopped, the total violations are punished and the relaxation gap will closely be zero. In summary, both the solving efficiency and the optimization precision can be guaranteed.

4 CASE STUDY

In this article, a real offshore wind farm in China is used as the testing system. The system consists of 91 wind turbines in 14 loops. The topology is shown in **Figure 3**.

In this system, the length of the submarine cable between most of the circuit is 735 m. In the circuit between No. 77 and No. 83 wind turbines and the circuit between No. 84 and No. 90 wind turbines, the length of the submarine cable is 1715 m. The selection of submarine cables between the wind turbines is decided according to the multiple factors such as the line's current carrying capacity, thermal stability, and voltage drop. The length of the high-voltage submarine cable between the wind turbine and the offshore substation is shown in **Table 1**.

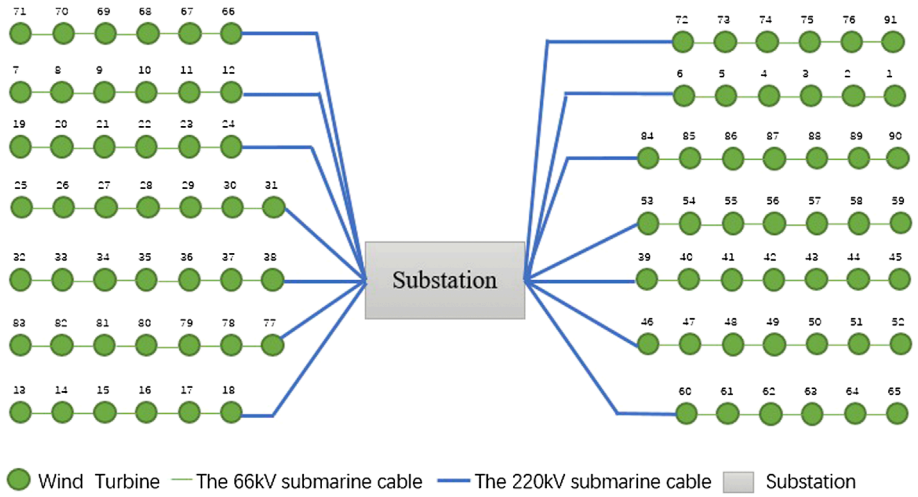

FIGURE 3 | Topology of the offshore wind farm system.

The relaxation model established above is built and written into Matlab through the Yalmip (Lofberg, 2004) toolbox, and solved by the IBM commercial solver CPLEX (Shinano and Fujie, 2007). The CPLEX is called to solve the convex optimization in the iterative process. In this case, the active power, reactive power, node voltage of each wind turbine node, and current and power on the lines between wind turbines are the variables to be optimized. At the same time, the upper and lower limits of the active power and reactive power of the wind turbine node, the upper and lower limits of the nodes' voltage, and the upper and lower limits of the active power and reactive power transmission of the line are known quantities. In this optimization, the output of the active power and reactive power of the wind turbine will affect the node voltage and the current of the line connected to it, thereby affecting the line loss, resulting in the change of the on-grid power of the wind farm. If the line loss is reduced, the on-grid power will increase. Conversely, if the line loss increases, the on-grid power will decrease.

In the test, by setting the wind turbines' output level with 25, 50, 75, and 100%, the optimized power loss is shown in **Figure 4**. From this, it can be found that within four times of the iterations, the objective function will no longer be changing in all scenes. In addition, in the iteration, the power loss will be smaller. That is to say, with the convex–concave procedure implemented, the objective function changes toward a better result.

As mentioned earlier, **Eq. 43** is a standard convex optimization, whose equality constraints are linear and the inequality constraints are all convex. To compare the relaxation gap of **Eq. 43** and the one in **Eq. 44**, we have conducted the following tests when the output level of the wind turbine is 100%.

TABLE 1 | Information of the connected wind turbines and their offshore submarine cables.

Loop no.	Wind turbine no.	Length of cables (km)	Cross section of cables (mm)
1	18	13,581	3 × 300
2	12	17,413	3 × 300
3	6	22,178	3 × 300
4	31	5,339	3 × 500
5	46	5,303	3 × 500
6	72	22,190	3 × 300
7	77	1,609	3 × 500
8	24	9,773	3 × 300
9	38	1,117	3 × 500
10	39	1,609	3 × 500
11	53	9,753	3 × 500
12	66	18,067	3 × 300
13	84	12,783	3 × 500
14	60	14,217	3 × 300

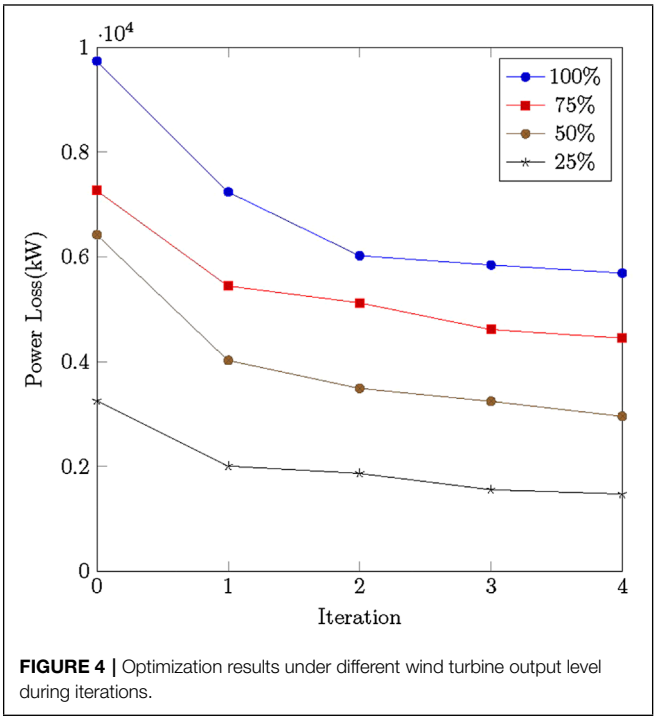

FIGURE 4 | Optimization results under different wind turbine output level during iterations.

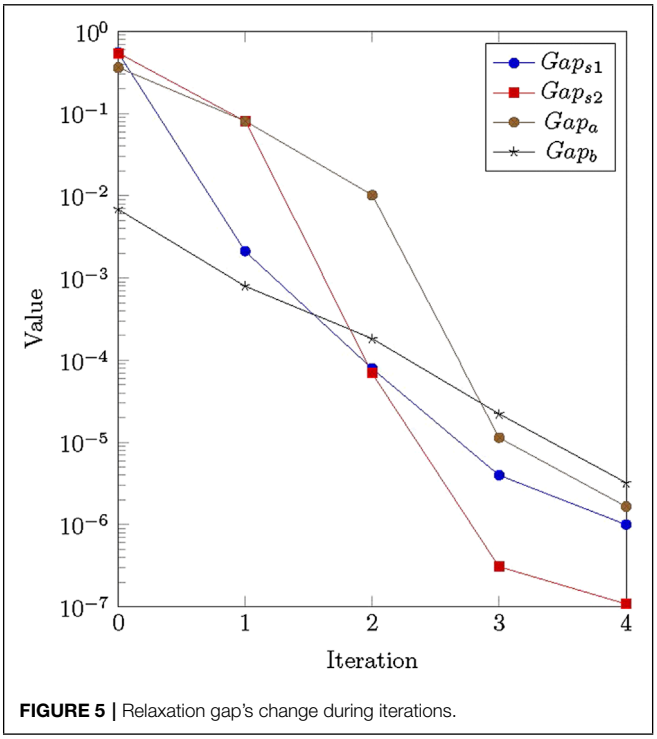

FIGURE 5 | Relaxation gap's change during iterations.

The relaxation gap is defined as

$$Gap_{s1} = \frac{\sum_{ij\in E}\left(|s_{ij}^2 - a_i b_j|\right)}{n} \tag{50}$$

$$Gap_{s2} = \frac{\sum_{ij\in E}\left(|s_{ji}^2 - a_j b_i|\right)}{n} \tag{51}$$

$$Gap_{a} = \frac{\sum_{ij\in E}\left(|a_{ij}^2 - a_i a_j|\right)}{n} \tag{52}$$

$$Gap_{b} = \frac{\sum_{ij\in E}\left(|b_{ij}^2 - b_i b_j|\right)}{n} \tag{53}$$

In the aforementioned equations, set E denotes all the branches of the system and n is the total number of transmission lines in the power system. Thus, Gap_{s1}, Gap_{s2}, Gap_a, and Gap_b are the average gap of four sets of the relaxed cones, respectively. In each iteration, the value of Gap_{s1}, Gap_{s2}, Gap_a, and Gap_b are shown in **Figure 5**. From this figure, it can be found that the second-order cone relaxation gap is reduced during iterations. Without the convex–concave procedure implemented, the initial value of the relaxation gap is around 0.5. With iterations, the gap is driven to be less than $10e-6$ and can be regarded as zero.

In summary, the proposed method is tested on a real offshore wind system. Both the power loss of the transmission lines and the relaxation gap are reduced by iterations of the convex–concave procedure.

5 CONCLUSION

In this article, a convex–concave procedure-based method for the optimal power flow of offshore wind farms is proposed.

1) It is established with the relaxation variables.
2) Two sets of the inequality constraints are implemented to replace the nonlinear and non-convex equality constraints.
3) To drive the gap of the second-order cone relaxations to be zero, the first-order Taylor expansion-based iteration is imposed.

From the test results of the real wind farm, the superiority of the proposed method is verified. It can be found that the proposed method can optimize the power loss of the transmission lines and improve the power transmitted to the power grid. Moreover, the relaxation gap is tested to be around zero with the proposed iterations.

In the future work, this method will be improved with high solving efficiency.

DATA AVAILABILITY STATEMENT

The original contributions presented in the study are included in the article/Supplementary Material; further inquiries can be directed to the corresponding author.

AUTHOR CONTRIBUTIONS

YC: methodology, software, visualization, writing—original draft preparation, and writing—reviewing and editing.

HL: supervision and writing—reviewing and editing. QC: methodology and software. RX: methodology and reviewing. XW: visualization and reviewing.

FUNDING

This project was supported by the National Key R&D Program of China (2021YFB2400600).

REFERENCES

Abdelouadoud, S. Y., Girard, R., Neirac, F. P., and Guiot, T. (2015). Optimal Power Flow of a Distribution System Based on Increasingly Tight Cutting Planes Added to a Second Order Cone Relaxation. *Int. J. Electr. Power and Energy Syst.* 69, 9–17. doi:10.1016/j.ijepes.2014.12.084

Apostolaki-Iosifidou, E., Mccormack, R., Kempton, W., Mccoy, P., and Ozkan, D. (2019). Transmission Design and Analysis for Large-Scale Offshore Wind Energy Development. *IEEE Power Energy Technol. Syst. J.* 6, 22–31. doi:10.1109/jpets.2019.2898688

Bourguignon, S., Ninin, J., Carfantan, H., and Mongeau, M. (2015). Exact Sparse Approximation Problems via Mixed-Integer Programming: Formulations and Computational Performance. *IEEE Trans. Signal Process.* 64, 1405–1419. doi:10.1109/TSP.2015.2496367

Boyd, S., Boyd, S. P., and Vandenberghe, L. (2004). *Convex Optimization*. Los Angeles: Cambridge University Press.

Chen, Y., Xiang, J., and Li, Y. (2021). A Quadratic Voltage Model for Optimal Power Flow of a Class of Meshed Networks. *Int. J. Electr. Power and Energy Syst.* 131, 107047. doi:10.1016/j.ijepes.2021.107047

Cremers, D., and Kolev, K. (2010). Multiview Stereo and Silhouette Consistency via Convex Functionals over Convex Domains. *IEEE Trans. Pattern Anal. Mach. Intell.* 33, 1161–1174. doi:10.1109/TPAMI.2010.174

Fazlyab, M., Paternain, S., Preciado, V. M., and Ribeiro, A. (2017). Prediction-Correction Interior-point Method for Time-Varying Convex Optimization. *IEEE Trans. Automatic Control* 63, 1973–1986.

Goli, A., Khademi-Zare, H., Tavakkoli-Moghaddam, R., Sadeghieh, A., Sasanian, M., and Malekalipour Kordestanizadeh, R. (2021). An Integrated Approach Based on Artificial Intelligence and Novel Meta-Heuristic Algorithms to Predict Demand for Dairy Products: a Case Study. *Netw. Comput. Neural Syst.* 32, 1–35. doi:10.1080/0954898x.2020.1849841

Guirguis, D., Romero, D. A., and Amon, C. H. (2016). Toward Efficient Optimization of Wind Farm Layouts: Utilizing Exact Gradient Information. *Appl. Energy* 179, 110–123. doi:10.1016/j.apenergy.2016.06.101

Hijazi, H., Coffrin, C., and Hentenryck, P. V. (2017). Convex Quadratic Relaxations for Mixed-Integer Nonlinear Programs in Power Systems. *Math. Prog. Comp.* 9, 321–367. doi:10.1007/s12532-016-0112-z

Jubril, A. M., Olaniyan, O. A., Komolafe, O. A., and Ogunbona, P. O. (2014). Economic-emission Dispatch Problem: A Semi-definite Programming Approach. *Appl. Energy* 134, 446–455. doi:10.1016/j.apenergy.2014.08.024

Khan, A., Naeem, M., Iqbal, M., Qaisar, S., and Anpalagan, A. (2016). A Compendium of Optimization Objectives, Constraints, Tools and Algorithms for Energy Management in Microgrids. *Renew. Sustain. Energy Rev.* 58, 1664–1683. doi:10.1016/j.rser.2015.12.259

Konar, A., and Sidiropoulos, N. D. (2017). First-order Methods for Fast Feasibility Pursuit of Non-Convex Qcqps. *IEEE Trans. Signal Process.* 65, 5927–5941. doi:10.1109/tsp.2017.2736516

Li, Q., Yu, S., Al-Sumaiti, A. S., and Turitsyn, K. (2018). Micro Water–Energy Nexus: Optimal Demand-Side Management and Quasi-Convex Hull Relaxation. *IEEE Trans. Control Netw. Syst.* 6, 1313–1322.

Li, Y., Xiao, J., Chen, C., Tan, Y., and Cao, Y. (2018). Service Restoration Model with Mixed-Integer Second-Order Cone Programming for Distribution Network with Distributed Generations. *IEEE Trans. Smart Grid* 10, 4138–4150.

Li, Y., Zhang, H., Huang, B., and Han, J. (2020). A Distributed Newton-Raphson-based Coordination Algorithm for Multi-Agent Optimization with Discrete-Time Communication. *Neural Comput. Applic* 32, 4649–4663. doi:10.1007/s00521-018-3798-1

Li, Z., Xu, Y., Fang, S., Zheng, X., and Feng, X. (2020). Robust Coordination of a Hybrid Ac/dc Multi-Energy Ship Microgrid with Flexible Voyage and Thermal Loads. *IEEE Trans. Smart Grid* 11, 2782–2793. doi:10.1109/tsg.2020.2964831

Li, Z., Wu, L., Xu, Y., Moazeni, S., and Tang, Z. (2022). Multi-stage Real-Time Operation of a Multi-Energy Microgrid with Electrical and Thermal Energy Storage Assets: A Data-Driven Mpc-Adp Approach. *IEEE Trans. Smart Grid* 13, 213–226. doi:10.1109/TSG.2021.3119972

Lofberg, J. (2004). "YALMIP : A Toolbox for Modeling and Optimization in MATLAB," 2004 IEEE International Conference on Robotics and Automation (IEEE Cat. No.04CH37508) 41, 284–289. doi:10.1109/CACSD.2004.1393890

Ma, M., Fan, L., Miao, Z., Zeng, B., and Ghassempour, H. (2020). A Sparse Convex Ac Opf Solver and Convex Iteration Implementation Based on 3-node Cycles. *Electr. Power Syst. Res.* 180, 106169. doi:10.1016/j.epsr.2019.106169

Neftci, E. O., Mostafa, H., and Zenke, F. (2019). Surrogate Gradient Learning in Spiking Neural Networks: Bringing the Power of Gradient-Based Optimization to Spiking Neural Networks. *IEEE Signal Process. Mag.* 36, 51–63. doi:10.1109/msp.2019.2931595

Rokbani, N., Kumar, R., Abraham, A., Alimi, A. M., Long, H. V., Priyadarshini, I., et al. (2021). Bi-heuristic Ant Colony Optimization-Based Approaches for Traveling Salesman Problem. *Soft Comput.* 25, 3775–3794. doi:10.1007/s00500-020-05406-5

Ruan, G., Zhong, H., Wang, J., Xia, Q., and Kang, C. (2020). Neural-network-based Lagrange Multiplier Selection for Distributed Demand Response in Smart Grid. *Appl. Energy* 264, 114636. doi:10.1016/j.apenergy.2020.114636

Shafiee, M. (2015). Maintenance Logistics Organization for Offshore Wind Energy: Current Progress and Future Perspectives. *Renew. energy* 77, 182–193. doi:10.1016/j.renene.2014.11.045

Shinano, Y., and Fujie, T. (2007). Paralex:a Parallel Extension for the Cplex Mixed Integer Optimizer. *Recent Adv. Parallel Virtual Mach. Message Passing Interface* 4757, 97–106. doi:10.1007/978-3-540-75416-9_19

Xie, S., Xu, Y., and Zheng, X. (2022). On Dynamic Network Equilibrium of a Coupled Power and Transportation Network. *IEEE Trans. Smart Grid* 13, 1398–1411. doi:10.1109/tsg.2021.3130384

Zhang, D., Wang, J., Lin, Y., Si, Y., Huang, C., Yang, J., et al. (2017). Present Situation and Future Prospect of Renewable Energy in china. *Renew. Sustain. Energy Rev.* 76, 865–871. doi:10.1016/j.rser.2017.03.023

Conflict of Interest: YC, HL, QC, RX, and XW were employed by the company PowerChina Huadong Engineering Corporation Limited.

Publisher's Note: All claims expressed in this article are solely those of the authors and do not necessarily represent those of their affiliated organizations, or those of the publisher, the editors, and the reviewers. Any product that may be evaluated in this article, or claim that may be made by its manufacturer, is not guaranteed or endorsed by the publisher.

frontiers | Frontiers in Energy Research

TYPE Original Research
PUBLISHED 08 August 2022
DOI 10.3389/fenrg.2022.968873

OPEN ACCESS

EDITED BY
Yang Li,
Hohai University, China

REVIEWED BY
Mingfei Ban,
Northeast Forestry University, China
Lei Yan,
Illinois Institute of Technology,
United States

*CORRESPONDENCE
Xuanyi Xiao,
xiaoxy6@163.com

SPECIALTY SECTION
This article was submitted to Smart Grids,
a section of the journal
Frontiers in Energy Research

RECEIVED 14 June 2022
ACCEPTED 11 July 2022
PUBLISHED 08 August 2022

CITATION
Fan H, Wang H, Xu Y, Hu J, Zhang W and Xiao X (2022), Capacity value analysis of interruptible loads in regional power systems with intermittent renewable energy.
Front. Energy Res. 10:968873.
doi: 10.3389/fenrg.2022.968873

Capacity value analysis of interruptible loads in regional power systems with intermittent renewable energy

Hengjian Fan[1], Hongliang Wang[2], Yang Xu[2], Jiahua Hu[2], Weiwei Zhang[2] and Xuanyi Xiao[3]*

[1]Polytechnic Institute, Zhejiang University, Hangzhou, China, [2]Economic and Technological Research Institute of State Grid Zhejiang Electric Power Company, Hangzhou, China, [3]College of Electrical Engineering, Zhejiang University, Hangzhou, China

The proportion of renewable energy is increasing rapidly to develop low-carbon power systems and the intermittence nature of renewable energy harms the security operation of power systems. The participation of interruptible loads is an effective means to handle the intermittence of renewable energy. However, the capacity value of interruptible loads has not been fully recognized, which results in limited involvement of interruptible loads in power system operations. Hence, it is urgent to analyze the capacity value of interruptible loads. In this paper, a capacity value calculation method of interruptible loads is proposed. A joint optimal operation model of interruptible loads and multiple power sources including thermal power units, hydropower units, and wind turbines is established to realize the application paradigm of power system operations with interruptible loads. Case analysis based on the operation data of the power system in a particular area verifies that the proposed method can effectively recognize the capacity value of interruptible loads and reduce the installed capacity of thermal power units. It thereby lays the theoretical foundation for analyzing the role of interruptible loads in the low-carbon transition of the electric energy industry.

KEYWORDS

interruptible loads, capacity value, energy transition, operation simulation, optimized operation, unit aggregation

1 Introduction

The electric energy industry accelerates the transformation to low-carbon nowadays. In the future, power systems will use a high proportion of renewable energy as the main body of the power system. However, due to the uncertainty, volatility, and intermittence of renewable energy, the power system operations in the future will face severe challenges (Mashhour et al., 2010; Sarkhani. et al., 2011). In power systems, if conventional generators are the only type of means used to handle the intermittence of renewable energy, these generators are started and stopped frequently or their outputs are changed

dramatically. This increases the difficulty of dispatching and reduces the economy of power systems (Sampang et al., 2018). Demand response has developed rapidly in recent years. It has gradually become a vital force that can support power systems to peak load shifting, and absorb renewable energy (Bessler and Jung, 2016), and its status is becoming more and more critical (Sivaneasan et al., 2016). Hence, measures to maintain the security operation of power systems with high proportion of intermittent renewable energy should not only be implemented on the power resource side but also the demand side.

Demand response is generally divided into incentive-based demand response and price-based demand response according to the response mode of the demand side (Devatgaran et al., 2013). Interruptible loads are an incentive-based demand response (Li et al., 2013). According to the contracts signed by users in advance, the loads will be cut off according to the agreement when the peak load is very high, or the security operation of power systems is threatened. Users will be given specific compensations after the loads are cut off (Sharma et al., 2018; Wang et al., 2020). The interruptible loads are developing rapidly and have enormous potential. In recent years, plenty of regions have successively introduced relevant policies on interruptible loads (Argiento et al., 2012). With the advancement of the electricity market, it has become inevitable for interruptible loads to participate in the electricity market in the future (Sampang et al., 2018). At this stage, the interruptible loads pricing mechanism is still dominated by the government, which cannot fully reflect the value of interruptible loads to power systems. Therefore, the value of the interruptible loads deserves careful analysis to develop effective price mechanisms in the future electricity market. Interruptible loads mainly play the role of peak load shifting in power systems (Mashhour et al., 2010). The effect of interruptible loads in power system operations is similar to energy storage systems. Therefore, interruptible loads have a particular capacity value. In the crucial period when interruptible loads need to be developed urgently, research on capacity value analysis has essential theoretical and practical value.

Some papers have had some exploratory analysis on the value of interruptible loads. Wang et al. (2004) analyzed the value of interruptible loads under different conditions such as advance time of interrupting notification and the duration of interrupting. Li (2017) analyzed the value brought by demand-side users of different scales as the interruptible loads; however, few types of users were analyzed, which ultimately failed to reflect the capacity value of interruptible loads. Shao et al. (2012) studied the value of interruptible loads to different bodies such as users, electricity companies, and society; however, the analysis process lacked quantitative calculations and could not expressly reflect capacity value. Li et al. (2013) analyzed the benefit of interruptible loads under different subsidy schemes from load aggregators; however, the load aggregators' scale was small. Zhang et al. (2016) uses the stochastic operation simulation method to analyze the value of interruptible loads participating in the electricity market; however, the analyzed capacity value is not comprehensive enough.

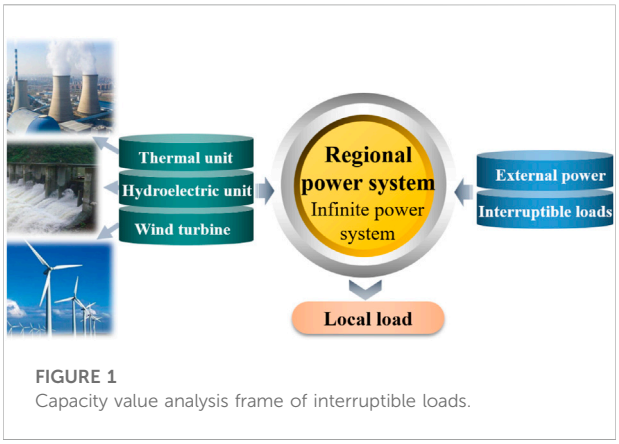

FIGURE 1
Capacity value analysis frame of interruptible loads.

Based on the above analysis, the research gap in the existing literature is that there is no unified method and standard for analyzing the capacity value of interruptible loads, which results in limited involvement of interruptible loads in power system operations and hinders the improvement of power system security while incorporating a high proportion of renewable energy. Hence, this paper proposes a capacity value calculation method of interruptible loads and establishes a mathematical model for the optimal joint operation of interruptible loads, thermal power units, hydropower units, and wind turbines. The proposed method can effectively recognize the capacity value of interruptible loads and reduce the installed capacity of thermal power units. The content is arranged as follows. Section 2 introduces the methodology, framework, and vital technologies of the capacity value analysis of interruptible loads; Section 3 presents the operation simulation model of interruptible loads and the calculation process of the capacity value; Section 4 shows the case analysis on a power system in a particular region; Section 5 is the conclusion of this paper.

2 Methodology

2.1 Research fundamentals

The coordinated operation of interruptible loads and power systems can enhance the security and sustainability of power systems. In this paper, the capacity value of the interruptible loads is a value brought to the security operation of power systems. However, the capacity value is difficult to be reflected in power systems directly. Theoretically, the installed capacity of thermal power units can reflect the capacity value of interruptible

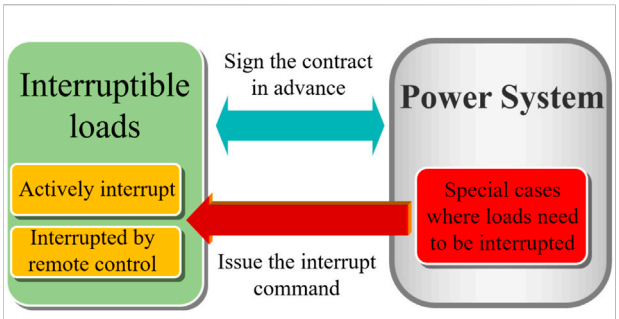

FIGURE 2
The realization process of interruptible loads.

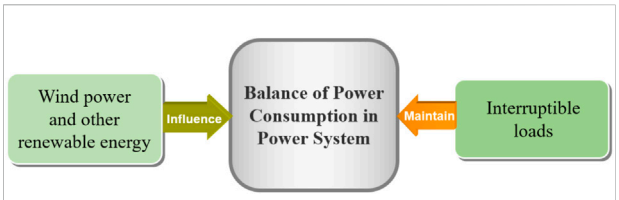

FIGURE 3
The function of interruptible loads.

loads on the premise of ensuring the balance of power consumption.

To address the above issue, we proposed a calculation method of the capacity value of interruptible loads and established a mathematical model of the coordinated operation of thermal power units, hydropower units, wind turbines, and interruptible loads in a regional power system that ensures the balance of power consumption with external electricity. The regional power system is considered infinite, ignoring the internal operation constraints and the grid structure. The frame of the value analysis of interruptible loads capacity is shown in Figure 1.

2.2 The function of interruptible loads

Interruptible load controlling is a load regulation method that considers both the system security and the users' wishes. The users sign agreements with the relevant departments of power systems in advance. During the peak period of power consumption, the interruptible loads can be activated to maintain the power balance of the systems. When the interruptible load needs to be activated to maintain the security operation of power systems, the dispatching department will interrupt them according to the former agreements (Sivaneasan et al., 2016). The realization process of interruptible loads is shown in Figure 2.

Early interruptible loads only existed among large industrial users for various reasons: single management means, low management efficiency, and insufficient power grid intelligence. Due to the lack of experience managing interruptible loads and imperfect value analysis, large industrial users did not attend early interruptible loads practices for a large amount. With the continuous improvement of the intelligence level of power systems in recent years, the types of users that can participate in the implementation of interruptible loads have been expanded from single large industrial users to medium and small industrial users and even commercial users. Medium and small users will participate in interruptible loads mainly through load aggregators.

In the foreseeable future, the proportion of renewable energy units such as wind turbines in power systems will increase, and the power balance of power systems will face new challenges. Interruptible loads will play a more important role in peak shaving and maintaining the balance of power consumption with intermittent renewable energy in the future, as shown in Figure 3.

2.3 Aggregated modeling of conventional generation units

2.3.1Aggregation of thermal units

The aggregation modeling method of thermal power units mainly superimposes the output constraints and ramping constraints, installs the capacity of all thermal power units in the regional power system, and obtains the new output constraints, ramping constraints, and installed capacity of the aggregation thermal power unit

$$P_c^{\max} = \sum_{j=1}^{n} P_{c,j}^{\max} \tag{1}$$

$$P_c^{\min} = \sum_{j=1}^{n} P_{c,j}^{\min} \tag{2}$$

$$R^{\max} = \sum_{j=1}^{n} r_j^{\max} \tag{3}$$

$$R^{\min} = \sum_{j=1}^{n} r_j^{\min} \tag{4}$$

$$W_c = \sum_{j=1}^{n} w_{c,j} \tag{5}$$

Where $P_c^{\max}$ is the maximum output of the thermal power unit after the aggregation; $p_{c,j}^{\max}$ is the maximum output of the thermal power unit j; $P_c^{\min}$ is the minimum output of the thermal power unit after the aggregation; $p_{c,j}^{\min}$ is the minimum output of the thermal power unit j. $R^{\max}$ is the upper ramping limit of the thermal power unit after the aggregation; $r_j^{\max}$ is the upper ramping limit of the thermal power unit j; $R^{\min}$ is the lower

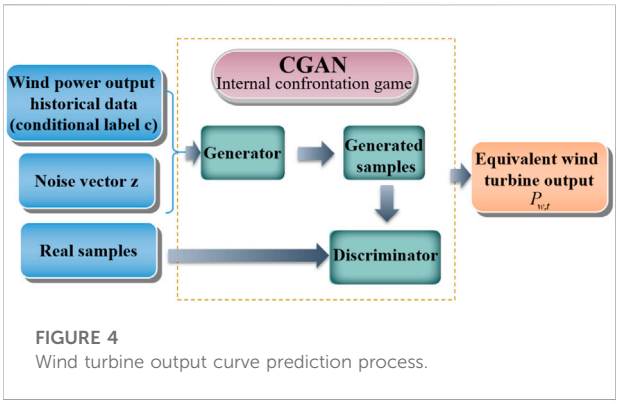

FIGURE 4
Wind turbine output curve prediction process.

ramping limit of the thermal power unit after the aggregation; $r_j^{\min}$ is the lower ramping limit of the thermal power unit j. W_c is the total installed capacity of thermal power units after the aggregation; $w_{c,j}$ is the installed capacity of thermal power unit j.

2.3.2Aggregation of hydropower units

The aggregation modeling method of the hydropower unit is similar to the aggregation modeling method of the above-mentioned thermal power unit. Superimpose the upper and lower limits of all hydropower units in the regional power system within a dispatch period to obtain the upper and lower limits of the aggregation hydropower unit; superimpose the installed capacity of all hydropower units to get the installed capacity of the aggregation hydropower unit:

$$S_h^{\max} = \sum_{j=1}^{o} S_{h,j}^{\max} \tag{6}$$

$$S_h^{\min} = \sum_{j=1}^{o} S_{h,j}^{\min} \tag{7}$$

$$W_h = \sum_{j=1}^{o} w_{h,j} \tag{8}$$

Where $S_h^{\max}$ is the upper limit of the hydropower unit in one dispatch period after the aggregation; $S_{h,j}^{\max}$ is the upper limit of the hydropower unit j in one dispatch period; $S_h^{\min}$ is the lower limit of the hydropower unit after the aggregation in one dispatch period; $S_{h,j}^{\min}$ is the lower limit of the hydropower unit j in one dispatch period; W_h is the total installed capacity of the hydropower unit after the aggregation; $w_{h,j}$ is the installed capacity of the hydroelectric unit j.

2.4 Conditional prediction of wind power output

The wind power output curve is generated using Conditional Generative Adversarial Networks (CGAN) (Kim, 2021). The generator maps the noise vector z in the low-dimensional space to the high-dimensional space to generate new samples close to the actual data (Xu et al., 2020). The discriminator's function is judging whether the input data is actual data. Usually, the generator and the discriminator are two convolutional neural networks with symmetrical structures. The robust feature extraction capability of the convolutional network can improve the quality of the generated data (Mohseni et al., 2020). Through the adversarial training of the two networks, the generator finally learns the distribution characteristics of the original data and can generate data that conforms to the real laws. The wind turbine output curve prediction process is shown in Figure 4.

First, the noise vector z is sampled from a Gaussian distribution with a mean of 0 and a standard deviation of 1. It is horizontally spliced with the wind power output historical data (conditional label c) and input to the generator to generate the generated samples. The generated and actual samples are combined with the corresponding condition labels and then input to the discriminator. In the game training process, the generator tries to generate new samples close to the actual data under condition c. The discriminator tries to distinguish between actual data or generated data under condition c, and the two progress together in this process. Finally, the output of the aggregation wind turbine $P_{w,t}$ is obtained through training.

The loss functions of the discriminator and generator are:

$$L_G = -E_{z\sim p_z(z)}[D(G(z|c)|c)] \tag{9}$$

$$L_D = \begin{cases} -E_{x\sim P_r(x)}[D(x|c)]+ \\ E_{z\sim p_z(z)}[D(G(z|c)|c)] \end{cases} \tag{10}$$

Where E is the expectation; $x \sim p_r(x)$ is the probability that a set of actual samples x, $D(\cdot)$ is the probability of the discriminator to judge that the input samples are actual; is the noise vector collected in the Gaussian distribution $p_z(z)$; $G(z|c)$ is the generated data under the condition c.

The objective function of the CGAN prediction process is:

$$\min_G \max_D V(G,D) = \{E_{x\sim P_r(x)}[D(x|c)] - E_{z\sim P_z(z)}[D(G(z|c)|c)]\} \tag{11}$$

The principle of constructing the objective function is that while training the generator, the generator tries to generate data that meets the mapping of condition c and the distribution of actual data to deceive the discriminator. At this time, the training objective of CGAN is to minimize the above objective function. While training, the discriminator tries to distinguish between actual data and generated data under condition c, so the objective function needs to be maximized while training the discriminator. The CGAN training process is essentially a game of minimum and maximum values. After the training is over, the generator can learn the mapping relationship between the actual data and condition c to generate data that obey the real law under condition c.

3 Design of interruptible loads operation model

3.1 Objective function

To minimize the total cost of regional power system operation, the power generation cost of aggregation thermal power units and the power abandonment penalty of renewable energy are considered to meet regional power system power consumption balance constraints, thermal power unit output constraints, and ramping constraints. The objective function is as follows:

$$\min\left\{\sum_{t=1}^{T} D_{c,t}\cdot G_{c,t}\left(P_{c,t}\right)+k_1\sum_{t=1}^{T}E_{w,t}+k_2\sum_{t=1}^{T}E_{h,t}\right\} \tag{12}$$

Where T is the total number of periods; $D_{c,t}$ is the 0–1 variable representing the operation state of the aggregation thermal power unit at the moment t, 0 means the unit is not running, and 1 means the unit is running; $P_{c,t}$ is the output of the aggregation thermal power unit at the moment t; k_1 is the wind power abandonment penalty factor; $E_{w,t}$ is the abandoned wind power in the system at the moment t; k_2 is the hydropower abandonment penalty factor; $E_{h,t}$ is the abandoned hydropower in the system at the moment t; $G_{c,t}$ is the cost function of the aggregation thermal power unit at the moment t, its expression is as follows (Dey and Basak, 2017; Yang et al., 2020):

$$G_{c,t}=a\cdot P_{c,t}^2+b\cdot P_{c,t}+d \tag{13}$$

Where a, b, and d are the coefficients between the thermal power unit's power and the generator's cost.

The abandoned wind power and hydropower in the system are calculated as follows:

$$E_{w,t}=W_{w,t}-P_{w,t} \tag{14}$$

$$E_{h,t}=W_{h,t}-P_{h,t} \tag{15}$$

Where $W_{w,t}$ is the theoretical output power of the aggregation wind turbine at time t; $P_{w,t}$ is the actual output power of the aggregation wind turbine at time t. $W_{h,t}$ is the theoretical output power of the aggregation hydropower unit at time t; $P_{h,t}$ is the actual output power of the aggregation hydropower unit at time t.

3.2 Constraints

In the operation simulation model of interruptible loads, the regional power system is regarded as an infinite power system. The constraints within the system and the power consumption of the lines in the system are ignored.

3.2.1 Balance of power consumption constraints

$$P_{c,t}+P_{w,t}+P_{h,t}+P_{i,t}+P_{l,t}=L_t \tag{16}$$

Where $P_{i,t}$ is the power of the interruptible loads responding to the interruption command at time t; $P_{l,t}$ is the power of external power in the regional power system at time t; $P_{l,t}$ is the local load in the system at time t.

3.2.2 Output constraints

$$P_c^{\min}\le P_{c,t}\le P_c^{\max} \tag{17}$$

Where $P_c^{\min}$ is the minimum output allowed by the aggregation thermal power unit at any time; $P_c^{\max}$ is the maximum output allowed by the aggregation thermal power unit.

3.2.3 Ramping constraints

$$P_{c,t}-P_{c,t-1}\le -R^{\min} \tag{18}$$

$$P_{c,t}-P_{c,t-1}\le R^{\max} \tag{19}$$

Where $P_{c,t-1}$ is the output of the aggregation thermal power unit at time t-1; $R^{\min}$ is the lower limit of the aggregation thermal power unit at any time; $R^{\max}$ is the upper limit of the aggregation thermal power unit at any time.

3.2.4 Aggregation hydropower unit's constraints

$$E_h^{\min}\le\sum_{t=1}^{T}\left(P_{h,t}+E_{h,t}\right)\le E_h^{\max} \tag{20}$$

Where $E_h^{\min}$ is the lower limit of the aggregation hydropower unit in a dispatch period; it $E_h^{\max}$ is the upper limit of the aggregation hydropower unit in a dispatch period.

3.2.5 Reserve capacity constraint

$$H^{\min}\le H_t \tag{21}$$

where $H^{\min}$ is the lower limit of the reserve capacity in the regional power system at any time; H_t is the reserve capacity in the regional power system at the time t.

3.2.6 Interruptible loads constraints

The constraints of interruptible loads include interruption quantity constraint, maximum interruption time constraint, minimum interruption time constraint, maximum interruption number of times constraint, and minimum interruption interval constraint (Sousa et al., 2017). Because the interruptible loads in the model are the actual interruptible loads in the regional power system, the operation is simulated on a typical day. The constraints of the maximum interruption time, the maximum number of interruptions, and the minimum interruption interval are not considered. However,

the total outage power constraint of the interruptible loads in 1 day is added.

3.2.6.1 Interruption quantity constraint

$$P_{i,\min} \le P_{i,t} \le P_{i,\max} \tag{22}$$

Where $P_{i,\min}$ is the minimum interruption a quantity of the interruptible loads at any time; $P_{i,\max}$ is the maximum interruption quantity of the interruptible loads.

3.2.6.2 Minimum interruption time constraint

$$T_i \ge T_0 \tag{23}$$

Where T_i is the interruption time of the interruptible loads; T_0 is the minimum interruption time of the interruptible loads.

3.2.6.3 Total interruption power constraint

$$\sum_{t=1}^{T} P_{i,t} \le Q_{\max} \tag{24}$$

Where $Q_{\max}$ it is the maximum quantity of the total interruption power of the load that can be interrupted in 1 day.

3.3 Linearization of aggregation thermal unit cost

Due to the existence of the generator cost function of the aggregation thermal power unit in the objective function, the model of the interruptible loads and the coordinated operation of thermal power, hydropower, wind turbine, and the regional power system, which comprehensively considers the constraints in 3.2, is a mixed-integer nonlinear programming problem. When solving, the power generator cost of the aggregation thermal power unit should be linearized by the following formula:

$$G_{c,t} = \sum_{s=1}^{n} K_s P_{c,s} \tag{25}$$

$$P_{c,t} = \sum_{s=1}^{n} P_{c,s} \tag{26}$$

$$F = \frac{P_c^{\max} - P_c^{\min}}{n} \tag{27}$$

$$K_s = a(2s-1)F + b \tag{28}$$

Where K_s is the slope of the aggregation thermal power unit in the s segment interval; n is the number of segments; $P_{c,s}$ is the actual output of the aggregation thermal power unit in the s segment; F is the maximum output of the aggregation thermal power unit in the s segment.

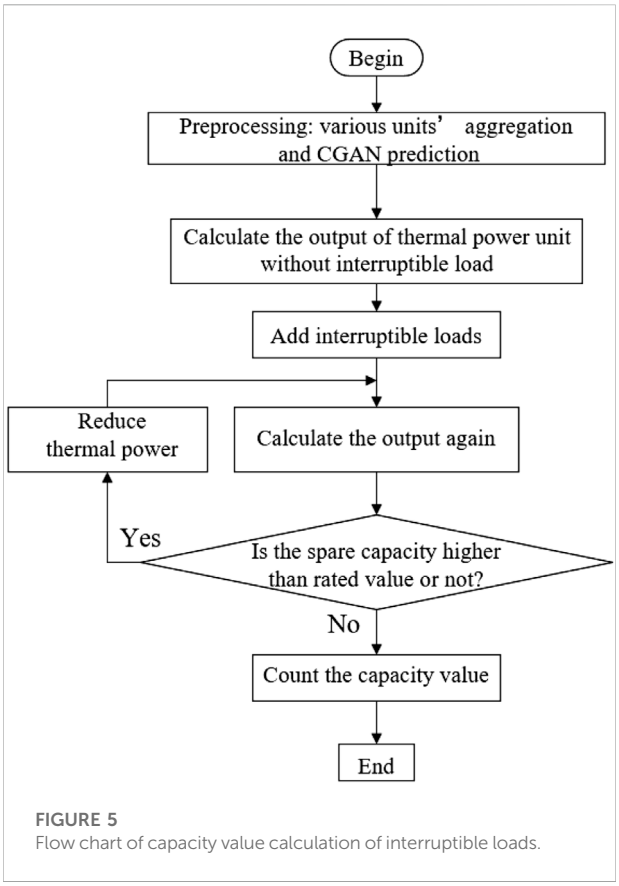

FIGURE 5
Flow chart of capacity value calculation of interruptible loads.

After piecewise linearization of the power generator cost of the aggregation thermal power unit, the model becomes a mixed-integer linear programming problem in each piecewise interval, which can be solved by using the mature linear programming commercial solver, Gurobi.

3.4 Calculation process

Figure 5 shows the flow of capacity value calculation for interruptible loads

(1) Data preprocessing: thermal units' and hydropower units' aggregation; use CGAN to predict the output curve of the aggregation wind turbine; linearize the power generator cost of the aggregation thermal power unit;
(2) On a typical day, simulate the operation of the regional power system when there are no interruptible loads; obtain the output of the aggregation thermal power unit;
(3) Add the interruptible loads to the system; all other parameters remain unchanged and perform the operation simulation on the same typical day again;
(4) In the case of the interruptible loads and the coordinated operation of the regional power system, calculate the output of the thermal power unit in the system;

TABLE 1 Predicted generation and interruptible load capacities in 2025.

Unit type	Predicted capacities in 2025/10 MW
Thermal unit	7,200
Hydropower unit	800
Wind turbine	2,800
Interruptible loads	200

(5) Judge whether the capacity of thermal power units in the system put into operation is higher than the rated value. If it is not higher than the rated value, perform step (7); if it is higher than the rated value, perform step (6);
(6) Reduce the installed capacity of the thermal power unit, and then perform step (4);
(7) Calculate the difference between the capacity of the thermal power unit after and before the interruptible loads are added to the system. The formula for calculating the benefit of interruptible loads capacity is:

$$F_i = W_c - W_c^{'} \tag{29}$$

Where F_i is the capacity value of the interruptible loads; $W_c^{'}$ is the installed capacity of the thermal power unit under the condition that the interruptible loads are added to the operation of the regional power system to ensure the security operation of the system and the system reserve capacity meets the constraints.

4 Case analysis

We designed the following cases to quantitatively calculate the value of interruptible loads in regional power systems with intermittent renewable energy in the future.

4.1 Related parameters

The data in the calculation example is based on the actual installed capacity and actual local loads of a regional power system in a particular region. The parameters of the system in 2025 and the annual load growth rate are set as 5.0. The data sampling interval is 1 h. The data of external power is the planned external power in the region in 2025. The minimum output of thermal power units is 50% of the installed capacity. Interruptible load refers to a load that can be positively activated 1 hour in advance. Its capacity forecasts in 2025, according to the growth rate of 5.0%, is about 2,000 MW, and the other scenarios, including the capacity of 4,000 and 6,000 MW, are used for comparison. The minimum interruption time is set to 1 h, and the maximum interruption energy in 1 day in the three scenarios is set to 16,000, 32,000, and 48,000 MWh, respectively. Other parameters of the system are shown in Table 1:

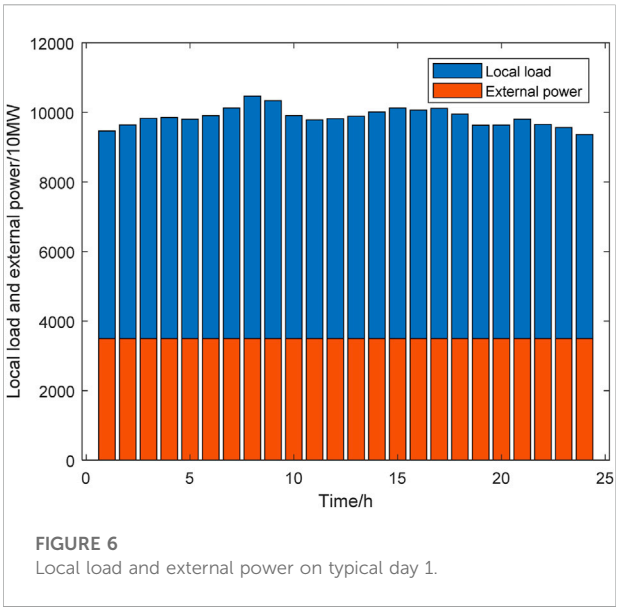

FIGURE 6
Local load and external power on typical day 1.

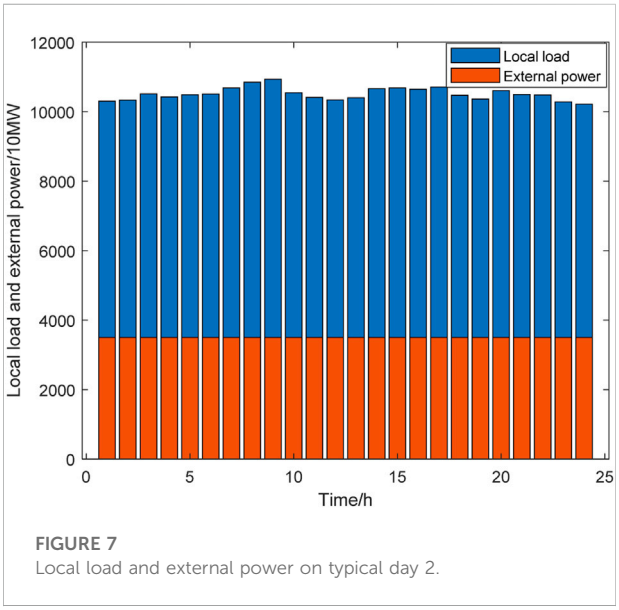

FIGURE 7
Local load and external power on typical day 2.

4.2 Results and analysis

In this regional power system in 2025, the day with the largest daily peak-to-valley difference was selected as typical day 1, and the day with the highest load was selected as typical day 2. The change of the installed capacity of thermal power units before

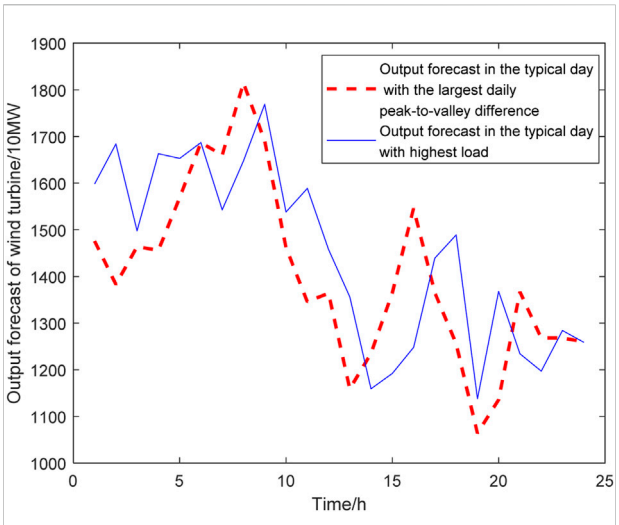

FIGURE 8
Output forecast of wind turbines on two typical days.

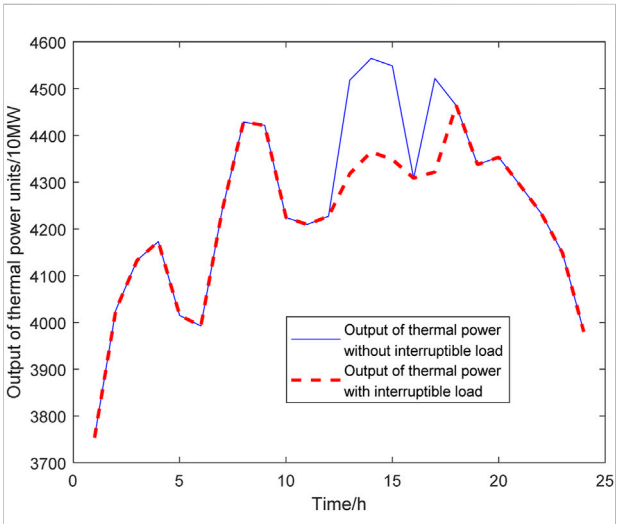

FIGURE 9
Comparison of the output of thermal power units on typical day 1 with two million kW interruptible loads.

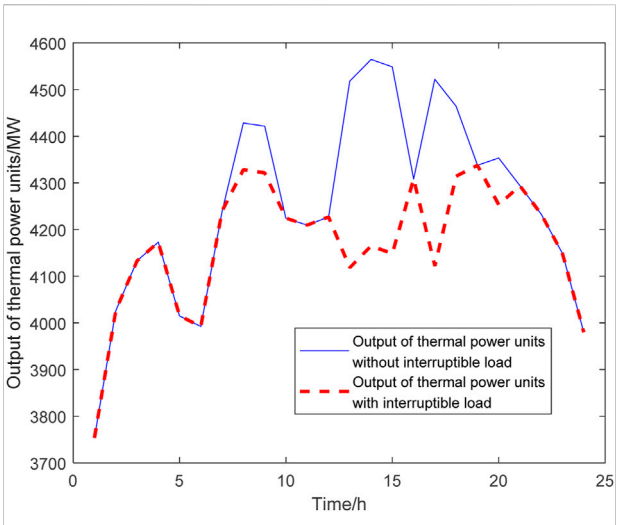

FIGURE 10
Comparison of the output of thermal power units on typical day 1 with 4 million kW interruptible loads.

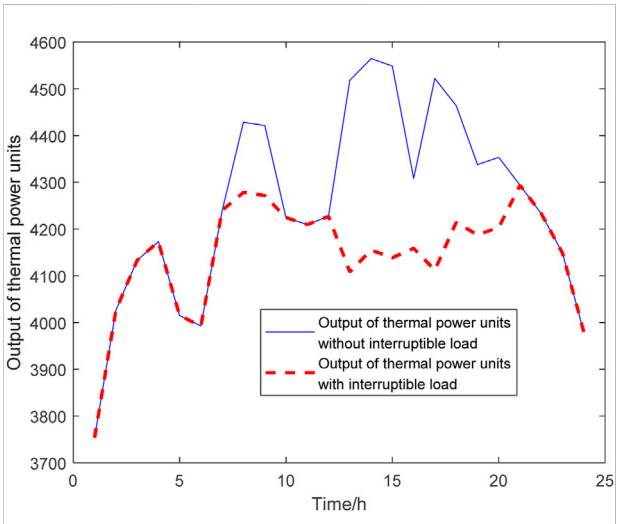

FIGURE 11
Comparison of the output of thermal power units on typical day 1 with 6 million kW interruptible loads.

and after the interruptible loads participated in the operation of power systems is calculated. The local load and external power on the typical day 1 and 2 are shown in Figures 6, 7, respectively. The output forecast of wind turbines on two typical days is shown in Figure 8.

Figures 9–11 are the comparison of the thermal power unit's output before and after the interruptible loads participate in the system operation under three different scenarios on typical day 1; Figures 12–14 are the comparison of thermal power unit's output before and after the interruptible loads participate in the system operation under three different scenarios on typical day 2.

On typical day 1, the operation simulation is carried out for two cases whether the interruptible loads participate in the operation of power systems. Compared with the time when the interruptible loads do not participate in the operation of power systems when the interruptible loads capacity is 2,000 MW, the addition of the interruptible loads can

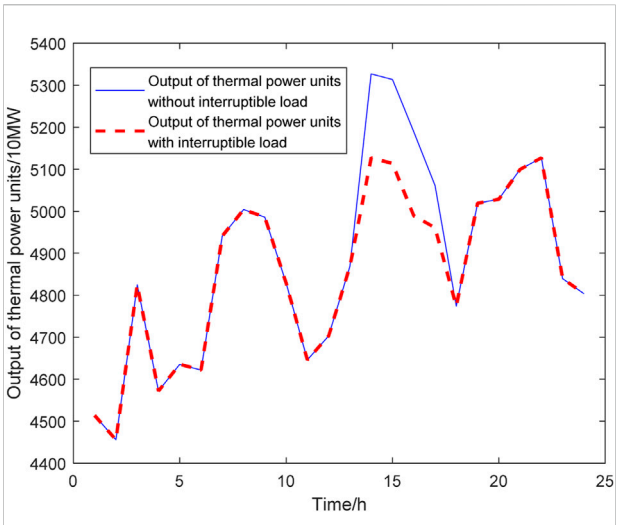

FIGURE 12
Comparison of the output of thermal power units on typical day 2 with 2 million kW interruptible loads.

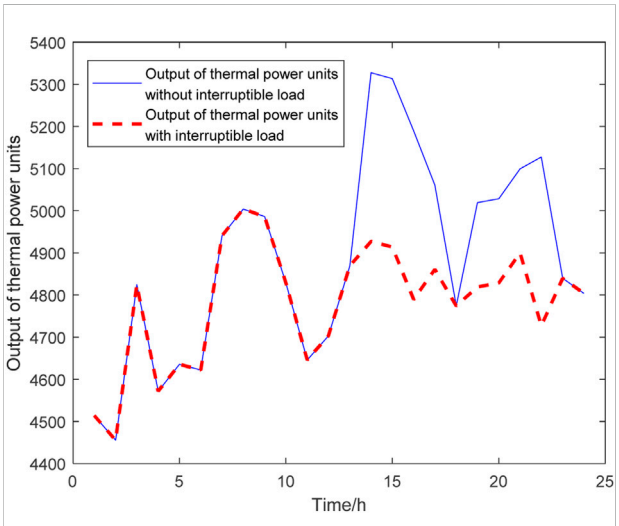

FIGURE 13
Comparison of the output of thermal power units on typical day 2 with 4 million kW interruptible loads.

reduce 1,005.84 MW of thermal power units; when the interruptible loads capacity is 4,000 MW, the addition of interruptible loads can reduce the thermal power assembly by 2,270.40 MW of thermal power units; when the interruptible loads capacity is 6000MW, the addition of interruptible loads can reduce 2,712.21 MW of thermal power units. On typical day 2, the operation simulation is carried out for two cases whether the interruptible loads

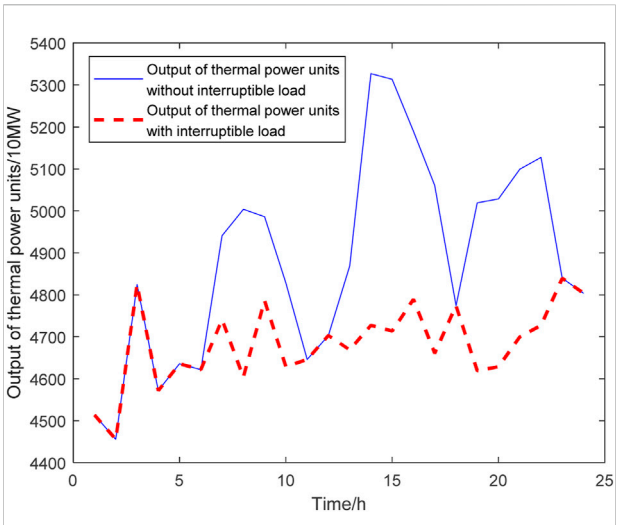

FIGURE 14
Comparison of the output of thermal power units on typical day 2 with 6 million kW interruptible loads.

participate in the operation of power systems. Compared with the time when the interruptible loads do not participate in the operation of power systems when the interruptible loads capacity is 2 MW, the addition of the interruptible loads can reduce 1999.73 MW of thermal power units; when the interruptible loads capacity is 4 MW, the addition of interruptible loads can reduce 3,232.26 MW of thermal power plants; when the interruptible loads capacity is 6 MW, the addition of interruptible loads can reduce 4,876.73 MW of thermal power units.

In summary, the benefit statistics of interruptible loads capacity are shown in Table 2:

In the simulation analysis of the operation of the interruptible loads, the multiple units, and power systems, it is undeniable that interruptible loads have plenty of capacity value in the operation of power systems. However, this paper uses the data of typical days for analysis. The response time of the interruptible loads used is short, which cannot wholly reflect the capacity value of different types of interruptible loads. The interruptible loads capacity in the calculation example is predicted according to the electricity consumption growth rate according to the current interruptible loads capacity of power systems in a particular region. The proposed method effectively calculates the value of interruptible loads in regional power systems with intermittent renewable energy. In the future construction of power systems, the capacity of the interruptible loads will be higher than that in the calculation example, and the interruptible loads will be able to reflect a higher capacity value.

TABLE 2 Results of the capacity value of interruptible loads.

The capacity of interruptible loads	The typical day with the largest daily peak-to-valley difference	The typical day with the highest load
S/MW	F_i/MW	F_i/MW
2,000	1,005.84	1,999.73
4,000	2,270.40	3,232.26
6,000	2,712.21	4,876.73

5 Conclusion

The participation of interruptible loads is an effective means to handle the intermittence of renewable energy, so the capacity value analysis of interruptible loads is an urgent problem. In this paper, combined with the functional characteristics of interruptible loads in power systems, a mathematical model for the optimal joint operation of interruptible loads, several units, and the operation simulation analysis are carried out based on actual operation data of power systems in a particular region. By comparing the changes in the installed capacity of thermal power units in power systems under the two conditions of whether the interruptible loads participate in the operation of power systems, the capacity value of the interruptible loads is calculated quantitatively. The installed capacity of thermal power units can be reduced obviously. The proposed method can effectively promote the participation of interruptible loads in power systems with intermittent renewable energy.

Data availability statement

The original contributions presented in the study are included in the article/supplementary material, further inquiries can be directed to the corresponding author.

Author contributions

HF: Conceptualization, Methodology, Software, and Writing—Original Draft. HW: Methodology, Software, and Validation. YX: Investigation, Data Curation. JH: Visualization, Writing—Original Draft. WZ: Software. XX: Supervision, Project administration, Writing—Review, and Editing.

Conflict of interest

Authors HW, YX, JH, and WZ were employed by Economic and Technological Research Institute of State Grid Zhejiang Electric Power Company.

The remaining authors declare that the research was conducted in the absence of any commercial or financial relationships that could be construed as a potential conflict of interest.

Publisher's note

All claims expressed in this article are solely those of the authors and do not necessarily represent those of their affiliated organizations, or those of the publisher, the editors and the reviewers. Any product that may be evaluated in this article, or claim that may be made by its manufacturer, is not guaranteed or endorsed by the publisher.

References

Argiento, R., Faranda, R., Pievatolo, A., and Tironi, E. (2012). Distributed interruptible load shedding and micro-generator dispatching to benefit system operations. *IEEE Trans. Power Syst.* 27 (2), 840–848. doi:10.1109/tpwrs.2011.2173217

Bessler, S., and Jung, O. (2016). "Energy management in microgrids with flexible and Interruptible load," in 2016 IEEE Power & Energy Society Innovative Smart Grid Technologies Conference (ISGT), 06-09 September 2016 (Minneapolis, MN, USA: IEEE), 1–6. doi:10.1109/ISGT.2016.7781238

Davatgaran, V., Mortazavi, S. S., Saniei, M., and Khalifeh, M. (2013). "Different strategies of Interruptible load contracts implemented in reliability constrained unit commitment," in 2013 21st Iranian Conference on Electrical Engineering (ICEE), 14-16 May 2013 (Mashhad, Iran: IEEE), 1–6. doi:10.1109/iraniancee.2013.6599884

Dey, D., and Basak, C. K. (2017). "Cost optimization of a wind power integrated thermal power plant," in 2017 International Conference on Computer, Electrical & Communication Engineering (ICCECE), 22-23 December 2017 (Kolkata, India: IEEE), 1–5. doi:10.1109/iccece.2017.8526198

Kim, M. (2021). ML/CGAN: Network attack analysis using CGAN as meta-learning. *IEEE Commun. Lett.* 25 (2), 499–502. doi:10.1109/lcomm.2020.3029580

Li, H. Z., Wang, B., Su, C. B., Guo, S., and Li, C. J. (2013). Selection assessment of Interruptible load participating in market reserve during peak period and benefit measurement. *Power Syst. Prot. Control* 41 (10), 39–44. doi:10.7667/j.issn.1674-3415.2013.10.007

Li, J. (2017). Analysis on application and benefit of interruptible load in power demand side management. *Ind. Technol. Innov.* 04 (02), 153–155. doi:10.14103/j.issn.2095-8412.2017.02.042

Mashhour, M., Golkar, M. A., and Tafreshi, S. M. (2010). "Efficient aggregation of distributed generations and interruptible load: A new tool for market integration of distributed recourses," in 2010 7th International

Conference on the European Energy Market, 23-25 June 2010 (Madrid, Spain: IEEE), 1–6. doi:10.1109/EEM.2010.5558776

Mohseni, S., Brent, A. C., Burmester, D., and Browne, W. (2020). "A game-theoretic approach to model interruptible load: Application to micro-grid planning," in 2020 IEEE Power & Energy Society General Meeting (PESGM), 02-06 August 2020 (Montreal, QC, Canada: IEEE), 1–5. doi:10.1109/PESGM41954.2020.9281836

Sampang, C., Ibarbia, P. I. S. D., Laxamana, C. T., and Nerves, A. C. (2018). "Optimal scheduling strategy for virtual power plants with interruptible load," in 2018 IEEE PES Asia-Pacific Power and Energy Engineering Conference (APPEEC), 07-10 October 2018 (Kota Kinabalu, Malaysia: IEEE), 616–620. doi:10.1109/APPEEC.2018.8566675

Sarkhani, S., Soleymani, S., Mozafari, B., and Afaghzadeh, H. (2011). "Impact of distributed generation and Interruptible load on energy supply strategies of distribution companies in day-ahead market," in 16th Electrical Power Distribution Conference, 19-20 April 2011 (Bandar Abbas, Iran: IEEE), 1.

Shao, S., Pipattanasomporn, M., and Rahman, S. (2013). Development of physical-based demand response-enabled residential load models. *IEEE Trans. Power Syst.* 28 (2), 607–614. doi:10.1109/tpwrs.2012.2208232

Sharma, J., Prakash, V., and Bhakar, R. (2018). "Interruptible load constrained primary frequency response scheduling with photovoltaic generation," in 2018 20th National Power Systems Conference (NPSC), 14-16 December 2018 (Tiruchirappalli, India: IEEE), 1–6. doi:10.1109/npsc.2018.8771760

Sivaneasan, B., Thachinamoorthi, K., and Goh, K. P. (2016). "Interruptible load scheme: Demand response management for buildings," in 2016 IEEE Region 10 Conference (TENCON), 22-25 November 2016 (Singapore: IEEE), 1716–1719. doi:10.1109/tencon.2016.7848311

Sousa, J. C., Saavedra, O. R., and Lima, S. L. (2018). Decision making in emergency operation for power transformers with regard to risks and interruptible load contracts. *IEEE Trans. Power Deliv.* 33 (4), 1556–1564. doi:10.1109/tpwrd.2017.2764466

Wang, B., Li, Y., Ming, W., and Wang, S. (2020). Deep reinforcement learning method for demand response management of interruptible load. *IEEE Trans. Smart Grid* 11 (4), 3146–3155. doi:10.1109/tsg.2020.2967430

Wang, J., Wang, X., Zhang, X., and Zhang, Z. (2004). Interruptible load management in power market and interim system Part 2 Operation of Interruptible load. *Electr. Power Autom. Equip.* 6, 1–5. doi:10.3969/j.issn.1006-6047.2004.06.001

Xu, H., Geng, S., Qiao, Y., Xu, K., and Gu, Y. (2020). "Combining CGAN and mil for hotspot segmentation in bone scintigraphy," in ICASSP 2020 - 2020 IEEE International Conference on Acoustics, Speech and Signal Processing (ICASSP), 04-08 May 2020 (Barcelona, Spain: IEEE), 1404–1408. doi:10.1109/icassp40776.2020.9052946

Yang, B., Cao, X., Cai, Z., Yang, T., Chen, D., Gao, X., et al. (2020). "Unit commitment comprehensive optimal model considering the cost of wind power curtailment and deep peak regulation of thermal unit," in IEEE Access (IEEE), 871318–871325. doi:10.1109/ACCESS.2020.2983183

Zhang, J., Wang, L., and Liu, S. (2016). Cost-benefit analysis of load aggregator participating in interruptible load program. *South. Power Syst. Technol.* 10 (08), 74–81. doi:10.1109/PESGM.2016.7741264

frontiers | Frontiers in Energy Research

TYPE Original Research
PUBLISHED 09 August 2022
DOI 10.3389/fenrg.2022.967290

OPEN ACCESS

EDITED BY
Yang Li,
Hohai University, China

REVIEWED BY
Meng Song,
Southeast University, China
Xu Wang,
Shanghai Jiao Tong University, China

*CORRESPONDENCE
Xiangyu Ma,
maxiangyu@zju.edu.cn

SPECIALTY SECTION
This article was submitted to Smart Grids,
a section of the journal
Frontiers in Energy Research

RECEIVED 12 June 2022
ACCEPTED 12 July 2022
PUBLISHED 09 August 2022

CITATION
Xu Q, Qiao S, Zhou H, Luo R, Ma X and Gong J (2022), Mechanism design and consumption certification of differentiated green electricity trading: A Zhejiang experience.
Front. Energy Res. 10:967290.
doi: 10.3389/fenrg.2022.967290

Mechanism design and consumption certification of differentiated green electricity trading: A Zhejiang experience

Qifeng Xu[1], Songbo Qiao[1], Huijie Zhou[2,3], Renjie Luo[2], Xiangyu Ma[2,3]* and Jianrong Gong[1]

[1]Zhejiang Power Exchange Center, Hangzhou, China, [2]College of Electrical Engineering of Zhejiang University, Hangzhou, China, [3]Polytechnic Institute of Zhejiang University, Hangzhou, China

The carbon neutrality strategy marks that green electricity will replace fossil energy as the main power source in the future power system. The trading varieties in the electricity market will be more diverse, and the demand for green electricity by consumers will grow significantly. This paper innovatively proposes a provincial market framework for voluntary flexible trading of green electricity while elaborating on the conceptual design of differentiated green electricity trading processes in a systematic way for Zhejiang province. The proposed framework can not only reflect the carbon emission reduction attributes of green electricity but also fully exploit its commercial and social values. Moreover, the proposed green electricity trading certificate can realize the authoritative certification of green electricity consumption and help the construction of a carbon traceability mechanism. The proposed trading mechanism is expected to give rise to a new green electricity service industry and deepen the reform of the carbon and electricity synergy mechanism. The experience of green electricity trading in the Zhejiang province is expected to reveal the promotive impact of the electricity market on the carbon neutrality strategy.

KEYWORDS

electricity market, green electricity, differentiated trading, consumption certification, mechanism design

1 Introduction

In recent years, the issue of climate warming is continued to attract attention and a wave of global carbon emission reduction is rising. At the 75th session of the United Nations General Assembly, President Xi made an important commitment on behalf of China to the international community to "achieve peak carbon and carbon neutrality". In the process of realizing the carbon neutrality strategy, green electricity (i.e., non-water renewable energy) will become the main source of incremental energy supply in China and gradually transform into various market entities of energy supply, which requires corresponding technological and institutional innovation. As stated in gov (2021),

market-based construction is the key means to addressing the low-carbon transformation of the energy and power system. Nevertheless, how to build a differentiated green electricity trading mechanism with reasonable prices and high market satisfaction is the key challenge that has long plagued the effective synergy between the current electricity market reform and green electricity development.

At the same time, multinational enterprises and foreign trade enterprises are highly concerned about green electricity consumption in the whole industry chain, and the demand for relevant certifications is increasingly urgent. For example, internationally renowned enterprises such as Apple Apple (2020), Amazon (sustainability, 2020), and Facebook (sustainability) have also announced implementation plans for 100% green electricity supply and low-carbon emission reduction initiatives. As an eastern coastal province with a large scale of export-oriented enterprises, Zhejiang urgently needs to rely on the power trading platform to address the certification needs of corporate users to consume green electricity throughout the production and operation life cycle. Although power users should collaboratively assume the responsibility of consumption and the amount of consumption should correspond to the annual electricity consumption (zfxxgk.nea.gov, 2019), no clear green electricity quota approach and assessment methods have been introduced for power users, and no mention has been made of how to guide power users to actively participate in the consumption apportionment, and the huge user-side dormant resources have not yet been awakened. Therefore, the necessity of constructing an electricity market that can guide power users to participate in green electricity consumption is becoming more and more obvious.

Currently, some countries have initially implemented mechanisms related to green electricity trading. The United States has a variety of mechanisms to support the development of green electricity, and the system varies from state to state. The green electricity certificate mandatory trading market, or "green certificate market", promotes green electricity development through a mandatory quota system, which is essentially a secondary financial market for green electricity generation, i.e., a "separate certificate and electricity" trading mechanism. Some states have also established voluntary green electricity trading markets, and have opened a market model in which green electricity and green certificates are bundled and traded, i.e., a "certificate and electricity" system in which electricity users can voluntarily apply directly to electricity sellers or generating companies to purchase specified green electricity and obtain a "green certificate" at the same time (Overview of U.S., 2019). In addition, Europe has also established the Guarantees of Origins (GO) certificate mechanism to form a voluntary market for "green electricity", in which customers and power producers trade green electricity bilaterally across borders, and the price of electricity with GO certificates is slightly higher than that of electricity without certificates (Shi, 2019).

China has carried out an initial exploration of market-based trading of green electricity certificates ("green certificates"). 2017 saw the introduction of a voluntary subscription program for green certificates (nea.gov, 2017), and further, the introduction of a green electricity quota mechanism to promote green certificate trading (zfxxgk.nea.gov, 2019; nea.gov, 2020), which specifies that provinces and regions can allocate targets for green electricity consumption weights, and for provinces that cannot meet the quota requirements, they can purchase excess green electricity consumption from other provinces or purchase green certificates to supplement it. For provinces that cannot meet the quota requirements, they can purchase excess green electricity consumption in other provinces and regions or purchase green certificates to supplement and replace them. However, the existing green certificate mechanism is too expensive, the certification system is not yet sound, and the acceptance of users is not high, resulting in low transaction volume and making it difficult to play its proper role. Although the voluntary subscription of green certificates can guide consumers to green consumption, and to a certain extent can also alleviate the financial subsidy gap, from the fact that the difference between the amount of subscription and the amount of certification is large, the market regulation is very limited.

Furthermore, direct market-based electricity trading is an important means to promote green electricity consumption. Some scholars have conducted relevant research on green electricity trading, covering market mechanism design, trading decision optimization, green certificate accounting and issuance, market impact analysis, etc., but generally speaking, it is still in the initial stage. At the same time, the design of a green electricity trading mechanism involving the "unification of certificates and electricity" is still relatively small. In terms of the market mechanism, literature (Zhang et al., 2019a) proposed an electricity market system in the context of a renewable energy quota system; literature (He et al., 2020) proposed a market mechanism scheme in line with renewable energy quantity and price preservation, and discussed the interrelationship within the market mechanism; literature (Qian et al., 2020) explored in-depth the coordination mechanism of constructing national green certificate trading and provincial day-ahead electricity market; Literature (Shan et al., 2020) explored the construction of green electricity market from the perspectives of market mechanism and policy rules based on the experience of foreign electricity market construction; literature (Liu et al., 2020a) proposed the design of green certificate trading system for charging load aggregators. The literature (Li et al., 2019) analyzed and discussed the implementation problems and the reasons for the low trading volume of the green certificate mechanism in China and introduced the corresponding green certificate trading improvement model. In terms of market behavior decisions, literature (Zhou et al., 2020) investigated

the bidding strategies of the offering power producers in the context of the GO certificate and quota system; literature (An et al., 2017) modeled and analyzed the possibility of green electricity generators using market forces to pull up the price of green certificates in the green certificate trading market; literature (Wang et al., 2020) proposed a power insurance design scheme for power selling companies to reduce the impact of green certificate price fluctuations. The literature (Guo et al., 2020) proposes a market equilibrium model that integrates energy and green certificate trading, simulates the decision-making process of renewable energy generators, and analyzes and discusses their market behavior under different scenarios. In terms of green certificate tracking and issuance, literature (Cai et al., 2020) proposed a blockchain-based GO certificate trading platform implementation scheme to solve the green certificate tracking problem; literature (Liu et al., 2020b) further considered the calculation and allocation method of GO certificates. In terms of market impact analysis: literature (Feng, 2016) proposed a coupling model to portray carbon trading, electricity trading and green certificate trading, and analyzed the mutual influence among the three; literature (Yao et al., 2020) proposed an optimization model of electricity trading considering both green certificate market and carbon trading market, and simulated and measured the influence of carbon quota coefficient and green certificate ratio on the carbon emission reduction effect of power producers; The literature (Zhang et al., 2019b) explored the main influencing factors affecting the willingness to trade green certificates and analyzed the impact of relevant policies on green certificate pricing by constructing a marginal price dynamics model; the literature (Qu et al., 2020) established a medium- and long-term secondary trading model for green certificates under the quota system policy and measured and analyzed the national provincial green certificate market trading volume; The literature (Lin et al., 2021) constructed a market decision model considering green electricity quota system and discussed the impact of green certificate price and quota weight on market equilibrium point.

The construction of the provincial electricity market in China is still in its initial stage, and there is still a lack of effective market-based means to recover the investment costs of green electricity power plants and the supporting grid construction and operation costs, resulting in the low carbon value of green electricity not yet effectively explored, and the increasing pressure of government financial subsidies. In particular, the consumption rate of green electricity in China's receiving power system is generally low, and the market competitiveness of the relevant power generation entities is generally weak. In Zhejiang Province, for example, although green electricity is developing rapidly [expected to account for up to 26.05% in 2025 (Zhejiang Provincial Energy Adminis tration, 2021)], unit utilization hours are low [electricity generation in 2019 accounted for only 6.7% of the total social electricity consumption (gov.cn, 2020)], and green electricity units and conventional units have not been effectively distinguished in the regular market-based trading process, and the low carbon value of green electricity is seriously underestimated. In fact, Zhejiang Province needs to consume non-water renewable energy up to 7.5% of the total social electricity consumption in 2020 (nea.gov, 2020), however, due to the relative lack of utilization hours of green electricity units in the province, it is difficult to fully meet the green electricity consumption weighting target. In view of the objective status quo of green electricity scarcity in Zhejiang Province, the provincial green electricity market space in Zhejiang presents a situation of less supply than demand, which in turn has the economic foundation conditions for green electricity marketization, especially for customer-side bidding. 2020 pilot trading example in the Fan Meishan demonstration area was a complete success, which practically verified the feasibility and effectiveness of the market system for differentiated green electricity trading and laid the foundation for the official operation of the subsequent market opening. On 13 May 2021, Zhejiang Province launched the preparation of a pilot implementation plan for green electricity market-based trading, aiming to further stimulate market vitality and deepen the reform of green electricity market-based trading.

This paper provides the market design principles considering green electricity differentiated trading, constructs the corresponding trading framework system, and proposes derivative mechanisms such as green electricity trading certificates based on the operation practice and experience of Zhejiang Province. Our contributions aim to actively respond to the growing demand for green electricity consumption in the whole society, reasonably discover the value attributes of green electricity, and optimize the solution of the problem of the construction and operating costs of new power systems with renewable energy as the mainstay energy sources. The remaining contents of this article are as follows: Section 2 will introduce the green electricity market-oriented trading mechanism and market organization process; Section 3 will analyze the characteristics and connotations of green electricity differentiated trading by comparing the existing green certificate trading mechanism; Section 4 will discuss the value and extension of green electricity from the three aspects of commercial value, social value and carbon market cooperative operation; Section 5 will analyze the results in combination with simulation cases, and Section 6 will discuss practical experience and further market start-up implementation suggestions and expected results Section 7 summarizes the paper.

2 Design of green electricity differentiated trading framework

This paper follows the general idea of separating green electricity with gray electricity. Organizing differentiated trading to construct a framework system of provincial

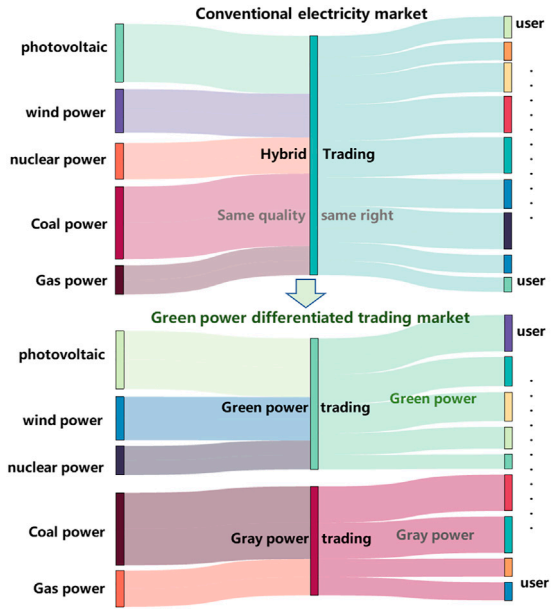

FIGURE 1
Comparison of traditional and differentiated trading.

voluntary differentiated green electricity trading market in conjunction with the actual situation in Zhejiang.

As shown in Figure 1, the conventional electricity market does not distinguish between power source categories, while power generation enterprises and consumers participate in the unified market, and all transactions are of the same quality and right, which makes it difficult to highlight the value of green electricity. Under the differentiated trading model, green electricity and traditional fossil power generation ("gray electricity") can be decoupled by setting the access conditions for market entities, and trade with consumers in batches, thus consumers' willingness can be meet to choose the quality of the purchasing power in a targeted manner, and the commodity attributes of green electricity can be fully reflected. Furthermore, the current main position of gray electricity trading can still follow the original market model. Differentiated green electricity trading is regarded as a new trading variety to open up a dedicated market module and an effective diversion of gray electricity without major adjustments to the original market system. The following parts discuss the design concept and market rules of differentiated green electricity trading.

2.1 Market access and trading mechanism

Market entities include power generation entities and consumer entities. In the initial stage of the differentiated trading market, the power generation entity is temporarily limited to green electricity power generation enterprises whose voltage and capacity meet certain conditions. Specifically, Solar, wind, and other green electricity power generation enterprises that have the national capital construction approval process and obtain or are exempt from the power business license (power generation) of 6,000 kW or above can participate in the differentiated green electricity trading as a market entity in Zhejiang province. Considering the technical constraints of metering, the consumer entities need to meet the grid access specifications, meet the technical requirements of grid security, open an independent account in the grid enterprise, separate metering and sign a formal power supply contract.

On this basis, the power trading center can regularly organize green electricity contract transactions based on market demand and transaction scale, taking annual, multi-month, and single month as the time scale, and adopting the mode of centralized bidding or listing transactions. Considering the scale and maturity of green electricity generation entities, it is more appropriate to adopt the unilateral centralized bidding model at the initial stage of the market in order to avoid collusion between power generation enterprises and keep the normal operation of the market (i.e., the demand-side entity submits the price and quantity while the generation-side entity only submits the quantity but not the price). Therefore, the following analysis only focuses on the green electricity differentiated trading model based on unilateral centralized bidding. The bidding model defaults to a unilateral centralized bidding model if no special instructions are given.

2.2 Bidding and clearing mechanism

Electricity consumers use the benchmark price of coal-fired power generation as the reference benchmark and declare the purchase price according to the market regularity. After the declaration is completed, the trading center will conduct market clearing according to the marginal price. Moreover, in the initial stage of the market, electricity consumers may not yet have the ability to make skilled market bidding decisions, and the prediction of the low carbon value of green electricity may significantly deviate. Power generation enterprises, as the recipients of the price, may have the risk of damage to their interests. Therefore, the trading center may set a price floor based on actual needs to protect the basic interests of power generation enterprises and promote the further development of the green electricity industry, while guiding consumers to discover the scarcity of the low-carbon value attached to the green electricity.

Take Zhejiang as an example, the declared price floor in annual trading is set at 10 CNY/MWh for the base price of coal-fired power generation on the grid, and the declared price floor $\underline{\rho}_m$ in monthly trading is set as follows:

$$\underline{\rho}_m = \rho_b + (\rho_c - \rho_b) \times \alpha \quad (1)$$

Where ρ_c is the annual transaction clearing price, ρ_b is the coal-fired power generation benchmark price, and α is the adjustment factor for the lower price limit. When α is 1, the lower price limit of the monthly trading declaration is the annual trading clearance price. When α is increased, the lower price limit is raised and the minimum value of green electricity is pulled up. To avoid the unintentional overvaluation of green electricity and low market participation on the demand side, it is not advisable to set too high a lower limit of the transaction price at the beginning of the market. Usually, α can be taken as 1.2, which means 1.2 times of the difference between the annual transaction clearing price and the benchmark price of coal-fired power generation feed-in price. Furthermore, when the market entities corresponding to the marginal price are not unique, the electricity quantity to be cleared in the marginal price segment is allocated in proportion to the electricity quantity declared by the market entities in that segment.

The market supply and demand balance analysis under unilateral centralized bidding by consumers is shown in Figure 2, where P_t is the benchmark feed-in price for coal-fired power generation, P_n is the ideal clearing price, and P_r is the minimum bid by consumers. The minimum bid limit is set to ensure that green electricity generators receive additional revenue corresponding to the low carbon value of green electricity (represented by the rectangular area of A + B in the figure). Moreover, the determination of the reasonableness of the minimum bid limit requires analysis and assessment based on the actual market bidding situation. Assuming that the market-clearing price is significantly higher than the set lower price limit, it indicates that the set price limit is more conservative and can ensure the smooth operation of the market in its initial stage to a certain extent. If the clearing price is close to the lower price limit for a long period of time, as shown in the bidding curve 1, it proves that the set minimum bid limit is too high and does not reasonably reflect the low carbon value of green electricity, and even inhibits the green electricity consumption demand. In this situation, if the price limit is released, the actual bid curve may shift into bidding curve 2, where the clearing price is lower than the lower price limit. The formed rectangular area of area B represents the real value of green electricity. Compared to the case of setting a price floor, the rectangular area of area A is reduced which indicates there is room for a price reduction for green electricity. In the future, under the condition that new energy subsidies are gradually withdrawn, the cost recovery of renewable energy power generation enterprises is limited, which is not conducive to promoting the healthy development of the renewable energy industry, and the willingness to promote the construction of supporting energy storage facilities may also be hindered. Therefore, setting the lower limit of the bid is conducive to guiding consumers to discover the price of green electricity and protecting the income of renewable energy generation enterprises. With the continuous development of renewable energy generation technology, the scarcity value of green electricity is gradually diluted, and green electricity will be gradually priced at parity. The price floor should be withdrawn at this time.

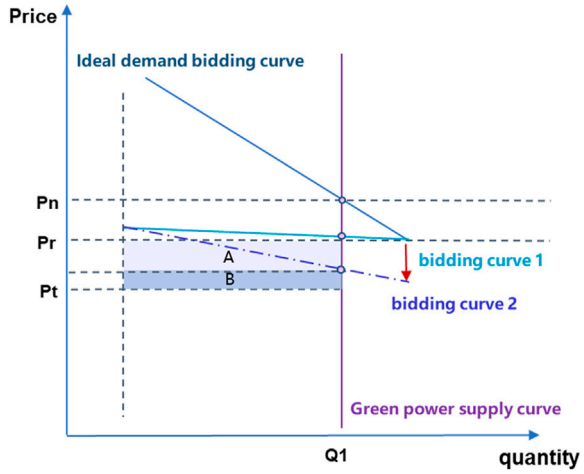

FIGURE 2
Analysis of market equilibrium under the one-sided customers' centralized bidding mode.

2.3 Settlement mechanism

The settlement of green electricity differential trading can be carried out in the way of "monthly settlement". Specifically, the uncompleted portion of the monthly contract power of each market entity will not be rolled over to the next month for settlement. The deviation will be settled according to the absolute value of the difference between the average price of the contract and the integrated price of coal-fired power generation on the grid. The actual monthly electricity generation and consumption of each market entity greater than the contracted electricity consumption are settled in accordance with the approved feed-in price and the consumer directory electricity price.

Taking Zhejiang as an example, the settlement price for consumers ρ_s^d is calculated as follows:

$$\rho_s^d = \rho_e + T + \rho_a + F \tag{2}$$

ρ_e is the green electricity clearing price, T is the transmission and distribution price (including line loss), ρ_a is the apportioned cost of auxiliary services, F is the governmental funds and surcharges. For customers with peak and valley time-sharing prices, the settlement of their time-sharing prices is based on the same range of increases or decreases in the difference between the settlement prices and catalog prices. The settlement price for power generation enterprises ρ_e is consistent with the clearing price,

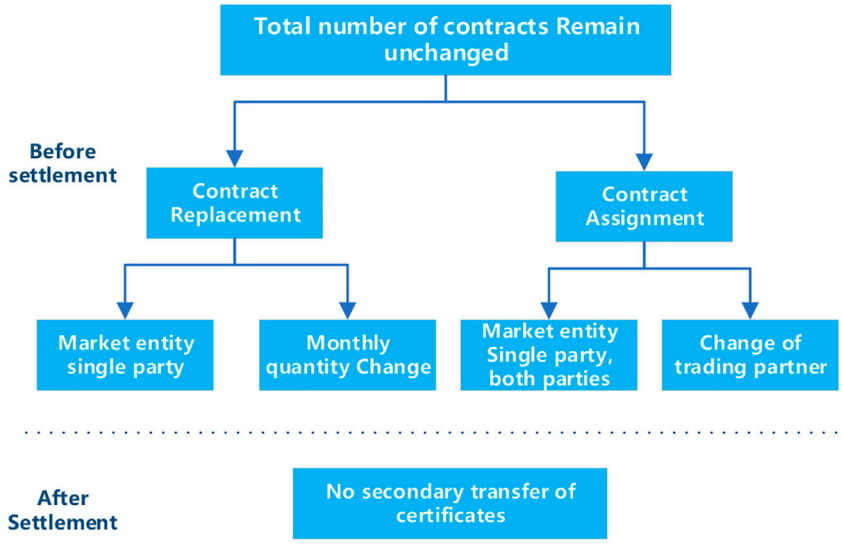

FIGURE 3
Deviation adjustment mechanism.

which includes the energy storage quota component and the discretionary income component, which is as follows:

$$\rho_e = \rho_k + G_1 \tag{3}$$

where G_1 is the unit power revenue formed by the price difference between the differentiated green electricity trading price and the benchmark feed-in price of coal-fired power generation in Zhejiang Province (converted by a proportional coefficient); ρ_k is the unit power revenue of the discretionary part of power generation enterprises. The special subsidy policy for clean energy has already provided policy subsidies to relevant power generation enterprises. If the entire share of differentiated green electricity trading is attributed to the power generation enterprises participating in the market, there is a risk of duplication of subsidies. Therefore, we should set a reasonable G_1 to guide the power generation enterprises to use part of the proceeds for the construction of energy storage quotas, and then build the positive cycle of "Take from the market, Benefit the society" on the basis of stimulating the willingness of green electricity enterprises to participate in the green electricity differentiated trading market.

2.4 Contract deviation adjustment mechanism

Market entities are required to bear the cost of deviation penalties when there are deviations in contract execution. To help market entities eliminate deviations and avoid deviation penalties, the market operation needs to consider a deviation adjustment mechanism to further improve the forecast accuracy of power generation and ensure the standardized rules.

The contract deviation adjustment mechanism is shown in Figure 3. Specifically, after reaching a green electricity transaction, market entities can adjust the transaction contract through market-based transactions including contract replacement and transfer on the premise that it does not affect the interests of related parties or the consensus of related parties. The purchase and sale of the two sides reach agreement and do not affect the implementation of other market entities' trading contract on the basis of the following month before the implementation of the transaction is allowed to adjust the subsequent months of the contract sub-month plan. However, the total number of differentiated green electricity trading contracts must remain unchanged. Based on the deviation adjustment mechanism set up, market entities can take the initiative to adjust the contract power deviation through ex-ante and ex-post contract replacement and contract transfer. However, it is worth pointing out that it is limited to contract replacement and transfer transactions before trade settlement.

2.5 Trading verification and authentication mechanism

After the green electricity transaction is completed and the contract is fulfilled, the trading center can issue the "Green electricity Trading Certificate" to the electricity consumers according to the settlement results. The certification process

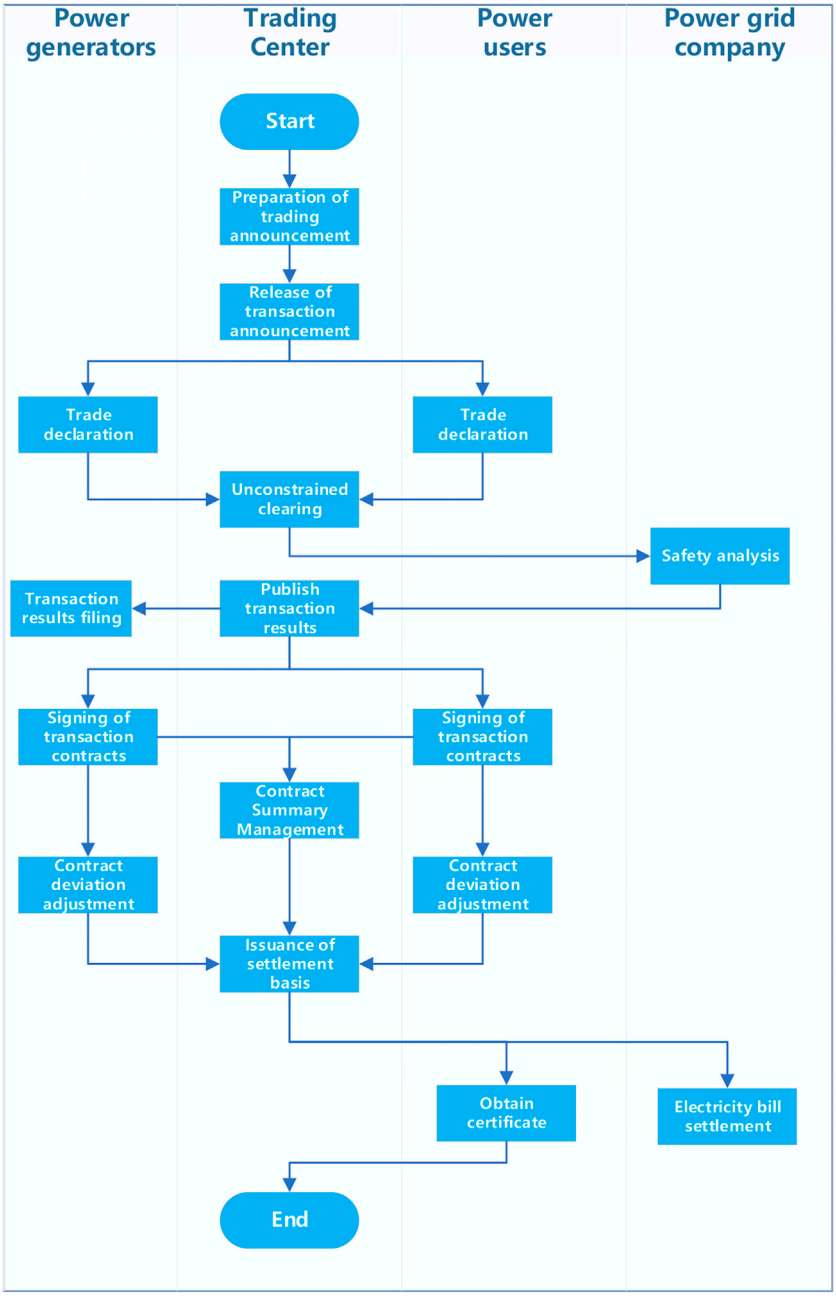

FIGURE 4
Process of market organization.

will be strictly in accordance with the settlement results record settlement power to ensure the uniqueness of the green attributes of each kilowatt-hour power purchased by the electricity consumers. It is worth pointing out that this type of certificate is mainly used to prove the authenticity of the consumer's consumption of green electricity, and cannot be transferred for secondary trading. With the gradual clarification of the principles of calculating carbon emission indicators for electricity consumption, such certificates are expected to be incorporated into the carbon emission indicator management system on their own initiative and used as the basis for reducing carbon emissions for consumers. At the same time, the issuance and certification of such certificates need to comply with the physical constraints of power balance and keep the synchronization of issuance and consumption.

Therefore, the power grid company must be deeply involved in the process of trade organization and execution of trade results, and guarantee the trade execution under the premise of ensuring the safe operation of the power grid. Especially in the initial stage of the market, the trading center and the power grid company should fully combine the actual needs of the market entities and consider the synergistic operation of the carbon market, which should play the following key roles:

1) Auxiliary role: provide a trading platform for green electricity power generation enterprises and electricity consumers, and guide market entities to discover the economic value attributes of green electricity.
2) Safeguarding role: providing power system security analysis services to safeguard the physical execution of the transaction, and strengthen the physical trading attributes of electricity.
3) Service role: it should play its own advantages in the construction of the carbon market to provide consumers with corresponding emission reduction services, and actively serve the needs of market entities to achieve their own emission reduction goals.

In summary, the organization process of green electricity differentiated trading can be summarized as shown in Figure 4. Power generation enterprises, electricity consumers, trading centers and power companies, and other multi-party entities collaborate to complete the financial settlement and physical delivery of green electricity, so as to realize the large-scale optimization of green electricity resources.

3 Differentiated trading features and connotations of green electricity

By effectively dividing the market-based trading process of green electricity and gray electricity, Green electricity differentiated trading can not only promote the zero-carbon power generation attributes of green electricity to be effectively quantified as market value but also reduce the design difficulty and reform cost of the electricity market mechanism. Moreover, the green electricity trading certificates delivered with power trading have the characteristics of traceability, which help clarify the rights and interests of green electricity consumers and stimulate the willingness of the whole society to reduce carbon emissions.

3.1 Inherent characteristics of green electricity trading certificates

Differentiated green electricity trading under the government's authorization and supervision, each market entity relies on the provincial power trading platform to bid and then produce the contract price. The trading results are physically executed, and the trading contract and settlement documents can form a strong evidence chain. On this basis, the trading center issues green electricity trading certificates to the settled green electricity based on credibility, which proves those market entities (especially consumers) have substantially participated in the green electricity trading. In turn, it is a more convenient and direct way to promote the concept of green electricity consumption to the whole society. Compared with the conventional green certificate "certification and electricity separation" mode, the green electricity trading certificate has obvious "certification and electricity unity" characteristics. In the trading process, the consumption of electricity can be traced, the footprint of carbon emission streams can be tracked, and the potential market acceptance space is large. Essentially, green electricity trading certificates are markers of the green electricity production and consumption process, which are by-products of green electricity differentiated trading. Green electricity trading certificates themselves have no additional value and cannot be separated from green electricity and traded. In contrast, the green certificate trading market is a secondary financial trading market. Taking the mandatory green certificate trading under the renewable energy quota system as an example, it lacks a mandatory binding relationship with the renewable energy power trading, but mainly stimulates the green electricity consumption demand of market entities by forming a matching relationship with the renewable energy quota system. It is worth pointing out that the differentiated green electricity trading mechanism has certain limitations in terms of flexibility in the use of certificates, which has constraints in terms of both consumption time and consumption quantity.

Table 1 presents a detailed comparison between green electricity trading certificates and conventional green certificates. On the one hand, green certificates are approved and issued on a monthly basis and are limited to onshore wind power projects and photovoltaic projects within the national renewable energy price surcharge fund subsidy catalog. The trading price of electricity corresponding to conventional green certificates is not allowed to be higher than the renewable energy price surcharge fund subsidy. Differentiated green electricity trading can be oriented to market demand and different uses, relying on the power trading platform to organize different time scales of market transactions. Differentiated green electricity trading can be also extended to biomass power generation, hydropower, and nuclear power as needed. Through market-based means, conduct reasonable pricing to a variety of clean energy carbon emission reduction values. On the other hand, the characteristics of green certificates "separation of certificates and electricity" make it difficult for consumers to strictly declare the green electricity consumption process. It is difficult for government departments and power grid enterprises to effectively track the carbon footprint, and consumers are not

TABLE 1 Comparison of green electricity trading certificates and green certificates.

Attribute	Green electricity trading certificates	Green certificates
Relying on electricity trading	Yes	No
Real power consumption	Certain	Uncertain
flexibility in the use of certificates	Limited	Flexible
Carbon-electric synergy tracking	Yes	No
Price range	Wider	Narrower
Range of market entities	Wider	Narrower
promoting the development of energy storage	Yes	No

highly motivated to participate. The green electricity trading certificate is only issued after the real delivery and settlement of electricity. The green electricity consumption and carbon emission reduction rights and interests are clearly defined. Moreover, differentiated green electricity trading based on unilateral centralized bidding by consumers can directly reflect the green electricity price level acceptable to the whole society and contribute to the integration of the electricity market and carbon trading market.

3.2 Merits of the differentiated trading mechanism

Differentiated green electricity trading explores the key role of green electricity in the process of achieving the carbon neutrality strategy through market-oriented and differentiated bilateral trading to stimulate the sustainable development of the green electricity industry after the withdrawal of government subsidies, specifically including:

1) Solve the problem that the traditional electricity market model cannot highlight the exclusive low-carbon value of green electricity. Through the establishment of a differentiated trading system, a reasonable green electricity price system will be gradually discovered and formed.
2) Promote the construction of supply capacity and cultivation of the consumption system of green electricity. Guide the flow of funds in the direction of increasing social welfare by enhancing the adaptability of the power system to green electricity.
3) Facilitate bilateral matchmaking of market entities. Discover the true value of green electricity through transaction price signals, relieve the pressure of the national green electricity subsidy funding gap, and provide a transition path for green electricity subsidy withdrawal.
4) Help enterprises to enhance their international competitiveness and social responsibility. Both foreign-funded enterprises, export-oriented enterprises, and high-energy-consuming enterprises can hedge their business risks under the pressure of carbon emission reduction in advance by participating in green electricity trading.

Green electricity differential trading is essentially a customized market mechanism for green electricity special trading in the medium and long-term electricity market environment. To realize the diversion of green electricity and gray electricity in the electricity market operation stage, its main differences from the traditional medium and long-term electricity market can be divided into three aspects: trading timing, market entities and trading methods, which are as follows:

1) Trading timing: differentiated green electricity trading in the total monthly electricity consumption of consumers has priority over ordinary direct trading and electricity sales market to conduct settlement, which aims to achieve the diversion of green electricity and gray electricity in the time scale.
2) Market entity: the traditional medium and long-term electricity market in the power generation entity, no restrictions on the type of power generation, coal power units, and gas units can participate. While the green electricity differentiated trading market has an entry threshold, limited to green electricity enterprises and electricity consumers to participate. The gray electricity represented by coal power is diverted to the traditional medium and long-term electricity market for trading, to realize the differentiation of market entities. It is worth emphasizing that, unlike ordinary direct trading policy price reductions that require considerable consumer access thresholds, green electricity is traded competitively with no thresholds required for consumers. Therefore, it is a truly voluntary market. As the market develops and matures, non-operating consumers including individuals can participate, which will greatly enrich the participation of green electricity trading, importing traffic for the market, and promoting market prosperity.

3) Trading method: the traditional medium and long-term electricity market in the centralized bidding trading method usually uses the seller and the buyer are both submit quantity and price, while the green electricity differential trading uses the demand-side submits quantity and price, the power generation enterprises only submit quantity for centralized clearing. Furthermore, Green electricity can be designed as a standard product and sold on the trading counter (OTC) with reference to the annual trading price according to market conditions. For example, for residential consumers, the price is increased by one cent per kWh, and 100 kWh is one trading unit, which can be bought and sold immediately. This will greatly reduce the complexity of trading and the threshold of participation to truly achieve the popularity of green electricity trading.

4 Value and outreach of differentiated green electricity trading

Market-oriented and differentiated intra-provincial green electricity trading is not only an effective transition for green electricity generation entities in the Zhejiang power system to participate in the electricity market, but also an important exploration to relieve the pressure of government financial subsidies. It has important commercial and social values to awaken the consensus of carbon neutrality strategy in the whole society and guide the transformation of the energy supply side.

4.1 The value space of green electricity trading

"Green, low-carbon, clean and environmental protection" will be the core competitiveness of multinational enterprises and foreign trade enterprises to participate in international trade under the pressure of global carbon emission reduction. For example, Europe has gradually implemented a carbon tax policy. Green electricity consumption can bring tangible economic benefits to enterprises. It is also an important step to enhance the image of enterprises' social responsibility. Important technology giants such as Apple and Facebook have already reaped wide acclaim for announcing and implementing green electricity programs. In this context, multinational and foreign trade enterprises that are in urgent need of environmental protection or carbon emission reduction recognition can participate in differentiated green electricity trading and obtain credible certification from provincial power trading centers, while being able to gain revenue or reduce corresponding expenses in the carbon emission market.

Currently, China has started to implement an enterprise-level carbon emission quota system, which has greatly increased the demand for lower carbon emissions from electricity consumers, implying a potentially broad market demand for green electricity with low-carbon attributes. In addition, China's Ministry of Ecology and Environment has made further regulation of national carbon emissions trading (Measures for the Administration, 2020). However, at present, China is still in the initial stage of carbon emission reduction process, and the carbon emission reduction technology of each market entity is not yet perfect, so carbon emission rights will have a large market demand. At the same time, in order to reduce carbon emissions of the power system to achieve the goal of carbon peak, it is still necessary to further cultivate green electricity enterprises and their supporting industrial construction. Therefore, it is especially important to lead and encourage the orderly development of the green electricity industry chain through market-based means, and further release low-carbon values to meet the carbon emission reduction needs of corporate consumers.

The differentiated green electricity trading mechanism is significantly different from that of gray electricity trading, which can play a positive incentive and guiding role in the development of the green electricity industry and further empower the whole society to make the low-carbon transformation. The differentiated green electricity trading highlights the added value of green electricity, which can not only broaden the profit channel of green electricity generation enterprises but also transfer the carbon emission reduction cost from the energy supply side to the demand side, thus helping to form a carbon neutrality strategy consensus in the whole society and forcing the structural transformation of the energy supply side. Furthermore, it can encourage green electricity power generation enterprises to help the construction of new power systems in a more active and forward-looking way by guiding the surplus funds of differentiated green electricity trading to be used for the construction of energy storage quota according to a certain proportion.

4.2 Cohesive and coherence with carbon emission allowances

The National Development and Reform Commission issued the "Corporate Greenhouse Gas Emissions Accounting Measures", which has explicitly included the carbon emissions embedded in the net purchased electricity of enterprises into the scope of corporate carbon emission calculation (ndrc.gov, 2013). However, the electricity carbon emission calculation of enterprises in China is still based on the emission factors of electricity consumption in their regions. Therefore, in order to further release the outward application value of green electricity trading certificates, it is necessary to differentiate the calculation of carbon emissions of electricity consumption of enterprise users, reflecting the low carbon benefits that users consuming

green electricity should have. Specifically, power users can choose to purchase relatively high-cost green electricity and relatively low-cost gray electricity, and the price difference between the two reflects the low carbon value obtained by power users. With the further establishment of a national carbon trading market, the carbon allowance system will stimulate companies to create a real demand for constraining their own carbon emissions.

In fact, green electricity production and consumption are natural measures of carbon emissions reduction. The corresponding differentiated green electricity trading can also accurately measure and calibrate the carbon reduction cost and contribution of the whole society. Moreover, green electricity trading certificates are effective proof of the physical delivery of green electricity for consumers. Compared to the consumption of gray electricity, it reduces the enterprise's own carbon emissions. With the continuous improvement of carbon trading, the purchase price difference based on green electricity and carbon emission rights may become one of the profit ways for electricity consumers. Specifically, consumers who switch from using gray electricity to using 100% green electricity or those who generate carbon surplus can trade their surplus carbon emission rights to gain economic benefits. However, the final revenue still depends on the price level of green electricity differentiated trading and carbon trading.

Theoretically, meeting carbon allowance requirements can be divided into indirect method and direct method. The indirect method refers to the market entity buying the remaining carbon emission allowances of other market entities by participating in the carbon market. The direct method refers to the direct adoption of emission reduction means by market entities to reduce their own carbon emissions. Green electricity differential trading is precisely to provide electricity consumers with new options in addition to the conventional carbon emission trading varieties. This means that consumers can not only indirectly meet carbon emission allowances by purchasing carbon emission rights but also directly reduce carbon emissions by purchasing green electricity.

In summary, as shown in Figure 5, promoting the use of green electricity consumption certification as a certification mechanism for cutting carbon emissions is conducive to encouraging the development of the green electricity industry and helps provide a channel for green electricity consumption certification for enterprises, which enhances the competitiveness of Zhejiang enterprises in green trade. It also helps to realize enterprise carbon verification to prove the carbon footprint of products. From the perspective of promoting the construction of a carbon market, promoting the construction of green electricity differentiated trading market is precisely a practical attempt to realize the synergistic operation of the electricity market and carbon market and jointly serve the carbon neutrality strategy, which is expected to release additional social and environmental values. Combined with Zhejiang's practical experience, two possible cohesive mechanisms are proposed as follows:

FIGURE 5
Applications of green electricity trading certificate.

1) Promote as soon as possible the transformation of green electricity trading certificates from common in Zhejiang province to national common certificates. At the same time, the international influence of China's green electricity certification will be enhanced to further promote the development of the green trade industry.
2) Scientifically design the mutual recognition and deduction mechanism between green electricity trading certificates and carbon emission management indicators (such as peer-to-peer conversion). The certificate can be directly calculated as carbon emission reduction by a certain factor.

5 Simulation analysis

In December 2020, the Zhejiang Provincial Power Trading Center organized the first pilot green electricity market-based trading in Ningbo Fan Meishan Highly Resilient Grid Demonstration Zone. Green electricity generation enterprise and power user complete green power trading through bilateral negotiations with the trading price for the feed-in tariff up 0.01 RMB/kWh. The scale of traded green electricity is about 14 million kWh from December 1st to 31st, 2020, which attracted wide attention from society and provided Zhejiang experience of green electricity trading.

Furthermore, to demonstrate in detail the process of green electricity differentiated trading based on unilateral centralized bidding by consumers, three scenarios are considered: 1) green electricity is in short supply; 2) green electricity is in oversupply

TABLE 2 Buyer's bidding behaviors of three scenarios.

Scenario name	Buyer entity	Price 1/CNY	Quantity 1/MWh	Price 2/CNY	Quantity 2/MWh	Price 3/CNY	Quantity 3/MWh
Scenario 1	A	380	2,000	387	1,000	401	1,000
	B	379	2,500	385	1,400	400	1,100
	C	376	2,000	385	2000	397	2000
	D	382	3,000	390	1,200	407	800
	E	374	4,000	379	2,800	389	1,200
	F	381	2,000	389	1,200	405	800
	G	375	3,000	382	1,500	390	500
Scenario 2	A	366	1,800	378	1,200	386	1,000
	B	357	2,000	375	1,600	382	1,600
	C	368	2,000	379	1,200	388	800
	D	355	2,000	365	1,400	379	1,200
	E	363	1,500	376	1,200	384	1,000
	F	356	1,500	372	1,500	381	800
	G	364	2,000	377	1,500	385	800
Scenario 3	A	346	1,500	353	1,200	368	1,000
	B	348	1,800	354	1,200	369	1,000
	C	346	1,500	351	1,500	366	800
	D	347	2,000	354	1,500	369	800
	E	348	2,000	355	1,200	372	800
	F	345	2,000	350	1,400	365	1,200
	G	346	2,000	352	1,600	367	1,600

with minimum price limit protection; 3) green electricity is in oversupply without minimum price limit.

5.1 Market declaration stage

Assuming the benchmark price of coal-fired power generation is 345 CNY/MWh and the minimum price limit is 10 CNY/MWh above the benchmark price of coal-fired power generation. There are 5 green electricity plants (including 2 wind farms and 3 photovoltaic farms). The seller entities of green electricity (power generation enterprises) participate in the market declaration by only submitting the quantity but not price. The buyer entities (power users) are 7 foreign trade enterprises (including textile group A, textile group B, refining group C, refining group D, electromechanical manufacturing group E, automobile group F, and automobile group G).

Scenario 1: The declared information by the buyer entities and their bids are shown in Table 2. The total quantity declared by the buyer is 37,000 MWh and the total quantity declared by the seller is 33,000 MWh. Since the market indicates that the demand for green electricity exceeds the supply, it is more likely that the power declared by the buyer entities will not all win the bid, and thus there may be a higher declared price. The highest bid of the seven buyer entities is 401 CNY/MWh, the lowest bid is 374 CNY/MWh, and the average bid price is 383.78 CNY/MWh.

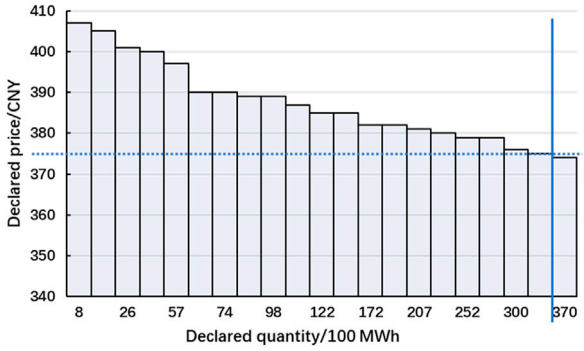

FIGURE 6
The results of clearing in the market of Scenario 1.

TABLE 3 Buyer's winning bid of Scenario 1.

Buyer entity	Declared quantity/MWh	Clearing quantity/MWh
A	4,000	4,000
B	5,000	5,000
C	6,000	6,000
D	5,000	5,000
E	8,000	4,000
F	4,000	4,000
G	5,000	5,000

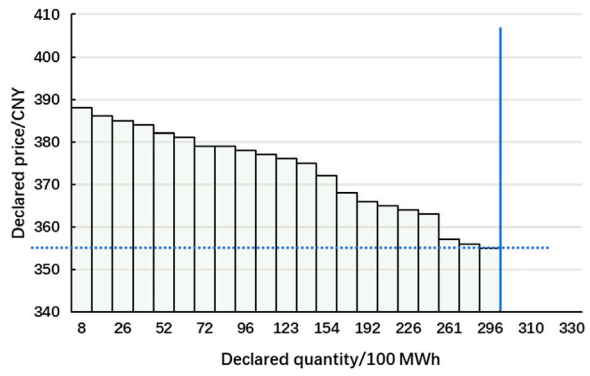

FIGURE 7
The results of clearing in the market of Scenario 2.

Scenario 2: the total declared volume of buyers is 29600 MWh and the total declared volume of sellers is still 33000 MWh. Due to the oversupply state of the market, the probability of not winning the bid for the buyer entities is relatively low. The highest declared price of seven buyer entities is $388/MWh and the lowest declared price is $355/MWh, which triggers the minimum price limit and the average declared price is 370.90/MWh.

Scenario 3: The total quantity of green electricity declared by buyers and sellers is the same as in Scenario 2, and the lowest declared price of the seven buyer entities is 345 CNY/MWh, the highest declared price is 372 CNY/MWh, and the average declared price is 353.69/MWh. Since green electricity is in oversupply and there is no protection of the lowest declared price limit, the buyer entities may use the market power to make the average declared price significantly lower compared with other scenarios.

5.2 Analysis of market clearing results

Scenario 1: As shown in Figure 6, the overall supply of green electricity is in short supply, the final traded volume is 33000 MWh, the clearing price is 375 CNY/MWh, and the market entity corresponding to the marginal electricity price is power user E. Table 3 is the specific winning bid of the buyer entities. As shown in Table 3, among the seven buyer entities, except for the power user E which has not won the bid in full, the rest of the power users' declared quantity of green electricity is fully traded.

Scenario 2: The total quantity of green electricity declared by the buyer entities is 29,600 MWh and the total quantity declared by the seller entities is 33,000 MWh, which indicates the green electricity oversupply. As shown in Figure 7, the final traded volume is 29,600 MWh, and the clearing price is 355 CNY/MWh, which is close to the lowest price limit. At this time, all buyer entities win the bids, while the winning bids of seller entities need to be allocated according to the declared quantity. The market clearing results are shown in Table 4.

Scenario 3: The green electricity still shows oversupply and the seller's clearing power allocation is consistent with Scenario 2. As shown in Figure 8, the final traded quantity is 29,600 MWh, and the corresponding unified clearing price is 345 CNY/MWh, which is close to the benchmark price of coal power. The clearing results show that the low carbon value of green electricity can hardly be effectively reflected in the oversupply scenario if the protection of the minimum bid limit is lost.

5.3 Market settlement

Without considering the transmission and distribution price (including line loss) and the apportionment cost of auxiliary services, the settlement of each market entity can be calculated and analyzed based on formula (2) and formula (3).

Scenario 1: Since the difference between the benchmark price of coal-fired power generation and the price of green electricity is 30 yuan/MWh, G1 should be 15 yuan/MWh (assuming that the proportion of allocated funds for energy storage priority construction is 50% and all electricity revenue paid to the power generation enterprise). The five seller entities received electricity revenue of 1.875 million yuan, 2.25 million yuan, 1.5 million yuan, 2.625 million yuan, and 4.125 million yuan

TABLE 4 Seller's winning bid of Scenario 2.

Seller entity	Declared quantity/MWh	Declared quantity percentage/%	Clearing quantity/MWh
A	5,000	15.15	4,484.85
B	6,000	18.18	5,381.82
C	4,000	12.12	3,587.88
D	7,000	21.21	6,278.79
E	11,000	33.33	9,866.67

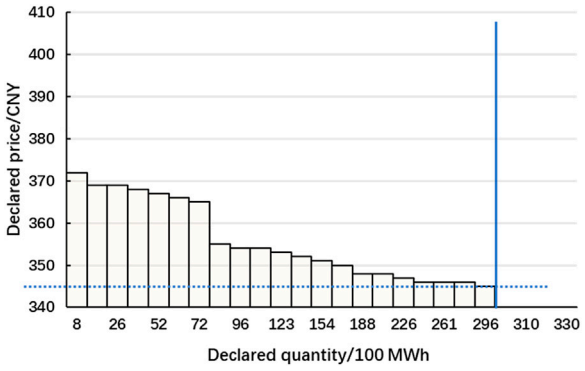

FIGURE 8
The results of clearing in the market of Scenario 3.

respectively, and the power generator obtained considerable income; while the 7 buyer entities spent 1.5 million yuan, 1.875 million yuan, 2.25 million yuan, 1.875 million yuan, 1.5 million yuan, 1.5 million yuan, and 1.875 million yuan respectively, and the detailed transaction situation and the allocation of energy storage priority construction funds are shown in Table 5.

Scenario 2: The settlement results are shown in Table 5. In the oversupply situation of green electricity, the buyer entity is less likely to not win the bid, which leads to a clearing price close to the minimum price limit. Although the revenue of seller entities decreases compared to the scenario of green electricity demand exceeding supply, they still earn additional revenue compared to the benchmark price of coal power, and the green electricity differentiated trading market is still attractive. Moreover, the settlement results also indicate that in the initial stage of the market, the scale of market entities should be expanded as much as possible. Power users should be actively cultivated and encouraged to participate in the green electricity differentiated trading market to promote the discovery of green electricity value for maintaining the stable market operation.

Scenario 3: The market settlement result is shown in Table 5. Without considering the minimum declared price limit, the low bid price of the buyer entity in the oversupply scenario may lead to serious damage to the interests of seller entities and weaken their driving force to participate in the green electricity differentiated trading, which is not conducive to the smooth start of the market. Therefore, if the scale of the buyer entities is significantly smaller than the seller entities, a minimum price limit should be established to protect the basic interests of seller entities and promote the expansion of the market scale of green electricity differentiated trading.

5.4 Pricing mechanism

The above clearing and settlement analyses all use the uniform clearing price mechanism. However, in terms of pricing mechanism, there are two mainstream models namely unified clearing pricing and pay-as-bid pricing. In the case of pay-as-bid pricing, the buyer entity is required to settle separately according to its price and the corresponding quantity, and the seller entity is required to settle in proportion to the amount of declared quantity because the seller entities don't offer price. Take Scenario 2 as an example, the market settlement using the pay-as-bid pricing mechanism is shown in Table 6.

As shown in Table 6, it can be seen that the adoption of the pay-as-bid pricing model can result in more additional green electricity benefits for the seller entity. However, it is also necessary to consider the possible impact of adopting the pay-as-bid pricing model on the bidding behavior of the buyer entity.

As the buyer entity needs to settle according to the declared price, compared with the unified pricing mechanism, the buyer entity's enthusiasm to achieve the full amount of the winning bid by increasing the bid price is inhibited. Therefore, the probability of a high bid price is relatively low. Especially in the situation of green electricity oversupply, the buyer entity may further depress the green electricity price level. In turn, it may cause the main interests of seller entities to be damaged, which is not conducive to the discovery of the low carbon value of green electricity. In addition, the adoption of the pay-as-bid pricing model as shown in Table 6 may result in the differences of green electricity purchase prices among buyer entities, which is not conducive to enhancing power users' recognition of the fairness of

TABLE 5 Settlement of the differentiated green electricity trading market of three scenarios.

Scenario name	Buyer entity	Electricity cost/ten thousand CNY	Seller entity	Electricity revenue/ten thousand CNY	Energy storage funds/ten thousand CNY
Scenario 1	A	150	A	187.5	7.5
	B	187.5	B	225	9
	C	225	C	150	6
	D	187.5	D	262.5	10.5
	E	150	E	412.5	16.5
	F	150			
	G	187.5			
Scenario 2	A	142	A	159.21	2.24
	B	184.6	B	191.05	2.69
	C	142	C	127.37	1.79
	D	163.3	D	222.90	3.14
	E	131.35	E	350.27	4.93
	F	134.9			
	G	152.65			
Scenario 3	A	127.65	A	154.73	0
	B	138	B	185.67	0
	C	131.1	C	123.78	0
	D	148.35	D	216.62	0
	E	138	E	340.40	0
	F	158.7			
	G	179.4			

TABLE 6 Settlement of market entity under the paid as bid mechanism.

Seller entity	Electricity revenue/ten thousand CNY	Revenue change/ten thousand CNY	Average electricity price CNY/MWh
A	166.34	+7.13	370.90
B	199.61	+8.56	370.90
C	133.07	+5.70	370.90
D	232.88	+9.98	370.90
E	365.95	+15.69	370.90

Buyer entity	Electricity cost/ten thousand CNY	Cost change/ten thousand CNY	Average electricity price CNY/MWh
A	149.84	+7.84	374.60
B	192.52	+7.92	370.23
C	150.12	+8.12	375.30
D	167.58	+4.28	364.30
E	137.97	+6.62	372.89
F	139.68	+4.78	367.58
G	160.15	+7.5	372.44

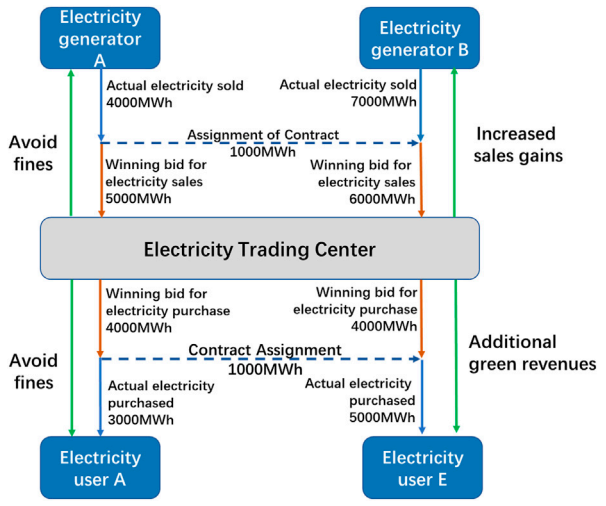

FIGURE 9
Case of contract deviation adjustment.

differentiated green electricity trading. Furthermore, users may pay higher fees which results in a poorer sense of market experience for users compared to the unified clearing pricing mechanism. Therefore, in the early stage of the green electricity differentiated trading market, it is more appropriate to adopt the uniform clearing pricing mechanism.

5.5 Deviation adjustment mechanism

Considering the randomness and volatility of green electricity generation, there may be deviations in the actual execution of the contract. Take Scenario 1 as an example. As shown in Figure 9, assume that power generator A forecasts its actual monthly green electricity generation to be 4000 MWh, which is lower than the contract quantity. Power generator B forecasts its actual green electricity generation to be 7000 MWh, which is higher than the contract quantity. According to the market rules, the over-generated portion can only be settled at the benchmark price of coal-fired power generation.

If power generator A and power generator B can transfer part of the contract power, then power generator A can avoid the annual settlement penalty of 30,000 CNY and power generator B makes an additional profit of 30,000 CNY (15,000 CNY of which can be used for supporting energy storage construction in priority) relative to the settlement at the base price of coal-fired power generation, achieving mutual benefit and a win-win situation. Another case considers there is a deviation in the green electricity consumption of users. Assuming that the actual electricity consumption of power user A is 3000 MWh, which is lower than the contract quantity of 1000 MWh, a penalty of 30,000,000 CNY shall be paid by power user A according to the market rules. However, if power user A transfers 1000 MWh to power user E, then power user E purchases additional green electricity in need, and power user A avoids paying the penalty. The total green electricity traded volume is not reduced severely by the change in actual power generation, thus realizing a win-win situation for the market operator, power users, and generators.

5.6 Analysis of implementation effect

Take Scenario 1 as an example as well. For the seller entity, the profit space is further enhanced (additional profit of 150,000 CNY, 180,000 CNY, 120,000 CNY, 210,000 CNY, and 330,000 CNY respectively) compared with the direct settlement based on the coal-fired power generation benchmark feed-in tariff. For the buyer entity, although it pays an extra cost of 30 CNY/MWh for green electricity, it can obtain green electricity trading certificates to enhance the competitiveness and honor of international trade. Furthermore, with the continuous improvement of the carbon emission index certification mechanism, the buyer entity has the opportunity to obtain additional benefits of carbon emission reduction. For instance, the formula for calculating the net purchased electricity carbon emissions of enterprises (ndrc.gov, 2013) indicates that net purchased electricity carbon emissions = net purchased electricity × electricity consumption emission factor in the region. It is possible that the electricity consumption emission factor corresponding to the part of green electricity purchased by users can be adjusted to 0, thus reducing the risk of purchasing carbon emission rights due to carbon emission overage. According to Scenario 1, the total CO2 reduction for customers is 13,200 tons assuming a carbon emission factor is 0.4tCO2/MWh. In terms of social welfare, a total of 495,000 CNY funds can be used for the green electricity storage quota construction project to continuously promote the low-carbon development of power systems.

6 Experiences and suggestions of differentiated green electricity trading

The successful implementation of the pilot trading in the Fan Meishan demonstration zone in Zhejiang Province means that the basic links and key processes of green electricity differentiated trading have been effectively verified. At present, the provincial electricity market still stays at the stage of promoting green electricity trading and consumption. In order to fully release the potential market value of green electricity and promote the formation of the environmental protection concept of “energy transition and green development”, the green electricity

differentiated trading mechanism needs to be further improved in the following aspects:

6.1 Market entity cultivation

It is recommended to conduct in-depth research on the needs of market entities. Through the digital training system and cloud training platform, providing training services for the whole process of differentiated green electricity trading operation, thereby improving the maturity, satisfaction, and sense of acquisition of market entities. Moreover, it should also fully draw on the experience of power demand-side response trial operation, actively guide eligible market entities to participate in the trial operation of green electricity differentiated trading through market invitation and participation incentives, etc.

6.2 Credit supervision and management

It is recommended to actively introduce third-party credit institutions and power trading platforms to supervise the signing of green electricity trading contracts and strengthen the credit supervision of market entities. In addition, the performance of market entities is included in the credit appraisal system. Adopt punitive measures for market entities with behaviors that disrupt market trading order and untrustworthy conduct following law and compliance, thereby ensuring orderly market operation. In addition, the introduction of blockchain technology is considered to build a security management mechanism for the whole life cycle of green electricity trading certificates covering issuance, maintenance, and audit functions to strictly prevent double counting and invalid issuance. The green electricity trading certificates adopts the issuance method of "one certificate and one code" to ensure the authenticity of green electricity consumption based on the technical advantage of blockchain technology of data traceability and anti-tampering. Furthermore, the security and trustworthiness of the blockchain-based consumer certification platform can further simplify the certification process of carbon emission reduction and reduce the cost of using the certificate.

7 Conclusion

This paper makes the mainly following contributions to meeting the growing demand for green electricity consumption in Zhejiang Province:

- This paper illustrates the design of a differentiated green electricity trading mechanism applicable to the Zhejiang objective situation and sustainable development needs combining the practical experience of electricity market reform with carbon neutrality strategy in Zhejiang province.
- This paper provides a market mechanism to support the low-carbon transformation of China's receiving-end power system and alleviate the pressure of government financial subsidies.
- The proposed derivative mechanisms such as green electricity trading certificates can meet the practical needs of power users for green electricity consumption certification and explore new paths to further enhance China's international trade image.

We hope that this paper and the related practice in Zhejiang Province can inspire more policymakers and researchers to further improve the green electricity market trading mechanism. Our next work aims to optimize the operation mode and product design to explore the path of market-oriented reform of the green power system.

Data availability statement

The original contributions presented in the study are included in the article/supplementary material, further inquiries can be directed to the corresponding author.

Author contributions

QX and SQ contributed to writing parts of the manuscript and the conceptual design of the market mechanism. HZ and RL contributed to the revision of manuscript and provided useful suggestions. XM contributed to writing parts manuscripts and designing the structure of manuscript. JG contributed to the improvement of the market mechanism design.

Funding

This work is supported by the Science and Technology Project of State Grid Zhejiang Electric Power Company Limited (No. B311DJ220002).

Conflict of interest

The authors declare that the research was conducted in the absence of any commercial or financial relationships that could be construed as a potential conflict of interest.

Publisher's note

References

An, X., Zhang, S., and Xue, L. I. (2017). Equilibrium analysis of oligopolistic electricity markets considering tradable green certificates[J]. *Automation Electr. Power Syst.* 41 (09), 84–89. doi:10.7500/AEPS20160516008

Apple (2020). Apple commits to be 100 percent carbon neutral for its supply chain and products by 2030[EB/OL]. Available at: https://www.apple.com/newsroom/2020/07/apple-commits-to-be-100-percent-carbon-neutral-for-its-supply-chain-and-products-by-2030/(Accessed 07 21, 2020).

Cai, Y., Gu, Y., Luo, G., Jenkinsd, D., McCallumd, P., Peacockd, A., et al. (2020). Blockchain based trading platform of green power certificate: Concept and practice [J]. *Automation Electr. Power Syst.* 44 (15), 1–9. doi:10.1016/j.rser.2018.10.014

Feng, Tiantian (2016). Coupling induction analysis model of tradable green certificates and carbon emission trading acting on electricity market in China[D]. *Resour. Conservation Recycl.* 163, 105487. doi:10.1016/j.resconrec.2021.105487

gov (2021). Guiding opinions of the state council on accelerating the establishment and improvement of a green and low-carbon circular development economic system[EB/OL]. Available at: http://www.gov.cn/zhengce/content/2021-02/22/content_5588274.htm(Accessed 02 02, 2021).

gov.cn (2020). Announcement of the national energy administration on the 2019 national renewable energy development monitoring and evaluation. Available at: http://www.gov.cn/zhengce/zhengceku/2020-05/16/content_5512148.htm (Accessed 05 06, 2020).

Guo, H., Qixin, C., Qing, X., and Kang, C. (2020). Modeling strategic behaviors of renewable energy with joint consideration on energy and tradable green certificate markets. *IEEE Trans. Power Syst.* 35 (3), 1898–1910. doi:10.1109/tpwrs.2019.2953114

He, J., Xu, S., Mi, C., Yu, T., et al. (2020). Design improvement of renewable portfolio standard, green electricity certificate and carbon trading mechanisms against a background of electric spot market[J]. *Sino-Global Energy.* 25 (10), 19–25.

Li, Z., Wang, C., Ye, X., Wang, W., and Hao, S. (2019). China's green certificate trading mode design and trading volume evaluation model establishment. *Chin. Autom. Congr.* 2019, 4868–4872. doi:10.1109/CAC48633.2019.8996576

Lin, X., Zeng, J., and Feng, D. (2021). Optimization decision model of electricity market under renewable portfolio standards[J]. *Automation Electr. Power Syst.* 45 (06), 158–168. doi:10.1016/j.gloei.2021.07.007

Liu, D., Liu, M., Wang, W., Peng, X., Xv, C., and Wang, J. (2020). Operation mode and key technology of charging load aggregator participating in green certificate trading[J]. *Automation Electr. Power Syst.* 44 (10), 1–9. doi:10.7500/AEPS20190813005

Liu, Q., Yuan, H., Yang, Z., Fan, H., and Xu, C. (2020). Discussion on compensation ancillary service scheme of green certificates based on renewable portfolio standard[J]. *Automation Electr. Power Syst.* 44 (06), 1–8. doi:10.7500/AEPS20191108007

Measures for the Administration (2020). Measures for the administration of carbon emissions trading (for trial implementation). Available at: http://www.gov.cn/gongbao/content/2021/content_5591410.htm (Accessed 12 25, 2020).

ndrc.gov (2013). Notice of the general office of the national development and reform commission on issuing the first batch of accounting methods and reporting guidelines for Greenhouse gas emissions by enterprises in 10 industries (for trial implementation). Available at: https://www.ndrc.gov.cn/xxgk/zcfb/tz/201311/t20131101_963960.html (Accessed 10 15, 2013).

nea.gov (2020). Notice of the national development and reform commission and the national energy administration on issuing the responsibility weights of renewable energy electricity consumption in provincial administrative regions in. Available at: http://www.nea.gov.cn/2020-06/01/c_139105253.htmp (Accessed 06 01, 2020).

nea.gov (2017). Notice of the national development and reform commission, the Ministry of finance and the national energy administration on the trial implementation of the renewable energy green power certificate issuance and voluntary subscription trading mechanism. Available at: http://www.nea.gov.cn/2017-02/06/c_136035626.htm (Accessed 02 06, 2017).

Overview of U.S. (2019). Green power market[EB/OL]. Available at: https://www.wri.org.cn/green-power-market-us-experience (Accessed 02 01, 2019).

Qian, P., Zhou, X., and Yang, R. (2020). Design of coordination and balance mechanism between national green power certificate trading market and provincial day-ahead power market[J]. *Power Syst. Technol.* 44 (07), 2565–2571.

Qu, M., Ding, T., Bai, J., He, Y., Liu, R., and Chen, T. (2020). Green certificate transaction analysis in China under responsibility for non-water renewable energy integration ratio. Power system technology[J]. *Power Syst. Technol.* 44 (10), 3885–3894. doi:10.13335/j.1000-3673.pst.2019.2405

Shan, M., Tang, H., Geng, M., Cao, Y., Yang, Z., and Wang, Y. (2020). Essential cause and design thinking of green electricity market[J]. *Automation Electr. Power Syst.* 44 (16), 12–20. doi:10.7500/AEPS20200109003

Shi, Jingli (2019). Comparison and enlightenment: The pros and cons of green certificate mechanisms in Europe, the United States and China. *Energy* (11), 37–40.

sustainability (2020). Amazon sustainability all in: Staying the course on our commitment to sustainability[EB/OL]. Available at: https://sustainability.aboutamazon.com/?energyType=true&workerCount=true&engagementProgram=true&productCategory=true (Accessed 12 01, 2020).

sustainability Facebook's net zero commitment[EB/OL]. Available at: https://sustainability.fb.com/our-climate-commitment/.

Wang, T., Wang, H., Leng, Y., Chen, B., Wang, J., and Zhao, W. (2020). Power insurance based support optimal decision of electricity market subjects[J]. *Automation Electr. Power Syst.* 44 (12), 56–63. doi:10.7500/AEPS20190426003

Yao, J., He, J., Wu, Y., et al. (2020). Energy optimization of electricity wholesale market with carbon emissions trading and green power certificate trading system[J. *J. Electr. Power.*, 1–9.

zfxxgk.nea.gov (2019). Notice of the national development and reform commission and the national energy administration on establishing and improving the guarantee mechanism for renewable energy consumption[EB/OL]. Available at: http://zfxxgk.nea.gov.cn/auto87/201905/t20190515_3662.htm (Accessed 05 10, 2019).

Zhang, H., Zhao, Q., Shi, J., Ye, X., and Zhang, X. (2019). Research on the trading pricing strategy of Chinese tradable green certificate[J]. *Price Theory & Pract.* 423 (09), 42–45.

Zhang, X., Zheng, C., Ma, Z., Zhanga, Z., Shib, Y., Lia, W., et al. (2019). Study on electricity market trading system Adapting to renewable portfolio standard[J]. *Power Syst. Technol.* 43 (08), 2682–2690. doi:10.1016/j.egyr.2021.08.119

Zhejiang Provincial Energy Administration (2021). The 14th five-year plan for energy development in Zhejiang province (draft for solicitation of comments. Available at: http://fzggw.zj.gov.cn/art/2021/3/12/art_1229123367_2251024.html (Accessed 03 12, 2021).

Zhou, X., Peng, Q., Yang, R., Han, Z., Wang, M., et al. (2020). Power price marketing strategy of comprehensive energy-based electricity sales company participating in electricity market competition under ubiquitous environment of internet of things[J]. *Power Syst. Technol.* 44 (04), 1317–1324. doi:10.13335/j.1000-3673.pst.2019.1906

frontiers | Frontiers in Energy Research

TYPE Methods
PUBLISHED 25 August 2022
DOI 10.3389/fenrg.2022.974365

OPEN ACCESS

EDITED BY
Yang Li,
Hohai University, China

REVIEWED BY
Han Wang,
Shanghai Jiao Tong University, China
Meng Song,
Southeast University, China
Yifei Wang,
Southeast University, China

*CORRESPONDENCE
Linjuehao Mei,
22010126@zju.edu.cn

SPECIALTY SECTION
This article was submitted to Smart Grids, a section of the journal Frontiers in Energy Research

RECEIVED 21 June 2022
ACCEPTED 18 July 2022
PUBLISHED 25 August 2022

CITATION
Shen Z, Dan Y, Qi M, Sun F, Sun Y and Mei L (2022), Efficient whole-process carbon intensity calculation method for power users in active distribution networks.
Front. Energy Res. 10:974365.
doi: 10.3389/fenrg.2022.974365

Efficient whole-process carbon intensity calculation method for power users in active distribution networks

Zhiheng Shen[1], Yangqing Dan[1], Mengxue Qi[2], Feifei Sun[1], Yikai Sun[1] and Linjuehao Mei[2]*

[1]Economic Research Institute of State Grid Zhejiang Electric Power Company, Hangzhou, China, [2]College of Electrical Engineering, Zhejiang University, Hang Zhou, China

With the tightening restrictions on carbon emission globally, the carbon intensity of the economic is receiving more attention than ever, but the results obtained by conventional methods are not accurate enough for the responsibility division. To change this situation, a power flow tracking method aimed at the distribution networks and an electricity-consumption-based carbon intensity calculation framework are proposed in this paper. Firstly, to overcome the obstacles created by the three-phase asymmetries and the scale expansion of the networks while processing power flow tracing, a phase-split calculation regime and a high-efficiency power flow tracing method are proposed, respectively. On that basis, a whole-process carbon intensity calculation framework is reported. By adding simplified models about industrial production processes, this paper gives the calculation route from the energy consumption to the carbon intensity for each user in the distribution network. Finally, we emulated with the IEEE 34 bus and 123 bus test feeders and analyze the numerical results, to prove the efficiency and effectiveness of the framework proposed.

KEYWORDS

active distribution network, carbon intensity, asymmetric distribution, power flow tracing, power flow modeling

1 Introduction

As the world pays more attention to the emissions of greenhouse gases, how to achieve the balance between carbon emission reduction and economic development has become a common concern of all social groups (Song and Xia, 2022; Yuan and Zheng, 2022). The carbon intensity of the economy (called carbon intensity, CI) refers to the carbon emission per unit GDP (U.S. Energy Information Administration, 2022), which represents the advanced level of low-carbon technology for a company or a group, comparing with peers. In order to make people more active in the low-carbon career, it is necessary to provide appropriate rewards and punishments for enterprises with different CI. The electricity carbon emissions account for nearly 50% of the total (Zhang et al., 2021), with the

improving electrification in the production processes (Ciller et al., 2019; Wu et al., 2022), the carbon emissions related to the usage of the electricity should be taken into consideration when calculating CI. However, this type of carbon emission is unintuitive, so the tracking of the carbon emissions flow in the power system has become an integral part of CI calculations (Kang et al., 2015).

At present, two categories of methods are used to extract the corresponding relationship between electricity consumption and carbon emission, namely the statistical methods (Wang et al., 2013; Chen et al., 2018) and the carbon flow analysis methods (Sun et al., 2016; Cheng et al., 2020). On the one hand, the statistical methods calculate the total energy consumption in a long period of time. While being utilized in traditional distribution networks, the slight inaccuracy of these methods can be ignored considering the low penetration rate of renewable sources in the network, and its high-efficiency advantage is highlighted. However, for the active distribution networks with distributed renewable sources (Le et al., 2022; Ma et al., 2022), the calculation results of the statistical methods are too rough, to deduce the load users' whole-process CI.

On the other hand, the carbon flow analysis methods are based on active power flow in the distribution network. The first step of these methods is to associate the electricity consumption of each load with the output electricity of the sources in the distribution network (power flow tracing, PFT). The second step is to calculate the carbon emissions efficiency of each power source in the distribution network, by dividing the gross carbon emission by the output active power of the source. Finally, calculate the carbon emission corresponding to all electricity consumption according to the above results. The utilization of these methods relies heavily on the amount and accuracy of data. As the distribution networks grow in size and operational complexity, the loss and the inaccuracy of required data are becoming inevitable (Deka et al., 2018; Huang et al., 2021), which causes difficulty in striking a balance between economy and accuracy when tracing the power flow by the conventional methods. Additionally, these PFT methods can only analyze the three-phase balanced power grids, which is unsuitable for the distribution networks with asymmetric loads and lines (Kwon et al., 2015; Tellez et al., 2015). However, the carbon flow analysis methods can achieve a fair division of carbon emission responsibilities in theory. Therefore, after correcting the deficiencies above, the carbon flow analysis methods can be utilized to calculate the CI of the distribution network's users, efficiently and accurately.

After simplifying the power flowing model in the transformer with delta connections, this paper proposes a high-efficiency PFT method for the active distribution networks based on the radial nature (Arefi et al., 2020; Shaheen et al., 2021) of the networks. On that basis, a framework is proposed to calculate load users' CI, which only needs the users' electricity consumption and a small amount of the state information of the related distribution network. The innovations are as follows:

1) A method to separate the distribution network into three independent one-phase networks.
2) A subgraph selecting method for the selection of the required data, together with a high-efficiency PFT method for the selected data.
3) A CI calculation framework considering the carbon emissions related to the electricity consumption.

The remainder of this paper is organized as follows: Section II introduces the proposed PFT method for a three-phase unbalanced distribution network; Section III shows the CI calculation framework for the load users, and demonstrates the application mode of the framework with simplified models; Section IV verifies the efficiency and effectiveness of the proposed method and framework by analyzing the structures and numerical results of several IEEE test feeders; Section V concludes the paper and introduces the work plans in the future.

2 Power flow tracing method for asymmetric distribution networks

2.1 Phase separation for the distribution networks

Due to the possible asymmetries in the loads, lines, and other equipment in the distribution networks, the power flow and the loads' electricity consumption are relatively independent between phases. Therefore, for the accuracy of the final results, the proposed PFT method separates the three phases of the distribution network and calculates them independently. However, there are two major types of participants in the distribution networks that have power flow between phases, the loads and the transformers, and the solutions to these two obstacles are introduced respectively as follows.

For the loads. The active power input to each phase of all loads can be measured by the smart meters, and the values of the phase-wise loads are recorded as a matrix P_M in the form of L*3, L is the quantity of the loads, the 1^{st}, 2^{nd}, and 3^{rd} element in the i^{th} row of the matrix represent the power absorbed by the load i from the 1^{st}, 2^{nd}, and 3^{rd} phase of the buses, respectively.

As for the transformers. On the one hand, the transformers without delta connections can be directly regarded as the lines in the power-flow perspective, because there is no power flowing between phases. On the other hand, since the current in the delta circuit is not acceptable for the safety and stability of the distribution networks, the conditions that the asymmetric power flowing into the delta-connected transformers are

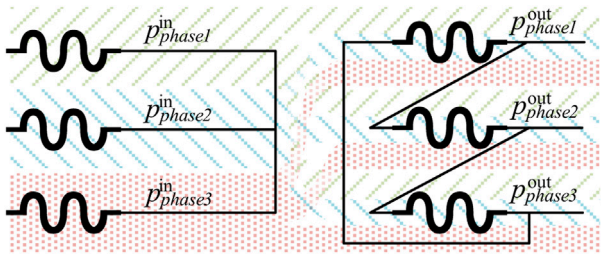

FIGURE 1
Power flow diagram of the star-delta transformer.

extremely rare, and such situation will not be discussed in this paper. Additionally, the power flow in the transformer is distinct between different operation states, so further research about it is expensive and with limited benefits. Accordingly, we assume that the output power of each phase has the same power composition, that is, the output power of each phase is provided by all input phases, and each input phase accounts for 1/3. Figure 1 shows the power flow of a star-delta transformer. Assuming the transformers as the loads is good enough for the calculation process of the proposed PFT method, and the utilization of this power flow model is illustrated in Section 2.1.

In practice, the first thing to do is to convert the other transformers into the lines firstly. At the same time, convert each transformer with delta connection into three loads, each load in a phase. Then, record the power flowing into each phase of the transformer as the related load in that phase. Considering that the load data is recorded phase by phase at the beginning, the distribution network has already divided into three independent networks after the above processes. Figure 2 shows the process of converting a three-phase asymmetric distribution network into three independent one-phase networks.

2.2 Process of the efficient power flow tracing method

Due to the scale expansion of the distribution network, the cost for the data collection has risen sharply (Kaiyuan and Xueshun, 2018; Yahya et al., 2020). Thus, a PFT method that only utilizes minimal data is helpful to deal with this situation. To this end, we define the subnet in the distribution network with the following rules: all buses in the subnet can be connected to any bus in the subnet, and the connection route is composed of the buses and lines that belong to that subnet. At the same time, record the proportion of the power from different sources in the load as the power proportion (PP) of that load. It is obvious that in each one-phase network, the PP of the loads will be the same when the subnet's power injection only happens in one bus. Based on the radial feature of the distribution network, this paper uses the above settings and proposes a PFT method that requires less data. The process of the method can be divided into three main steps, and the first step is to find the redundant data while processing PFT:

1) Converting the transformers with delta connections into three loads, each in a phase, the value of each load is the input power to the related phase of the transformer
2) Representing the distribution network as a graph, in which edges represent lines and nodes represent buses (Rusek et al., 2020), the features of each node is the same as those of the related bus.
3) Finding all nodes that are connected to power sources, and find the shortest path between each pair of these nodes (Krasnobayev et al., 2020).Then, recording all nodes on these paths as the minimum node set (MNS), and record the subgraph only including the nodes in the MNS as the minimum subgraph.

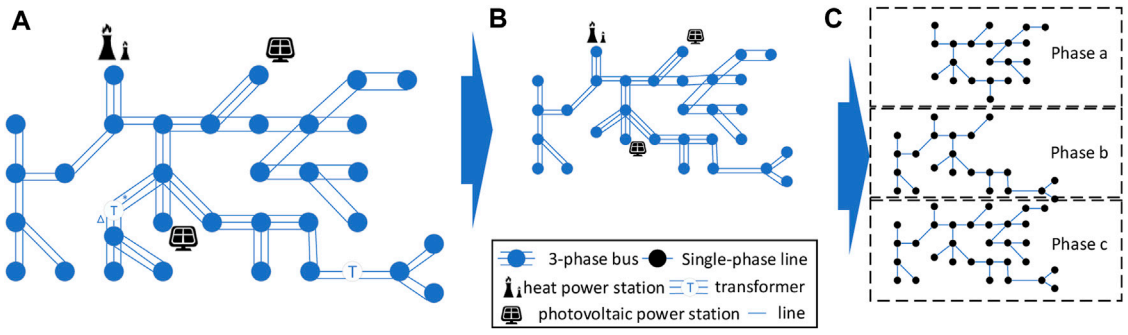

FIGURE 2
Flowchart of dividing the distribution network into three independent networks.

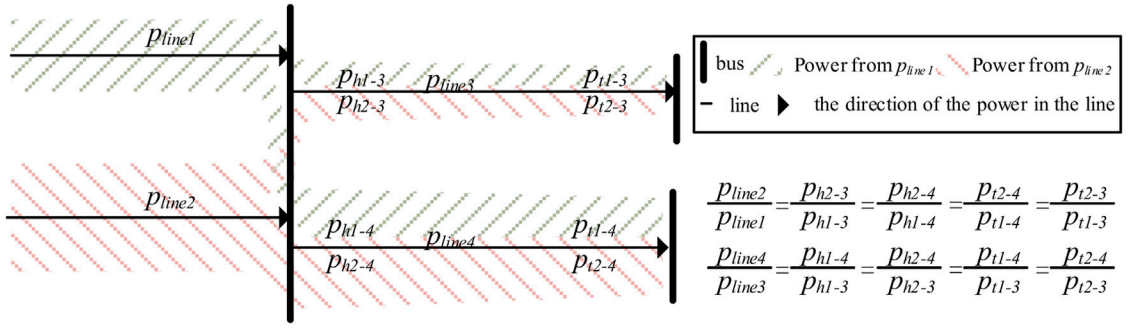

FIGURE 3
Schematic diagram of the proportion sharing principle.

Clearly, for each subgraph obtained by the above processes, the quantity of the buses that has inflowing power is equal or less than 1. Therefore, the PP of the loads in the whole distribution network can be broadcasted by those in the minimum subgraphs. So, the second step is to analyzing the topology and power flow of the minimum subgraph, and calculate the PP of the loads in each phase of it. The specific method is as follows:

1) Generate three independent networks by the method in Section 2.2 and transform them into three one-phase graphs as in the first step.
2) For each graph, delete the nodes in the MNS, and divide the nodes and the lines remained into multiple subgraphs according to their connectivity.
3) Add the nodes in the MNS that are directly connected to each subgraph to that subgraph, if a node in the MNS is connected to multiple subgraphs, merge the node and the subgraphs into one subgraph. The subgraphs created in this step are denoted as remained subgraphs (RS), each RS is related to a single node in the MNS.
4) Record the total power consumption of each RS as the load of the related node. Then, use the traditional PFT method, to calculate the PP of the loads in the minimum subgraph.

The traditional power flow tracking method uses the proportion sharing principle (Rao et al., 2012) to analyze the power flow of the network, and obtain the position where all power from each source is finally consumed. The proportion sharing principle can be explained from two aspects: for the lines, among the power flowing at the beginning and end of a single line, the proportion of power from different power sources is the same; for the buses, the percentage of power from each input terminal is the same in each output terminal. Figure 3 shows the schematic diagram of the proportion sharing principle. Under the constraints of the above principles, a bus-by-bus iteration is used to calculate the PP for the loads in the minimum subgraph related to the three phases. The three-phase PP of the loads can be represented as the proportional matrix $\mathrm{E}_i = [\varepsilon_i^{(1)}, \varepsilon_i^{(2)}, \varepsilon_i^{(3)}]^T$, where i is the id of each load; $\varepsilon_i^{(k)} = [\varepsilon_{i1}^{(k)}, \varepsilon_{i2}^{(k)}, ..., \varepsilon_{iJ}^{(k)}]$; J is the total amount of power generation equipment; $\varepsilon_{ij}^{(k)}$ represents the proportion of the power flowing to the k^{th} phase of load i that comes from source j.

The results above can be broadcasted to the loads outside the minimum subgraph, and by which, the result of the PFT can be deduced in the third step as:

1) While regarding the delta-connected transformers as loads, for each RS in each one-phase graph, the PP of loads in that RS is the same as the PP of the load which that RS was equivalented to.
2) According to the simplified power flow model of the transformer with delta connections in Section 2.2, for the transformer iu that the input power of which was equivalented as load iu in the previous steps, the proportional matrix of the downstream loads can be calculated as:

$$E_{id^{(o)}} = [\varepsilon_{iu}^m, \varepsilon_{iu}^m, \varepsilon_{iu}^m]^T \quad (1)$$

$$\varepsilon_{iu}^m = \left(\varepsilon_{iu}^{(1)} + \varepsilon_{iu}^{(2)} + \varepsilon_{iu}^{(3)}\right)/3 \quad (2)$$

where $\mathrm{E}_{id^{(o)}}$ is the proportional matrix of the load $id^{(o)}$ downstream of the transformer iu. $\varepsilon_{iu}^{(k)}(\forall k \in (1,2,3))$ is the k^{th} row of the loadiu's proportional matrix.

3) For each load in the distribution network, obtain the power magnitude from the sources as: $S_i = P_M[i] \cdot \mathrm{E}_i$, where $P_M[i]$ is the i^{th} row of P_M, and the j^{th} value of S_i $(\forall j \in \{1,2,...,J\})$ represents the active power in load i from generator j.

The introduction of the proposed PFT method is above, and the flowchart of it is shown in Figure 4.

According to the differences between the process of the proposed and the conventional PFT methods, it is clearly that the proposed method reduces the requirement of the data and while remaining the accuracy of the results, which will be verified in Section 2.2.

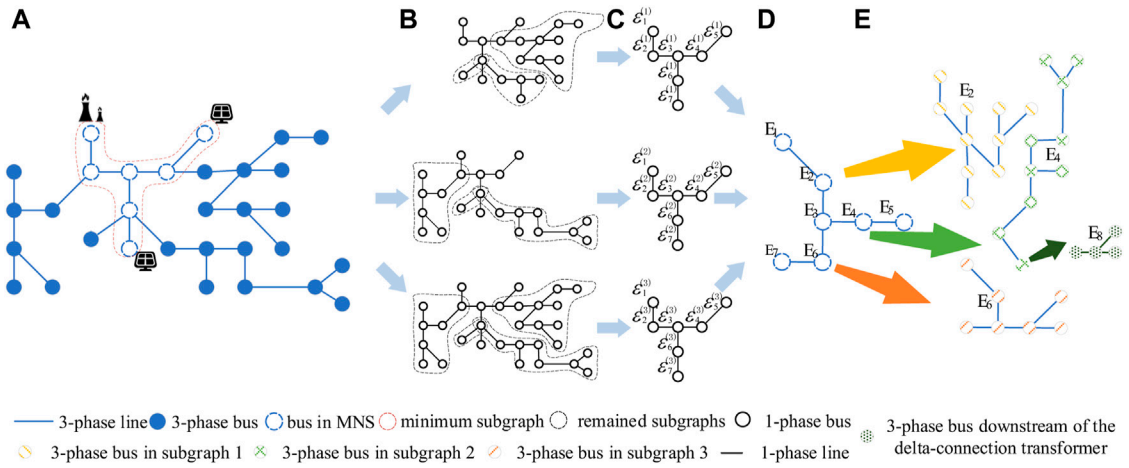

FIGURE 4
Flowchart of PFT method proposed in this paper.

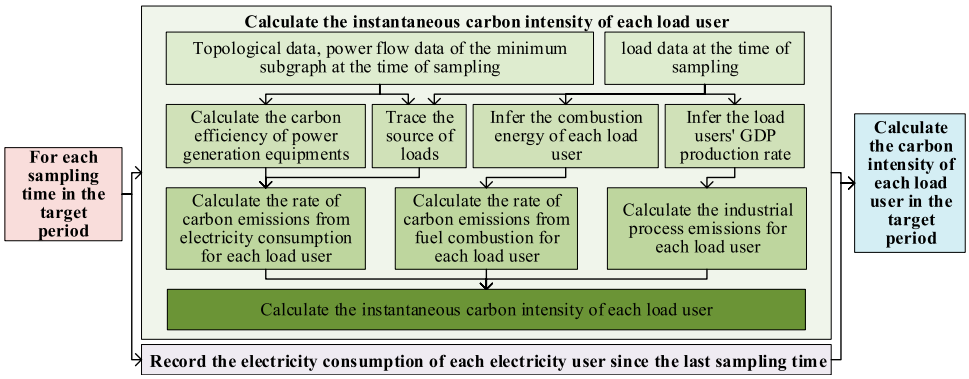

FIGURE 5
Flowchart of the CI calculation framework.

It is worth noting, when there are sources in both sides of the delta-connected transformer, the power-injection side should be calculated as a load firstly. Then, calculate the PP for the output power of each phase of the transformer. By treating the output of the transformers as the power sources, the PP of all loads in the network can be calculated by the proposed method.

3 Whole-process CI calculation framework

Industrial Carbon emissions can be divided into the industrial process emissions and the energy consumption emissions. The former refers to the carbon emissions produced by physical or chemical changes other than combustion. The latter refers to carbon emissions deduced by fuel combustion and other forms of energy usage. At present, the carbon emissions related to the usage of combustion energy are based on the statistical methods. In those methods, the industrial process emissions are calculated by multiplying the referred carbon emission ratio by the product output, for each production. The energy consumption emissions are calculated likewise, and the referred ratio is multiplied by the consumption of electricity and fuels. Due to the uncertainty of combustion efficiency under different production environment conditions, the results are often insufficient. Considering the strong correlations between the usage of different types of energy, this paper makes a few assumptions and simplified models. Accordingly, we report a framework to calculate the

whole process carbon emissions of the load users based on their electricity consumption, as shown in Figure 5.

3.1 Related models and parameters

For the high-accuracy of the framework, the detailed information that describing the generation processes is indispensable for the construction of the models. Due to the fact that no model can achieves absolute unity in all situations, the simplified models are utilized to illustrate how the proposed framework extract CI from the electricity consumption. The models and the parameters are as follows:

The user corresponding to load i is marked as user i, and we assume that the industrial process emission per GDP is a constant value for user i, denoted as μ_i^t. For each industrial power user, we assume that the required energy from electricity and combustion are constant when generating each unit of GDP, and the demands are p_i^E and p_i^B for user i, respectively. The corresponding relationship between carbon emissions and power generation (Wang et al., 2022) of thermal power source j is:

$$\lambda_j = \varsigma_j \tau_j \left(1 - \upsilon_j\right) \frac{M_{co_2}}{M_c} \sum_{n=0}^{2} b_j^{(n)} Power\left(P_j^E, n-1\right)$$

where λ_j is the tons of carbon emission per kWh of the power source j. $b_j^{(n)}$ is the characteristic parameter related to the carbon emission efficiency of the source j. ς_j, τ_j, and υ_j are the carbon content rate, carbon oxidation rate and carbon capture rate of the source j, respectively. M_{co_2} and M_c are the molar masses of carbon and carbon dioxide, 12 g/mol and 44 g/mol, respectively. P_j^E is the output power of the source j. $Power\left(P_i^B, n-1\right)$ is the $(n-1)^{th}$ power of P_j^E. The c_j of each renewable power source is 0, and the λ_j of all power sources constitute the vector $\gamma_G = [\lambda_1, \lambda_2, ..., \lambda_J]$.

The corresponding relationship between the combustion power and carbon emissions of industrial users is similar to that of thermal power plants, and the expression is:

$$\lambda_i^B = \varsigma_i \tau_i \left(1 - \upsilon_i\right) \frac{M_{co_2}}{M_c} \sum_{n=0}^{2} b_i^{(n)} Power\left(P_i^B, n-1\right)$$

where λ_i^B is the carbon emission generated by user i per kWh combustion energy. $b_i^{(n)}$ is the characteristic parameter related to the carbon emission efficiency of user i. ς_i, τ_i, and υ_i are the carbon content rate, carbon oxidation rate and carbon capture rate of the user i 's combustion equipment, respectively. P_i^B is the combustion power of user i.

3.2 Calculation process of CI

For the calculation of instantaneous CI: According to the operating status of the distribution network and the active power flowing to each load, by the PFT method Section 2.2 in and the parameters in Section 3.1, the instantaneous CI of the related user can be obtained. The calculation is as follows:

The carbon emission ratio conducted by electricity consumption for user i is $c_i^e = S_i \cdot \gamma_G^T$, where γ_G^T is the transpose of γ_G. Besides, the GDP generation rate of user i can be calculated by the related active power usage P_i and the parameter P_i^E, as $g_i = P_i / p_i^E$. Accordingly, the combustion power of user i can be calculated like $P_i^B = g_i * p_i^B$, the carbon emission related to which is calculated by $c_i^B = P_i^B * \lambda_i^B$. Therefore, the energy consumption emissions ratio of user i is $c_i = c_i^B + c_i^e$, and the energy-consumption-part CI μ_i^c is obtained by dividing c_i by g_i. Combining the above results, the instantaneous CI of user i is $\mu_i = \mu_i^c + \mu_i^t$.

As for the CI calculations in a period of T seconds. The sampling frequency of the input power and the energy consumption of each user is ϕ hertz, and the sampling time points are denoted in sequence as $\{t_0, t_1, ..., t_{T*\phi}\}$. The long-term carbon intensity of the users can be calculated by the instantaneous carbon intensity $\mu_i^{(t_m)}$ at each time point, with the electricity consumption $w_i^{(t_m)}$ in the corresponding time period. where $w_i^{(t_m)}$ is the power consumption of the load i between time t_{m-1} and time t_m, the unit is kWh. With the above parameters, the total GDP and the total carbon emission of user i can be calculated as $G_i = \sum_{m=1}^{T*\phi} w_i^{(t_m)} / p_i^E$ and $C_i = \sum_{m=1}^{T*\phi} w_i^{(t_m)} * (\mu_i^{(t_m)} + \mu_i^{(t_{m-1})})/2 p_i^E$, respectively. Therefore, the CI of user i in the target time period is $M_i = C_i / G_i$.

4 Case study

We use IEEE 37-bus and 123-bus test feeder (namely feeder1 and feeder2) to verify the advancement and effectiveness of the method in this paper.

Firstly, we prove the necessity of dividing the distribution network into three phases for the PFT. There are only delta-connected generators in feeder1, the topology and the lines parameters of all three phases are the same, the phases are also symmetric. So, the result of the PFT will remain accurate whether the distribution network is divided into three independent networks. However, the topology diagram of each phase in feeder two is shown in Figure 6. There is topology inconsistency among different phases, and most of the loads are only connected to 1 or 2 phases of the network. Therefore, it is more convincing to divide the distribution network into three before processing PFT.

Then, this paper verifies the efficiency and the effectiveness of the data usage by using the method we proposed, the verification is divided into two aspects.

On the one hand, we calculated the reduction of the required data by comparing the quantity of the nodes in the minimum subgraph and the whole graph. Specifically, we add N_{dg} $(\forall N_{dg} \in \{1, ..., 20\})$ distributed photovoltaic devices at the

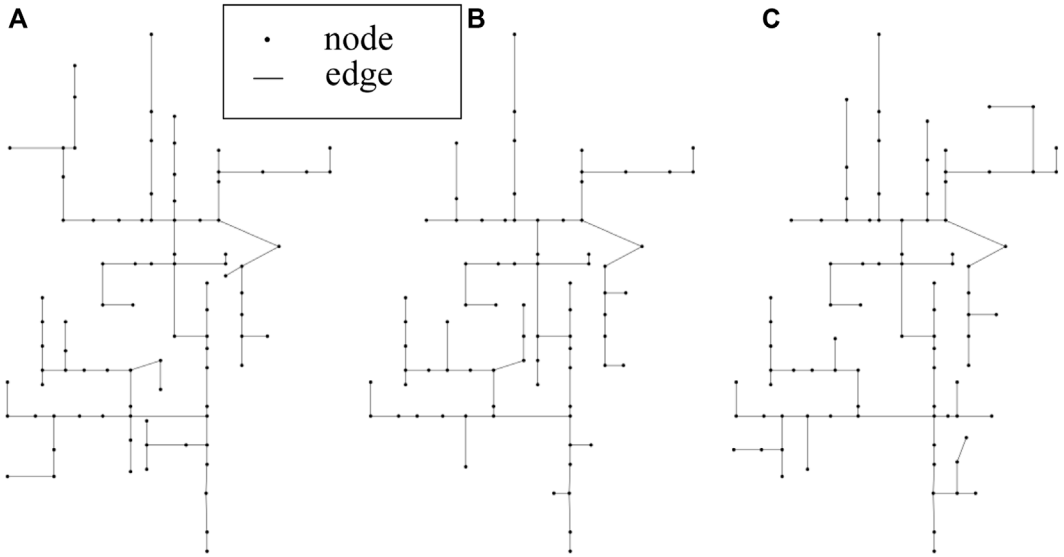

FIGURE 6
The topology of each phase in feeder2.

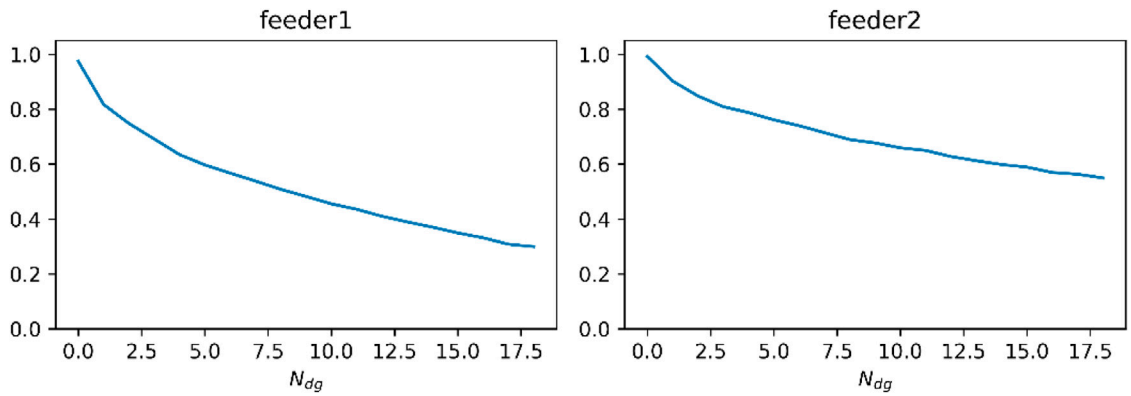

FIGURE 7
Percentage of data requirement reduction.

non-repetitive random buses in both test feeders, then calculate the number of buses that are needed for the proposed PFT method. Repeat 1,000 times and average the number of required nodes, divide by the number of buses in the feeder, and get the proportion of nodes that need to be sampled. The values obtained by subtracting this proportion from 1 can infer the improvement of data utilization efficiency when using the method proposed in this paper. The values correspond to different N_{dg} in both feeders are shown in Figure 7.

As shown in the figure above, the amount of the required data is greatly reduced by using the proposed method when processing PFT. When the quantity of the distributed sources is less than 1/5 of the number of buses, the amount of the required data is decreased by over 50%, and the efficiency of data usage is boosted by more than 100% in average. The result proves that the requirement of data has significantly reduced, which demonstrates the high efficiency of the method we proposed.

On the other hand, we verify the effectiveness of the proposed method. On the basis that the PFT is processed phase by phase, the conventional PTF method has already achieved people's expectations to the fairness (Wang et al.,

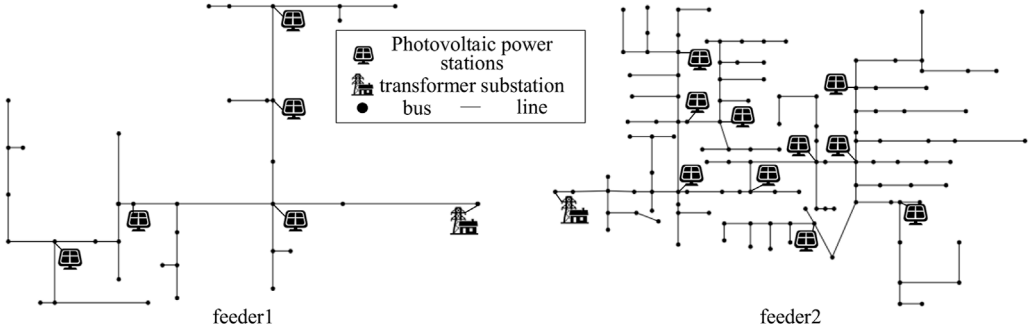

FIGURE 8
Schematic diagram of topology and photovoltaic location of feeder 1 and feeder two.

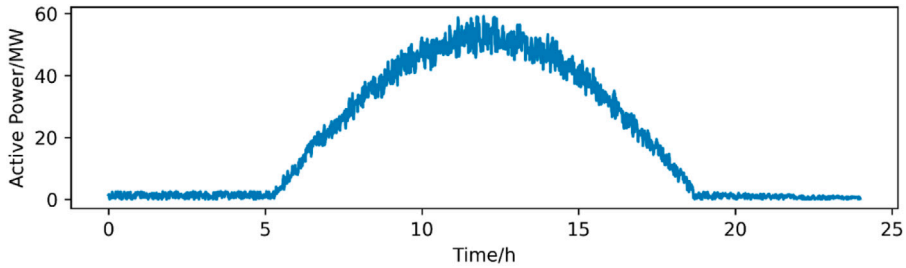

FIGURE 9
Standard curve of photovoltaic output.

2022). Therefore, we verify the effectiveness of the proposed method by comparing the users' carbon emission, which are deduced by the proposed method (PM) and the conventional method (CM), respectively. The emulation software is OpenDSS. 5 and 10 distributed photovoltaics are set in the feeder1 and feeder2 respectively, the power from the abspanntransformator is regarded as the power from one thermal power station, and its carbon emission efficiency is calculated by the formula in 3.1. The topology of the distribution network and the location of each distributed power generation equipment are shown in Figure 8. The photovoltaic output curve of each day is the standard curve shown in Figure 9 multiplied by a random number from 0 to 1. All parameters related to industrial production are random numbers. The input power of each load is generated by the minute as the average power for that minute, and the value of it fluctuates randomly between 0 and 1 times the initial value of the feeders. The load is sampled every 15 min to obtain the active power consumption of the load within 15 min, as well as the power at that moment. We use both PFT methods to obtain the carbon emissions related to the electricity consumption of each load in 1 month. The results are shown in Table 1, where each users' ID (UI) corresponds to a load user.

By comparing the results calculated by the two methods, it can be found that the carbon emissions calculated by the two methods are equal for all users. Therefore, the method described in this paper uses only a small amount of data to achieve the trustworthy results that traditional methods require several times the data.

The monthly CI of each load users in both feeders are given in Table 2, in t/GDP.

The data requirement of the conventional CI accounting method is different from which of the proposed method, these two methods are not comparable. So, we analyze the advantages of our method from a mechanism prospect. The proposed method has a much smaller requirement of the data quantity, because the usage of each type of production raw materials are not indispensable. At the same time, the proposed method can tell the difference in CI under different working conditions, instead of calculating all carbon emissions from energy usage by a standard ratio. In conclusion, the proposed framework has the potential boost the accuracy and efficiency when calculating the CI of each user.

TABLE 1 Monthly carbon emission calculated by TM and PM.

	UI	0	1	2	3	4	5	6	7	8	9	10
Feeder1	CM(t)	20,515	1,479	1869	883	2,377	33,608	1,365	1,076	3,010	1,493	3,306
	PM(t)	20,515	1,479	1869	883	2,377	33,608	1,365	1,076	3,010	1,493	3,306
	UI	**11**	**12**	**13**	**14**	**15**	**16**	**17**	**18**	**19**	**20**	**21**
	CM(t)	960	1716	3,061	918	3,160	838	1704	945	34,173	2,840	1825
	PM(t)	960	1716	3,061	918	3,160	838	1704	945	34,173	2,840	1825
	UI	**22**	**23**	**24**								
	CM(t)	807	1900	4,157								
	PM(t)	807	1900	4,157								
Feeder2	CM(t)	3,914	2,154	4,837	2,121	4,774	1951	4,466	3,409	4,434	2,100	318,651
	PM(t)	3,914	2,154	4,837	2,121	4,774	1951	4,466	3,409	4,434	2,100	318,651
	UI	**11**	**12**	**13**	**14**	**15**	**16**	**17**	**18**	**19**	**20**	**21**
	CM(t)	1938	3,855	11,471	3,367	3,784	3,632	3,674	3,485	1741	1776	3,820
	PM(t)	1938	3,855	11,471	3,367	3,784	3,632	3,674	3,485	1741	1776	3,820
	UI	**22**	**23**	**24**	**25**	**26**	**27**	**28**	**29**	**30**	**31**	**32**
	CM(t)	3,964	3,721	3,689	1881	1961	2,419	1890	3,940	1846	4,706	33,327
	PM(t)	3,964	3,721	3,689	1881	1961	2,419	1890	3,940	1846	4,706	33,327
	UI	**33**	**34**	**35**	**36**	**37**	**38**	**39**	**40**	**41**	**42**	**43**
	CM(t)	22,191	3,270	3,810	5,351	4,034	4,951	3,363	2015	1960	2,293	1925
	PM(t)	22,191	3,270	3,810	5,351	4,034	4,951	3,363	2015	1960	2,293	1925
	UI	**44**	**45**	**46**	**47**	**48**	**49**	**50**	**51**	**52**	**53**	**54**
	CM(t)	4,046	3,817	7,928	9,319	7,700	1889	3,827	1925	3,773	3,786	4,315
	PM(t)	4,046	3,817	7,928	9,319	7,700	1889	3,827	1925	3,773	3,786	4,315
	UI	**55**	**56**	**57**	**58**	**59**	**60**	**61**	**62**	**63**	**64**	**65**
	CM(t)	3,734	130,596	8,382	6,753	4,305	6,069	1949	2,340	9,841	2,685	5,803
	PM(t)	3,734	130,596	8,382	6,753	4,305	6,069	1949	2,340	9,841	2,685	5,803
	UI	**66**	**67**	**68**	**69**	**70**	**71**	**72**	**73**	**74**	**75**	**76**
	CM(t)	5,305	5,070	4,646	5,060	2,668	2,592	3,787	6,492	4,005	2023	4,357
	PM(t)	5,305	5,070	4,646	5,060	2,668	2,592	3,787	6,492	4,005	2023	4,357
	UI	**77**	**78**	**79**	**80**	**81**	**82**	**83**	**84**			
	CM(t)	4,061	12,540	4,222	32,744	1792	37,410	3,961	1804			
	PM(t)	4,061	12,540	4,222	32,744	1792	37,410	3,961	1804			

TABLE 2 The CI of users in both feeders.

	UI	0	1	2	3	4	5	6	7	8	9	10	11	12	13	14
Feeder1	CI	234	138	163	48	272	331	26	26	126	54	80	257	144	47	73
	UI	**15**	**16**	**17**	**18**	**19**	**20**	**21**	**22**	**23**	**24**	**15**	**16**	**17**	**18**	**19**
	CI	80	113	243	50	690	216	106	211	60	127	80	113	243	50	690
Feeder2	CI	95	102	38	106	76	24	91	67	67	69	368	92	90	54	20
	UI	**15**	**16**	**17**	**18**	**19**	**20**	**21**	**22**	**23**	**24**	**25**	**26**	**27**	**28**	**29**
	CI	47	62	57	76	80	10	120	117	80	114	108	95	41	104	25
	UI	**30**	**31**	**32**	**33**	**34**	**35**	**36**	**37**	**38**	**39**	**40**	**41**	**42**	**43**	**44**
	CI	26	41	74	38	117	81	108	103	75	64	42	59	21	58	94
	UI	**45**	**46**	**47**	**48**	**49**	**50**	**51**	**52**	**53**	**54**	**55**	**56**	**57**	**58**	**59**
	CI	114	140	107	129	86	52	42	84	43	47	96	55	27	92	51
	UI	**60**	**61**	**62**	**63**	**64**	**65**	**66**	**67**	**68**	**69**	**70**	**71**	**72**	**73**	**74**
	CI	86	89	91	7	59	86	39	67	136	86	39	110	127	72	64
	UI	**75**	**76**	**77**	**78**	**79**	**80**	**81**	**82**	**83**	**84**					
	CI	30	112	95	70	84	520	112	192	81	8					

5 Conclusion

In order to obtain a more accurate CI for the load users in the distribution network, this paper proposes a high-efficiency PFT method suitable for three-phase-asymmetric distribution networks. The proposed method splits the distribution network into three one-phase networks, and solves the obstacles brought by the asymmetries of the lines and loads in the network. Additionally, the method makes the best of the radial feature of the distribution network, and overcomes the challenges brought by the scale expansion of it. Furthermore, we proposed the simplified models describing the energy-carbon relationship of power sources, as well as the production processes of the load users. On that basis, a calculation framework about the users' whole process CI is proposed. Although there are a few assumptions in the proposed framework, after perfecting the simplified model, the user's CI can be obtained more precisely by the user's electricity consumption.

In the future, we intend to additionally increase the precision and practicality of the CI calculation in two aspects. Firstly, we intend to focus on the distribution network with distributed storage devices, and study the flow of carbon emissions in the temporal and spatial dimensions. Secondly, we plan to use deep learning methods to replace the simplified models in this paper, and improve the accuracy of the results of the CI while maintaining the calculation speed.

Data availability statement

The original contributions presented in the study are included in the article/Supplementary Material, further inquiries can be directed to the corresponding author.

Author contributions

All authors listed have made a substantial, direct, and intellectual contribution to the work and approved it for publication.

Funding

This study received funding from the Science and Technology Project of State Grid Zhejiang Electric Power Company Limited (No. B311JY21000B). The funder was not involved in the study design, collection, analysis, interpretation of data, the writing of this article or the decision to submit it for publication. All authors declare no other competing interests.

Conflict of interest

Authors ZS, YD, FS, and YS were employed by the company Economic Research Institute of State Grid Zhejiang Electric Power Company.

The remaining authors declare that the research was conducted in the absence of any commercial or financial relationships that could be construed as a potential conflict of interest.

Publisher's note

References

Arefi, A., Ledwich, G., Nourbakhsh, G., and Behi, B. (2020). A Fast Adequacy Analysis for Radial Distribution Networks Considering Reconfiguration and DGs. *IEEE Trans. Smart Grid* 11 (5), 3896–3909. doi:10.1109/tsg.2020.2977211

Chen, L., Sun, T., Zhou, Y., Fang, C., and Feng, D. (2018). Method of Carbon Obligation Allocation between Generation Side and Demand Side in Power System [J]. *Automation Electr. Power Syst.* 42 (19), 6. doi:10.7500/AEPS20171113004

Cheng, Y., Zhang, N., Zhang, B., Kang, C., Xi, W., and Feng, M. (2020). Low-Carbon Operation of Multiple Energy Systems Based on Energy-Carbon Integrated Prices. *IEEE Trans. Smart Grid* 11 (2), 1307–1318. doi:10.1109/tsg.2019.2935736

Ciller, P., Ellman, D., Vergara, C., Gonzalez-Garcia, A., Lee, S. J., Drouin, C., et al. (2019). Optimal Electrification Planning Incorporating on- and Off-Grid Technologies: The Reference Electrification Model (REM). *Proc. IEEE* 107 (9), 1872–1905. doi:10.1109/jproc.2019.2922543

Deka, D., Backhaus, S., and Chertkov, M. (2018). Structure Learning in Power Distribution Networks. *IEEE Trans. Control Netw. Syst.* 5 (3), 1061–1074. doi:10.1109/tcns.2017.2673546

Huang, C., Wang, W., Lu, J., and Kurths, J. (2021). Asymptotic Stability of Boolean Networks with Multiple Missing Data. *IEEE Trans. Autom. Contr.* 66 (12), 6093–6099. doi:10.1109/tac.2021.3060733

Kaiyuan, H., and Xueshun, Y. (2018). "A Data-Upload Strategy of Measurements for Lean Management in Distribution Network under Certain Communication Cost[C]," in 2018 China International Conference on Electricity Distribution (CICED), Tianjin, China, 17-19 September 2018.

Kang, C., Zhou, T., Chen, Q., Wang, J., Sun, Y., Xia, Q., et al. (2015). Carbon Emission Flow from Generation to Demand: A Network-Based Model. *IEEE Trans. Smart Grid* 6 (5), 2386–2394. doi:10.1109/tsg.2015.2388695

Krasnobayev, V., Kuznetsov, A., Yanko, A., and Kuznetsove, T. (2020). "Solving the Shortest Path Problem Using Integer Residual Arithmetic," in 2020 IEEE International Conference on Problems of Infocommunications. Science and Technology, Kharkiv, Ukraine, 06-09 October 2020.

Kwon, J. H., Seo, M. C., Lee, H. S., Gu, J. h., Ham, J. h., Hwang, K. C., et al. (2015). Broadband Doherty Power Amplifier Based on Asymmetric Load Matching Networks. *IEEE Trans. Circuits Syst. Ii.* 62 (6), 533–537. doi:10.1109/tcsii.2015.2407197

Le, F. L., Martinez, M., Leonardo, J. O., and Pedro, E. M. (2022). Devices and Control Strategies for Voltage Regulation under Influence of Photovoltaic Distributed Generation. A Review[J]. *IEEE Lat. Am. Trans.* 20 (5), 731–745.

Ma, X., Liu, S., Liu, H., and Zhao, S. (2022). The Selection of Optimal Structure for Stand-Alone Micro-grid Based on Modeling and Optimization of Distributed Generators. *IEEE Access* 10, 40642–40660. doi:10.1109/access.2022.3164514

Rao, N. V. S., Rao, G. K., and Sivanagaraju, S. (2012). "Power Flow Tracing by Graph Method Using BFS Technique," in 2012 International Conference on Advances in Power Conversion and Energy Technologies, Mylavaram, India, 02-04 August 2012.

Rusek, K., Suárez-Varela, J., Almasan, P., Barlet-Ros, P., and Cabellos-Aparicio, A. (2020). RouteNet: Leveraging Graph Neural Networks for Network Modeling and Optimization in SDN. *IEEE J. Sel. Areas Commun.* 38 (10), 2260–2270. doi:10.1109/jsac.2020.3000405

Shaheen, A. M., Elattar, E. E., El-Sehiemy, R. A., and Elsayed, A. M. (2021). An Improved Sunflower Optimization Algorithm-Based Monte Carlo Simulation for Efficiency Improvement of Radial Distribution Systems Considering Wind Power Uncertainty. *IEEE Access* 9, 2332–2344. doi:10.1109/access.2020.3047671

Song, Z., and Xia, Z. (2022). Carbon Emission Reduction of Tunnel Construction Machinery System Based on Self-Organizing Map-Global Particle Swarm Optimization with Multiple Weight Varying Models. *IEEE Access* 10, 50195–50217. doi:10.1109/access.2022.3173735

Sun, T., Feng, D., Ding, T., Chen, L., and You, S. (2016). "Directed Graph Based Carbon Flow Tracing for Demand Side Carbon Obligation Allocation [C]," in 2016 IEEE Power and Energy Society General Meeting, Boston, MA, USA.

Tellez, A. A., Galarza, D. F. C., and Matos, L. O. (2015). Analysis of Power Losses in the Asymmetric Construction of Electric Distribution Systems[J]. *IEEE Lat. Am. Trans.* 13 (7), 2190–2194. doi:10.1109/TLA.2015.7273776

U.S. Energy Information Administration (2022). 2005-2016 Independent Statistics and AnalysisEnvironment - Analysis & Projections State-Level Energy-Related Carbon Dioxide Emissions. Available at https://www.eia.gov/environment/emissions/state/analysis/.

Wang, C., Chen, Y., Wen, F., Tao, Y., Tao, C., and Jiang, X. (2022). Some Problems and Improvement of Carbon Emission Flow Theory in Power Systems[J]. *Power Syst. Technol.* 46 (5), 1683–1691.

Wang, C., Lu, Z., and Qiao, Y. (2013). A Consideration of the Wind Power Benefits in Day-Ahead Scheduling of Wind-Coal Intensive Power Systems. *IEEE Trans. Power Syst.* 28 (1), 236–245. doi:10.1109/tpwrs.2012.2205280

Wu, T., Wei, X., Zhang, X., Wang, G., Qiu, J., and Xia, S. (2022). Carbon-Oriented Expansion Planning of Integrated Electricity-Natural Gas Systems with EV Fast-Charging Stations. *IEEE Trans. Transp. Electrific.* 8 (2), 2797–2809. doi:10.1109/tte.2022.3151811

Yahya, S., Ndyetabura, H., Mvungi, N., and Lujara, S. (2020). "Low Cost Data Acquisition System for Electrical Secondary Distribution Network," in 2020 6th IEEE International Energy Conference, Gammarth, Tunisia, 28 September 2020 - 01 October 2020.

Yuan, X. M., and Zheng, C. C. (2022). Evolutionary Game and Simulation Analysis of Low-Carbon Technology Innovation with Multi-Agent Participation. *IEEE Access* 10, 11284–11295. doi:10.1109/access.2022.3143869

Zhang, Y., Zhang, N., Dai, H., Zhang, S., Wu, X., and Xue, M. (2021). Model Construction and Pathways of Low-Carbon Transition of China's Power System[J]. *Electr. Power* 54 (03), 11. doi:10.11930/j.issn.1004-9649.202101058

frontiers | Frontiers in Energy Research

TYPE Original Research
PUBLISHED 05 September 2022
DOI 10.3389/fenrg.2022.964216

OPEN ACCESS

EDITED BY
Changsen Feng,
Zhejiang University of Technology, China

REVIEWED BY
Shubo Wang,
Qingdao University, China
Zhijing Liao,
Queen Mary University of London, United Kingdom
Yongfeng Lyu,
University of Warwick, United Kingdom

*CORRESPONDENCE
Xian Wang,
wanglywxian@163.com

SPECIALTY SECTION
This article was submitted to Smart Grids, a section of the journal Frontiers in Energy Research

RECEIVED 08 June 2022
ACCEPTED 12 July 2022
PUBLISHED 05 September 2022

CITATION
Xi X, Shi Z, Wang X, Xing C and Li S (2022), Adaptive finite-time parameter estimation for grid-connected converter with LCL filter.
Front. Energy Res. 10:964216.
doi: 10.3389/fenrg.2022.964216

Adaptive finite-time parameter estimation for grid-connected converter with LCL filter

Xinze Xi[1], Zhenghao Shi[2,3], Xian Wang[2,3]*, Chao Xing[1] and Shengnan Li[1]

[1]Electric Power Research Institute of Yunnan Power Grid Co., Ltd., Kunming, China, [2]Faculty of Mechanical and Electrical Engineering, Kunming University of Science and Technology, Kunming, China, [3]Yunnan International Joint Laboratory of Intelligent Control and Application of Advanced Equipment, Kunming, China

This study proposes an online finite-time adaptive parameter estimation method for grid-connected voltage source inverter (VSI) with LCL filter. In this framework, a time-continuous state-space system model is first developed, which is different from the nonparametric frequency-response-based method. Then, the parameter estimation error information is extracted by introducing a series of filter operations. Moreover, a sliding mode term is studied and cooperated with the obtained parameter estimation error to design the parameter estimation error-based finite-time adaptive parameter estimation algorithm. With the help of this novel adaptive law, the physical parameters of electrical components can be driven to their true values accurately and fast. Theoretical analysis is conducted in terms of the Lyapunov theory to demonstrate the convergence of the parameter estimation error. Finally, numerical simulation results are provided to illustrate the superiority of the proposed method over the conventional method.

KEYWORDS

adaptive parameter estimation, finite-time convergence, LCL filters, voltage source inverters, parameter identification

1 Introduction

Voltage source inverters (VSIs) are widely implemented in many grid-connected applications due to their capability of converting the DC source to an AC output. In order to convert the current, the inverter is required to implement the pulse modulation technique which will cause high-order harmonic pollution and may trigger a negative impact on grid-connected performance; especially, it may disturb the supply voltage of sensitive loads or devices tied to the grid (Mohamed (2010); Feng et al. (2022)). In order to attenuate the switching frequency harmonics caused by the VSI and improve the quality of the grid capability, a proper filter is needed and implemented between the VSI and the grid practically (Reznik et al. (2013)). Compared with a traditional L-filter (Gomes et al. (2018)), a high-order LCL filter has been generally used in the electrical power system because of its higher attenuation ability and better dynamic characteristics (Tang et al. (2011; 2015)). Moreover, when the range of power levels up to hundreds of

kW, the LCL filter can effectively reduce the overall size and weight of the componentswith a small value of inductors and capacitors (Liserre et al. (2005a)).

However, the three-order LCL filter suffers from the resonance problem, which may lead to oscillation of the power grid (Tang et al. (2015)). Although the LCL filter can accommodate the oscillation phenomenon by properly designing the filter parameters (Massing et al. (2011)), some of these parameters may have uncertainties due to the manufacturing tolerances, temperature changes, and the aging of electrical components in practical application. Moreover, if there is a transformer between the filter and the grid, the leakage inductance of the transformer will also lead to uncertainties in the filter (Schlesinger and Biela (2020)), and these lumped uncertainties will impact the overall grid performance.

Since the proper estimation of grid impedance including the LCL filter and VSI has a significant influence on the grid-connected quality, various work based on frequency-response estimation methods (i.e., also known as nonparametric methods) and model-based estimation methods has been done. This kind of method does not assume an exact model and only requires the injected stimulus and the responses. In the work of Liserre et al. (2005b) and Reigosa et al. (2012)), the grid impedance is identified by injecting sinusoidal currents into a grid, in which the Fourier analysis is introduced at a steady state by using the grid-side current and voltage responses. The utilization of sine sweeps provides the highest signal-to-noise ratio (SNR), and thus, it can achieve high-precision identification of the grid impedance. However, this method is not suitable for online identification due to the measurement time and additional power of electronic hardware.

Though frequency-response-based methods are able to describe the dynamic characteristics of the grid, they cannot get the physical parameters of electrical components directly. Furthermore, in many VSI control applications, model-based methods are commonly employed (the controller gains are related as a function of the LCL filter and VSI parameters), such that the prior-knowledge of these uncertain physical parameters is of vital importance. To address the uncertain parameters that existed in electrical power systems, model-based estimation methods are studied in recent years. In (Mohamed and El-Saadany (2008)), the neural networks (NN) based estimation method is proposed, it can obtain great estimation performance, but the NN-based control performance heavily depends on the convergence estimation and rate of NN weights which leads to heavy computational burden. In (Hoffmann and Fuchs (2013)), an extended Kalman filter (EKF) is applied to estimate the electrical components connected in the grid, but the covariance matrices need a tedious parameter tuning procedure.

According to the certainty equivalence principle, the overall performance of the grid will be greatly improved provided that the high accuracy and fast converge rate of online physical parameter estimation in the grid can be obtained. Especially, the start-up performance of the inverter can be simplified and the transient response can be improved. In the traditional adaptive parameter estimation algorithm framework such as the gradient descent method, a predictor and/or observer are generally used to generate predictor and/or observer error to design the adaptive law (de Mathelin and Lozano (1999)). However, the utilization of the gradient descent method may suffer from the potential bursting phenomenon, especially when the system is subject to the external disturbances. In order to overcome this issue, several prevalent robust adaptive laws have been successively proposed such as e-modification (Ioannou and Kokotovic (1983)), and σ-modification (Ortega and Tang (1989)). One salient of such robust adaptive law is that a leakage term is established to ensure the boundedness of the estimated parameters. However, the introduced damping term prevents the estimated parameters from converging to their true values, which means that there is a trade-off between accuracy and boundedness. It is worth noting that the online test of persistent excitation (PE) condition which is used to prove the parameter estimation convergence still remains a difficult challenge in the parameter estimation field. Therefore, it is worthy to further investigate a novel adaptive parameter estimation algorithm, which can not only estimate the system parameter accurately but also provide an intuitive approach to verity the PE condition.

Motivated by the above discussions, this study will propose a novel parameter estimation algorithm for the grid-converter system with LCL filter. To realize this purpose, a series of filter operations and auxiliary variables are used to extract the parameter estimation error information, which is used to construct a novel leakage term and online validate the PE condition. Then, a sliding mode term is studied and cooperated with a new leakage term to design the adaptive finite-time parameter estimation algorithm, by which the system parameters can be driven to their true values accurately and fast. The parameter estimation error convergence is rigorously proved in terms of the Lyapunov theory. Finally, simulation results are provided to demonstrate the effectiveness of the proposed method.

This study is organized as follows. **Section 2** provides the dynamic modeling of the grid-connected VSI with LCL filter in continuous-time model. **Section 3** presents the finite-time adaptive estimation algorithm design and analysis, and a comparison to another estimation algorithm. Comparison simulations are given in **Section 4**. Some conclusions are summarized in **Section 5**.

2 Dynamic modeling

In this section, continuous-time model for grid-connected VSI with LCL filter is first described. As shown in **Figure 1**,

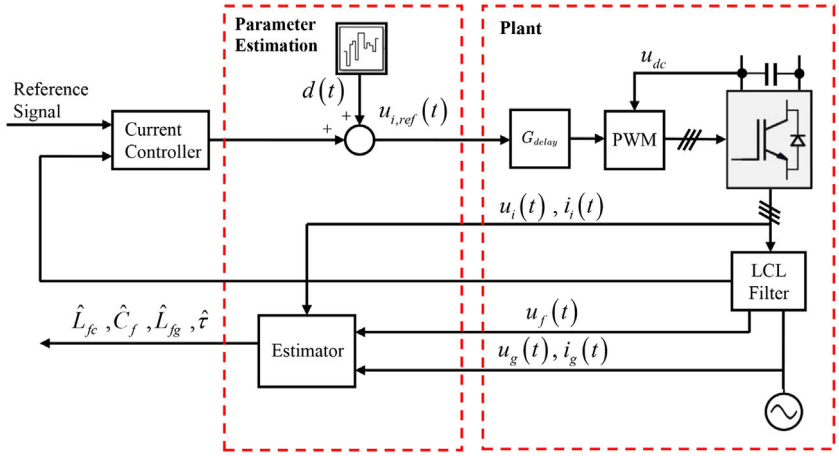

FIGURE 1
Schematic diagram of the estimation setup.

the inverter is supplied with a constant DC voltage $u_{dc}$and an LCL filter is inserted between VSI and the grid to attenuate the switching frequency harmonics caused by VSI. A current controller is applied to regulate the grid-side inductor current and digital control delay G_{delay} of the controller is also considered. Moreover, a parameter estimation scheme is added to the system with external disturbances $d(t)$. Note that the aim of this study is to propose a novel parameter estimation scheme to identify the physical parameters of the LCL filter and the digital control delay of VSI with accuracy and fast converge rate.

2.1 Model of LCL filter

For the ease of subsequent analysis, a single-phase equivalent circuit model of a typical LCL filter is shown in Figure 2, which is widely used in the grid application. As shown in Figure 2, the symbols u_i and i_i denote the inverter voltage and inverter current. u_f is the voltage across the shunt branch's filter capacitor, u_g and i_g represent the grid-side voltage and grid-side current. L_i, L_g, and C_f represent the inverter side inductance, the grid-side inductance, and the filter capacitance, respectively. Note that in practical engineering applications, the electrical components such as L_i, L_g, and C_f exist uncertainties because of the manufacturing tolerances, temperature changes, and aging phenomenon. Moreover, inductive grid impedance and the leakage inductance caused by the transformer will also lead to the parameter changing of L_i and L_g. In order to estimate the physical parameters of electrical components online, the dynamic of the LCL filter can be given by applying the Krichhoff's law (Massing et al. (2011)), note that equivalent resistors could be ignored since their impedances of them are far less than the one of inductance L_i and L_g.

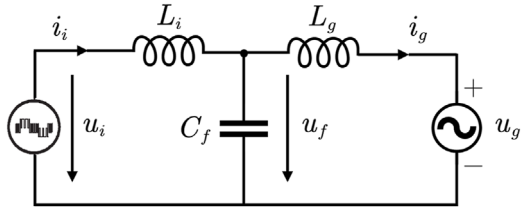

FIGURE 2
Single-phase equivalent circuit diagram.

$$\begin{cases} L_i \dot{i}_i = u_i - u_f \\ C_f \dot{u}_f = i_i - i_g \\ L_g \dot{i}_g = u_f - u_g \end{cases} \tag{1}$$

To facilitate the estimator design, we define the system states as $x_{ig} = \left[i_i, \quad u_f, \quad i_g\right]^T \in \Re^3$, and hence, the state-space form of system (1) can be written as

$$\begin{cases} \dot{x}_{ig} = A_{ig} x_{ig} + B_i u_i + B_g u_g \\ y = C x_{ig} \end{cases} \tag{2}$$

$$A_{ig}=\begin{bmatrix}0 & -\frac{1}{L_i} & 0\\ \frac{1}{C_f} & 0 & -\frac{1}{C_f}\\ 0 & \frac{1}{L_g} & 0\end{bmatrix},$$
$$B_i=\begin{bmatrix}\frac{1}{L_i}\\ 0\\ 0\end{bmatrix},\quad (3)$$
$$B_g=\begin{bmatrix}0\\ 0\\ -\frac{1}{L_g}\end{bmatrix},$$
$$C_i=\begin{bmatrix}0 & 0 & 1\end{bmatrix},$$

where $A_{ig}\in\Re^{3\times3}$ and $B_i\in\Re^{3\times1}$ and $C_i\in\Re^{1\times3}$ denote the system matrix, input matrix and output matrix, respectively. B_g represents the unknown parameter of the grid-side voltage.

2.2 Model of digitally controlled VSI

The digitally controlled inverters existing time delay includes the computation delay of the microprocessor, sampling period time delay, and time delay of the zero-order hold in the pulse width modulation converter (Agorreta et al. (2010)). Though the three elements are analyzed in the z-domain, few research works focused on the time-domain analysis. In this sense, the following time-continuous model is given:

$$G_{delay}=\frac{e^{-\tau\cdot s}\cdot(1-e^{-\tau\cdot s})}{\tau\cdot s},\quad (4)$$

where τ denotes the sampling period.

Note that **Eq. 4** cannot be used to establish the desired state-space form due to its complex transfer function. As analyzed by Agorreta et al. (2010); Houpis (1999); and Houpis and Sheldon (2013), **Eq. 4** can be rewritten in terms of the Pade approximation technique as follows:

$$G_{delay}=\frac{e^{-\tau\cdot s}\cdot(1-e^{-\tau\cdot s})}{\tau\cdot s}\approx\frac{1}{\tau\cdot s+1}\cdot\frac{1}{\tau}\cdot\frac{\tau}{0.5\tau\cdot s+1}\approx\frac{1}{0.5\tau^2s^2+1.5\tau s+1}.\quad (5)$$

Based on **Eq. 5**, a new G_{delay1} can be obtained:

$$G_{delay1}\approx G_{delay}=\frac{1}{1.5\tau s+1}.\quad (6)$$

Based on **Eq. 2** and **6**, the comprehensive state-space form of grid-connected VSI with LCL filter can be formulated as follows:

$$\begin{cases}\dot{x}=Ax+B_{uref}u_{i,ref}+B_{ga}u_g+\delta\\ y=Cx\end{cases}\quad (7)$$

where $x=\begin{bmatrix}i_i, & u_f, & i_g, & u_i\end{bmatrix}^T\in\Re^4$ is the overall system state. δ denotes approximation error and measurement noise which can be considered as a bounded disturbance i.e., $\|\delta\|\leqslant\varepsilon_\delta$ for a positive constant $\varepsilon_\delta>0$.

$$A=\begin{bmatrix}0 & -\frac{1}{L_i} & 0 & \frac{1}{L_i}\\ \frac{1}{C_f} & 0 & -\frac{1}{C_f} & 0\\ 0 & \frac{1}{L_g} & 0 & 0\\ 0 & 0 & 0 & -2/(3\tau)\end{bmatrix},$$
$$B_{uref}=\begin{bmatrix}0\\ 0\\ 0\\ 2/(3\tau)\end{bmatrix},\quad (8)$$
$$B_{ga}=\begin{bmatrix}0\\ 0\\ -\frac{1}{L_g}\\ 0\end{bmatrix}$$
$$C=\begin{bmatrix}0 & 0 & 1 & 0\end{bmatrix},$$

where $A\in\Re^{4\times4}$ and $C\in\Re^{1\times4}$ denote the augmented system matrix and augmented output matrix. $B_{ref}\in\Re^{4\times1}$ represents the augmented input matrix corresponding with the control input u_{ref} while $B_{ga}\in\Re^{4\times1}$ denotes the unknown parameter of the grid-side voltage u_g. Different from nonparametric frequency-response-based identification, model-based estimation method can describe the power electrical system by modelling with physical laws i.e., Kirchhoff's law. It is not difficult to find out that inductances, capacitances and digital control delay in the grid are directly included in the model **Eq. 7** which paved a new way to estimate these components directly.

ASSUMPTION 1: The system state and the reference control input of the system **Eq. 7** are bounded and accessible for measurement.

Note that Assumption 1 has been widely used in the estimation field [marino1995adaptive, adetola2008finite], and it can be satisfied by applying a proper controller.

3 Online parameter estimation

In this section, we will propose a finite-time adaptive parameter estimation algorithm to online estimate the unknown parameters encountered in the VSI with LCL filter.

3.1 Finite-time adaptive parameter estimation

For the ease of subsequent analysis, **Eq. 7** can be rewritten as

$$\dot{x}=\Phi(x,u)\,\Theta+\delta,\quad (9)$$

where $\Theta=\begin{bmatrix}1/L_i, & 1/C_f, & 1/L_g, & -2/(3\tau)\end{bmatrix}^T\in\Re^4$ is the augmented parameter to be estimated and $\Phi(x,u)=$

$\mathrm{diag}\left(-u_f+u_i,\quad i_i-i_g,\quad u_f-u_g,\quad -u_c+u_{ref}\right)\in\Re^{4\times4}$ represents the augmented regressor matrix. To extract the estimation error, a low-pass filter operation is imposed on both sides of **Eq. 9**, and the filtered variables x_f, $\Phi_f\left(x_f,u_f\right)$, δ_f of $x,\Phi(x,u)$ and δ can be defined as:

$$\begin{cases}\kappa\dot{x}_f+x_f=x,x_f(0)=0\\ \kappa\dot{\Phi}_f+\Phi_f=\Phi,\Phi_f(0)=0\\ \kappa\dot{\delta}_f+\delta_f=\delta,\delta_f(0)=0\end{cases}\tag{10}$$

where $\kappa>0$ is a positive filter parameter. Note that δ_f is only used for analysis.

The motivation for adopting the low-pass filter operation can be divided into two aspects. First, the low-pass filter can significantly eliminate the effect of the high-frequency noises (such as measurement noise), which is contributed to improving parameter estimation performance. Second, the measurement of the derivative terms such as $\dot{i}_i$, $\dot{u}_f$ and $\dot{i}_g$ is not an easy task, such that the adopted low-pass filter operation can avoid using such derivative.

Substituting **Eq. 10** into **Eq. 9**, one can deduce that

$$\Phi_f\Theta=\dot{x}_f-\delta_f=\frac{x-x_f}{\kappa}-\delta_f.\tag{11}$$

It should be pointed out that the non-zero initial condition $x(0)$ may bring an exponentially decaying term $\frac{1}{\kappa}e^{\frac{-t}{\kappa}}x(0)\to0$ when $t\to\infty$. Based on this conclusion, the effect of the initial condition will not be considered in the subsequent analysis as (Ortega et al. (2018); Aranovskiy et al. (2016, 2015))

In order to extract the parameter estimation error information with simple algebraic calculation, the auxiliary matrix $P\in\Re^{4\times4}$ and vector $N\in\Re^4$ are first defined as follows:

$$\begin{cases}\dot{P}=-lP+\Phi_f^T\Phi_f,P(0)=0\\ \dot{N}=-lN+\Phi_f^T\left[\left(x-x_f\right)/\kappa\right],N(0)=0\end{cases}\tag{12}$$

where the parameter $l>0$ is designed to guarantee the boundness of auxiliary matrix P and vector N. By integrating on both sides of **Eq. 12**, one can deduce that

$$\begin{cases}P(t)=\int_0^t e^{-l(t-r)}\Phi_f^T(r)\,\Phi_f(r)\,dr\\ N(t)=\int_0^t e^{-l(t-r)}\Phi_f^T(r)\left[\left(x(r)-x_f(r)\right)/k\right]dr\end{cases}\tag{13}$$

Furthermore, another auxiliary vector $H\in\Re^4$ is designed along with **Eq. 7** as

$$H=P\hat{\Theta}-N=-P\tilde{\Theta}+\Psi,\tag{14}$$

where $\hat{\Theta}$ denotes the estimation, i.e., error of unknown system parameters. $\tilde{\Theta}=\Theta-\hat{\Theta}$ is the parameter estimation error. $\Psi=\int_0^t e^{-\ell(t-r)}\phi_f^T(r)\delta_f(r)\mathrm{d}r$ represents the bounded residual error since state x is assumed to be bounded which further means that Φ and Φ_f are also bounded. Hence, the condition $\|\Psi\|\leqslant\delta_\psi$ is true for a positive constant $\delta_\psi>0$. Moreover, we can see that the parameter estimation error information is included in H, which will used to construct a new leakage term to design the adaptive parameter estimation algorithm.

Generally, the persistent excitation (PE) condition is required to guarantee the parameter estimation convergence in the adaptive parameter estimation. To verify the PE condition online, the following Lemma is given.

Lemma 1:

If the regressor matrix Φ defined in **Eq. 9** fulfils the PE condition, the matrix P is positive define, i.e., the minimum eigenvalue of P in **Eq. 12** fulfils the condition $\lambda_{\min}(P)>\sigma>0$ for a positive constant σ.

Proof: According to the definition of PE (Na et al. (2015)) condition, the inequality $\int_t^{t+T}\Phi_f^T\Phi_f dr\geqslant\rho I$ is equivalent to $\int_{t-T}^t\Phi_f^T\Phi_f dr\geqslant\rho I$ for $t>T>0$. Therefore, one can deduce that the inequality $\int_{t-T}^t\Phi_f^T\Phi_f dr\geqslant\rho I$ is true for $t>T>0$ provided that the filtered regressor matrix Φ_f satisfies the PE condition. Note that the Φ_f is the filtered variable of Φ, such that the PE condition for Φ is equivalent for Φ_f. Therefore, considering the integrating interval $\lambda\in[t-T,t]$, the inequality $e^{-l(t-\lambda)}\geqslant e^{-lT}>0$ is true for $t-\lambda<T$, one can deduce that

$$\int_{t-T}^t e^{-l(t-\lambda)}\Phi_f^T\Phi_f d\lambda\geqslant\int_{t-T}^t e^{-lT}\Phi_f^T\Phi_f d\lambda\geqslant e^{-lT}\rho I.\tag{15}$$

For $t>T>0$, **Eq. 15** can be rewritten as

$$\int_0^t e^{-l(t-\lambda)}\Phi_f^T\Phi_f d\lambda>\int_{t-T}^t e^{-l(t-\lambda)}\Phi_f^T\Phi_f d\lambda.\tag{16}$$

Based on **Eq. 15** and **16**, we can obtain

$$P=\int_0^t e^{-l(t-\lambda)}\Phi_f^T\Phi_f d\lambda>e^{-lT}\int_{t-T}^t\Phi_f^T\Phi_f d\lambda\geqslant e^{-lT}\rho I.\tag{17}$$

According to **Eq. 17**, we can claim that if the matrix P is positive definite, the condition $\lambda_{\min}(P)>\sigma>0$ is true for $\sigma=e^{-lT}\rho$.

Remark 1: In order to increase the excitation level, an excitation signal in $\alpha\beta$ frame is added to the output of the current loop controller which is also the reference input voltage of inverter u_{ref}. The excitation signal is given as $u_n=u_{n\alpha}+ju_{n\beta}$. We add the excitation signal in β-direction since it can reduce the effects of the inverter nonlinearities on the PWM generator and parameter estimation (Koppinen et al. (2017)). Moreover, the trade-off between excitation power and current harmonic distortion should be carefully considered since a small amplitude of excitation signal will not excite the desired frequency components, while a larger one will cause harmonic distortion in the grid current.

Given the fact that the utilization of parameter estimation error $P\tilde{\Theta}$ in adaptation will be beneficial for the parameter estimation performance, a finite-time adaptive parameter estimation scheme is developed as follows:

$$\dot{\hat{\Theta}}=-\Gamma_1\frac{P^TH}{\|H\|},\tag{18}$$

where $\Gamma_1>0$, $\Gamma_1\in\Re^{4\times4}$.

Theorem 1:

For inverter system with LCL filter Eq. 9 and the parameter adaptation law in Eq. 18, the estimation parameter $\hat{\Theta}$ is bounded and the estimation error $\tilde{\Theta}$ will converge to a small set around zero i.e., $\tilde{\Theta}$ is uniformly ultimately bounded (UUB) in a finite time satisfying $\lim_{t\to\infty} P_1\tilde{\theta} = \Psi$.

Proof:

In the inverter system equipped by LCL filter with extra excitation signal, we assume that Φ fulfils the PE condition. And based on Lemma 1, we can guarantee that $\lambda_{\min}(P) > \sigma > 0$. Then, we first proof that the estimation parameter $\hat{\Theta}$ is bounded. By calculating the time derivative of $P^{-1}H = -\tilde{\Theta} + P^{-1}\Psi$, one can get

$$\begin{aligned}\frac{\partial P^{-1}H}{\partial t} &= -\dot{\tilde{\Theta}} + \frac{\partial P^{-1}}{\partial t}\Psi + P^{-1}\dot{\Psi} = \dot{\hat{\Theta}} - P^{-1}\dot{P}P^{-1}\Psi \\ &\quad + P^{-1}\dot{\Psi} = \dot{\hat{\Theta}} + \Psi', \end{aligned} \tag{19}$$

where $\Psi' = -P^{-1}\dot{P}P^{-1}\Psi + P^{-1}\dot{\Psi}$; we then choose the Lyapunov function as $V = 1/2H^T P^{-1}P^{-1}H$, and its derivation can be deduced as

$$\begin{aligned}\dot{V} &= H^T P^{-1}\frac{\partial P^{-1}H}{\partial t} = -H^T P^{-1}\Gamma_1\frac{P^T H}{\|H\|} + H^T P^{-1}\Psi' \\ &\leqslant -\left(\lambda_{\min}(\Gamma_1) - \|P^{-1}\Psi'\|\right)\|H\|. \end{aligned} \tag{20}$$

Focusing on the term $\|P^{-1}\Psi'\|$, one can find that Ψ and $\dot{\Psi}$ is bounded since the disturbance δ and filtered residual error Ψ_f are bounded, P and P^{-1} are also bounded for bounded Ψ_f. Furthermore, PE condition can further ensure that P^{-1} is bounded. Hence, if Γ_1 is large enough to satisfy $\lambda_{\min}(\Gamma_1) > \|P^{-1}\Psi'\|$, the estimation error $\tilde{\Theta}$ and estimation parameter are all bounded.

According to Eq. 20 and rewrite it as $\dot{V} \leqslant -\mu\sqrt{V}$ with $\mu = \sqrt{2}\sigma\left(\lambda_{\min}(\Gamma_1) - \|P^{-1}\Psi'\|\right)$ which is a positive scalar and needs to be selected large enough. From finite-time convergence of Lyapunov solution V, that the auxiliary vector with parameter error will converge to zero in finite time, i.e., $\lim_{t\to\infty} H = 0$ in $t_f = 2\sqrt{V(0)}/\mu$. Based on $\dot{V} \leqslant -\mu\sqrt{V}$ we can claim that in $t \in \left[0, t_f\right]$, the plant Eq. 18 evolves in a sliding mode along the surface $H = 0$, which further means that $\lim_{t\to\infty} P\tilde{\Theta} = \Psi$ is true in finite time. It should be noted that the sliding mode term in Eq. 18 will not lead to severe chattering problem in the estimated parameters as the integrating operation imposed on term $H/\|H\|$ (Na et al. (2019)).

Remark 2:

From the above proof, one can find that the convergence rate of estimation error depends on the learning gain Γ_1 and excitation level σ. Generally, a large learning gain and excitation level can obtain a faster converge rate, while too large gain may trigger parameter oscillation. The forgetting factor l in Eq. 12 is set to the penalty of the initial condition which is not suggested to be large. Filter parameter κ in Eq. 10 denotes the "bandwidth" of the filter. Hence, there is also a trade-off between converge rate and robustness in selecting the value of the forgetting factor and filter parameter.

3.2 Gradient-based adaptive parameter estimation

In order to further show the superiority of the proposed adaptive law over conventional method, a brief discussion of gradient-based adaptive parameter estimation algorithm is provided in this subsection. First, an observer is designed for the system in Eq. 7:

$$\dot{\hat{x}} = \Phi(x,u)\hat{\alpha} + \lambda(x - \hat{x}), \tag{21}$$

where $\lambda > 0$ denotes the observer gain, $\Phi(x,u) = \mathrm{diag}\left(-u_f + u_i,\ \ i_i - i_g,\ \ u_f - u_g,\ \ -u_c + u_{ref}\right) \in \mathfrak{R}^{4\times 4}$ denotes the regressor matrix and $\hat{\alpha} = \left[1/\hat{L}_i,\ \ 1/\hat{C}_f,\ \ 1/\hat{L}_g,\ \ -2/(3\hat{\tau})\right]^T \in \mathfrak{R}^4$ represents the unknown parameter. $\hat{x} = \left[\hat{i}_i,\ \ \hat{u}_f,\ \ \hat{i}_g,\ \ \hat{u}_i\right]^T \in \mathfrak{R}^4$ is the observer state which is needed to be observed. First, we design the observer error $e = x - \hat{x}$, $e \in \mathfrak{R}^4$ and the corresponding time derivative can be calculated as

$$\dot{e} = -\lambda e + \Phi(x,u)\tilde{\alpha}. \tag{22}$$

In order to minimize the power of the estimation error e by $\partial e^2/\partial\alpha = 0$, one can design the adaptive law by using the observer error e as

$$\dot{\hat{\alpha}} = \Gamma_2\Phi^T\frac{e}{m^2}, \tag{23}$$

where Γ_2 denotes the learning gain of gradient-based adaptive law, m^2 is a normalizing signal designed by $m = 1 + \|\Phi\|$ as explained by de Mathelin and Lozano (1999). According to Eq. 23, we can find that different from the finite-time estimation algorithm Eq. 18 with parameter estimation error, the gradient-based method depends on a predictor/observer to create the predictor/observer error for driving the adaptive law which may indirect for online parameter estimation.

Remark 3: Grid converters are usually controlled by model-based control algorithms, which means that the estimated parameters like the LCL filter will participate directly/indirectly in the design of the controller. Moreover, from (Xie and Chen (2021); Tao et al. (2022)) we can find that the accuracy and the converge rate of the estimated parameter can impact the overall control performance, which further suggests that a proper estimation algorithm dedicates to grid-connected control. Though there exist some online parameter estimation methods such as gradient-based adaptive law and σ-modification, the estimated parameters may need a fairly time to converge or even not able to converge to the real value. On the contrary, the proposed finite-time adaptive estimation algorithm can drive the estimated parameters toward the real value in finite time. In this sense, the overall control performance can be improved, the controller's overall performance, especially during the start-up period.

4 Simulation

In this section, the parameter estimation of the LCL filter with VSI is simulated in MATLAB/SimPowerSystems software environment. Comparative simulation results are given to demonstrate the effectiveness of the proposed method. The parameters to be estimated and the associate parameters are listed in **Table 1** (Koppinen et al. (2017)). Note that the DC voltage is constant and the time delay of digitally control in VSI is considered. Moreover, the sampling frequency is set as $f_s = 10\text{kHz}$ and the inverter switching frequency is set at half of the sampling frequency i.e., $f_{PWM} = 5\text{kHz}$.

The current controller implemented in this simulation is a typical PI controller based on dq synchronous reference frame and the purpose of the controller is to regulate the grid-side inductor current i_q. Note that some existing PWM-based control strategies such as repetitive controllers (De Almeida et al. (2014)) and resonant integrator controllers (Yepes et al. (2010)) can be used instead. Moreover, the up-to-date grid-voltage angle ω_g can be calculated from the measured grid voltage by the phase-locked loop (PLL) method.

Comparison to gradient-based algorithms: For a fair comparison, the control parameters in the current controller and PLL are taken as the same value, which means that the input signal u_{ref} is the same in two estimation process. Moreover, an extra noise $d = 10rand(0.1)$ with mean 0 and variance 0.1 is added into the system to increase the excitation level.

From **Figure 3**, it can be found that the minimum eigenvalue of matrix $P(t)$ is larger than zero (e.g., $\lambda_{\min}(P(t)) > \sigma > 0$). Therefore, the regressor vector Φ satisfies the PE condition according to Lemma 1. Moreover, by calculating the $\lambda_{\min}(P(t))$, we can online validate the PE condition, which is helpful in practical application. Note that in finite-time estimation, as one can find in previous proof of the theorem, input signals with high excitation levels may improve the convergence rate of estimation errors.

The associated parameters are chosen as $\Gamma_1 = 5\text{diag}\left(50, 5\times10^6, 5, 1\right)$, filter constant $\kappa = 0.01$ and forgetting factor $l = 0.2$ via a trial-and-error method. Note that the initial values in the simulation are set as zero. And the parameters in gradient-based parameter estimation **Eq. 23** are set as $\Gamma_2 = 5\text{diag}\left(400, 5\times10^6, 6, 1\right)$ and $\lambda = 5\text{diag}\left(30, 5\times10^3, 50, 20\right)$.

Figure 4 illustrates the comparative parameter estimation performance between the proposed adaptive estimation algorithm and gradient-based estimation algorithm. The estimated parameters based on the aforementioned algorithms are listed in **Table 2**. As shown in **Figure 4** and **Table 2**, we can find that the proposed adaptive estimation algorithm **Eq. 18** obtains a fast parameter convergence speed and accuracy than that of the gradient-based algorithm. The reason for this phenomenon is that the information of parameter estimation error $P\tilde{\Theta}$ in H is used to drive the adaptive law **Eq. 18**, while only the observer error e is employed in the gradient-based algorithm, and it can again verify the effectiveness of the proposed algorithm.

Figure 5 provides the frequency responses of the proposed adaptive law and gradient-based adaptive law in terms of the Bode diagram, respectively. We can find from **Figure 5** that the proposed adaptive law can accurately estimate the resonant peak and slopes at the high frequency of the LCL filter in the presence of time delay compared with the gradient-based adaptive law due to the precise parameter estimation performance. The improved performance can be also found from the phase angle. Based on the above simulation results, we can further deduce that the proposed parameter estimation method for the LCL filter may provide an alternative way to carry out the corresponding controller design to attenuate the resonant peak to obtain a stable grid current.

TABLE 1 Simulation system parameters.

Symbol	Value	Symbol	Value
u_{dc}	800 V	L_i	3.3 mH
u_g	$400\sqrt{2/3}$ V	C_f	8.8 μF
ω_g	$2\pi \cdot 50$ rad/s	L_g	3.0 mH
f_s	10 kHz	f_{PWM}	5 kHz

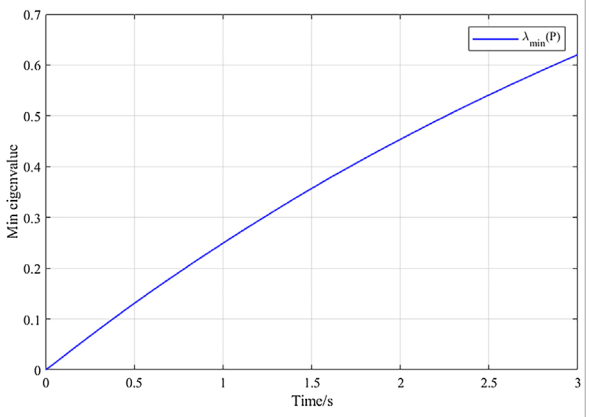

FIGURE 3
Minimum eigenvalue of $P(t)$.

TABLE 2 Estimation of parameters.

Symbol	Reference value	Finite time	Gradient based
$1/L_i$	303.03	302.14	334.33
$1/C_f$	113636.36	113510.83	94854.50
$1/L_g$	333.33	332.46	340.10
$1/\tau$	10000.00	9920.66	10288.59

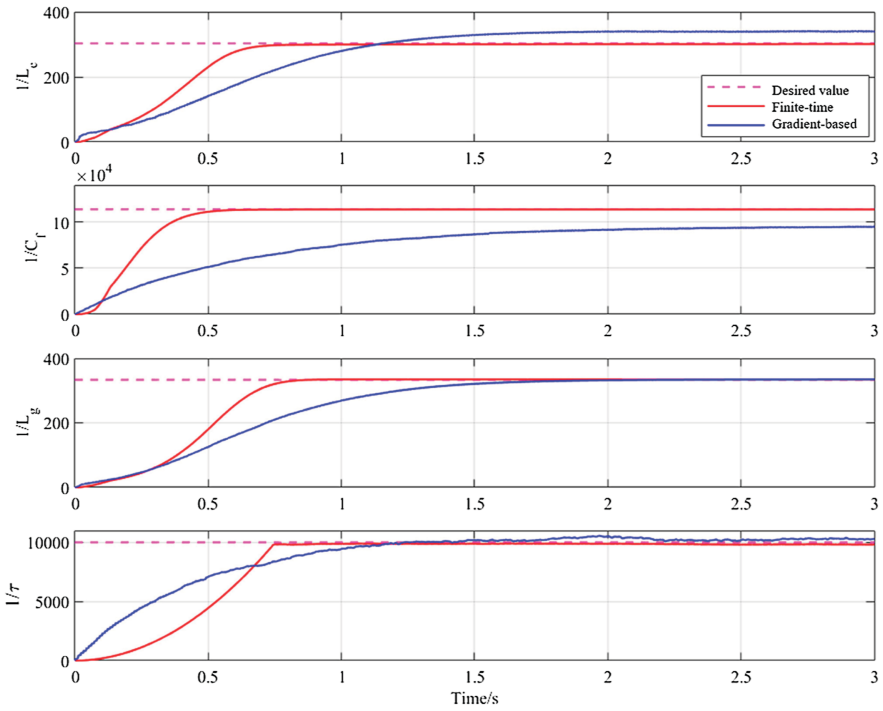

FIGURE 4
Parameter estimation compared with the proposed method and gradient-based method.

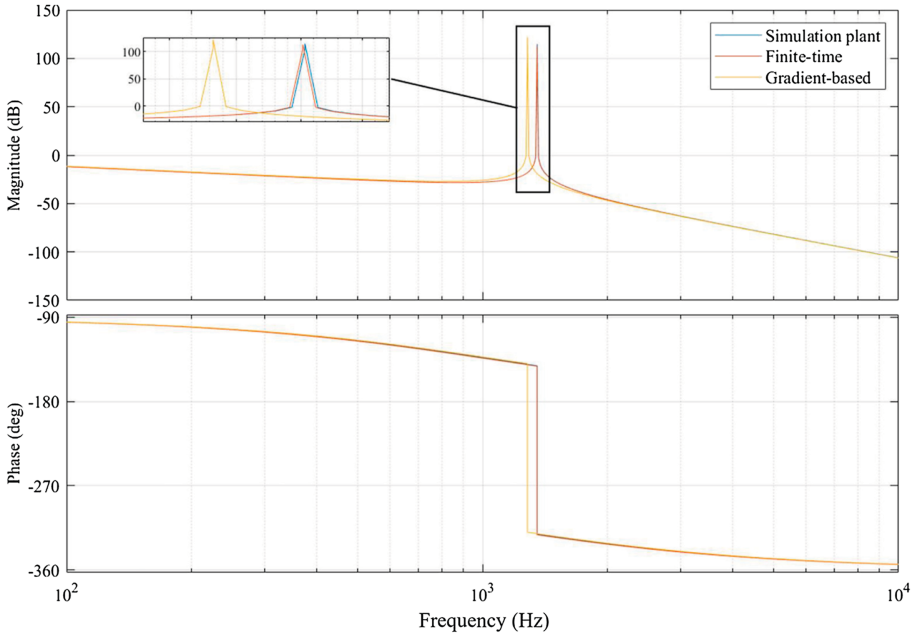

FIGURE 5
Frequency responses of LCL filter with two estimation methods.

5 Conclusion

In this study, an online finite-time adaptive parameter estimation method was proposed for a grid-converter system with LCL filter in time-continuous state-space form. Different from the conventional predictor/observer-based method, the proposed framework could achieve high accuracy and fast converge rate by applying parameter estimation error in driving adaptive law and a sliding mode term is studied and cooperated with new leakage term to design the finite-time adaptive parameter estimation algorithm. Theoretical analysis was studied by Lyapunov theory to demonstrate the convergence of the estimation error. Moreover, a comparative simulation was developed to illustrate the effectiveness of the proposed method. Applying the proposed method to estimate the electrical components can be beneficial for fault diagnosis of the electrical power system. The future work will focus on combining the proposed parameter estimation method with a certain controller to enhance the overall control performance of the grid, and experiments will also carry out in the future.

Data availability statement

The original contributions presented in the study are included in the article/Supplementary Material; further inquiries can be directed to the corresponding author.

Author contributions

XX: analysis, modeling, and writing—original draft. ZS: data curation and writing—original draft. XW: conceptualization and methodology. CX: writing—reviewing the draft. SL: writing—reviewing and editing.

Funding

This work was supported in part by the National Natural Science Foundation of China under Grant 52167011; in part by the National Key Research and Development Program of China under Grant 2019YFE0118000; and in part by the Yunan Fundamental Research Projects under Grant 202001AU070056.

Conflict of interest

XX, CX, and SL were employed by the Electric Power Research Institute of Yunnan Power Grid Co., Ltd.

The remaining authors declare that the research was conducted in the absence of any commercial or financial relationships that could be construed as a potential conflict of interest.

Publisher's note

All claims expressed in this article are solely those of the authors and do not necessarily represent those of their affiliated organizations, or those of the publisher, the editors, and the reviewers. Any product that may be evaluated in this article, or claim that may be made by its manufacturer, is not guaranteed or endorsed by the publisher.

References

Agorreta, J. L., Borrega, M., López, J., and Marroyo, L. (2010). Modeling and control of *N*-paralleled grid-connected inverters with LCL filter coupled due to grid impedance in PV plants. *IEEE Trans. Power Electron.* 26, 770–785. doi:10.1109/TPEL.2010.2095429

Aranovskiy, S., Bobtsov, A. A., Pyrkin, A. A., Ortega, R., and Chaillet, A. (2015). Flux and position observer of permanent magnet synchronous motors with relaxed persistency of excitation Conditions∗∗This article is supported by government of Russian federation (grant 074-U01, GOSZADANIE 2014/190 (project 2118)), the ministry of education and science of Russian federation (project 14.Z50.31.0031). *IFAC-PapersOnLine* 48, 301–306. doi:10.1016/j.ifacol.2015.09.202

Aranovskiy, S., Bobtsov, A., Ortega, R., and Pyrkin, A. (2016). "Parameters estimation via dynamic regressor extension and mixing," in 2016 American Control Conference (ACC) (Boston, MA, USA: IEEE), 6971–6976. doi:10.1109/ACC.2016.7526771

De Almeida, P. M., Duarte, J. L., Ribeiro, P. F., and Barbosa, P. G. (2014). Repetitive controller for improving grid-connected photovoltaic systems. *IET Power Electron.* 7, 1466–1474. doi:10.1049/iet-pel.2013.0546

de Mathelin, M., and Lozano, R. (1999). Robust adaptive identification of slowly time-varying parameters with bounded disturbances. *Automatica* 35, 1291–1305. doi:10.1016/S0005-1098(99)00026-6

Feng, C., Liang, B., Li, Z., Liu, W., and Wen, F. (2022). Peer-to-peer energy trading under network constraints based on generalized fast dual ascent. *IEEE Trans. Smart Grid* 1, 3162876. doi:10.1109/tsg.2022.3162876

Gomes, C. C., Cupertino, A. F., and Pereira, H. A. (2018). Damping techniques for grid-connected voltage source converters based on lcl filter: An overview. *Renew. Sustain. Energy Rev.* 81, 116–135. doi:10.1016/j.rser.2017.07.050

Hoffmann, N., and Fuchs, F. W. (2013). Minimal invasive equivalent grid impedance estimation in inductive–resistive power networks using extended kalman filter. *IEEE Trans. Power Electron.* 29, 631–641. doi:10.1109/TPEL.2013.2259507

Houpis, C. H. (1999). *Quantitative feedback theory: Fundamentals and applications*. Boca Raton, FL, USA: CRC Press. doi:10.4324/9780203908051

Houpis, C. H., and Sheldon, S. N. (2013). *Linear control system Analysis and design with MATLAB®*. Boca Raton, FL, USA: CRC Press.

Ioannou, P. A., and Kokotovic, P. V. (1983). *Adaptive systems with reduced models*. Berlin, Germany: Springer. doi:10.1007/BFb0006363

Koppinen, J., Kukkola, J., and Hinkkanen, M. (2017). Plug-in identification method for an lcl filter of a grid converter. *IEEE Trans. Ind. Electron.* 65, 6270–6280. doi:10.1109/TIE.2017.2787546

Liserre, M., Blaabjerg, F., and Hansen, S. (2005a). Design and control of an lcl-filter-based three-phase active rectifier. *IEEE Trans. Ind. Appl.* 41, 1281–1291. doi:10.1109/TIA.2005.853373

Liserre, M., Blaagjerg, F., and Teodorescu, R. (2005b). "Grid impedance detection via excitation of lcl-filter resonance," in Fourtieth IAS Annual Meeting. Conference Record of the 2005 Industry Applications Conference, 2005 (Hong Kong, China: IEEE), 910–916. Vol. 2.

Massing, J. R., Stefanello, M., Grundling, H. A., and Pinheiro, H. (2011). Adaptive current control for grid-connected converters with lcl filter. *IEEE Trans. Ind. Electron.* 59, 4681–4693. doi:10.1109/TIE.2011.2177610

Mohamed, Y. A.-R. I., and El-Saadany, E. F. (2008). Adaptive discrete-time grid-voltage sensorless interfacing scheme for grid-connected dg-inverters based on neural-network identification and deadbeat current regulation. *IEEE Trans. Power Electron.* 23, 308–321. doi:10.1109/TPEL.2007.911879

Mohamed, Y. A.-R. I. (2010). Mitigation of dynamic, unbalanced, and harmonic voltage disturbances using grid-connected inverters with LCL filter. *IEEE Trans. Ind. Electron.* 58, 3914–3924. doi:10.1109/TIE.2010.2098372

Na, J., Mahyuddin, M. N., Herrmann, G., Ren, X., and Barber, P. (2015). Robust adaptive finite-time parameter estimation and control for robotic systems. *Int. J. Robust Nonlinear Control* 25, 3045–3071. doi:10.1002/rnc.3247

Na, J., Wang, S., Liu, Y.-J., Huang, Y., and Ren, X. (2019). Finite-time convergence adaptive neural network control for nonlinear servo systems. *IEEE Trans. Cybern.* 50, 2568–2579. doi:10.1109/TCYB.2019.2893317

Ortega, R., Praly, L., Aranovskiy, S., Yi, B., and Zhang, W. (2018). On dynamic regressor extension and mixing parameter estimators: Two luenberger observers interpretations. *Automatica* 95, 548–551. doi:10.1016/j.automatica.2018.06.011

Ortega, R., and Tang, Y. (1989). Robustness of adaptive controllers — A survey. *Automatica* 25, 651–677. doi:10.1016/0005-1098(89)90023-X

Reigosa, D., Briz, F., Charro, C. B., García, P., and Guerrero, J. M. (2012). Active islanding detection using high-frequency signal injection. *IEEE Trans. Ind. Appl.* 48, 1588–1597. doi:10.1109/TIA.2012.2209190

Reznik, A., Simões, M. G., Al-Durra, A., and Muyeen, S. (2013). LCL filter design and performance analysis for grid-interconnected systems. *IEEE Trans. Ind. Appl.* 50, 1225–1232. doi:10.1109/TIA.2013.2274612

Schlesinger, R., and Biela, J. (2020). Comparison of analytical models of transformer leakage inductance: Accuracy versus computational effort. *IEEE Trans. Power Electron.* 36, 146–156. doi:10.1109/TPEL.2020.3001056

Tang, Y., Loh, P. C., Wang, P., Choo, F. H., and Gao, F. (2011). Exploring inherent damping characteristic of lcl-filters for three-phase grid-connected voltage source inverters. *IEEE Trans. Power Electron.* 27, 1433–1443. doi:10.1109/TPEL.2011.2162342

Tang, Y., Yao, W., Loh, P. C., and Blaabjerg, F. (2015). Design of lcl filters with lcl resonance frequencies beyond the nyquist frequency for grid-connected converters. *IEEE J. Emerg. Sel. Top. Power Electron.* 4, 3–14. doi:10.1109/JESTPE.2015.2455042

Tao, M., Chen, Q., He, X., and Xie, S. (2022). Fixed-time filtered adaptive parameter estimation and attitude control for quadrotor uavs. *IEEE Trans. Aerosp. Electron. Syst.* 1, 3159770. doi:10.1109/TAES.2022.3159770

Xie, S., and Chen, Q. (2021). Adaptive nonsingular predefined-time control for attitude stabilization of rigid spacecrafts. *IEEE Trans. Circuits Syst. Ii.* 69, 189–193. doi:10.1109/TCSII.2021.3078708

Yepes, A. G., Freijedo, F. D., López, O., and Doval-Gandoy, J. (2010). High-performance digital resonant controllers implemented with two integrators. *IEEE Trans. Power Electron.* 26, 563–576. doi:10.1109/TPEL.2010.2066290

frontiers | Frontiers in Energy Research

TYPE Mini Review
PUBLISHED 07 September 2022
DOI 10.3389/fenrg.2022.1002973

OPEN ACCESS

EDITED BY
Changsen Feng,
Zhejiang University of Technology, China

REVIEWED BY
Zhanhong Wei,
Lanzhou University of Technology, China
Ying Han,
Southwest Jiaotong University, China

*CORRESPONDENCE
Shuaibing Li,
lishuaibing1105@163.com

SPECIALTY SECTION
This article was submitted to Smart Grids, a section of the journal Frontiers in Energy Research

RECEIVED 25 July 2022
ACCEPTED 15 August 2022
PUBLISHED 07 September 2022

CITATION
Li S, Li X, Kang Y and Gao Q (2022), Load capability assessment and enhancement for transformers with integration of large-scale renewable energy: A brief review. *Front. Energy Res.* 10:1002973. doi: 10.3389/fenrg.2022.1002973

Load capability assessment and enhancement for transformers with integration of large-scale renewable energy: A brief review

Shuaibing Li*, Xinchen Li, Yongqiang Kang and Quanyi Gao

School of New Energy and Power Engineering, Lanzhou Jiaotong University, Lanzhou, China

With the rapid development of large-scale distributed renewable energy in China, the load factor of distribution transformer increases year by year, this directly become a new challenge to the load capacity of the transformer. Once subjected to this condition for a long time will have an impact on the hotspot temperature and consequently, the useful life of the transformer. In this regard, load capacity assessment of the distribution transformer becomes an essential work for unit upgrading or even replacement. This article systematically summarized the evaluation methods of transformer load capacity, as well as the load capacity prediction and dynamic capacity enhancement strategies of transformer. Discussions for the future work regarding this topic are also carried out.

KEYWORDS

renewable energy, distribution transformer, hotspot temperature, load capacity, dynamic capacity

1 Introduction

To fulfill the goal of carbon neutral, the Chinese power utilities are advancing the development of a new power system dominated by new energy, especially for large-scale integrated wind and solar power generations and the distributed renewable energy resources, as shown in Figure 1. This directly leads to the increase of the load factor of transformers year by year. On the distribution side, the power flow is no longer one direction, i.e., flowing from the distribution transformer to users, but becomes a bi-direction mode as distributed renewable energy resources integrated to the network (Feng et al., 2018; Feng et al., 2022; Jiang et al., 2022). Figure 1 shows a schematic diagram of a distribution network dominated by new energy generation, demonstrating the load changes from the traditional single distribution load curve to a composite load combining distribution load and new energy online load.

The introduction of large-scale distributed renewable energy sources poses a great threat to the safe operation of the power grid. If the load capacity assessment and dynamic capacity enhancement of the transformer can be realized, the load potential can be fully exploited and the threat posed to the grid by the composite load can be controlled. This enables real-time regulation of the transformer load, so intelligent transformers (Ma et al., 2015) with information sensing technology become a new trend. To improve the

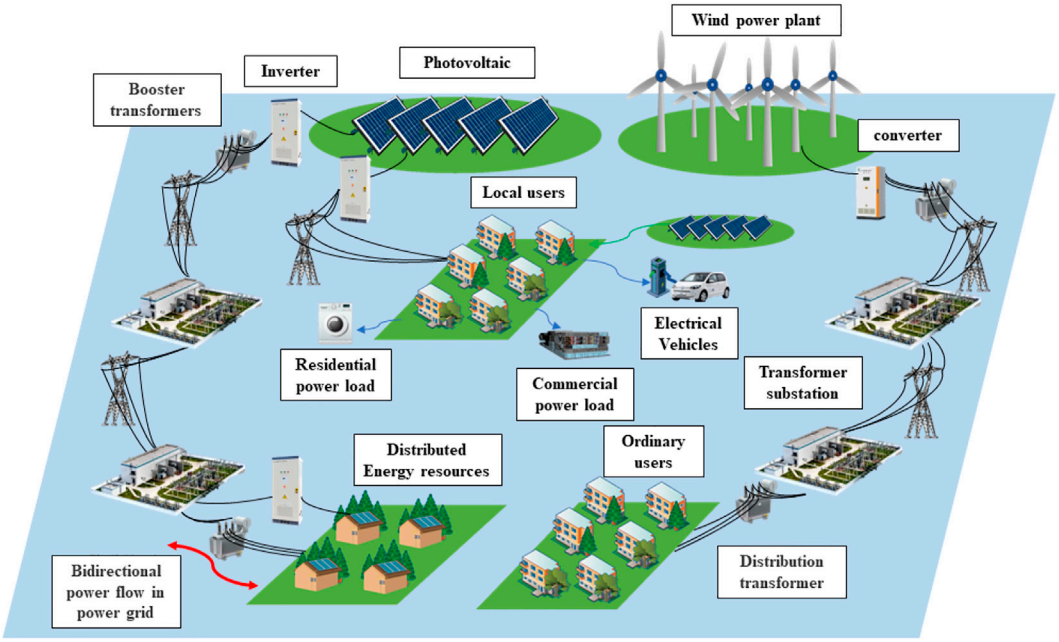

FIGURE 1
A schematic of the new energy power generation dominated distribution network.

intelligence of transformer, the condition assessment model, overload model, insulation aging model, heat balance model, cooling model, etc. have been established to assess and predict the condition of the transformer. This greatly advances the condition-based maintenance of the transformer.

Therefore, the study of the load capacity of transformers is essentially a matter of ensuring that the actual maximum load that a transformer can withstand and the duration it can last without the hotspot temperature (HST) exceeding the limit (Tang et al., 2017). In the standards of IEC 60076-7, GB/T 1094.7 and IEEE Std C57.91-2011, the limits for overload operation of oil-immersed power transformers are specified. The HST of the transformer winding insulation system is the main determinant of the load capacity, and when the HST exceeds the limit, it will lead to insulation damage or loss of life (Zhong et al., 2021).

This paper briefly summarizes the current load capacity assessment methods and expounds the load prediction methods, as well as the necessity of dynamic capacity enhancement. The problems of current load capacity assessment methods are discussed and suggestions for the future study are proposed.

2 Influence factor of transformer load capacity

The load capacity of a transformer is determined by factors such as material selection and process control during its manufacturing phase, which reflects the inherent level of transformer load capacity. The load capacity of a transformer in operation is not only determined by its inherent level, but is also influenced by the operating factors such as the HST, ambient temperature, and cooling method. This section will detail such factors one by one.

2.1 Hot spot temperature

The core and winding of the transformer are the main source of the heat generation, where the temperature of the hottest spot in the winding is called the HST. Currently, there are three kinds of method to obtain the HST of transformers, including the direct method, the numerical analysis method, and the thermoelectric analogous model. The HST temperature limit for transformers is specified in GB/T 1094.7, which can be expressed as Eq. 1. The load condition of the transformer can have an effect on the HST.

$$\theta_h(t) = \theta_a + \Delta\theta_{or} + \left\{\Delta\theta_{or} \times \left[\frac{1 + R \times K^2}{1 + R}\right]^x - \Delta\theta_{or}\right\} \times f_1(t) + \Delta\theta_{hr} + \left\{Hg_r K^y - \Delta\theta_{hr}\right\} \times f_2(t) \quad (1)$$

where, θ_a is the ambient temperature, $\Delta\theta_{or}$ is the standard oil temperature rise, $\Delta\theta_{hr}$ is the oil temperature gradient, R is the loss ratio, K is the ratio of actual load to rated load, x is top oil index,

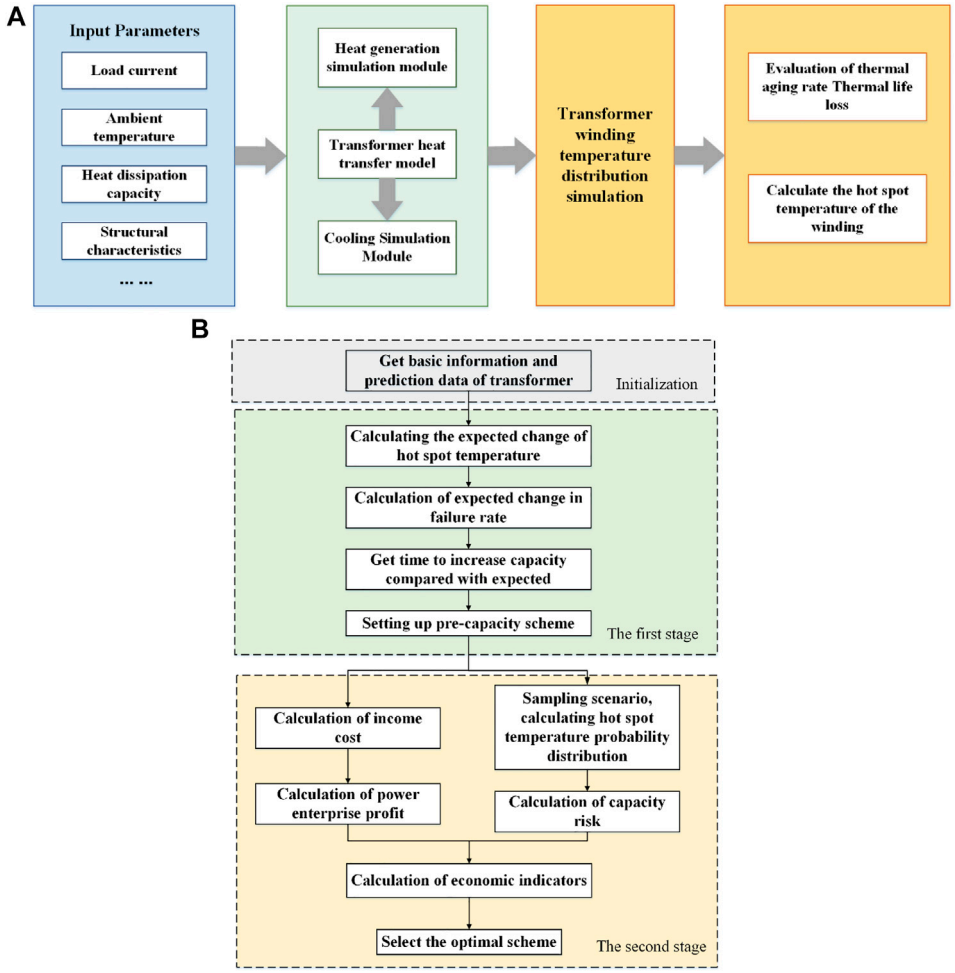

FIGURE 2
Online evaluation model and calculation process for load capacity assessment. **(A)** Online evaluation model for load capacity of oil-immersed power transformers, **(B)** calculation process of multi-risk transformer dynamic capacity increase strategy.

H is HST coefficient, g_r is the temperature difference between the average temperature of the winding and oil temperature measured by the test, y winding index, $f_1(t)$, $f_2(t)$ are in the exponential form, indicating the slow process of internal temperature rise or fall.

2.1.1 Direct detection method

The direct detection methods incorporate two categories: invasive measurements (Qian et al., 2003; Lobo Ribeiro et al., 2008; Liu et al., 2020) and non-invasive measurements (Ruan et al., 2020).

The invasive detection of winding HST is mainly realized by direct measurements. For example, the U. S. Luxtron Corporation applies a stable light body temperature sensor (Qian et al., 2003) to sense the HST of a transformer, and a multipoint fiber optic temperature sensor network system is integrated inside the transformer (Lobo Ribeiro et al., 2008). Some built-in distributed fibers combined with thermocouple are also introduced to for direct measurement (Liu et al., 2020).

In comparative, the non-invasive measurement of HST is mainly realized by infrared techniques with interpreting the streamline heat dissipation model of the internal heat source of the equipment (Ruan et al., 2020). The mapping relationship between the shell characteristic temperature measurement point and the internal HST of the transformer is established.

2.1.2 Numerical analysis method

The numerical analysis methods predict transformer temperature rise based on multi-physics field coupling calculations. The establishment of the solution model and the determination of the boundary conditions are complicated. Experts use the fluid-solid coupling method (Xie et al., 2016) to calculate the HST of the transformer, or use magnetic-thermal coupling (Liao et al., 2021) to solve the temperature distribution

to improve the accuracy of the internal temperature calculation results. For the simulation model, the shortcoming lies that it is difficult to reflect the real oil flow and heat transfer inside the transformer and the final temperature rise distribution cannot reflect the temperature rise in the full domain. For load capacity analysis, the numerical analysis is often realized by Ansys Fluent and COMSOL, and the results are used as complementary to experimental testing verification to justify and support the overall analysis.

2.1.3 Thermoelectric analogy model

Considering the heat flow is similar to the current flow in circuit, the hot circuit model of transformer conduction is constructed by thermoelectric analogy (Swift et al., 2001). In load capacity assessment, researchers (Susa and Nordman, 2009) considered the change in oil viscosity and winding loss with temperature and established a simplified model of HST based on the top oil temperature. Such models greatly reduce the demand of input parameters. Some experts also use a thermoelectric analogous model to estimate the HST, thermal resistance and thermal capacity to improve the dynamic response of the model, and propose a load capacity assessment model in consequence (Li et al., 2018). Besides, the influence of HST on the load capacity of traction transformers is also studied and a collector heat path model is established to simplify the nonlinear thermal resistance to real-time thermal capacity evaluation (Zhou et al., 2021).

Since the results of transformer HST directly affect the accuracy of transformer load capacity, a large number of scholars have conducted research in HST calculation. At present, the HST is mainly obtained by direct measurements, analyzed and demonstrated by applying numerical analysis method, and estimated by the idea of thermoelectric analogy.

2.2 Dissipation mode

The dissipation theory of the transformer assumes part of the heat generated by the core and coil can be dissipated by transformer oil and dissipated by dissipaters. The process of heat dissipation is actually the process of reducing the internal temperature and increasing the load factor. It is suggested to introduce dissipation mode as a factor of load capability assessment to provide better guidance for transformer optimization (Li et al., 2018). If damage to the fan occurs when the transformer has to withstand an overload situation, it can lead to an impact on the overload capacity.

2.3 Ambient temperature

As one of the important parameters affecting the load capacity of transformer, ambient temperature plays a key role. In order to establish a more accurate load prediction model, the highest as well as the lowest temperature of the day needs to be taken into account, and the ambient temperature will be fuzzy discretized according to the standard GB/T 1094.7-2008. Moreover, under different initial loads, the change of allowable overload time has similar characteristics: it decreases rapidly with the increase of ambient temperature. Therefore, the accuracy of ambient temperature has a great influence on the calculation of transformer overload capacity.

3 Progress on load capacity assessment

With the integration of large-scale new energy, load capacity assessment becomes a critical task for the new energy power systems. In this regards, it is necessary to pay more attention to load capacity prediction as well as the dynamic capacity enhancement strategy of transformer.

3.1 Load capacity prediction

According to the prediction requirement in temporal dimension, load capacity prediction can be classified as ultra-short-term prediction (in hours and minutes), short-term prediction (in days), medium-term prediction (in months) and long-term prediction (in years). The accuracy of load capacity prediction requires both the reliability of data and the applicability of the prediction algorithm. Load capacity prediction mainly focuses on two types: one is prediction based on actual transformer measurement data, such as top oil temperature and HST, and the other is simulation results prediction based on computational model.

3.1.1 Measured data-based prediction

The top oil temperature prediction based on Kalman filtering combines current data with historical loads to predict the trend of transformer load capacity (Zhou et al., 2020). For such method, an evaluation model would be constructed with multiple data inputs, as shown in Figure 2A, but it has not been applied in practices.

3.1.2 Computational model-based prediction

Computational model-based load capacity prediction methods mainly include statistical methods as well as machine learning methods. For statistical methods, the typical algorithms include Kalman filter, linear extrapolation and wavelet fractional solution method (Shen et al., 2016). Since statistical methods require high stability of time series, so it is difficult to reflect the non-linear influence of weather, events and other factors. In comparison, the machine learning algorithms such as fuzzy inference (Wang et al., 2022), support vector machines, artificial neural networks (Fan et al., 2022) and cluster

analysis (Shen et al., 2016) have demonstrated their capability of improving the non-linear fitting ability of the models. It is believed that the computational model-based load capacity prediction methods have a good prospect. However, its ability of extracting deep features from actual highly fluctuating time series is still a problem to be solved in the future.

3.2 Dynamic load capacity enhancement

Dynamic load capacity enhancement refers to the operation of power transmission line or transformation equipment with load exceeding rated capacity under the premise of ensuring safety and reliability. The existing studies on dynamic load capacity enhancement of transformer pays more attention to the evaluation of HST and failure rate, and also combines economic indicators (Zhang et al., 2013; Dong et al., 2021). In this regard, the load curve, ambient temperature and relevant operation and maintenance information of the transformer are firstly obtained to determine the scenario and operating conditions of dynamic load. The equipment load scenario, service age and condition monitoring information are then taken to carry out thermal ageing for health state evaluation. Based on that, load constraints and corresponding threshold values can be determined for dynamic load capacity enhancement.

Besides, some researchers also use the Weibull model to calculate the real-time failure rate and risk of transformer when the load capacity increases (Qian et al., 2015). Under constrains like temperature, failure rate and economic investment, dynamical load capacity enhancement approaches are proposed (Zhang et al., 2017). The flow chart for this solution is shown in Figure 2B. The method is carried out in two stages: firstly, the working condition prediction data is used to obtain a pre-capacity enhancement solution under the HST temperature and fault rate constraints, with load reduction if any of the constraints are not met to ensure the safety and reliability of the capacity increase. Afterwards, the economics of each capacity enhancement decision is evaluated and the economically optimal solution is selected. Such method can be taken as a typical solution for dynamic transformer capacity enhancement.

4 Discussion

For a long time, studies on transformer load capability assessment mainly concentrated on remaining useful life of the insulation system as well as the economy investment. For the equipment installed in the new energy power system, the traditional load capacity evaluation approach becomes no longer adaptive due to the following issues:

- Some factors like historical health condition, dissipation mode and ambient parameters are not fully considered, since they can affect the load potential of the transformer.
- Load capability forecasting did not attract enough attention. With large-scale integration of new energy and impulsive loads like electrical vehicles, uncertainties in both source side and load side become a new factor for influence the load capability of the transformer.
- In terms of dynamic load capacity of transformer, the constraints are limited to HST, failure rate and investment. To meet the goal of carbon neutrality, the constraints of load capacity should consider the health status and power loss or carbon emission of transformer itself, residual life and other factors, and increase the constraints of dynamic difference.

In the new power system, the distribution transformer plays a vital role, dynamic capacity enhancement can improve the transformer load capacity, and more accurate load capability assessment model should be constructed to consider different factors. The objective function and the adaptive adjustment scheme of the cooling system should be determined to adapt to minimize transformer loss and maximize its insulation life.

Author contributions

SL proposed the idea and wrote the draft of the manuscript, XL orgnized the references, YK and QG proofread the manuscript.

Conflict of interest

The authors declare that the research was conducted in the absence of any commercial or financial relationships that could be construed as a potential conflict of interest.

Publisher's note

References

Dong, X., Zhang, S., Ruan, J., Du, Z., Deng, Y., and Cheng, S. (2021). Research and application of dynamic load assessment technology for oil-immersed power transformers. *High. Volt. Technol.* 47 (06), 1959–1968. doi:10.13336/j.1003-6520.hve.20210788

Fan, Q., Wen, Q., Lu, Q., Zhang, X., Xiao, N., and Liu, J. (2022). Transformer load forecasting and risk assessment based on main transformer load conditions. *Electr. Meas. Instrum.* 1-11. Available: http://kns.cnki.net/kcms/detail/23.1202.th.20220527.1737.006.html.

Feng, C., Li, Z., Shahidehpour, M., Wen, F., Liu, W., and Wang, X. (2018). Decentralized short-term voltage control in active power distribution systems. *IEEE Trans. Smart Grid* 9 (5), 4566–4576. doi:10.1109/tsg.2017.2663432

Feng, C., Liang, B., Li, Z., Liu, W., and Wen, F. (2022). Peer-to-peer energy trading under network constraints based on generalized fast dual ascent. *IEEE Trans. Smart Grid* 1. doi:10.1109/TSG.2022.3162876

Jiang, Z., Li, S., Ma, X., Li, X., Kang, Y., Li, H., et al. (2022). State estimation of regional power systems with source-load two-terminal uncertainties. *Comput. Model. Eng. Sci.* 132 (1), 295–317. doi:10.32604/cmes.2022.019996

Li, Y., Liu, N., Liang, J., Xu, S., Lin, D., Mu, H., et al. (2018). Oil-immersed transformer load capacity evaluation model based on temperature rise characteristics. *Chin. J. Electr. Eng.* 38 (22), 6737–6746. doi:10.13334/j.0258-8013.pcsee.180075

Liao, C., Ruan, J., Liu, C., Wen, W., and Wang, S. (2021). Three-dimensional electromagnetic-fluid-temperature field coupling analysis method for oil-immersed transformers. *Power autom. Equip.* 35 (9), 50–155.

Liu, Y., Li, X., Li, H., Yin, J., and Gao, S. (2020). Development of a 35 kV oil-immersed transformer with built-in distributed fiber optic sensing. *High. Volt. Technol.* 46 (06), 1886–1894. doi:10.13336/j.1003-6520.hve.20200615005

Lobo Ribeiro, A. B., Eira, N. F., Sousa, J. M., Guerreiro, P. T., and Salcedo, J. R. (2008). Multipoint fiber-optic hot-spot sensing network integrated into high power transformer for continuous monitoring. *IEEE Sens. J.* 8 (7), 1264–1267. doi:10.1109/jsen.2008.926926

Ma, H., Saha, T. K., Ekanayake, C., and Martin, D. (2015). Smart transformer for smart grid—Intelligent framework and techniques for power transformer asset management. *IEEE Trans. Smart Grid* 6 (2), 1026–1034. doi:10.1109/tsg.2014.2384501

Qian, H., Wang, Q., and Chen, X. (2015). Dynamic capacity increase scheduling of transmission cross sections considering multiple risks to the grid. *China Electr.* 48 (10), 60–64. doi:10.19595/j.cnki.1000-6753.tces.2014.04.029

Qian, Z., Sun, J., Yuan, K., and Sun, D. (2003). Online monitoring technology for hot spot condition of power transformer windings. *High. Volt. Technol.* 29 (9), 26–28. doi:10.13336/j.1003-6520.hve.2003.09.012

Ruan, J., Deng, Y., Huang, D., Duan, C., Gong, R., Quan, Y., et al. (2020). HST calculation of a 10 kV oil-immersed transformer with 3D coupled-field method. *IET Electr. Power Appl.* 14 (5), 921–928. doi:10.1049/iet-epa.2019.0469

Shen, C., Qin, J., Sheng, W., and Fang, H. (2016). Wavelet clustering-based short-term load forecasting method for distribution substations. *Grid Technol.* 40 (02), 521–526. doi:10.13335/j.1000-3673.pst.2016.02.027

Susa, D., and Nordman, H. (2009). A simple model for calculating transformer hot-spot temperature. *IEEE Trans. Power Deliv.* 24 (3), 1257–1265. doi:10.1109/tpwrd.2009.2022670

Swift, G., Molinski, T. S., and Lehn, W. (2001). A fundamental approach to transformer thermal modeling. I. Theory and equivalent circuit. *IEEE Trans. Power Deliv.* 16 (2), 171–175. doi:10.1109/61.915478

Tang, W., Qian, T., Huang, J., Lu, G., Wang, Y., and Luan, L. (2017). Improved thermoelectric analog model for transformer load capacity assessment. *J. South China Univ. Technol. Nat. Sci. Ed.* 45 (10), 71–77+86. doi:10.3969/j.issn.1000-565X.2017.10.010

Wang, C., Wang, Y., Ding, Z., Zheng, T., Hu, J., and Zhang, K. (2022). A based transformer-based method of multi-energy load forecasting in integrated energy system. *IEEE Trans. Smart Grid*. doi:10.1109/TSG.2022.3166600

Xie, Y., Lin, L., Song, Y., and Wang, S. (2016). Multi-physics field coupling calculation method for temperature rise of oil-immersed power transformer windings. *Chin. J. Electr. Eng.* 36 (21), 5957–5965. doi:10.13334/j.0258-8013.pcsee.160806

Zhang, X., Song, Z., and Yang, Z. (2013). An oil-immersed transformer fault rate model based on load factor and equipment detection information. *Grid Technol.* 37 (4), 1159–1165. doi:10.13335/j.1000-3673.pst.2013.04.019

Zhang, Y., He, D., Xu, Y., Guo, C., Du, X., and Bai, D. (2017). Short-term capacity increase decision method for oil-immersed transformers taking into account comprehensive risks. *Power Syst. autom.* 41 (13), 86–91+118. doi:10.7500/AEPS20161121007

Zhong, X., Ekanayake, C., Ma, H., and Saha, T. K. (2021). Ageing analysis of solar farm inverter transformers. *IEEE Trans. Power Deliv.* 36 (6), 3815–3824. doi:10.1109/TPWRD.2021.3049505

Zhou, B., Xu, X., Wing, S., Li, Canbing., Wu, Q., Zhang, C., et al. (2020). Thermodynamic modelling of buried transformer substations for dynamic loading capability assessment considering underground heat accumulative effect. *Int. J. Electr. Power & Energy Syst.* 121, 106153–106615. doi:10.1016/j.ijepes.2020.106153

Zhou, L., Wang, L., Zhang, X., Liu, Q., Guo, L., and Wang, D. (2021). An estimation method for real-time thermal capacity of traction transformers under unbalanced loads. *IEEE Trans. Ind. Electron.* 68 (11), 11438–11446. doi:10.1109/tie.2020.3036252

frontiers | Frontiers in Energy Research

TYPE Original Research
PUBLISHED 23 September 2022
DOI 10.3389/fenrg.2022.1005281

OPEN ACCESS

EDITED BY
Shiwei Xia,
North China Electric Power University, China

REVIEWED BY
Lei Sun,
Hefei University of Technology, China
Amit Kumar,
Thapar Institute of Engineering and Technology, India

*CORRESPONDENCE
Yang Li,
eeliyang@hhu.edu.cn

SPECIALTY SECTION
This article was submitted to Smart Grids, a section of the journal Frontiers in Energy Research

RECEIVED 28 July 2022
ACCEPTED 23 August 2022
PUBLISHED 23 September 2022

CITATION
Wang Z, Wu F, Li Y, Huang W and Shi L (2022), Bi-layer optimal secondary frequency control approach for energy storage clusters considering wind power uncertainty.
Front. Energy Res. 10:1005281.
doi: 10.3389/fenrg.2022.1005281

Bi-layer optimal secondary frequency control approach for energy storage clusters considering wind power uncertainty

Zizhao Wang, Feng Wu, Yang Li*, Weidong Huang and Linjun Shi

College of Energy and Electrical Engineering, Hohai University, Nanjing, China

Increasing penetration of wind power with intermittency and variability threatens the stability of the power system frequency. The fast response capability of the energy storage system (ESS) makes it an effective measure to improve frequency regulation performance. However, designing an optimal control for numerous energy storage units (ESUs) with different power and energy characteristics is challenging. To solve the dilemma that the distributed control methods cannot achieve optimality over time horizons while the centralized optimization methods would cause high computational burdens, a bi-layer optimal control approach is proposed in this study. In the upper layer, a multi-area secondary frequency control (SFC) problem is established to determine control policies for ESS clusters under continuous wind power fluctuations and is solved by the Itô theory-based stochastic optimization (ITB-SO) method with high computational efficiency in a rolling-horizon manner. In the lower layer, the power output of ESUs is dispatched and coordinated using the distributed algorithm (DA) method via communication networks, considering different characteristics and the current state-of-charge (SoC) levels. Simulation studies carried out in a dual-region test system evidence the improvement of system frequency stability by compensating for rapid wind power fluctuations immediately *via* ESSs. The results show that the proposed ITB-SO method without scenario generation is suitable for real-time SFC for the ESS. The effectiveness of the DA method and its robustness in encountering loss of communication links are also verified.

KEYWORDS

energy storage, frequency regulation, wind power uncertainty, stochastic optimization, Itô theory, distributed algorithm

1 Introduction

In the past few decades, the penetration of renewable energy sources (RES) has been increasing rapidly. At the end of 2020, the RES capacity, including wind power and photovoltaic power generation, was 1300GW, accounting for 9.4% of the total installed power generation capacity in the world (Khan et al., 2021). The increasing RES penetration level in the interconnected power grids results in a decrease in the system inertia (Meegahapola and Flynn, 2010). For example, the wind turbine generators are decoupled from the system frequency by converters, so they cannot provide frequency regulation support for a long time (Tsili and Papathanassiou, 2009). Severer frequency fluctuations would happen in the areas with low system inertia than others in the interconnected power systems (Miller et al., 2011). Meanwhile, the intermittency and variability nature of RES power generation would lead to continuous power imbalances and system frequency deviations (Bidram and Davoudi, 2012). Therefore, the increasing integration of RES will inevitably bring challenges to the stability of system frequency.

Exploiting energy storage systems (ESSs) for maintaining frequency stability of the systems with high penetration levels of the RES has recently attracted attention both in industry and academia. In recent years, the application of the ESS is gradually becoming widespread. In 2021, the rated power of installed ESS was 173.7GW, and 1,363 ESS projects were operational globally (U.S.DOE, 2021). The ESS has higher ramping and faster response capability than conventional generators, so better dynamic tracking performance is available for frequency regulation control. Since the traditional automatic generation control (AGC) signal is unsuitable for ESSs with limited energy capacity, filtering mechanisms are developed to extract fast-moving and high-frequency components of the AGC signal for the ESS to participate in SFC (Cheng et al., 2014). Meanwhile, the management of state-of-charge (SoC) for ESS during frequency regulation is important as well. It needs to prevent the second frequency drop issue due to sudden withdrawals of some ESSs. Karrari et al. (2020) propose an SoC recovery mechanism for flywheel ESS so that the residual energy capacity is always in the optimal state. Garcia-Torres et al. (2021) apply the stochastic optimization (SO) method considering the management SoC level and address the prediction uncertainties of RES.

In order to further exploit the complementary advantages of different types of ESSs in terms of rated power and energy capacity, hybrid ESSs are developed and utilized in frequency regulation. The main ESS types, including batteries (Li-ion, Pb-Acid), flywheels, and supercapacitors, possess different power-to-energy ratio characteristics. Jan et al. (2020) used a fuzzy PI controller for ESSs to cater to the frequency variations adaptively. Shim et al. (2018) proposed droop control with the SoC feedback to improve their frequency response and regulation services to the grid. However, the control strategies in these studies are separate and independent, which means different ESSs cannot be coordinated, and hence unnecessary mutual regulation and waste of resources would be caused. Esmaili et al. (2013) decomposed the power signal into fast/slow components to allocate responsibility for hybrid ESSs. Oshnoei et al. (2020) adopted the model predictive control method to determine an ESS control scheme with various characteristics, which is robust to uncertain disturbances. Nevertheless, these centralized ways are sensitive to noise and communication failure (Zhao and Ding, 2018b). On the contrary, the distributed realizations relying on local and neighboring information can reduce computation time and take advantage of local intelligent agents (Anderson et al., 2021).

Distributed methods such as the consensus algorithm are widely used in economic dispatch problems (Li et al., 2019), control for photovoltaic arrays (Zhang et al., 2021) and batteries (Chen C. et al., 2019), etc. Alsharif et al. (2020) applied the distributed algorithm (DA) method coordinating ESS power output to enhance the frequency nadir and improve the dynamic performance. Lee et al. (2016) coordinated the group battery ESS by a distributed control algorithm for voltage and frequency deviation regulation. Cherukuri and Cortes (2018) developed a distributed method for ESSs considering the change of load, but uniform storage efficiency is assumed. However, these studies did not take into account random wind power generation or the influence of ESS control strategies on the frequency of interconnected grids. Zhao and Ding (2018a) present a DA method to maximize the total welfare of battery ESSs during frequency regulation considering changes in wind power. But, it relies on accurate predictions of wind power, which is difficult to accomplish, considering their inherent variability. As a result, the stochastic characteristics of RES should be taken into account when designing accurate control strategies for the ESS.

However, a disadvantage of the distribution methods is that the optimality of power dispatching between ESSs can only be achieved at the current time step, instead of considering the optimal solution over a future finite time horizon. The power output scheme is possibly not adapted to the energy-constrained ESSs when the signal is constantly biased, resulting in storage saturation. It indicates that the ESS can participate in the SFC only if the energy content of the signal is kept low (Megel et al., 2018). So, it is necessary to develop reasonable control strategies to maintain optimal energy levels of ESSs. But, on the other hand, if the power output of all ESSs is decided in a centralized optimization problem over a period, a large scale of variables would lead to computational burdens and intractability, which is unsuitable for real-time SFCs.

In order to fill the abovementioned research gap, a bi-layer SFC framework for the ESS is presented in this article. Different

energy storage units (ESUs) in the same area are combined as an ESS cluster to reduce the computational complexities of upper-layer control, and the optimal control policies are updated in a rolling-horizon manner to ensure frequency regulation performance. Then, the ESUs coordinate their power output *via* communication networks in real-time. Therefore, different from the previous studies, the proposed approach can achieve a balance between the optimization method considering wind power uncertainty and the distribution method with high efficiency. The main contributions of this article are summarized as follows:

1) An upper-layer optimization problem of multi-area frequency regulation considering stochastic wind power fluctuation is established to determine the optimal control policy of ESS clusters. The Itô theory-based stochastic optimization (ITB-SO) method is proposed to efficiently obtain the solutions, in which the wind power uncertainty is modeled by stochastic differential equations (SDE) without scenario generation. The computational burden is significantly reduced so that it is suitable for real-time frequency regulation.
2) To make full use of the local computing capability, a DA method with high efficiency and robustness is applied to dispatching power output among ESUs. The power command can be adaptively decomposed considering the different characteristics of power-type and energy-type units. The evaluation of the SoC level is improved by adopting the logistic function to better reflect the safe and dangerous SoC zones. Sudden withdrawal of ESUs due to energy saturation and violation of power limits can be avoided to guarantee power tracking performance.

The remainder of the article is organized as follows: Section 2 describes the multi-area frequency regulation model considering ESSs and wind power uncertainties. Section 3 proposes an optimal SFC approach for ESS clusters based on the ITB-SO method. Section 4 proposes a power dispatching approach for ESUs in the clusters based on the DA method. Case studies are presented in Section 5. Section 6 gives a conclusion.

2 System model

2.1 Dynamic model of frequency regulation considering the ESS

The system frequency is affected by load and generation sources, including conventional generators and ESSs. Regardless of the power loss, the dynamic frequency response model of multi-areas can be expressed as follows (Mauricio et al., 2009; Li et al., 2016):

$$\frac{d}{dt}\Delta f_i = -\frac{1}{2H_i}\left(D_i\Delta f_i - \Delta p_i^{\mathrm{M}} + p_i^{\mathrm{E}} + \Delta p_i^{\mathrm{L}} + \sum_{j:\, i\longrightarrow j}\Delta p_{ij}^{\mathrm{tie}}\right), \forall i, j \in \mathcal{A} \tag{1}$$

$$\frac{d}{dt}\Delta p_i^{\mathrm{M}} = -\frac{1}{T_i^{\mathrm{t}}}\left(\Delta p_i^{\mathrm{M}} - \Delta p_i^{\mathrm{AGC}} + \frac{1}{R_i}\Delta f_i\right), \forall i \in \mathcal{A} \tag{2}$$

$$\frac{d}{dt}\Delta p_{ij}^{\mathrm{tie}} = 2\pi\sum T_{ij}\left(\Delta f_i - \Delta f_j\right), \forall i, j \in \mathcal{A} \tag{3}$$

$$\frac{d}{dt}\Delta p_i^{\mathrm{AGC}} = -K_i^{\mathrm{I}}\left(B_i\Delta f_i + \sum_{j:\, i\longrightarrow j}\Delta p_{ij}^{\mathrm{tie}}\right), \forall i, j \in \mathcal{A} \tag{4}$$

where $\mathcal{A}$ is the set of area systems; Δf_i is the frequency deviation of the ith area from the rated value; Δp_i^{M} is the active power deviation of conventional generators from the nominal value in the ith area; p_i^{E} is the active power of the ith ESS cluster because numerous units can be equivalently combined to reduce the number of variables; Δp_i^{L} is the change of load; $\Delta p_{ij}^{\mathrm{tie}}$ represents the tie line power from the ith to the jth area; $\Delta p_i^{\mathrm{AGC}}$ is the AGC reference; H_i and D_i are the equivalent system inertia and damping, respectively; T_i^{t} is turbine time constant; R_i is the droop coefficient; T_{ij} is the synchronizing coefficient; B_i is the frequency bias factor; and K_i^{I} is the integral coefficient. Eq 1 gives the frequency dynamic characteristic; Eq. 2 shows the change of regulation output from the generators, including primary frequency regulation and AGC; Eq. 3 shows the power change on the tie line between different areas; tie-line bias control in Eq. 4 automatically adjusts the AGC reference by driving the area control errors (ACE) to zero.

The wind power output can be considered a negative system load as shown in Eq. (5), which is more difficult to accurately forecast than load. Hence, the continuous wind power fluctuations would pose a threat to the safety and stability of the system frequency.

$$\Delta p_i^{\mathrm{L}} = -\Delta p_i^{\mathrm{W}}, \forall i \in \mathcal{A} \tag{5}$$

where Δp_i^{W} is the deviation of wind power from its initial value in the ith area.

2.2 Energy storage model

Different ESUs are combined into an ESS cluster, so the overall power output and energy level of the ith cluster can be represented by the sum of that of the member ESUs as follows:

$$p_i^{\mathrm{E}} = p_i^{\mathrm{E,d}} - p_i^{\mathrm{E,c}} = \sum_k\left(p_k^{\mathrm{d}} - p_k^{\mathrm{c}}\right), \forall k \in \mathcal{S}_i \tag{6}$$

$$s_i^{\mathrm{E}} = \sum_k s_k, \forall k \in \mathcal{S}_i \tag{7}$$

$$\frac{d}{dt}s_k = p_k^{\mathrm{c}}\eta_k^{\mathrm{c}} - p_k^{\mathrm{d}}/\eta_k^{\mathrm{d}}, \left(\eta_k^{\mathrm{c}}, \eta_k^{\mathrm{d}}\right) \in (0, 1], \forall k \in \mathcal{S}_i \tag{8}$$

where $\mathcal{S}$ is the set of ESS clusters; $p_i^{\mathrm{E,d}}$ and $p_i^{\mathrm{E,c}}$ are the discharge and charge power of the ith ESS cluster, respectively; p_k^{d} and p_k^{c}

are the discharge and charge power of the kth ESU, respectively; s_i^{E} and s_k are the energy level of the ESS cluster and ESU, respectively; the initial condition is s_0; and η_k^{c} and η_k^{d} are the charge and discharge efficiencies, respectively. The power output and energy level satisfy the limit constraints as shown in (9 and 10), and the state-of-charge (SoC) can be obtained according to the energy level as shown in (11).

$$0 \le p_k^{\mathrm{d}} \le P_k{}^{\max}, 0 \le p_k^{\mathrm{c}} \le P_k{}^{\max} \tag{9}$$

$$0 \le s_k \le S_k{}^{\max} \tag{10}$$

$$SoC_k = \frac{s_k}{S_k{}^{\max}} \tag{11}$$

where $P_k{}^{\max}$ represents the rated power; $S_k{}^{\max}$ is the rated energy capacity; and SoC_k is the SoC level of the kth ESU.

2.3 Model of wind power prediction error

SDE has been widely used as an effective model of RES prediction error, such as wind power (Verdejo et al., 2016) and photovoltaic power (Lingohr and Müller, 2019). The probability distribution information and the temporal correlation characteristic could be simultaneously expressed. It is convenient to fit the non-Gaussian distribution *via* the Itô process by adopting different functions in SDE models so as to well-reflect the detailed characteristics of RES uncertainty. On the other hand, the SDE model can be embedded into SO problems without scenario generation in order to significantly release computational burdens.

Specifically, the wind power output value consists of the ultra-short-term prediction in a finite time period and the prediction error, which is modeled *via* the Itô process as follows:

$$\Delta p_i^{\mathrm{W}} = \Delta p_i^{\mathrm{W,pred}} + \xi_i, \forall i \in \mathcal{A} \tag{12}$$

$$d\xi_i = \mu(\xi_i)dt + \sigma(\xi_i)dW_t, \forall i \in \mathcal{A} \tag{13}$$

$$\mu(\xi_i) = -\frac{(\xi_i - b_1)}{\tau}, \sigma(\xi_i) = \frac{b_2}{\tau}(\xi_i - b_3)(b_4 - \xi_i) \tag{14}$$

where $\Delta p_i^{\mathrm{W,pred}}$ is the predicted wind power deviating from the initial forecast; ξ_i represents the prediction error; $\mu(\cdot)$ and $\sigma(\cdot)$ are the drift and diffusion function of SDE, respectively; W_t is a Wiener process; τ represents the time constant; parameter b_1 is the mean deviation from the predicted value; b_2 is the fluctuation intensity; and b_3 and b_4 indicate the fluctuation interval. The parameters can be easily adjusted in different time periods according to the preference of operators in advance.

2.4 Bi-layer SFC framework for ESS clusters

The optimal SFC for ESS clusters is divided into two control layers. In the upper layer, the convex SO problems are established to decide the optimal power output minimizing the frequency deviation. However, modeling numerous ESUs will result in a large number of decision variables for the optimization problem, which is difficult to solve rapidly. Therefore, optimal control policies for the overall power output of ESS clusters are determined to reduce computational complexities. The ITB-SO method is applied instead of scenario-based methods in order to quickly obtain the optimal solutions for the SFC.

In the lower layer, the total power command is dispatched between the ESUs in the same ESS cluster with a communication network. The optimal dispatching scheme is obtained by the DA method considering the current SoC levels and different characteristics of power-type and energy-type units. In summary, the framework of the bi-layer optimal SFC is shown in Figure 1.

3 Optimal SFC of ESSs based on ITB-SO

3.1 Objective function

The frequency regulation control problem to minimize the frequency deviation and operation cost of the ESS can be described as a SO problem over $\mathcal{T}: t \in [0, T]$, and the objective function is defined as

$$\begin{aligned}\min J = \mathbb{E}_{\xi_0}\left\{\int_0^T \left(\Delta \boldsymbol{f}_t^{\mathrm{T}} \boldsymbol{\Lambda}_f \Delta \boldsymbol{f}_t + \boldsymbol{R}_t^{\mathrm{T}} \boldsymbol{\Lambda}_R \boldsymbol{R}_t\right) dt\right\} \\ + \mathbb{E}_{\xi_0}\left\{\Lambda_S \sum_i \left(SoC_{i,T} - SoC^{\mathrm{ref}}\right)^2\right\}\end{aligned} \tag{15}$$

where $\mathcal{T}$ is the set of time index; T represents the terminal time; $\Delta \boldsymbol{f}_t$ is the vector form of the frequency deviation of each area shown in (16); $\boldsymbol{R}_t$ is the vector of control variables of the ESS shown in (17), including the discharge and charge components of power output. Since the objective is to achieve a minimum of the square power output, simultaneous non-zero charging and discharging power can be avoided; SoC^{ref} is the reference value for SoC, which is set as 0.5 in this study; $\boldsymbol{\xi}_t$ is the vector of wind power prediction error ξ_i; $\mathbb{E}_{\xi_0}\{\cdot\}$ denotes the expectation operator under the initial conditions $\boldsymbol{\xi}_0$; $\boldsymbol{\Lambda}_f$, $\boldsymbol{\Lambda}_R$, and Λ_S are the weight parameters.

$$\Delta \boldsymbol{f}_t = \left[\Delta f_{i,t}\right]^{\mathrm{T}}, \forall i \in \mathcal{A}, \forall t \in \mathcal{T} \tag{16}$$

$$\boldsymbol{R}_t = \left[p_{i,t}^{\mathrm{E,d}}, p_{i,t}^{\mathrm{E,c}}\right]^{\mathrm{T}}, \forall i \in \mathcal{A}, \forall t \in \mathcal{T} \tag{17}$$

Since different ESUs are combined into an ESS cluster and meet the power command, their overall SoC level can be estimated by

$$\frac{d}{dt} SoC_i = \frac{1}{S_i{}^{\max}}\left(p_i^{\mathrm{E,c}} \eta_i^{\mathrm{c,eq}} - p_i^{\mathrm{E,d}} / \eta_i^{\mathrm{d,eq}}\right), \forall i \in \mathcal{A} \tag{18}$$

where $\eta_i^{\mathrm{d,eq}}$ and $\eta_i^{\mathrm{c,eq}}$ are the equivalent discharge and charge efficiency, respectively, which are set as the average over ESUs; and $S_i{}^{\max}$ is the total rated energy capacity of the ith ESS cluster.

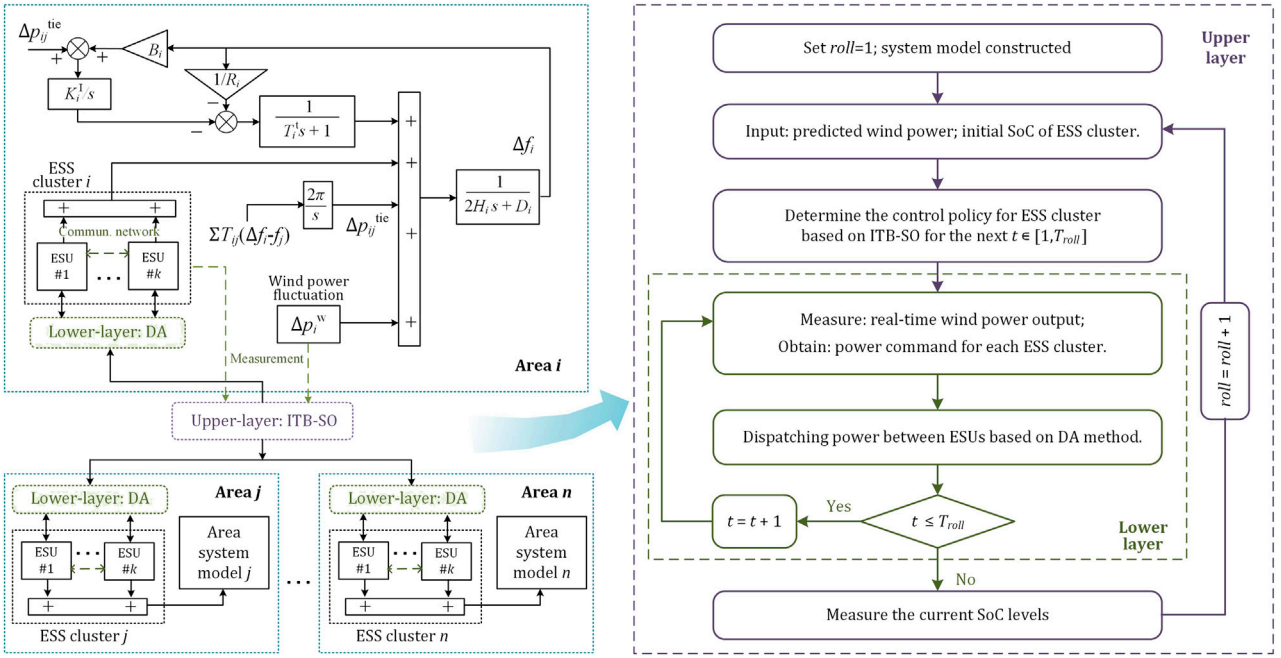

FIGURE 1
Framework of bi-layer secondary frequency control for energy storage clusters in multi-area systems.

It can be seen that the objective function (15) shows the trade-off between frequency regulation performance and the power and energy cost of the ESS. At the terminal time, the SoC level is forced to be close to the reference value by the objective function because it is necessary to maintain the feasibility of the next rolling horizon after the terminal time.

Moreover, the frequency deviation constraint and SoC constraint should be considered, as shown in (19) and (20), to enhance frequency regulation performance and guarantee the operation of the ESS. It is to be noted that constraint (19) could be violated sometimes when ESSs do not have enough power capacity to participate in frequency regulation, and hence it should be removed if the problem is infeasible.

$$-\Delta f^{\max} \le \Delta f_{i,t} \le \Delta f^{\max}, \forall i \in \mathcal{A}, \forall t \in \mathcal{T} \tag{19}$$

$$\underline{SoC} \le SoC_{i,t} \le \overline{SoC}, \forall i \in \mathcal{A}, \forall t \in \mathcal{T} \tag{20}$$

3.2 Itô theory-based stochastic optimization method

3.2.1 Series expansion of stochastic assessment function

To obtain the expected value of the objective function under all uncertainties, an ITB approximation method is adopted to evaluate it in a deterministic way (Chen et al., 2019c) so that the SO problem can be solved efficiently. For convenience, the stochastic system is expressed as (21) considering the stochastic resources $\boldsymbol{\xi}_t$ described by SDE.

$$\begin{aligned} d\boldsymbol{X}_t &= (\boldsymbol{A}\boldsymbol{X}_t + \boldsymbol{B}\boldsymbol{\xi}_t)dt \\ d\boldsymbol{\xi}_t &= \mu(\boldsymbol{\xi}_t)dt + \sigma(\boldsymbol{\xi}_t)dW_t \end{aligned} \tag{21}$$

where $\boldsymbol{X}_t$ represents the state variables, which is a $N_x \times 1$ column vector; $\boldsymbol{\xi}_t$ is a $N_\xi \times 1$ column vector representing wind power prediction error in this study; $\boldsymbol{A}$ and $\boldsymbol{B}$ are the coefficient matrices; and the initial condition of the stochastic system is $\boldsymbol{X}_0$ and $\boldsymbol{\xi}_0$.

The stochastic assessment function (SAF) is defined and denoted as $u(t, \boldsymbol{X}_0)$ when specific functions of $\boldsymbol{X}_t$ are given and can be expanded into a series of deterministic terms as follows:

$$u(t, \boldsymbol{X}_0) = \mathbb{E}_{\xi_0}\left\{\int_0^t g(\boldsymbol{X}_s)ds + h(\boldsymbol{X}_t)\right\} = \sum_n^\infty \tilde{u}_n(t, \boldsymbol{X}_0) \tag{22}$$

where $g(\cdot)$ and $h(\cdot)$ are functions of $\boldsymbol{X}_t$ with continuous second-order derivatives and $\tilde{u}_n$ is the nth order deterministic components of the SAF. Therefore, SAF can be approximately estimated by ignoring the high-order terms.

Specifically, the objective function (15) evaluated by SAF at time T can be decomposed into low-order terms as

$$J = u(T, \boldsymbol{X}_0) \approx \tilde{J}_0 + \tilde{J}_1 \tag{23}$$

Given that $g = \Delta \boldsymbol{f}_t^{\mathrm{T}} \Lambda_f \Delta \boldsymbol{f}_t + \boldsymbol{R}_t^{\mathrm{T}} \Lambda_R \boldsymbol{R}_t$ and $h = \Lambda_S \sum_i (SoC_{i,t} - SoC^{\mathrm{ref}})^2$, the 0-th and 1-st order terms of the objective function are defined as

$$\tilde{J}_0 = \int_0^T g(\tilde{\boldsymbol{X}}_t)dt + h(\tilde{\boldsymbol{X}}_T) \tag{24}$$

$$\tilde{J}_1 = \int_0^T \frac{1}{2}\sigma(\tilde{\boldsymbol{\xi}}_t)^{\mathrm{T}} \boldsymbol{\theta}_t \sigma(\tilde{\boldsymbol{\xi}}_t)dt \tag{25}$$

where $\tilde{\boldsymbol{X}}_t$ is the auxiliary state variables by ignoring $\sigma(\boldsymbol{\xi}_t)dW_t$ in (21). Hence, they can be recognized as the expected state variables in the deterministic system without the influence of uncertain resources; $\tilde{\boldsymbol{\xi}}_t$ is independent of the state variables, so $\sigma(\tilde{\boldsymbol{\xi}}_t)$ can be obtained once the initial condition $\boldsymbol{\xi}_0$ is given. $\boldsymbol{\theta}_t$ represents the second-order derivative of SAF components and is defined as

$$\boldsymbol{\theta}_t = \int_0^t \hat{\boldsymbol{X}}_s^{\mathrm{T}} [\nabla^2 g] \hat{\boldsymbol{X}}_s ds + \hat{\boldsymbol{X}}_t^{\mathrm{T}} [\nabla^2 h] \hat{\boldsymbol{X}}_t \tag{26}$$

where ∇^2 is the operator of the Hessian matrices and $\hat{\boldsymbol{X}}_t$ is another group of auxiliary state variables with $\hat{\boldsymbol{X}}_t = \partial \tilde{\boldsymbol{X}}_t / \partial \boldsymbol{\xi}_0, \hat{\boldsymbol{X}}_0 = \boldsymbol{0}_{N_\xi \times N_x}$. The detailed proof of the abovementioned series expansion method based on Itô theory can be found in (Chen et al., 2019c).

3.2.2 Control policy

The control output of the ESS should be appropriately adjusted in response to different wind power values. However, it is hard to accurately predict wind power so the design of the control strategy is challenging considering unrevealed uncertainties. Disturbance feedback control is needed to address the problem (Skaf and Boyd, 2010). An effective measure is parameterizing the control policies as an affine policy (Chen et al., 2019b; Qiu et al., 2020), which is expressed in (27). The control policy only needs to be updated once in each rolling period, and once $\boldsymbol{\xi}_t$ is measured, the control output can be determined in real-time.

$$\boldsymbol{R}_t = r(\boldsymbol{\xi}_t) = \boldsymbol{r}_{0,t} + \boldsymbol{K}\boldsymbol{\xi}_t, \forall t \in \mathcal{T} \tag{27}$$

where $\boldsymbol{r}_{0,t}$ is the base control output and $\boldsymbol{K}$ is the gain matrix which leads to correction of power output according to the disturbance $\boldsymbol{\xi}_t$. Thus, the auxiliary control variables are

$$\begin{aligned} \tilde{\boldsymbol{R}}_t &= \boldsymbol{r}_{0,t} + \boldsymbol{K}\tilde{\boldsymbol{\xi}}_t, \forall t \in \mathcal{T} \\ \hat{\boldsymbol{R}}_t &= \boldsymbol{K}\hat{\boldsymbol{\xi}}_t, \forall t \in \mathcal{T} \end{aligned} \tag{28}$$

where $\tilde{\boldsymbol{R}}_t$ and $\hat{\boldsymbol{R}}_t$ are included in $\tilde{\boldsymbol{X}}_t$ and $\hat{\boldsymbol{X}}_t$, respectively; there is $\hat{\boldsymbol{\xi}}_t = \partial \tilde{\boldsymbol{\xi}}_t / \partial \boldsymbol{\xi}_0, \hat{\boldsymbol{\xi}}_0 = \boldsymbol{I}_{N_\xi \times N_\xi}$. Based on the control variables, the auxiliary variables of SoC can also be obtained as

$$\begin{aligned} \frac{d}{dt}\widetilde{\boldsymbol{SoC}}_t &= \frac{1}{\boldsymbol{S}^{\max}} \boldsymbol{\eta} \tilde{\boldsymbol{R}}_t, \forall t \in \mathcal{T} \\ \frac{d}{dt}\widehat{\boldsymbol{SoC}}_t &= \frac{1}{\boldsymbol{S}^{\max}} \boldsymbol{\eta} \boldsymbol{K} \hat{\boldsymbol{\xi}}_t, \forall t \in \mathcal{T} \end{aligned} \tag{29}$$

where $\boldsymbol{SoC}_t$ and $\boldsymbol{\eta}$ are the vector forms of $SoC_{i,t}$ and $[\eta_i^{\mathrm{c,eq}}, 1/\eta_i^{\mathrm{d,eq}}]$, respectively. It can be seen that the auxiliary variable of SoC is related to the historical information of wind power uncertainties, so the assessment of SoC would be gradually inaccurate over time. Therefore, the rolling-horizon manner should be used to guarantee good control performance.

3.2.3 Chance constraint

In the established SO problem, the constraints are classified into equality constraints, including (1)–(6), (18), (28), and (29); and inequality constraints, including (9), (19), and (20). The linear inequality constraints are considered in a probabilistic way as chance constraints, expressed as

$$\Pr\{\boldsymbol{\phi}_r^{\mathrm{T}} \boldsymbol{X}_t \le \bar{\phi}_r\} \ge \gamma, \forall r \in \mathcal{C} \tag{30}$$

where $\mathcal{C}$ is the set of all inequality constraints; $\Pr\{\cdot\}$ represents the probability operator; $\boldsymbol{\phi}_r$ and $\bar{\phi}_r$ are the coefficients vector and the upper bound of the rth constraint, respectively; and γ is the chance tolerance. Chance constraint (30) can be rewritten as (31) for inner approximation with coefficient κ_γ under specific probability level (Calafiore and Ghaoui, 2006).

$$\kappa_\gamma \sqrt{\mathrm{var}\{\boldsymbol{\phi}_r^{\mathrm{T}} \boldsymbol{X}_t\}} + \boldsymbol{\phi}_r^{\mathrm{T}} \tilde{\boldsymbol{X}}_t \le \bar{\phi}_r \tag{31}$$

According to the abovementioned series expansion theory, the variance term can be evaluated by SAF as (32), and a detailed explanation of (31) and (32) can be found in Supplementary Appendix SA.

$$\mathrm{var}\{\boldsymbol{\phi}_r^{\mathrm{T}} \boldsymbol{X}_t\} = \int_0^t \sigma(\tilde{\boldsymbol{\xi}}_s)^{\mathrm{T}} \hat{\boldsymbol{X}}_s^{\mathrm{T}} \boldsymbol{\phi}_r \boldsymbol{\phi}_r^{\mathrm{T}} \hat{\boldsymbol{X}}_s \sigma(\tilde{\boldsymbol{\xi}}_s) ds \tag{32}$$

3.2.4 Convex optimization problem reformulation

The convexity of the SO problem can be guaranteed when the affine feedback policy is adopted, and the optimization problem is formed as a quadratically constrained quadratic programming (QCQP) problem. The trapezoidal rule (Sanchez-Gasca et al., 1995) can be used in the numerical calculation of the integral. To express the chance constraints as a second-order cone constraint form, the coefficient vector $\boldsymbol{\pi}_r$ is introduced to reformulate the variance term in (32), considering the accumulation characteristic of integral operator as

$$\begin{aligned} &\sqrt{\boldsymbol{\pi}_r^{\mathrm{T}} \boldsymbol{Y}_t \boldsymbol{Y}_t^{\mathrm{T}} \boldsymbol{\pi}_r} \le -\frac{1}{\kappa_\gamma}(\boldsymbol{\phi}_r^{\top} \tilde{\boldsymbol{X}}_t - \bar{\phi}_r), \forall r \in \mathcal{C} \\ &\text{where } \boldsymbol{Y}_t = \left[\hat{\boldsymbol{X}}_0^{\mathrm{T}}, \hat{\boldsymbol{X}}_1^{\mathrm{T}}, \cdots, \hat{\boldsymbol{X}}_t^{\mathrm{T}}\right]^{\mathrm{T}}, \forall t \in \mathcal{T} \end{aligned} \tag{33}$$

Moreover, the ' = ' in the objective function can be replaced by '≥' to relax and can be rewritten into second-order cone constraints similar to the method in (33). In summary, the overall optimization problem is expressed as

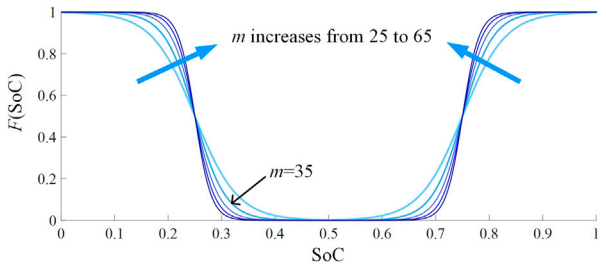

FIGURE 2
Different curves of F (SoC) when the value of the adaptive factor m increases from 25 to 65.

$$\min_{\boldsymbol{r}_{0,t},\boldsymbol{K},\tilde{\boldsymbol{X}}_t,\hat{\boldsymbol{X}}_t} J \geq \varphi^2$$

$$\| \boldsymbol{\omega}_0^{\mathrm{T}} \tilde{\boldsymbol{X}} \|_2 \leq \varphi_0, \| \boldsymbol{\omega}_1^{\mathrm{T}} \hat{\boldsymbol{X}} \|_2 \leq \varphi_1, \left\| \begin{matrix} \varphi_0 \\ \varphi_1 \end{matrix} \right\|_2 \leq \varphi \tag{34}$$

$$\text{s.t.} \quad \| \boldsymbol{\pi}_r^{\mathrm{T}} \boldsymbol{Y}_t \|_2 \leq -\frac{1}{\kappa_\gamma} \left(\boldsymbol{\phi}_r^{\top} \tilde{\boldsymbol{X}}_t - \bar{\phi}_r \right), \forall r \in \mathcal{C}$$

$$\text{equality constraints (1)} - \text{(6)}, \text{(18)}, \text{(28)}, \text{(29)}$$

where φ_0 and φ_1 are the square root value of $\tilde{J}_0$ and $\tilde{J}_1$, respectively; $\boldsymbol{\omega}_0$ and $\boldsymbol{\omega}_1$ are the introduced coefficient vectors; and $\| \cdot \|_2$ represents 2-norm operator.

4 Power dispatching approach for ESUs based on DA

Once the total power command is given by the upper-layer optimal SFC, different ESUs in the same ESS cluster are required to coordinate with each other to determine their power output and completely meet the command. However, the characteristics of different ESUs are probably inconsistent, including rated power, rated energy capacity, and the current SoC level. Thus, the possible energy saturation and violation of power limits would lead to sudden withdrawals of ESUs, which might influence the frequency regulation effect. Therefore, a DA method is proposed in this section to coordinate the power output of ESUs with communication networks and guarantee the frequency regulation performance.

4.1 Optimization control problem of ESUs

Similar to the cost of conventional generators in economic dispatch (Wen et al., 2018), the virtual cost function of ESUs can be defined as a quadratic function with respect to the power output of the ESU and the current SoC level (Megel et al., 2018) at each time step t as

$$C_{k,t}\left(p_{k,t}\right) = \frac{1}{2}\alpha_k p_{k,t}^2 + \beta_k \left(SoC_{k,t}\right) p_{k,t} \tag{35}$$

where $p_{k,t}$ denotes $p_{k,t}^{\mathrm{d}} - p_{k,t}^{\mathrm{c}}$; α_k is the quadratic term coefficient; and $\beta_k \left(SoC_{k,t}\right)$ is the linear term coefficient, used as an evaluation

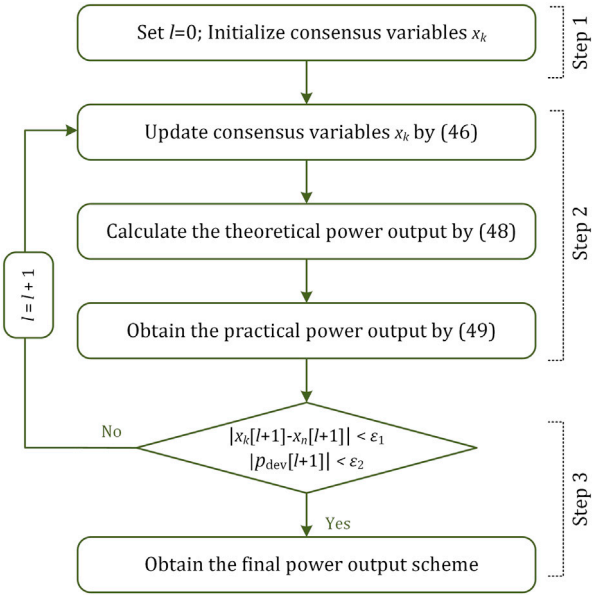

FIGURE 3
Flowchart of the DA method.

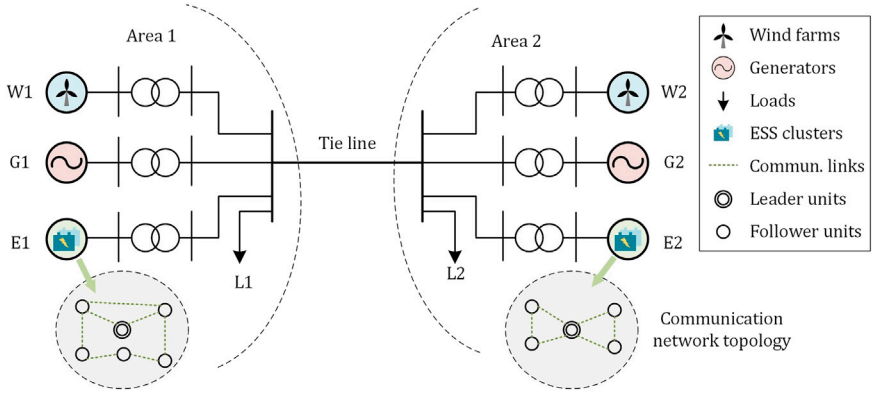

FIGURE 4
Structure of two-area systems considering wind power and energy storage systems.

function of the current SoC level. The detailed derivation of (35) can be found in Supplementary Appendix SB.

Thus, the optimization control problem of ESUs is to achieve the minimizing objective function (36) under equality constraint (37) and other inequality constraints.

$$\min \sum_{k=1}^{Ni} N_i C_{k,t}\left(p_{k,t}\right) \tag{36}$$

$$\sum_{k=1}^{Ni} N_i\, p_{k,t} = p_{i,t}^{\mathrm{E}}, \forall i \in \mathcal{A}, \forall k \in \mathcal{S}_i \tag{37}$$

where N_i is the number of ESUs in the ith ESS cluster and $p_{i,t}^{\mathrm{E}}$ is the total power command determined by the upper control layer for all ESUs in the same cluster.

In addition, the inequality constraints are twofold: power and energy limits, and power direction constraints, i.e., $\mathrm{sign}\left(p_{k,t}\right) = \mathrm{sign}\left(p_{i,t}^{\mathrm{E}}\right)$. It is to avoid the opposite direction of the ESU power output, which might cause some to charge others and result in a waste of resources.

This problem is a quadratic programming problem and can be solved in a centralized way (Yin et al., 2021). However, the local computing capability in a parallel way is not fully used, so the efficiency of solving optimization problems would be reduced. Therefore, the DA needs to be developed.

According to the general process of utilizing distributed methods to solve optimization problems (Wang et al., 2019), the Lagrange function $L(\boldsymbol{p}, \lambda)$ is constructed in (38) based on the objective function (36) and equality constraint (37). $\boldsymbol{p}$ represents the vector form of p_k. The inequality constraints are ignored here, which will be considered later in DA. For convenience, the time step label t is omitted hereafter.

TABLE 1 Parameters of the system frequency regulation model in p.u.

Parameters	Values	Parameters	Values
H_1	12	H_2	10
D_1	1.6	D_2	1.2
R_1	0.08	R_2	0.09
T_1^{t}	0.3	T_2^{t}	0.2
K_1^{I}	0.01	K_2^{I}	0.015
B_1, B_2	20	T_{12}	1.67

$$L(\boldsymbol{p}, \lambda) = \sum_{k=1}^{Ni} N_i C_k\left(p_k\right) + \lambda\left(p_i^{\mathrm{E}} - \sum_{k=1}^{Ni} N_i\, p_k\right) \tag{38}$$

where λ is the Lagrange multiplier. If $\partial L(\boldsymbol{p}, \lambda)/\partial p_k = 0, \forall k$, for any ESU, there is

$$\frac{\partial C_k\left(p_k\right)}{\partial p_k} - \lambda = 0, \forall k \tag{39}$$

In other words, when all $\partial C_k\left(p_k\right)/\partial p_k$ are equal to λ, the original objective function (36) can achieve its extreme value. Therefore, the value of the consensus variable x_k should approach the value of λ as shown in (40). In addition, x_k is the input for the dispatching scheme of p_k, where a higher x_k leads to a higher p_k and vice versa.

$$x_k = \frac{\partial C_k\left(p_k\right)}{\partial p_k} = \alpha_k p_k + \beta_k\left(SoC_k\right), \forall k \tag{40}$$

Specifically, the evaluation function $\beta_k\left(SoC_k\right)$ with the basic form of *logistic* function (Postnikov, 2020) is proposed in this article to better-reflect the safe and dangerous zones of SoC as shown in (41).

TABLE 2 Parameters of energy storage units.

	Number	Type	P^{max} (MW)	S^{max} (MWh)	η^c, η^d	SoC^0
ESS cluster 1	1	Power-type	20	1.085	0.80, 0.85	0.62
	2	Power-type	14	1.125	0.85, 0.95	0.58
	3	Power-type	14	1.755	0.95, 0.95	0.73
	4	Energy-type	10	4.36	0.80, 0.85	0.59
	5	Energy-type	6	6.0325	0.90, 0.85	0.66
	6	Energy-type	5	15.17	0.95, 0.85	0.51
ESS cluster 2	1	Power-type	11	2.1375	0.95, 0.85	0.47
	2	Energy-type	9	4.44	0.85, 0.85	0.39
	3	Energy-type	8	5.0625	0.95, 0.95	0.33
	4	Energy-type	6	10.325	0.80, 0.80	0.38
	5	Energy-type	2	10.625	0.95, 0.90	0.41

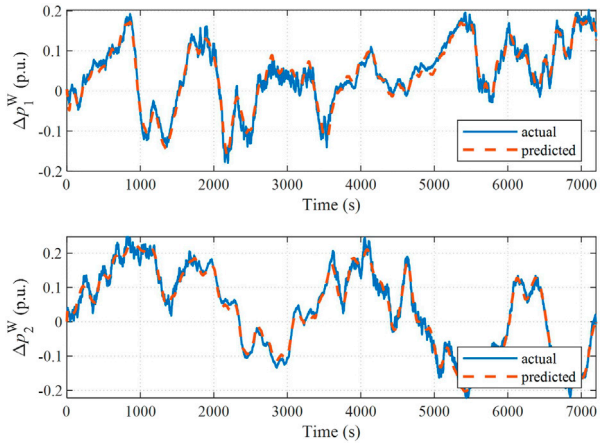

FIGURE 5
Predicted and actual wind power deviation in **(A)** area 1 and **(B)** area 2.

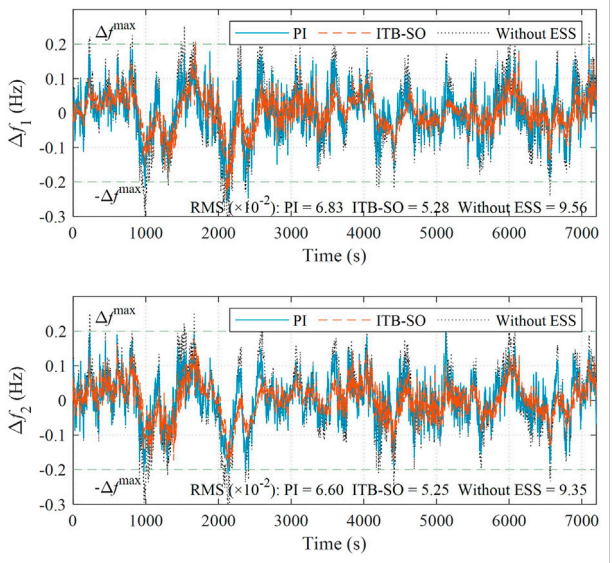

FIGURE 6
Comparison of frequency deviation under different control methods of **(A)** area 1 and **(B)** area 2.

$$\beta_k(SoC_k) = w_k \cdot \mathrm{sign}\left(SoC^{ref} - SoC_k\right) \cdot F(SoC_k) \quad (41)$$

where w_k is the weight factor with $w_k \in [0, 1]$ and $F(SoC_k)$ is constructed above and below the reference value and defined as

$$F(SoC_k) = \frac{e^{m\left(\left|SoC_k - SoC^{ref}\right| - \frac{1}{2}\left|SoC_k^{lim} - SoC^{ref}\right|\right)}}{1 + e^{m\left(\left|SoC_k - SoC^{ref}\right| - \frac{1}{2}\left|SoC_k^{lim} - SoC^{ref}\right|\right)}} \quad (42)$$

where SoC_k^{lim} is the SoC limit: when $SoC_k < SoC^{ref}$, there is $SoC_k^{lim} = SoC_k{}^{min}$; when $SoC_k > SoC^{ref}$, there is $SoC_k^{lim} = SoC_k{}^{max}$; and m is an adaptive factor used to adjust the steepness of $F(SoC_k)$ in (42), in order to adjust the scope of safe and dangerous SoC levels. After several comparative analyses, m is selected as 35 as shown in Figure 2.

4.2 Discrete consensus algorithm

The main idea of DA is that the agents use a communication network to share information to complete the iterative calculation. The communication network topology can be modeled by a directed or undirected graph denoted by $G = (V, E)$ (Pourbabak et al., 2018), where V is the set of nodes and E is the set of edges formed by adjacent nodes. A Laplace matrix $\boldsymbol{L} = [L_{kn}]$ is defined as shown in (43), where the diagonal element is the degree of nodes in graph G, and the non-diagonal

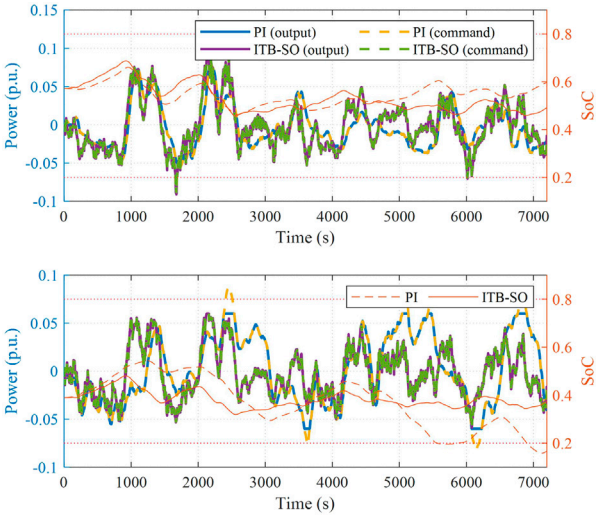

FIGURE 7
Comparison results under different control methods of **(A)** ESS cluster 1 and **(B)** ESS cluster 2.

element is the (0–1) element a_{kn}, which is determined by whether the nodes k and n are adjacent.

$$\begin{cases} L_{kk} = \sum_{k \neq n} a_{kn} \\ L_{kn} = -a_{kn} \end{cases} \tag{43}$$

The agents obtain information from their neighbors through the communication network and update their own information. All agents finally converge to the same value after several iterations. The first-order discrete consensus algorithm can be updated according to (44).

$$x_k[l+1] = \sum_{n=1}^{N} d_{kn}[l] x_n[l] \tag{44}$$

where l is the discrete sequence representing the lth iteration; x_k is the consensus variable of the kth agent; and $d_{kn}[l]$ is the element of $\boldsymbol{D}_{n\times n} = [d_{kn}]$ and is defined as

$$d_{kn}[l] = \frac{|L_{kn}|}{\sum_{n=1}^{N} |L_{kn}|} \tag{45}$$

4.3 Control procedure of DA

1) Step 1: Initializing power dispatch and consensus variables.

Set $l = 0$. Current SoC level information is measured to compute the evaluation function by (41). The total power command is allocated equally to each ESU as the initial condition, and the consensus variable is initialized by (40).

2) Step 2: Iterative calculation.

The consensus variables are iterated by DA. In order to ensure that the final dispatching scheme can match the total power command, a power correction term is introduced for the leader agent. The update rule is shown as

$$\begin{cases} x_k[l+1] = \sum_{n=1}^{Ni} N_i\, d_{kn}[l] x_n[l] + \delta p_{\text{dev}}[l], k \text{ is leader} \\ x_k[l+1] = \sum_{n=1}^{Ni} N_i\, d_{kn}[l] x_n[l], k \text{ is follower} \end{cases} \tag{46}$$

where δ is the convergence coefficient that determines the convergence speed of the leader and p_{dev} is the deviation from command at the current iteration:

$$p_{\text{dev}}[l] = p_i^{\text{E}} - \sum_{n=1}^{Ni} N_i\, p_k[l] \tag{47}$$

p_k is updated according to the consensus variable x_k by the following rules:

$$\bar{p}_k[l] = \frac{x_k[l] - \beta_k(SoC_k)}{\alpha_k} \tag{48}$$

$$p_k[l] = \{\bar{p}_k[l]\}_{\text{restriction}} \tag{49}$$

where (49) makes a restriction on the theoretical power output by (48), which is possibly infeasible due to inequality constraints, i.e., power and energy limits and power direction constraints.

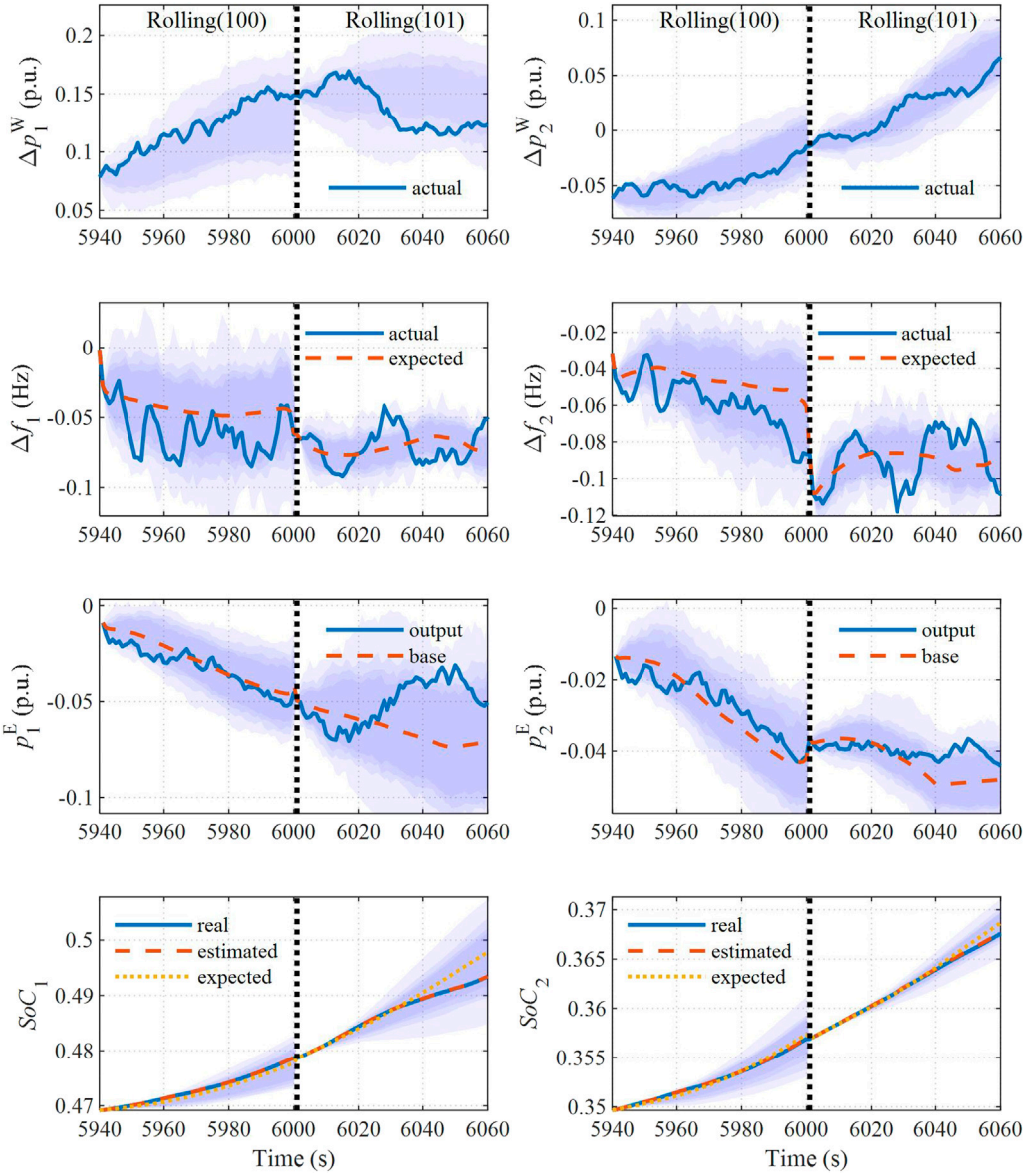

FIGURE 8
Actual results and Monte Carlo samples of **(A,B)** wind power deviation, **(C,D)** frequency deviation **(E,F)** power output of the ESS cluster, and **(G,H)** SoC level of the ESS cluster.

Then, the remaining power deviation would be fed back to the consensus variable through the correction term and shared by other neighbors.

3) Step 3: Judging the convergence condition.

First, each ESU agent should reach an agreement with the adjacent agents on their consensus variables. However, complete consensus cannot be achieved for all agents actually, so the approximate condition is implemented as

$$|x_k[l+1] - x_n[l+1]| < \varepsilon_1, k \leftrightarrow n \tag{50}$$

where $k \leftrightarrow n$ means adjacent and ε_1 is a small constant.

Second, the power deviation is also taken as a factor in the convergence condition as shown in (51). In order to avoid over-iteration, ε_2 is set as a small constant close to 0, and it determines the accuracy of tracking the command.

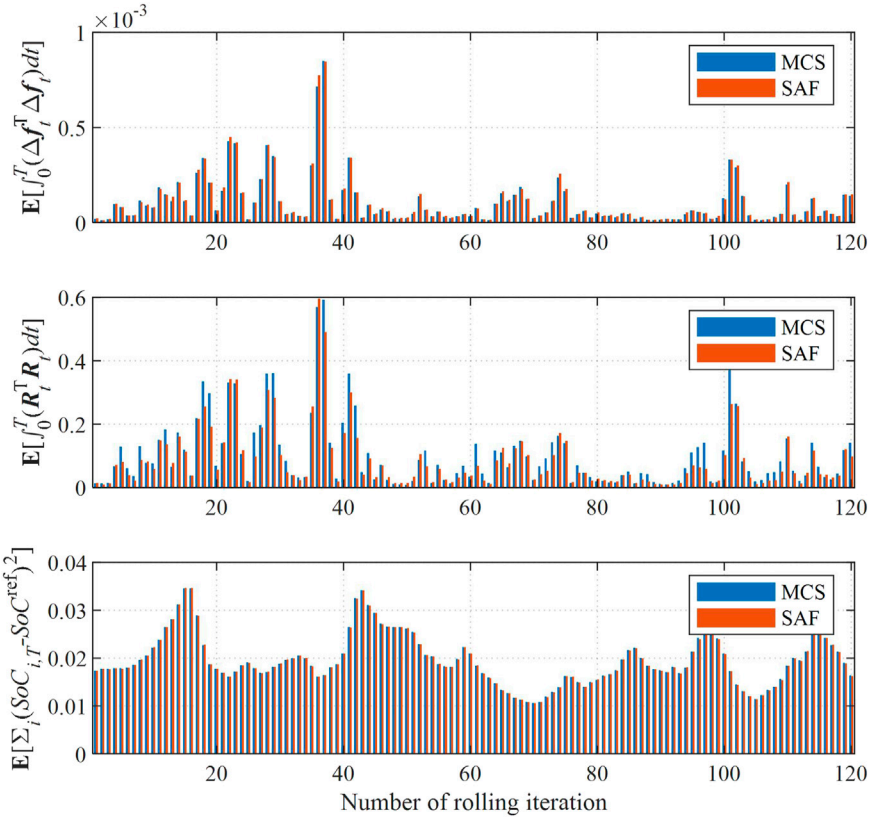

FIGURE 9
Objective value estimated by SAF compared with Monte Carlo samples: **(A)** objective of frequency deviations, **(B)** objective of control variables, and **(C)** objective of SoC deviations. Keywords: energy storage, frequency regulation, wind power uncertainty, stochastic optimization, Itô theory, distributed algorithm.

$$\left|p_{\text{dev}}[l+1]\right| < \varepsilon_2 \tag{51}$$

In summary, the flowchart of the control procedure of the DA method is shown in Figure 3.

5 Case study

5.1 Simulation model setting

The simulations are performed using Matlab software and run on a machine equipped with Intel i7 3.2 GHz CPU and 16 GB RAM. The established optimization problems are solved by the Yalmip toolbox called Gurobi optimizer. The test simulations based on the actual wind power scenario are conducted using the Simulink platform.

The structure of the simulation system for frequency regulation is shown in Figure 4 containing two areas with rated capacities of both 600 MW and a rated system frequency of both 50 Hz. The parameters of the simulation system are listed in Table 1 (Kundur et al., 1994; Pathak et al., 2018). The parameters and initial SoC levels of the ESSs are listed in Table 2. The predicted and actual wind power deviations in the two areas are shown in Figure 5. The total simulation time is set as 7200s; the time step is set as 1s; the parameters of the SDE models can be found in Supplementary Appendix SC; the upper-layer SO problem is solved every 60 s, in which the parameter $\Delta f^{\max}$ is set as 0.2Hz, κ_γ as 1.7, and $\underline{SoC}$ and $\overline{SoC}$ as 0.2 and 0.8, respectively; and the lower-layer DA is implemented at each time step, in which the matrices $\boldsymbol{D}_i$ are listed in Supplementary Appendix SD.

5.2 Frequency regulation results

In this section, two contrast cases are introduced for comparison. Contrast method 1: the contribution of the ESS is not considered during the frequency regulation, and Contrast method 2, namely, PI: the power command for the ESS is computed *via* PI controller, where the input signal of PI is

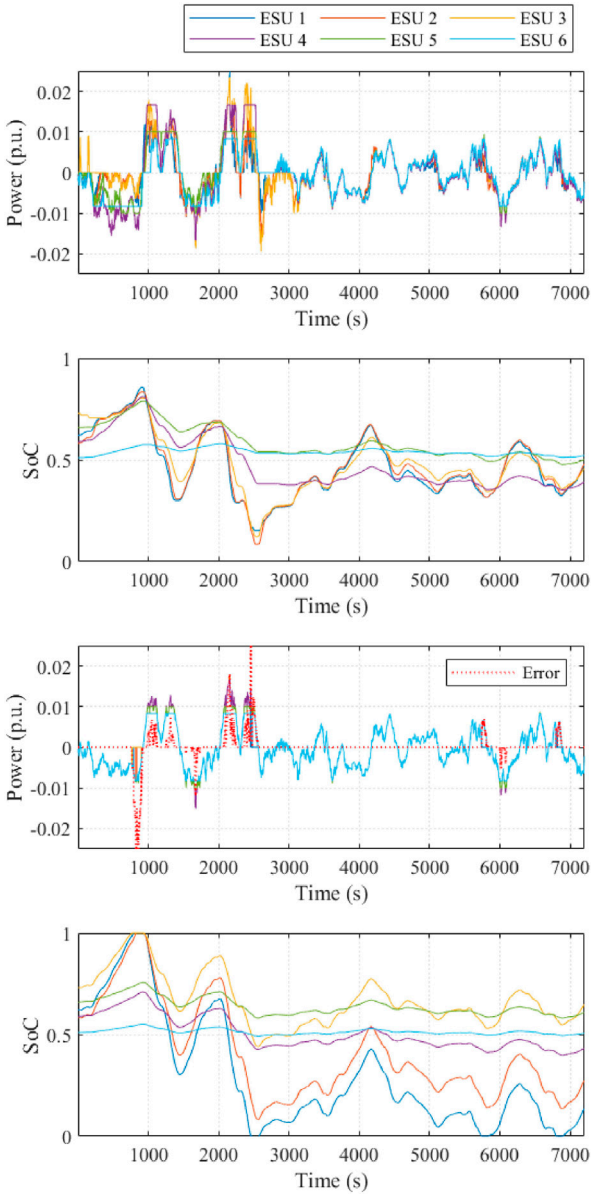

FIGURE 10
Power output and SoC level of each ESU compared under **(A,B)** DA control and **(C,D)** equally allocation method.

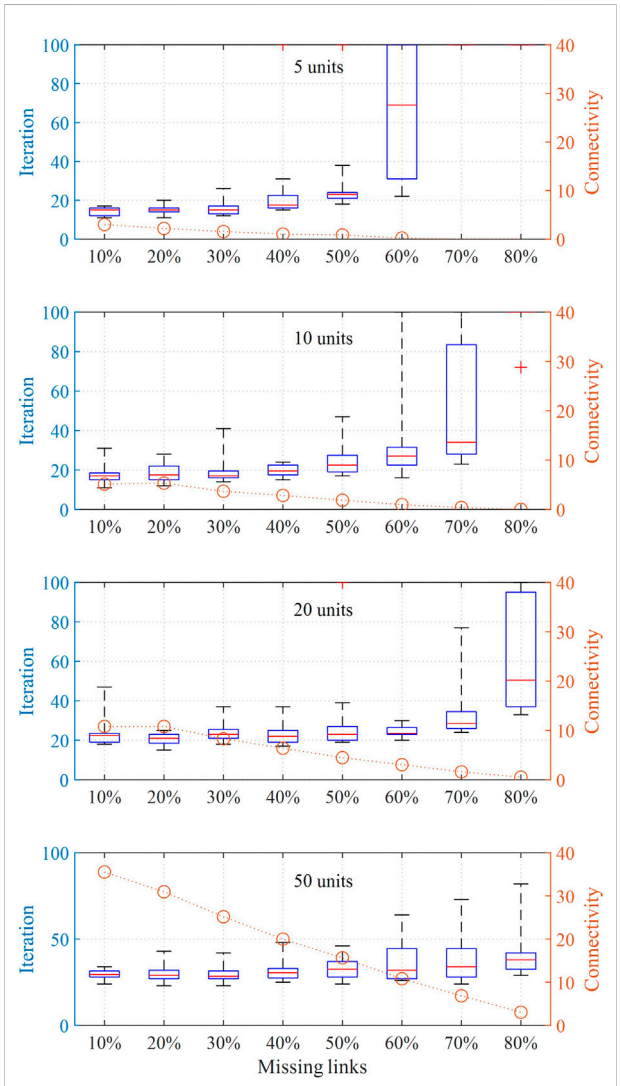

FIGURE 11
Results of iteration times and mean value of connectivity for simulation systems with different numbers of ESUs Nomenclature.

high-frequency components of the ACE signal *via* a high-pass filter. In addition, our proposed method is denoted as ITB-SO for convenience.

The results of frequency deviations under these different control methods are compared in Figure 6. It is clear that when the ESS participates in frequency regulation, the peak and nadir value of system frequency is always reduced and increased. Most of the time, the frequency deviations of the two areas can be limited within the ±0.2 Hz bounds, both under the PI and the ITB-SO methods. However, the PI method cannot respond immediately to wind power fluctuation, so it is difficult to make full use of the rapid adjustment capability of the ESS. The root mean squared (RMS) value of frequency deviations is given for comparison as shown in Figure 6. It can be seen that the RMS value under the ITB-SO method is the lowest, and that of the two different areas can be restricted to a similar level.

To verify that the proposed ITB-SO method can adaptively adjust the power output of the ESS considering different rated power and energy capacity, Figure 7 gives the simulation results under the PI and the ITB-SO methods. It can be seen that the power command for ESS cluster 2 cannot be accurately met by the actual output during several periods because the rated power of ESS cluster 2 is small. On the

contrary, the scheme determined by ITB-SO is based on the estimation of the future possible power and SoC in a finite horizon; therefore, the violation of power and energy restriction can be avoided, and the frequency regulation performance can be guaranteed.

In addition, the SoC level under ITB-SO is closer to the reference value than that of the PI method. For example, the ESS cluster 2 operates near the lower SoC bound, i.e., 0.2 after 5500 s under PI control, while under ITB-SO, ESS cluster 1, with a higher energy level, discharges more power to release the burden of ESS cluster 2. That is because the penalty of SoC deviation is also considered in the objective function in order to force the SoC to the reference value.

5.3 Accuracy and results of stochastic assessment

The effectiveness of the rolling-horizon manner is validated in this section by comparing it with Monte Carlo sample (MCS) simulations, where the MCS simulations are conducted under 100 wind power generation scenarios. Results of the two successive rollings (100th and 101st) are shown in Figure 8. The violet bands represent 85–100% (5% interval) of all 100 MCS results, and the actual operation results are clearly in the scope of the MCS. The four subgraphs in the left column show the wind power deviation, frequency deviation, power, and SoC of the ESS cluster in area 1, and those in area 2 are in the right column.

In Figures 8C and D, the expected value is obtained without taking into account wind power uncertainty, where the impact of stochastic fluctuation on the objective and chance constraints in the optimization problem cannot be considered. Therefore, the application of SO is necessary. In Figures 8E and F, it can be seen that the control output of the ESS can be further corrected according to the feedback policy and respond to the real-time wind power prediction error rapidly. In Figures 8G and H, the curve marked 'real' is the mean value of all ESUs in the ESS cluster, and the estimated results are obtained by equivalent discharge and charge efficiency as in (18). It indicates that accuracy can be ensured, and the effectiveness of ITB-SO can be verified.

To verify the effectiveness of the approximately decomposed reformulation of SAF in the first-order form, the objective value assessed by SAF of each rolling iteration is compared with the results *via* MCS simulations. The gross objective is divided into multi-objective for comparison as shown in Figure 9, including the objective of frequency deviations, control variables, and SoC deviations. It evidenced the accuracy of SAF without scenario generation; thus, the computational efficiency can be enhanced.

5.4 Results of DA

Taking the ESUs in the ESS cluster 1 as an example, Figure 10 shows their output power and SoC level under the DA method, compared with the contrast method, which is to reach the average command signals. It is easy to be implemented without iteration, and the power command can be met under ideal situations.

However, the tracking error cannot be eliminated because of the SoC saturation or violation of rated power in some cases when the power command is equally allocated to each ESU. For example, in Figures 10C and D, some ESUs withdraw from frequency regulation since their SoC level reaches the upper bound (such as 800 s) and the lower bound (such as 2500 s) or the power signal is larger than the rated output (such as 1080 s), while others with large energy capacity are barely used. Therefore, the effect of frequency regulation could deteriorate due to sudden withdrawals. In contrast, the proposed DA method enables all ESUs to coordinate their output power and adjust their SoC at optimal levels. It is clear from Figure 10B that the SoC level is attracted to their reference value and the saturation can be avoided. Therefore, the DA method can make full use of the characteristics and advantages of power-type and energy-type units effectively.

Random communication failure between the ESU agents is implemented to verify the robustness of the DA dispatching method. The results are studied in different simulation systems containing 5, 10, 20, and 50 ESUs. The situation with complete connectivity is defined as all units being connected with each other. Then, the proportion of missing communication links varies from 10 to 80% (10% interval) by disconnecting the communication links randomly. The boxplot of iteration times and the mean value of algebraic connectivity are shown in Figure 11. The algebraic connectivity is the second smallest eigenvalue of the Laplace matrix $\boldsymbol{L}$, which reflects the connectivity of the graph (Yoonsoo and Mesbahi, 2006).

When parts of the communication links disconnect between ESUs, they can still share information through other remaining links and successfully track the power command as well. It can be found in Figure 11 that with the increase in the number of missing links, the connectivity gradually decreases while iteration times increase. However, the trend is diverse with different numbers of units: iteration times with 20 and 50 units increase slower than that with 5 and 10 units, and the iteration characteristic is more stable. It indicates that random communication failure has a slight impact on the system with numerous ESUs and the robustness is higher.

6 Conclusion

In this article, a bi-layer optimal SFC approach is proposed for ESSs to participate in multi-area systems frequency regulation under

continuous wind power fluctuations. The upper-layer control based on the ITB-SO method in a rolling-horizon manner is implemented to determine the power command for different ESS clusters considering wind power uncertainties. The power output of ESUs in the same cluster is coordinated using the DA method in the lower-layer control to track the total power command. The simulation applications reveal that 1) the stability of the system frequency can be enhanced by compensating for wind power volatility immediately via ESSs. Moreover, the trade-off between frequency regulation performance and the operation cost of the ESS can be achieved. 2) The ITB-SO method can solve optimization problems precisely without generating scenarios of wind power. The computational efficiency is high, so it is suitable for real-time SFCs. 3) Sudden withdrawals of ESSs due to energy saturation and violation of power limit can be avoided by dispatching power signals using the DA method. The robustness of the DA method is also validated while missing limited communication links between ESUs. In future work, the addition of PV systems would be considered.

Data availability statement

The original contributions presented in the study are included in the article; further inquiries can be directed to the corresponding author.

Author contributions

ZW, FW, and LS contributed to the conception and design of the study. ZW and YL are responsible for providing experimental design and data analysis. ZW and WH are responsible for providing code implementation. All authors contributed to the manuscript writing revised, read, and approved the submitted version.

Funding

This work was supported in part by the Funds for International Cooperation and Exchanges of the National Natural Science Foundation of China under Grant 52061635102, and in part by the Overseas Expertise Introduction Project for Discipline Innovation ("111Project") under Grant B14022.

Conflict of interest

The authors declare that the research was conducted in the absence of any commercial or financial relationships that could be construed as a potential conflict of interest.

Publisher's note

All claims expressed in this article are solely those of the authors and do not necessarily represent those of their affiliated organizations, or those of the publisher, the editors, and the reviewers. Any product that may be evaluated in this article, or claim that may be made by its manufacturer, is not guaranteed or endorsed by the publisher.

Supplementary material

The Supplementary Material for this article can be found online at: https://www.frontiersin.org/articles/10.3389/fenrg.2022.1005281/full#supplementary-material

References

Alsharif, H., Jalili, M., and Hasan, K. N. 2020. "Analyzing the impact of distribution of battery energy storage system for participation in frequency regulation", in: 2020 Australasian Universities Power Engineering Conference (AUPEC), Hobart, Australia, 29 November 2020 - 02 December 2020, 1–6.

Anderson, T., Muralidharan, M., Srivastava, P., Haghi, H. V., Cortés, J., Kleissl, J., et al. (2021). Frequency regulation with heterogeneous energy resources: A realization using distributed control. *IEEE Trans. Smart Grid* 12 (5), 4126–4136. doi:10.1109/TSG.2021.3071778

Bidram, A., and Davoudi, A. (2012). Hierarchical structure of microgrids control system. *IEEE Trans. Smart Grid* 3 (4), 1963–1976. doi:10.1109/TSG.2012.2197425

Calafiore, G. C., and Ghaoui, L. E. (2006). On distributionally robust chance-constrained linear programs. *J. Optim. Theory Appl.* 130 (1), 1–22. doi:10.1007/s10957-006-9084-x

Chen, C., Bao, Y.-Q., Wu, X.-H., Wang, B., and Shen, C. (2019a). Battery energy storage system based on incremental cost consensus algorithm for the frequency control. *IEEE Access* 7, 147362–147372. doi:10.1109/access.2019.2946458

Chen, X., Lin, J., Liu, F., and Song, Y. (2019b). Optimal control of AGC systems considering non-Gaussian wind power uncertainty. *IEEE Trans. Power Syst.* 34 (4), 2730–2743. doi:10.1109/tpwrs.2019.2893512

Chen, X., Lin, J., Liu, F., and Song, Y. (2019c). Stochastic assessment of AGC systems under non-Gaussian uncertainty. *IEEE Trans. Power Syst.* 34 (1), 705–717. doi:10.1109/tpwrs.2018.2865502

Cheng, Y., Tabrizi, M., Sahni, M., Povedano, A., and Nichols, D. (2014). Dynamic available AGC based approach for enhancing utility scale energy storage performance. *IEEE Trans. Smart Grid* 5 (2), 1070–1078. doi:10.1109/TSG.2013.2289380

Cherukuri, A., and Cortes, J. (2018). Distributed coordination of DERs with storage for dynamic economic dispatch. *IEEE Trans. Autom. Contr.* 63 (3), 835–842. doi:10.1109/tac.2017.2731809

Esmaili, A., Novakovic, B., Nasiri, A., and Abdel-Baqi, O. (2013). A hybrid system of Li-ion capacitors and flow battery for dynamic wind energy support. *IEEE Trans. Ind. Appl.* 49 (4), 1649–1657. doi:10.1109/tia.2013.2255112

Garcia-Torres, F., Bordons, C., Tobajas, J., Real-Calvo, R., Santiago, I., and Grieu, S. (2021). Stochastic optimization of microgrids with hybrid energy storage systems for grid flexibility services considering energy forecast uncertainties. *IEEE Trans. Power Syst.* 36 (6), 5537–5547. doi:10.1109/tpwrs.2021.3071867

Jan, M. U., Xin, A., Abdelbaky, M. A., Rehman, H. U., and Iqbal, S. (2020). Adaptive and fuzzy PI controllers design for frequency regulation of isolated

microgrid integrated with electric vehicles. *IEEE Access* 8, 87621–87632. doi:10.1109/access.2020.2993178

Karrari, S., Baghaee, H. R., Carne, G. D., Noe, M., and Geisbuesch, J. (2020). Adaptive inertia emulation control for high-speed flywheel energy storage systems. *IET Gener. Transm. Distrib.* 14 (22), 5047–5059. doi:10.1049/iet-gtd.2020.0066

Khan, F. H., Pal, T., Kundu, B., and Roy, R. "Wind energy: A practical power analysis approach", in: 2021 Innovations in Energy Management and Renewable Resources,Kolkata, 07 February 2021, 1–6.

Kundur, P., Balu, N. J., and Lauby, M. G. (1994). *Power system stability and control*. New York: McGraw-Hill.

Lee, S.-J., Kim, J.-H., Kim, C.-H., Kim, S.-K., Kim, E.-S., Kim, D.-U., et al. (2016). Coordinated control algorithm for distributed battery energy storage systems for mitigating voltage and frequency deviations. *IEEE Trans. Smart Grid* 7 (3), 1713–1722. doi:10.1109/tsg.2015.2429919

Li, N., Zhao, C., and Chen, L. (2016). Connecting automatic generation control and economic dispatch from an optimization view. *IEEE Trans. Control Netw. Syst.* 3 (3), 254–264. doi:10.1109/tcns.2015.2459451

Li, Q., Gao, D. W., Zhang, H., Wu, Z., and Wang, F. y. (2019). Consensus-based distributed economic dispatch control method in power systems. *IEEE Trans. Smart Grid* 10 (1), 941–954. doi:10.1109/TSG.2017.2756041

Lingohr, D., and Müller, G. (2019). Stochastic modeling of intraday photovoltaic power generation. *Energy Econ.* 81, 175–186. doi:10.1016/j.eneco.2019.03.007

Mauricio, J. M., Marano, A., Gomez-Exposito, A., and Martinez Ramos, J. L. (2009). Frequency regulation contribution through variable-speed wind energy conversion systems. *IEEE Trans. Power Syst.* 24 (1), 173–180. doi:10.1109/tpwrs.2008.2009398

Meegahapola, L., and Flynn, D. 2010. "Impact on transient and frequency stability for a power system at very high wind penetration", in: IEEE PES General Meeting, Minneapolis, 29 July 2010, 1–8.

Megel, O., Liu, T., Hill, D. J., and Andersson, G. (2018). Distributed secondary frequency control algorithm considering storage efficiency. *IEEE Trans. Smart Grid* 9 (6), 6214–6228. doi:10.1109/tsg.2017.2706979

Miller, N. W., Clark, K., and Shao, M. "Frequency responsive wind plant controls: Impacts on grid performance", in: 2011 IEEE Power and Energy Society General Meeting, Detroit, 28 July 2011, 1–8.

Oshnoei, A., Kheradmandi, M., and Muyeen, S. M. (2020). Robust control scheme for distributed battery energy storage systems in load frequency control. *IEEE Trans. Power Syst.* 35 (6), 4781–4791. doi:10.1109/tpwrs.2020.2997950

Pathak, N., Bhatti, T. S., Verma, A., and Nasiruddin, I. (2018). AGC of two area power system based on different power output control strategies of thermal power generation. *IEEE Trans. Power Syst.* 33 (2), 2040–2052. doi:10.1109/tpwrs.2017.2734923

Postnikov, E. B. (2020). Estimation of COVID-19 dynamics "on a back-of-envelope": Does the simplest SIR model provide quantitative parameters and predictions? *Chaos Solit. Fractals* 135, 109841. doi:10.1016/j.chaos.2020.109841

Pourbabak, H., Luo, J., Chen, T., and Su, W. (2018). A novel consensus-based distributed algorithm for economic dispatch based on local estimation of power mismatch. *IEEE Trans. Smart Grid* 9 (6), 5930–5942. doi:10.1109/tsg.2017.2699084

Qiu, Y., Lin, J., Liu, F., Song, Y., Chen, G., and Ding, L. (2020). Stochastic online generation control of cascaded run-of-the-river hydropower for mitigating solar power volatility. *IEEE Trans. Power Syst.* 35 (6), 4709–4722. doi:10.1109/tpwrs.2020.2991229

Sanchez-Gasca, J. J., D'Aquila, R., Price, W. W., and Paserba, J. J. 1995. "Variable time step, implicit integration for extended-term power system dynamic simulation", in: Power Industry Computer Application Conference, Salt Lake City, 2 May 1995.

Shim, J. W., Verbic, G., Zhang, N., and Hur, K. (2018). Harmonious integration of faster-acting energy storage systems into frequency control reserves in power grid with high renewable generation. *IEEE Trans. Power Syst.* 33 (6), 6193–6205. doi:10.1109/tpwrs.2018.2836157

Skaf, J., and Boyd, S. P. (2010). Design of affine controllers via convex optimization. *IEEE Trans. Autom. Contr.* 55 (11), 2476–2487. doi:10.1109/TAC.2010.2046053

Tsili, M., and Papathanassiou, S. (2009). A review of grid code technical requirements for wind farms. *IET Renew. Power Gener.* 3 (3), 308–332. doi:10.1049/iet-rpg.2008.0070

U.S.DOE (2021). Global energy storage database projects. [Online]. Available: https://sandia.gov/ess-ssl/gesdb/public/projects.html (accessed 01Jun, 2022).

Verdejo, H., Awerkin, A., Saavedra, E., Kliemann, W., and Vargas, L. (2016). Stochastic modeling to represent wind power generation and demand in electric power system based on real data. *Appl. Energy* 173, 283–295. doi:10.1016/j.apenergy.2016.04.004

Wang, Y., Xu, Y., Tang, Y., Liao, K., Syed, M. H., Guillo-Sansano, E., et al. (2019). Aggregated energy storage for power system frequency control: A finite-time consensus approach. *IEEE Trans. Smart Grid* 10 (4), 3675–3686. doi:10.1109/TSG.2018.2833877

Wen, G., Yu, X., Liu, Z.-W., and Yu, W. (2018). Adaptive consensus-based robust strategy for economic dispatch of Smart grids subject to communication uncertainties. *IEEE Trans. Ind. Inf.* 14 (6), 2484–2496. doi:10.1109/tii.2017.2772088

Yin, J., Leon, J. I., Perez, M. A., Franquelo, L. G., Marquez, A., and Vazquez, S. (2021). Model predictive control of modular multilevel converters using quadratic programming. *IEEE Trans. Power Electron.* 36 (6), 7012–7025. doi:10.1109/tpel.2020.3034294

Yoonsoo, K., and Mesbahi, M. (2006). On maximizing the second smallest eigenvalue of a state-dependent graph Laplacian. *IEEE Trans. Autom. Contr.* 51 (1), 116–120. doi:10.1109/tac.2005.861710

Zhang, X., Yu, T., Yang, B., and Jiang, L. (2021). A random forest-assisted fast distributed auction-based algorithm for hierarchical coordinated power control in a large-scale PV power plant. *IEEE Trans. Sustain. Energy* 12 (4), 2471–2481. doi:10.1109/tste.2021.3101520

Zhao, T., and Ding, Z. (2018a). Cooperative optimal control of battery energy storage system under wind uncertainties in a microgrid. *IEEE Trans. Power Syst.* 33 (2), 2292–2300. doi:10.1109/tpwrs.2017.2741672

Zhao, T., and Ding, Z. (2018b). Distributed agent consensus-based optimal resource management for microgrids. *IEEE Trans. Sustain. Energy* 9 (1), 443–452. doi:10.1109/TSTE.2017.2740833

Glossary

RES Renewable energy sources

SFC Secondary frequency control

ESS Energy storage system

ESU Energy storage unit

SoC State-of-charge

AGC Automatic generation control

ACE Area control errors

ITB-SO Itô theory-based stochastic optimization

DA Distributed algorithm

SDE Stochastic differential equation

SAF Stochastic assessment function

MCS Monte Carlo samples

Variables

Δf_i Frequency deviation of the ith area

Δp_i^{M} Active power deviation of conventional generators in the ith area

p_i^{E} Active power of ith ESS cluster

Δp_i^{L} Change of load in the ith area

$\Delta p_{ij}^{\mathrm{tie}}$ Tie line power from the ith to the jth area

$\Delta p_i^{\mathrm{AGC}}$ AGC reference for the ith area

Δp_i^{W} Deviation of wind power in the ith area

$\Delta p_i^{\mathrm{W,pred}}$ Predicted wind power in the ith area

ξ_i Prediction error of wind power in the ith area

$p_i^{\mathrm{E,d}}$, $p_i^{\mathrm{E,c}}$ Discharge and charge power of ith ESS cluster

p_k^{d}, p_k^{c} Discharge and charge power of kth ESU

s_i^{E} Energy level of ith ESS cluster

s_k Energy level of kth ESU

SoC_k SoC level of kth ESU

$\boldsymbol{r}_{0,t}$ Base control output of the ESS

$\boldsymbol{K}$ Gain matrix of feedback control

Parameters

H_i Equivalent system inertia

D_i Equivalent system damping

T_i^{t} Turbine time constant

R_i Droop coefficient

T_{ij} Synchronizing coefficient

B_i Frequency bias factor

K_i^{I} Integral coefficient

η_k^{c}, η_k^{d} Charge and discharge efficiencies

$P_k^{\max}$ Rated power

$S_k^{\max}$ Rated energy capacity

$\Delta f^{\max}$ Bound of frequency

$\underline{SoC}$, $\overline{SoC}$ Lower and upper bound of SoC

$\boldsymbol{D}_i$ Communication matrix of ith ESS cluster

frontiers | Frontiers in Energy Research

TYPE Original Research
PUBLISHED 05 January 2023
DOI 10.3389/fenrg.2022.1007694

OPEN ACCESS

EDITED BY
Zhiyi Li,
Zhejiang University, China

REVIEWED BY
Yang Li,
Hohai University, China
Changsen Feng,
Zhejiang University of Technology, China
Yifei Wang,
Southeast University, China

*CORRESPONDENCE
Lingling Wang,
wanglingling1993@sjtu.edu.cn

SPECIALTY SECTION
This article was submitted to Smart Grids, a section of the journal Frontiers in Energy Research

RECEIVED 30 July 2022
ACCEPTED 20 September 2022
PUBLISHED 05 January 2023

CITATION
Guo M, Zhang K, Wang S, Xia J, Wang X, Lan L and Wang L (2023), Peer-to-peer energy trading and smart contracting platform of community-based virtual power plant.
Front. Energy Res. 10:1007694.
doi: 10.3389/fenrg.2022.1007694

Peer-to-peer energy trading and smart contracting platform of community-based virtual power plant

Mingxing Guo[1], Ke Zhang[2], Su Wang[1], Jinlei Xia[2], Xiaohui Wang[1], Li Lan[1] and Lingling Wang[2]*

[1]Economic and Technical Research Institute, Shanghai Municipal Electric Power Company, Shanghai, China, [2]Key Laboratory of Control of Power Transmission and Conversion, Shanghai Jiao Tong University, Shanghai, China

Traditional centralized transactions require a control center for user demand matching, settlement and other processes. However, with the increase in the penetration rate of distributed energy in the community, the explosive increase in the number of transactions leads to a decrease in efficiency and it is difficult to guarantee user privacy and information security. The smart contract technology based on blockchain technology has the characteristics of decentralization, traceability and tamper resistance, and these key factors show unique advantages in distributed energy transactions. This paper explores Ethereum and smart contract technology, designs a peer-to-peer energy sharing mechanism with reward and punishment incentives and establishes a smart contract trading platform for smart community-based virtual power plant (CVPP). This paper verifies the functionality and effectiveness of smart contract. The results show that when the supply and demand ratio changes, the user can conduct energy transactions according to the contract without a third-party organization, which solves the problem of trust between the two parties and achieves the expected effect and runs successfully. In addition, the simulation results show that the peer-to-peer transaction based on smart contracts reduces the energy cost per household and increases the total benefit of CVPP.

KEYWORDS

virtual power plant, electricity market, blockchain, smart contract, trading platform

1 Introduction

With the increasing maturity of distributed generation technology, the penetration rate of renewable energy such as solar energy and wind energy in the power system continues to increase (Wang, Li, Shahidehpour, and Jiang). Multi-energy entities are eager to participate in electricity market competition (Gong et al., 2110; Wang et al., 2019a; Wang et al., 2019b). Distributed energy nearby autonomous trading has become the future development trend of distribution network (Feng et al., 2022; Gan et al., 2022).

Among them, CVPP acts as an energy supplier by aggregating multiple types of distributed generator sets, energy storage facilities, etc.

Although some studies believe that CVPP energy trading can learn from the experience of traditional markets and establish a centralized trading center (Kristov et al., 2016). But in fact, there are big differences between distributed power trading and traditional power trading: 1) the number of prosumers is huge, but the scale of a single transaction is usually small; 2) prosumers have complete control over their own power generation and consumption equipment, but the power generation and consumption characteristics and quotation strategies have strong uncertainties and differences; 3) The self-interest of prosumers makes them have higher requirements for transaction fairness, privacy and non-discrimination (Masiello and Aguero, 2016). Facing the transformation and upgrading of the electricity market, the traditional centralized management method has great limitations: 1) the operation and maintenance costs of the trading center are high, the trading freedom is low, and the effective operation of the microgrid cannot be guaranteed; 2) It is difficult for users to trust third-party institutions, and management institutions have high trust maintenance costs, lack of transparency and credibility; 3) The trading center has a large target and is easily attacked, so there is the possibility of data loss or tampering, and information security risks are high.

Compared with traditional centralized energy trading, peer-to-peer (P2P) energy trading based on smart grid is safer, faster and more automated. It can effectively deal with the penetration of distributed energy and is more suitable for solving the problem of distribution network. The National Development and Reform Commission and the National Energy Administration of China issued the "Guiding Opinions on Accelerating the Construction of a Unified National Electricity Market System" (The National Development and Reform Commission and the National Energy Administration of China, 2022), which encourages distributed photovoltaics and other entities to trade directly with surrounding users. This policy pushes China to build a distributed trading market, which promotes the sharing of electricity, carbon emissions and backup resources. The Sonnen pilot, a community of owners of the Sonnen Batterie, was originally launched by the German business Sonnen and has continued to expand. There are Sonnen community members in Germany, Austria, Switzerland and Italy and Sonnen is currently developing a new community pilot in Australia. In the Sonnen pilot, there is a central software that connects and tracks all community members to balance energy supply and demand at all times (Clean Technica, 2015; IRENA, 2020). The UK Piclo pilot is one of the relatively mature peer-to-peer trading pilots currently. Based on this, the United Kingdom has launched an online peer-to-peer trading market for clean energy. In this pilot, the power generation entity can choose and know the counterparty to which it sells electric energy, and users can also choose which power generation entity to purchase electric energy on blockchain (Zhang et al., 2017; Open Utility, 2021). For the P2P transaction of electric energy between VPPs, the literature (Shan, Hu, Wu) established a P2P market transaction mechanism and model for VPP energy management, and realized the energy transaction between the prosumers within the VPP. The literature (Wu, Ma, Yang, Wu, Kong) established a P2P transaction model between VPPs to formulate the price and capacity of P2P transactions between VPPs.

In 2014, Buterin and Wood created Ethereum and firstly apply the smart contract to the blockchain (Buterin, 2014). The application of blockchain is no longer limited to digital cryptocurrency transactions. The two combine to complete more complex functions such as transaction settlement. Smart contract forces the execution of pre-implanted commands through code and the process done automatically and without intervention. The programmable features of smart contracts allow both parties to a transaction to agree on various transaction terms, ensuring the automation and integrity of transaction execution. This technology has been relatively mature in the fields of finance (Turkanović et al., 2018), medical (Angraal et al., 2017), and the Internet of Things (Zhang and Wen, 2017). In P2P energy trading, research on smart contract is still in its infancy. At present, there are some pilot projects. For example, LO3 Energy Company of the United States cooperated with Consensus System Company to design a distributed photovoltaic power sales platform based on blockchain technology (Mengelkamp, Garttner, Rock, Kessler, Orsini, and Weinhardt), which is the first time to apply the Ethereum blockchain technology in the field of energy trading. The Scenery-Project funded by European Union is studying ways to implement decentralized transactions based on blockchain technology to achieve high efficiency and high returns for peer-to-peer transactions (Mihaylov et al., 2014). The German electric power company RWE has cooperated with Slock.it to develop an electric vehicle charging station management system based on blockchain smart contracts to verify user identities and achieve independent billing and transaction settlement (Xu, 2016). In addition to this, there is the Brooklyn Microgrid Project (Molle, 2016). It enables residents to directly sell the electricity generated by rooftop solar equipment to nearby users, and the two parties trade directly without the participation of third-party companies.

In terms of the application of this technology in CVPP, American LO3 Energy and ConsenSys have developed the Trans Active Grid project in a community in Brooklyn (Orsini et al., 2019), which allows resident users in the community to participate in peer-to-peer electricity transactions within the community. Users can obtain real-time data such as electricity generation or electricity consumption by using smart meters and use the blockchain to sell or buy electricity energy. But the shortcomings are that the initially designed device is cumbersome, the user interface is not friendly enough, and there are very few users involved and the scale is small in a

community. Subsequently, the American Exergy Engineering pilot followed the application of Trans Active Grid to peer-to-peer distributed transaction technology, especially blockchain technology (Exergy, 2017).

Although the combination of blockchain technology and distributed energy trading has the advantages of safety, efficiency and automation, there are still some shortcomings and many risks in practical applications. On the one hand, the security of distributed energy transactions based on blockchain and smart contract technology needs to be improved. The evaluation revealed that 8,519 existing smart contracts contain at least one new defect (Wang et al., 2020). On the other hand, the transaction rules and settlement mechanisms in smart contracts still need to be improved. A more complete and reliable trading mechanism is needed to improve user income, enhance the enthusiasm and initiative of users to participate in transactions and ensure the development of the distributed energy trading market.

In summary, the P2P trading behaviors between the nodes during the negotiation process is studied to set up the P2P bidding system and corresponding smart contracts. Considering the negative impact of forecast error, this contract incorporates a reward and penalty mechanism according to The Incentive Principle of Positive Economics. Prosumers are encouraged to refine their models for predicting power generation, while consumers are urged to regulate their consumption habits. The feasibility of the smart contract on P2P energy trading under multiple conditions are verified and validated. Then the economic impact of P2P energy transactions conducted by this contract is further discussed.

2 Overall design

This paper learns the design science guidelines proposed by Hevner et al. (Hevner, March, Park, Ram), and the design idea is shown in Supplementary Material.

2.1 Trading rules

It is assumed that prosumers, including CVPP, generate electricity through distributed equipment and have reliable forecasting models. Prosumers are willing to sell their surplus energy and consumers with continuous demand for electricity intend to purchase energy from prosumers through the P2P market.

1) Prosumers and consumers upload their forecasted power generation and demand, as well as expected electricity prices.
2) The contract sorts consumers' bid amounts from high to low and then selects the optimal bid for each user. If multiple consumers give the same price, the system will preferentially match consumers with higher demand, thereby reducing the possibility of wasting energy. On the other hand, since each blockchain transaction needs to consume Gas, reducing the number of transactions under the premise of ensuring the efficacy of the contract is conducive to maximizing the overall benefit.
3) The contract matches all users in the queue. If the needs of both the prosumer and consumers are met, the transaction will be fired and then removed from the matching queue. Users who fail to match will complete the transaction with those who still have surplus power or their energy suppliers.
4) The smart meter reads the actual power generation and consumption of the previous transaction and uploads it to the platform.
5) The platform calculates the difference between the expected transaction volume and the actual power generation or consumption in this trading cycle.
6) The platform rewards and punishes users for this transaction performance according to the incentive policy.

2.2 Incentive policy

Although electricity is continuously generated in real time, it is usually traded in half-hour segments for ease of settlement. Both parties predict the supply and demand through the models, and the actual transaction volume may not be consistent with the predicted volume. For example, a consumer may purchase electricity without planning to use an air conditioner, but the weather is hotter than expected, the consumer finally uses the air conditioner. In this case, the agreed transaction volume does not match the actual situation and the system is difficult to maintain balance and becomes fragile, thereby increasing the operating cost of the microgrid (Chakraborty et al., 2018). According to The Incentive Principle of Positive Economics, a person is more likely to take an action if its benefits rises, and less likely to take it if its cost rise (Shen et al., 2008). This paper introduces an incentive mechanism into the contract to minimize the impact of residents' behavior and renewable energy uncertainty on P2P transactions. The contract records the number of users defaults and rewards or punishes accordingly to regulate electricity consumption, such as a higher P2P transaction probability as a reward and an appropriate fine as a punishment.

Referring to the current fault handling standard of the Short Term Operating Reserve (STOR) of the British power grid (National Grid, 2015), in order to facilitate settlement of the difference between the agreed electricity and the actual electricity, the system sets two unbalanced electricity prices (Elexon, 2020). System Buying Price (SBP) is the unit price paid by the grid to purchase excess electricity from prosumers. The System Selling Price (SSP) is the price paid by prosumers when they purchase energy from the distribution grid, measured in pennies per kilowatt-hour (p/kWh). User losses can be controlled within 30%.

Taking into account the uncertainty of renewable energy, this contract has been adjusted on the basis of the current STOR standard. The punishment is controlled within 15% and incentive measures have been added to the contract to fully mobilize the enthusiasm of users to participate in the P2P energy trading market. On the one hand, it ensures that users will not incur higher costs by participating in P2P transactions. On the other hand, this distribution method is more easily accepted by small-scale prosumers, incentivizing them to participate in P2P transactions and reducing the risk of energy waste. The reward and punishment incentive mechanism adopted is shown as follows:

For prosumers, if the actual power generation exceeds the forecast, the contract will record the excess power. Other users can continue to buy the excess and prosumers can choose to sell to the grid as well. If the actual power generation is less than the transaction volume, prosumers are slightly penalized to encourage them to improve their forecasting models. The specific punishment mechanism is as follows, and summarized in Figure 1:

1) Considering the uncertainty of renewable energy, the forecast error of prosumers is allowed to be between −5% and +5%. Prosumers are not penalized when actual production is higher than 95% of the forecast and receive payments that match the actual transaction volume. Consumers need to purchase the credits from the energy provider themselves. Since SSP is usually higher than the transaction price, in order to subsidize consumers, the system will waive the service fee for users participating in P2P transactions this time and next time.
2) When the actual power generation is less than 95% of the predicted amount, prosumers receive the amount corresponding to the actual transaction volume. Consumers purchase the shortage of electricity by themselves, and prosumers should subsidize consumers by 10% of the shortage amount. Considering that SSP is usually higher than the P2P transaction unit price, this contract waives the service fee for this and the next P2P transaction for consumers whose interests are damaged.
3) For consumers, if their actual power consumption exceeds the transaction volume, consumers should purchase the excess power by themselves. If the actual electricity consumption is lower than the transaction volume, the user still needs to pay the prosumers in full. But the consumers can sell the excess electricity to the grid or other consumers. The SBP is usually below the contract price, and other consumer bids may also be lower. Defaulting consumers could face some of the losses, prompting them to regulate their energy usage.
4) When the actual power generation or power consumption meets the agreed transaction volume, the user will be rewarded. If the forecast by the prosumers is accurate or the consumer's power consumption is consistent with the agreed amount, it is considered that the user has performed well in this transaction, and the system will record it. If the user has accumulated five good performances, each transaction can be reduced by 20% of the service fee. Accumulate ten good performances and get a 40% discount. Twenty well-performing user transactions get 60% off. And so on.

2.3 Safety measures

1) Function encapsulation. Encapsulates one or more functions and only provides a simple calling interface to external programs. The caller cannot access the internal logic of the function. Key variables and functions are declared as internal calls.
2) Declare main storage type variables and basic functions as internal parameters. In order to reduce the cost of data storage, data in the blockchain is divided into two types: storage variables and memory variables. Storage variables refer to variables stored in the blockchain, while memory variables are only for temporary storage. For example, public variables are forced to be of storage type, while function return parameters are defaulted to memorized types. For security reasons, critical storage variables and functions cannot be called directly by external accounts.
3) User transaction authorization. Users need to obtain transaction authorization from the management node before calling the contract function, which further helps the trading platform to screen individual users. Authorization information will be stored in the user structure.
4) Use a mapping structure to ensure that variables are unique. A map is a key-value store structure. In the Solidity language, "msg. sender" is a special mapping that represents the Ethereum address of the current function caller. When the user calls the contract function, this variable is automatically set as the sender's address, which ensures the unique correspondence between key values.

3 Smart contract based trading platform

The main functions of the contract include user registration, quotations uploaded by prosumers, sealed bids by consumers, system matching, smart meter reading, transaction balance settlement, and incentives for rewards and punishments. The contract also provides auxiliary functions to query order status based on ID or address. Figure 2 shows the logical relationship between contract functions.

3.1 User registration

Users participating in P2P energy trading need to register for a blockchain account. The account corresponds to a pair of public key and private key. The key serves as the account address and can be used to activate the account. The user enters information such

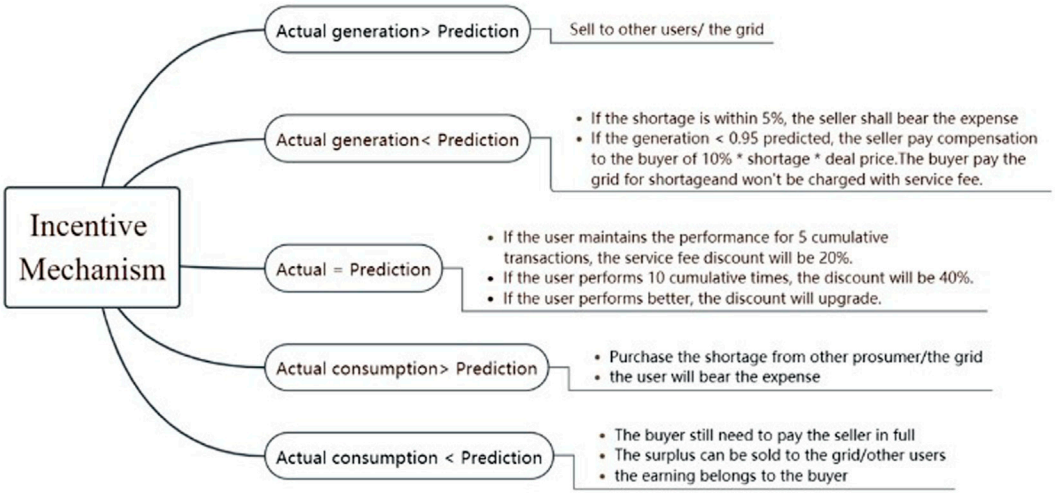

FIGURE 1
Illustration of incentive policy.

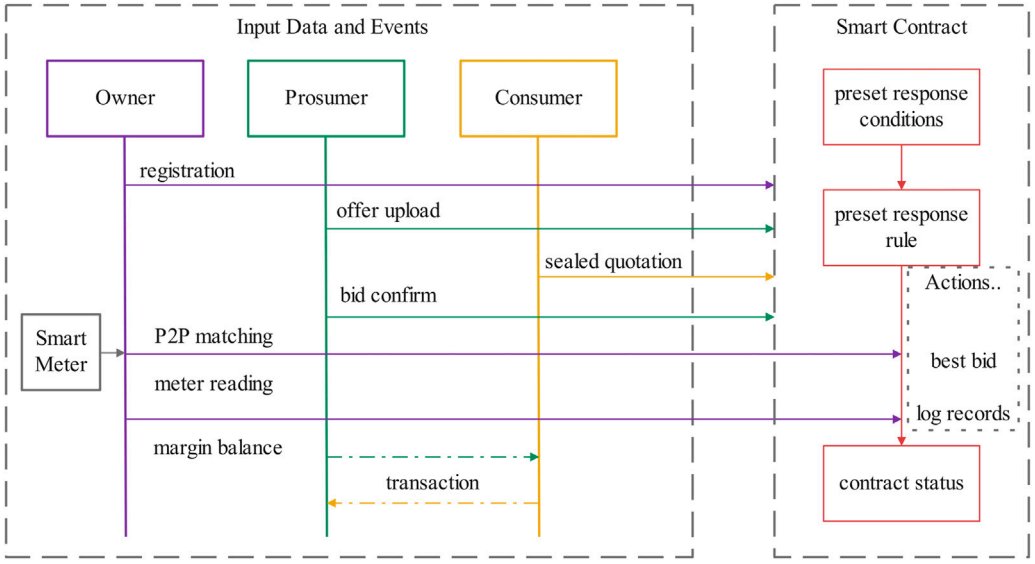

FIGURE 2
Logical relationship of contract functions.

as name, email address, zip code and smart meter number, and the registration is successful after obtaining authorization.

3.2 Upload quotation

The system queries the authorization information of the prosumers to ensure that only authorized prosumers can call this function. After passing the inspection, the prosumers enter the following information: 1) the quotation ID, which is used as an index label to find the quotation; 2) the total transaction volume, which represents the electricity expected by the prosumers; 3) the expected electricity price, the prosumers can decide the expected price selling price. After the quotation is submitted, the system automatically records the time stamp. Quote details are permanently stored on the

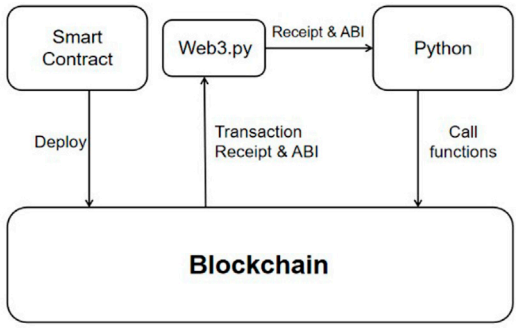

FIGURE 3
Platform data flow.

blockchain as transactions. The system defaults to this quote as "valid." All consumers are free to participate in bidding unless the prosumers actively mark the offer as invalid.

3.3 Sealed bid

After entering the address and quotation ID corresponding to the quotation, the consumer creates a bid ID and determines his expected unit price and demand. The system first verifies that the electricity purchased by the consumer does not exceed the electricity provided by the prosumers and then checks whether the bid already exists. If a bid already exists, duplicate submissions are not allowed, preventing malicious bidding behavior. After the bid passes the checks, the function will execute and record the bid on the blockchain. Bids in this contract can only be set to four states of "create," "reserved," "confirmed" and "rejected." At this point, the bid is in the "created" state and will be added to the sequence of consumers participating in the bid.

3.4 Contract matching

The bid confirmation function is called, and the system checks all bids and selects the best bid according to the transaction mechanism. The best bid is not selected based on unit price, but is prioritized based on the total bid amount. It can not only maximize the interests of both users, but also reduce energy waste. In the case of multiple users bidding the same total amount, the system will give priority to matching consumers with higher demand. Successfully matched bids have their status changed to "Accepted."

3.5 Smart meter reading

Call the smart meter to obtain the actual power generation and consumption of the user. Enter the smart meter number to verify against the smart meter number stored in the sealed user structure. After validation, the data will be imported into the corresponding user structure.

3.6 Transaction settlement

The system calculates the difference between the predicted transaction volume and the actual amount of electricity generated or consumed, and settles between prosumers and consumers, as well as energy suppliers. The blockchain stores the calculation results, and the user completes the token transfer. This function can only be called by the contract owner. Therefore, there is no interface for the user to input parameters. Supplementary Material shows the three basic built-in functions of this process.

3.7 Query function

The query function does not change any data in the blockchain, so calling the query function does not consume Gas. The query function returns the data in the caller's structure and outputs the requested information. Users can use the ID to get order details, including bid quantity, expected unit price, total supply and demand, and remaining unsold electricity.

4 Deploy contracting

All node data in the blockchain is synchronized (Vranken, 2017) and each node can fully participate in the negotiation process. Public blockchains allow everyone read and write access, while private blockchains limit the read or write rights of nodes. Public chains are open and allow anyone to access the blockchain network. There are many public chain nodes, it takes a lot of time to propagate transactions, the throughput of operations is limited, the latency is high, and the processing efficiency is relatively low (Hahn et al., 2017). The private chains are managed by administrators, and only specific nodes are allowed to join the negotiation process. Compared with public chains, private chains are in a sense more centralized and operate more efficiently (Xiaoling et al., 2019). This contract is more suitable to be deployed in a private chain with internal control, faster processing, lower cost and higher security.

Deploying a smart contract can be understood as a special transaction on the blockchain. Before deploying the contract, the destination address is empty. Transactions are sent from the deployer address and the destination is the contract address. When a transaction is recorded on the blockchain, a new address is automatically generated for the contract.

First, the constructor function which only executes once in a contract is called to input the necessary initial information,

including the address of the grid, SBP, SSP, and the service fee. Then, Web3 Provider is adopted to deploy smart contracts compiled with Remix to a private blockchain created by Ganache. Call the constructor and enter the necessary information, including the energy provider address, SBP, SSP, and service charge. Constructors can only be executed once in a contract. Several accounts can be created to test the smart contract. Specially, the first address who deploys the smart contract is default as the owner of the contract. Each account has an initial amount of ethers, which can be used to pay gas for making transactions on the blockchain. Those test account can be used to call the previously constructed functions in turn, and the running result of each function are written in the contract log.

However, the blockchain cannot store the calculation details of the smart contract. This is because the blockchain technology stores data in blocks of the blockchain network. Each node will get a copy of the data on the chain to be kept synchronized with the network. Therefore, there is no specific data storage zoom for the operating details of the smart contract. To further test the function of the contract, this paper uses the flask API to interact with Python as a tool for storing and analyzing contract operation data (Atia, 2016) The data flow is shown in Figure 3. After system interaction, the following functions can be realized: 1) Send ether from wallet to smart contract address in exchange for energy; 2) Call functions in the contract to execute transactions or access certain inform.

5 Case analysis

5.1 Evaluation standard

Based on the evaluation system of literature (Zhou et al., 2018a), this study uses two technical indicators and two economic indicators to evaluate the P2P energy trading platform. Technical indicators include validation basis and condition adaptation index. Economic indicators are made up of value utilization index and participation willingness index.

5.1.1 Verification basis

According to Magazzeni et al. (2017), verifying the validity of a smart contract should be based on five criteria: 1) whether the natural language contract accurately and adequately expresses the mutual intent of both parties; 2) whether the computer code is compiled correctly natural language contract; 3) whether the computer program can do what it is supposed to do; 4) whether the program only does what it is designed to do; 5) if multiple programs run in parallel, does the system operate only as expected and no errors. Through the five criteria, developers can test whether the contract structure conforms to the logical paradigm and requirements of the research, check whether the contract can adapt to different usage scenarios, and ensure the efficiency and effectiveness of the test.

Criteria 1 and 2 verify the validity of the contract's natural language and encoding. The most basic attribute of a smart contract is the accurate coding of requirements, and this contract conforms to the trading wishes of all users. Criteria 3 and 4 validate individual program properties. The contract is completed and only what is required to be done, subject to the agreement of the parties. Input that meets the criteria can lead to the desired result, whereas incorrect input will lead to incorrect results. Criterion 5 verifies the effectiveness of the platform as a whole. All nodes cooperate to execute the contract, the data in the block is kept synchronized, and the contract is locally valid, that is, globally valid. In conclusion, the contract conforms to the logical paradigm and requirements of this research.

5.1.2 Performance indicators

Zhou et al. (2018b) have developed an evaluation system P2P energy trading mechanism. The evaluation method of these contracts is adapted and built on this indexing scheme. Two economic indexes and one technical index are eventually adopted. The meaning of each indicator is described below.

1) Condition adaptation index, which measures how the contract operates under different conditions. This study explores the operation of the contract under two conditions of high supply-demand ratio and low supply-demand ratio.
2) Value mining index. Compare the energy cost of residents under the traditional transaction framework, measure the energy cost saved by P2P transaction, and reflect the overall benefit of CVPP. The higher the indicator value, the higher the CVPP return, that is, the higher the value obtained.
3) Participation willingness index. In addition to evaluating the overall benefit, the income per household is equally important. Participation willingness index reflects the benefits obtained by users after participating in the contract, thereby affecting the willingness of residents in the region to join the CVPP and P2P markets, which is crucial to the long-term development of the P2P ecosystem. If participating in P2P transactions leads to an increase in user energy costs, users will have sufficient incentives to return to the traditional transaction state. Therefore, the willingness to participate index measures the willingness of residents to participate in CVPP and P2P energy sharing mechanisms through user interests.

5.2 Example description

5.2.1 Power data

Al-Ammari and Al-Thani (2019) tested and compared blockchain transaction throughput for 10, 20, 30 to 140 nodes, proving that smart contracts in this range are capable of handling large numbers of transactions without

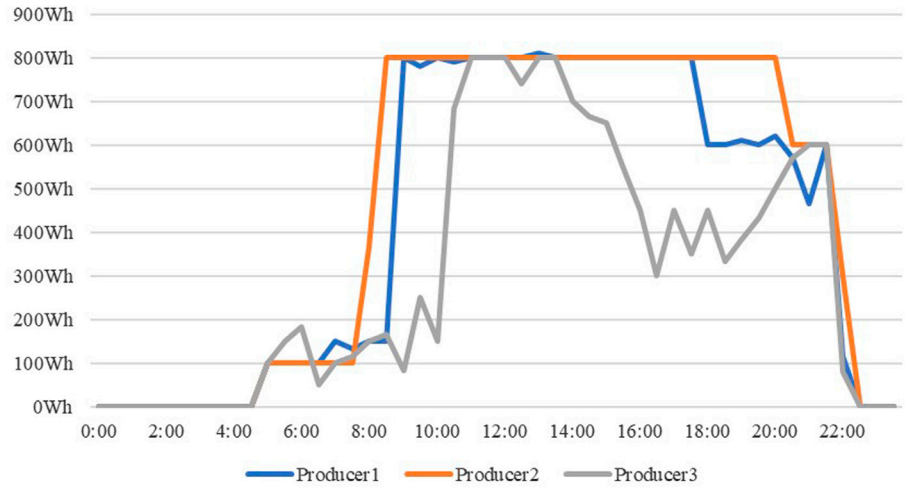

FIGURE 4
PV daily power generation curve of each prosumer.

sacrificing performance. Network expansion within a reasonable range will not affect the efficiency of the network. Therefore, this study tests 10 nodes of the system and performs economic analysis on each node.

In this paper, the photovoltaic power generation of each household collected by the Thames Valley Vision project (Potter et al., 2015) is selected as the data of the virtual power plant. The photovoltaic penetration level is 30%, the statistical accuracy is 30 min, and the data of smart meter uploaded in 24 h, the unit is watt per hour (Wh). This accuracy is not only in line with the general settlement time of the electricity trading market, but also better understand the customer's electricity consumption behavior.

The types of energy storage devices that provide or absorb energy are not discussed separately herein. Although energy storage technology can provide greater versatility for P2P energy trading, they are also very costly. The energy storage facility is equivalent to a special prosumer, which does not affect the feasibility and validity of the contract.

The blue part of Figure 4 is the energy consumption of all participants in the P2P market over a 24-h period. The orange part represents the net electricity generation after CVPP actual electricity generation minus electricity consumption. Assuming that all consumers put their excess electricity into the P2P market for sale, the net electricity generation is equal to the electricity available for sale. Figure 4 shows the daily power generation curve of prosumers participating in P2P transactions. Assuming that all consumers put their excess electricity into the P2P market for sale, the net electricity generation is equal to the electricity available for sale. Figure 5 shows the net production curve after integrating the power consumption of CVPP.

According to the electricity consumption characteristics of CVPP, electricity consumption is concentrated in lighting, kitchen supplies and electronic equipment. The use of home appliances is not completely random, which is largely affected by the living habits of residents (Torriti, 2017). Also, electricity usage varies by household size. These differences and fluctuations are verified in the Supplementary Material. This study focuses on whole-household energy costs and overall CVPP benefits and therefore does not consider the specific size within each household.

5.2.2 Pricing model

The electricity price of each user varies according to their needs, usage habits and the frequency of electricity price package updates. The price gap between energy suppliers does not exceed 10% (Quarterly Energy Prices, 2019). Therefore, the average electricity price is used for settlement between users and energy suppliers in this study. In 2019, the average retail price of electricity in the United Kingdom was 18 pence per kilowatt-hour (p/kWh) (Sönnichsen, 2021).

This article refers to energy prices in the market. Octopus Energy (Octopus Energy, 2020) is a new type of green energy supplier that emerged in the UK in 2016. The company buys energy from home solar at 6 p/kWh. Another British company, Green Energy, proposed tidal electricity pricing strategy (Green Energy UK, 2020). According to statistics, customers who choose this package have an average electricity price of 4.9 p/kWh between 11 p.m. and 6 a.m. However, electricity rates between 4 p.m. and 7 p.m. are five times the nightly rate. The source of energy supply in this study is solar energy and P2P transactions are concentrated during the day. Consumers only need to buy low-cost off-peak electricity from the grid at night, thus cutting their electricity bills during peak hours. Even taking into account

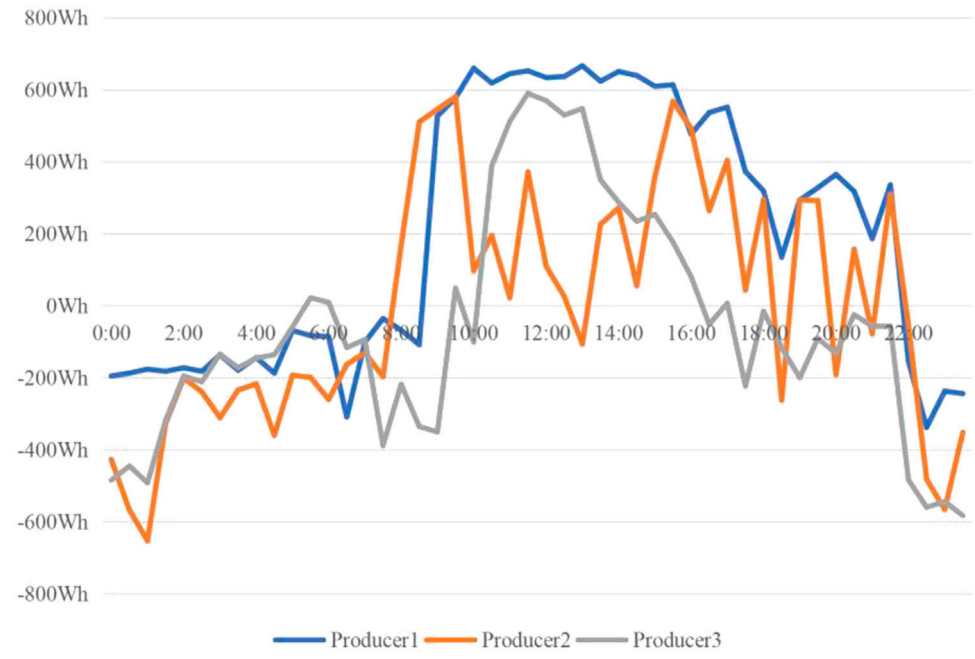

FIGURE 5
The daily net production curve of each prosumer.

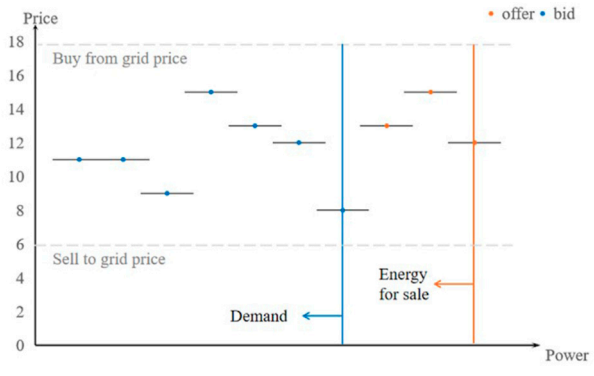

FIGURE 6
Auction-based pricing strategy.

tidal electricity prices, the economic advantages of P2P are further increased. Therefore, this paper only uses average prices to model P2P transactions. Although the effectiveness of the P2P transaction mechanism may be underestimated, this does not affect the verification results of contract validity.

Taking the above considerations into account, the electricity price for the user to sell the surplus energy to the grid is 6 p/kWh in this case. The price the user buys from the grid is 18 p/kWh. Usually the transaction price of P2P transactions will remain within this range.

Although prosumers can freely set energy prices under the auction-based market transaction mechanism, the settlement price is mainly affected by demand and power generation in the actual P2P market. Therefore, this study adopts the pricing model proposed by Amin et al. (2020) to simulate bidding. The purpose of the tender is to minimize the cost per household and the total CVPP cost to maximize benefits. Take the settlement time of 11:30 a.m. as an example. The energy supply in the P2P trading market is higher than the demand. According to the pricing strategy, the consumer's bid and the price of the consumer's bid are shown in Figure 6.

5.3 Result analysis

5.3.1 Technical performance

The supply-demand ratio (SDR) is defined as the ratio of total supply to total demand. When the SDR is greater than 1, it means that the production supply is oversupplied. If the SDR is equal to 1, it means that supply and demand are exactly the same. Likewise, if SDR is less than 1, it means that supply is not sufficient to meet demand. Figure 7 compares the shifts in the demand and supply curves over a day. Total supply is higher than demand during the settlement period in 11:30–12:30. In most other cases, the SDR is less than 1.

Figure 8 shows a trade settlement at 11:30 with an SDR greater than 1. For prosumers, the bar graph reflects the revenue they earn from selling energy. And for consumers, this represents their energy

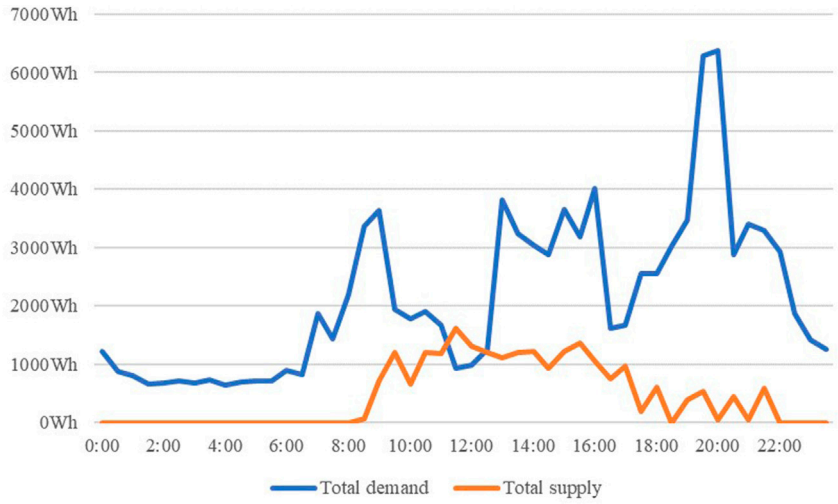

FIGURE 7
Comparison of daily supply and demand curves.

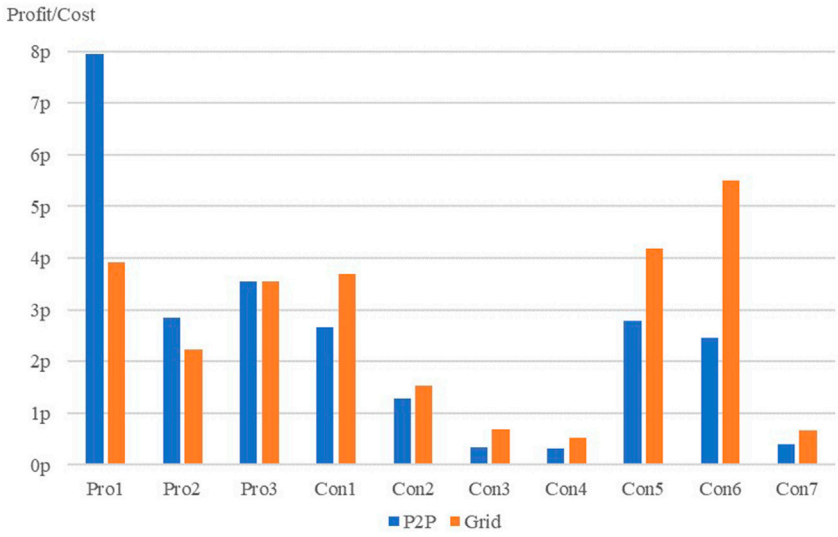

FIGURE 8
User energy costs (SDR > 1).

bills. It can be seen that the income of prosumers participating in P2P transactions is higher than that of directly selling energy to the grid. For users, the energy cost of P2P transactions is lower than that of direct transactions with the grid.

Figure 9 shows the settlement results at 17:00 with SDR less than 1. Although there is still enough solar energy to generate electricity at this time, the demand of prosumers has also increased. So there is less energy available for sale in the market. In this case, as long as the prosumers also provide electricity, the revenue from P2P transactions is much higher than that of selling electricity directly to the grid. However, if the net power generation is insufficient, participating in P2P transactions will improve the energy cost very little. At this time, the power generation in the CVPP area cannot meet the demand and some users who participate in the bidding may not be able to trade. Even for the winning bidder, the savings in energy costs are not significant due to the smaller transaction volume. However, it is still economical to participate in P2P transactions when all-day returns are taken into account.

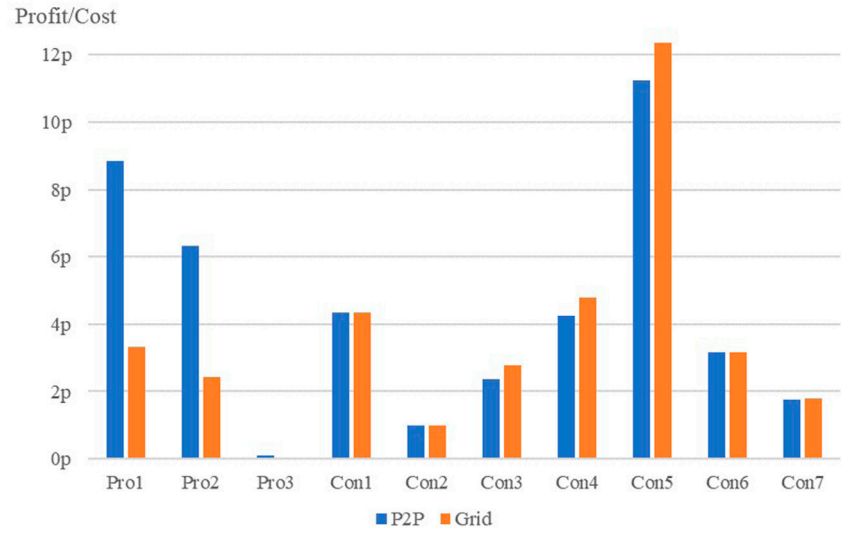

FIGURE 9
User energy costs (SDR < 1).

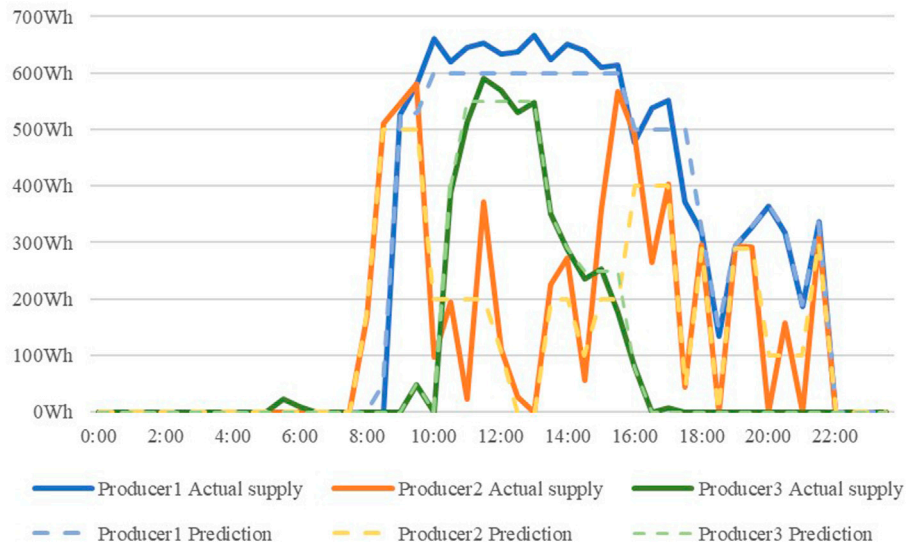

FIGURE 10
Producer forecast bias.

No matter how the SDR changes, the Condition Adaptation Index and Value Mining Index indicators are within the normal range and do not affect the validity of the contract. It indicates that the contract can accurately balance and settle transactions under different conditions. The contract performed well on the technical level including the extreme conditions. In addition, users participating in the energy sharing mechanism reduce energy costs to a certain extent.

5.3.2 Economic analysis

In this paper, all prosumers have their own forecasting methods and models by default. Does not focus on optimization of predictive models. The prosumers' forecast bias is shown in Figure 10.

Among the seven consumers, consumers 1 and 2 are set as users with extremely irregular usage behavior. In other words,

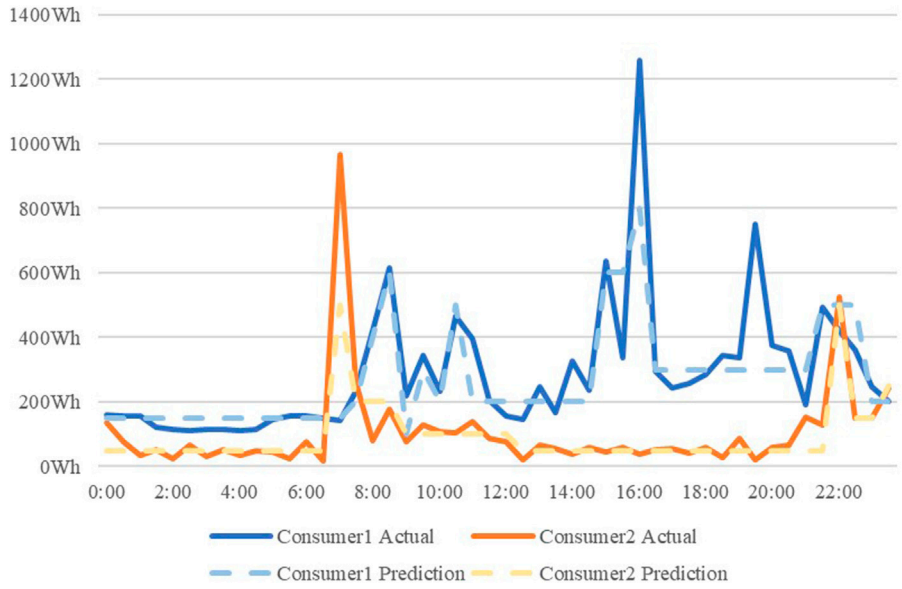

FIGURE 11
Electricity deviation of irregular consumers.

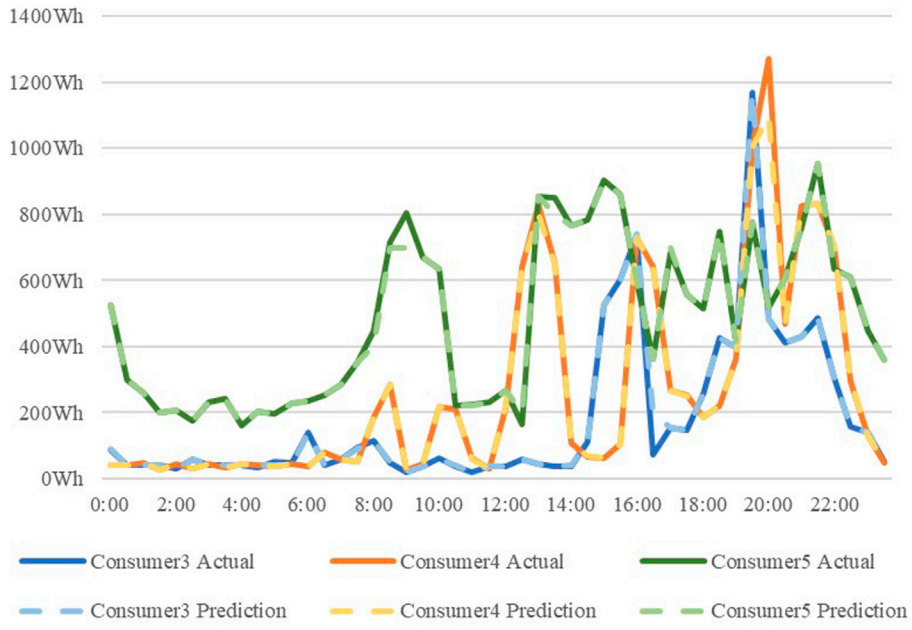

FIGURE 12
Electricity deviation of ordinary consumers.

they are not used to using appliances as planned. Consumers 3, 4 and 5 are considered to be slightly irregular users. Sometimes they follow the rules and sometimes they don't follow the plan. Consumers 6 and 7 are considered to have good electricity habits. The users' prediction errors are shown in Figures 11–13 respectively.

The cost of each household is obtained after the simulation shown in Figure 14. The negative bar represents the revenue

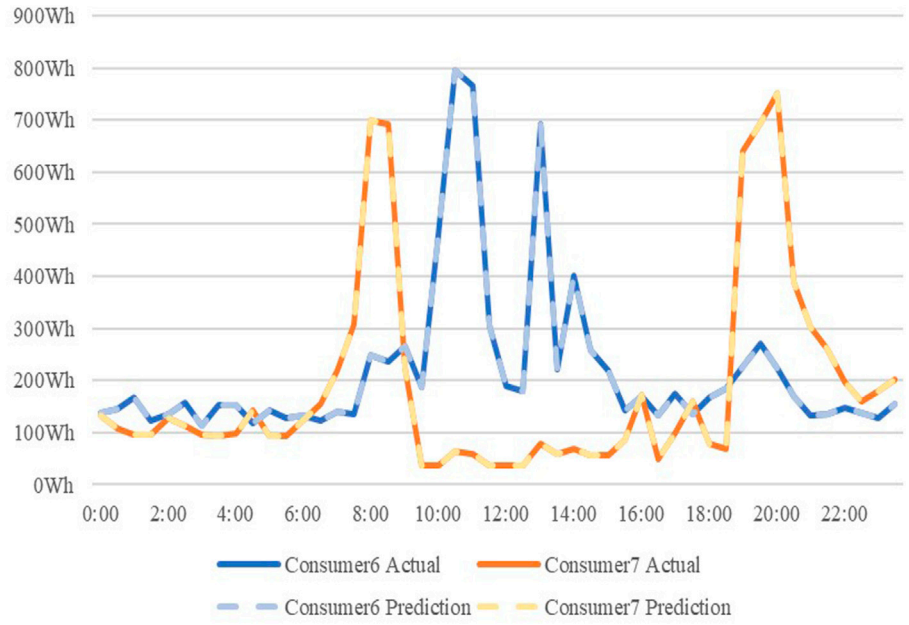

FIGURE 13
Electricity deviation of standardizing consumers.

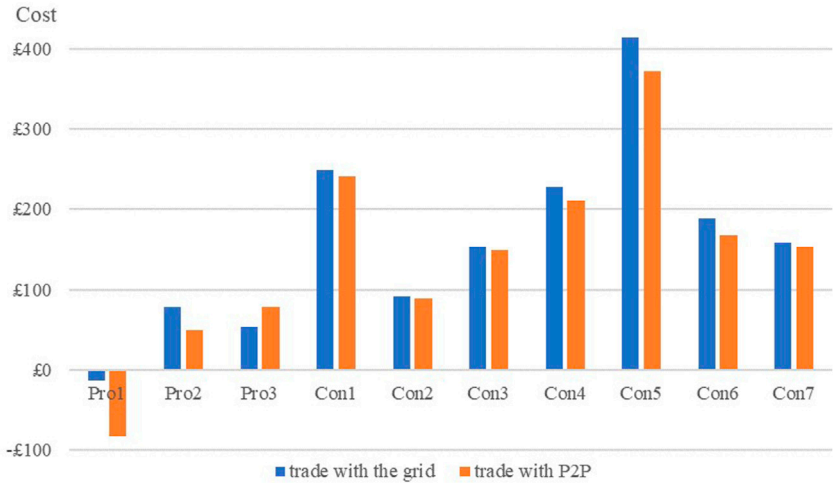

FIGURE 14
Daily energy consumption of each household.

that prosumers receive from selling surplus energy. Compared with trading directly with the grid, some prosumers participating in P2P transactions have increased their profits and the rest have also succeeded in further reducing energy costs. Likewise, consumer energy bills have been reduced to some extent.

The transaction results of each settlement period are affected by various factors, including bid price, estimated power generation or consumption, and user performance in previous P2P transactions. The contract calculates and compares the number of deals for each consumer and its deal probability is shown in Figure 15.

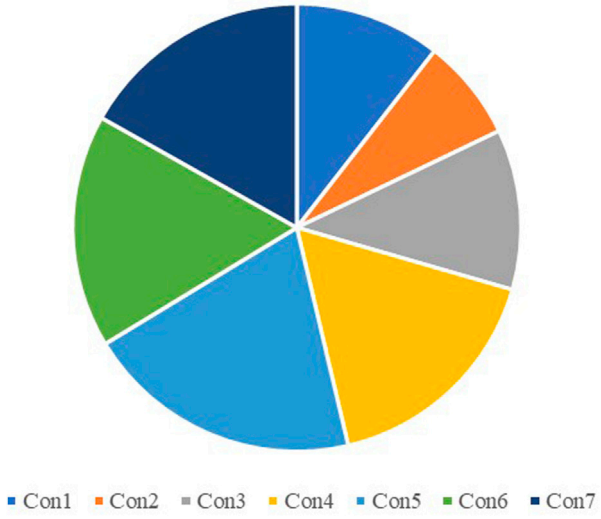

FIGURE 15
Consumer transaction probability.

While suppliers tend to seek high returns, buyers tend to go after low costs. However, users not only look at the price but also give more consideration to the credit of the trading partner under the incentive mechanism of reward and punishment. It turns out that the prosumer is more likely to prioritize the Consumer 6 and Consumer 7 transactions with good performance. It seems strange that Consumer 5 with normal performance also has a greater chance of clinching a deal than consumers with similar credits. This is because Consumer 5 usually has higher demand and the contract will recommend prosumers to make a deal with him preferentially. As for the ones with poor performance, Consumer1 and 2 have a much lower trading chance. The incentive system allows users who perform well to be rewarded, encouraging them to maintain a good state, and actively participate in P2P transactions. The penalty mechanism, on the one hand, encourages producers to improve their forecasting models. On the other hand, consumers who do not use electricity properly are urged to regulate their usage behaviours. However, the punishment is very humanized so as not to bring users too much loss, avoiding affecting their enthusiasm to participate in P2P transactions.

The case study shows that all households participating in P2P energy trading have reduced energy costs without reducing demand. In addition, P2P energy trading can balance local demand and reduce the transmission amount of electricity between CVPP and the grid, thereby reducing the risk of power system. The P2P transaction model is worthy of further promotion and becomes the soil for the growth of distributed energy.

6 Conclusion

This study proposes a smart contract model for P2P energy trading by taking advantage of the decentralized nature of the underlying technology of blockchain. On the one hand, user data is more secure, which solves the problem of trust between the two parties of the transaction. On the other hand, heavy maintenance costs such as unified management and data storage are avoided. At the same time, the transaction network based on blockchain technology can also ensure the traceability and real-time performance of transactions. In addition, this paper introduces a reward and punishment mechanism into the energy sharing mechanism to motivate participants to upgrade the prediction models and regulate electricity consumption behaviors. The simulation results show that the trading platform can reasonably and reliably complete resource allocation according to the trading mechanism and achieve a partial balance between distributed generation and regional demand. This paper conducts a preliminary study on the application of smart contract in the field of P2P energy trading. The research results provide theoretical basis and practical knowledge for the research and growth of future blockchain networks.

Smart contract is still a developing technology. Once the contract is deployed on the blockchain, it cannot be modified. If there is a breach, the consequences would be catastrophic. To avoid unnecessary losses, smart contracts need to be fully verified and tested. The prosumer data used in this case study is all photovoltaic power generation and there is almost no excess energy flow in the nighttime P2P market. Introducing other types of renewable power generation methods to extend the transaction time of P2P, the validity and practicality of the contract needs to be further explored. This paper does not consider the impact of power flow constraints and countermeasures on P2P energy trading. Future work can continue to study smart contracts combined with power grid models, expand security control and market assessment, and establish diversified P2P trading mechanism evaluation indicators. At the same time, the strategic behavior of participants deserves to be studied and modeled in detail to design a P2P energy trading mechanism that is more stable and friendly to the power system, and further develop an integrated, advanced and reliable P2P energy trading platform.

Data availability statement

Publicly available datasets were analyzed in this study. This data can be found here: R. Potter, N. SSEPD, C. Edwards, N. SSEPD, T. Leonard, and G. DNV, New Thames Valley Vision, 2015.

Author contributions

The contributions of all authors are listed in strict order. MG made the main contribution with the original design of the working concept. KZ is in charge of and drafted the thesis. JX approved the final version of the paper for publication. SW, XW, and LL were responsible for data collection. LW made important revisions to the paper.

Funding

This work was supported by the program of Research on multi-objective control strategy and business model of virtual power plant for new power system regulation needs of Economic and Technical Research Institute Shanghai Municipal Electric Power Company.

Conflict of interest

MG, SW, XW, and LL were employed by Shanghai Municipal Electric Power Company.

The remaining authors declare that the research was conducted in the absence of any commercial or financial relationships that could be construed as a potential conflict of interest.

Publisher's note

All claims expressed in this article are solely those of the authors and do not necessarily represent those of their affiliated organizations, or those of the publisher, the editors and the reviewers. Any product that may be evaluated in this article, or claim that may be made by its manufacturer, is not guaranteed or endorsed by the publisher.

Supplementary material

The Supplementary Material for this article can be found online at: https://www.frontiersin.org/articles/10.3389/fenrg.2022.1007694/full#supplementary-material

References

Al-Ammari, M. A., and Al-Thani, Mohamed M. (2019). *Dena (committee member); Oligeri, Gabriele (committee member) smart contract for P2P energy trading in smart grids: Ethereum Implementation and performance evaluation*. PQDT - Global, HAMAD BIN KHALIFA UNIVERSITY ProQuest Dissertations Publishing.

Amin, W., Huang, Q., Afzal, M., Khan, A. A., Zhang, Z., Umer, K., et al. (2020). Consumers' preference based optimal price determination model for P2P energy trading. *Electr. Power Syst. Res.* 187, 106488. doi:10.1016/j.epsr.2020.106488

Angraal, S., Krumholz, H. M., and Schulz, W. L. (2017). Blockchain technology: applications in health care. *Circ. Cardiovasc. Qual. Outcomes* 10, e003800. doi:10.1161/circoutcomes.117.003800

Atia, R. (2016). *Integration of renewable energy sources in microgrids: Sizing and intelligent management*. National Changgang University of Technology and Science.

Buterin, V. (2014). A next-generation smart contract and decentralized application platform. *white Pap.* 3, 37.

Chakraborty, N., Naskar, A., Ghosh, A., Chandra, S., Banerji, A., and Biswas, S. K. Multi-party energy management of microgrid with Heat and electricity coupled demand Response. In 2018 IEEE International Conference on Power Electronics, Drives and Energy Systems (PEDES). December 2018. Chennai, India. IEEE, 1–6.

Clean Technica (2015). Germany's sonnenbatterie launches energy trading platform. Available at: https://cleantechnica.com/2015/12/06/germanys-sonnenbatterie-launches-energy-trading-platform/(Accessed December 6, 2015).

Elexon (2020). *System sell price, system buy price and net Imbalance volume data*.

Exergy (2017). Electric power technical whitepaper. Available at: http://www.truevaluemetrics.org/DBpdfs/Initiatives/Exergy/Exergy-2018-Technical-Whitepaper-v8.pdf (Accessed December 14, 2017).

Feng, C., Liang, B., Li, Z., Liu, W., and Wen, F. (2022). Peer-to-Peer Energy Trading under network constraints based on generalized fast dual ascent. *IEEE Trans. Smart Grid* (Early Access), 1. doi:10.1109/TSG.2022.3162876 (Accessed March 29, 2022)

Gan, W., Yan, M., Yao, W., Guo, J., Fang, J., Ai, X., et al. (2022). Multi-network coordinated hydrogen supply infrastructure planning for the integration of hydrogen vehicles and renewable energy. *IEEE Trans. Ind. Appl.* 58 (2), 2875–2886. doi:10.1109/tia.2021.3109558

Gong, K., Wang, X., Jiang, C., Shahidehpour, M., Liu, X., and Zhu, Z. Security-constrained optimal sizing and siting of BESS in hybrid AC/DC microgrid considering post-contingency corrective rescheduling. *IEEE Trans. Sustain. Energy* 12 (4), 2110–2122.

Green Energy UK (2020). Green energy UK. [Online]. Available at: https://www.greenenergyuk.com (accessed July 19, 2020).

Hahn, A., Singh, R., Liu, C.-C., and Chen, S. Smart contract-based campus demonstration of decentralized transactive energy auctions. In 2017 IEEE Power & energy society innovative smart grid technologies conference (ISGT). April 2017. Washington, DC, USA. IEEE, 1–5.

Hevner, A. R., March, S. T., Park, J., and Ram, S. Design science in information systems research. *MIS Q.* 28, 75–105.

IRENA (2020). Peer-to-peer electricity trading: Innovation landscape brief. Available at: https://www.irena.org/-/media/Files/IRENA/Agency/Publication/2020/Jul/IRENA_Peer-to-peer_trading_2020.pdf?la=en&hash=D3E25A5BBA6FAC15B9C193F64CA3C8CBFE3F6F41 (Accessed November 15, 2021).

Kristov, L., De Martini, P., and Taft, J. D. (2016). A tale of two visions, Designing a decentralized transactive electric system. *IEEE Power Energy Mag.* 14 (3), 63–69. doi:10.1109/mpe.2016.2524964

Magazzeni, D., McBurney, P., and Nash, W. (2017). Validation and verification of smart contracts: A research agenda. *Computer* 50 (9), 50–57. doi:10.1109/mc.2017.3571045

Masiello, R., and Aguero, J. R. (2016). Sharing the ride of power: Understanding transactive energy in the ecosystem of energy economics. *IEEE Power Energy Mag.* 14 (3), 70–78. doi:10.1109/mpe.2016.2524965

Mengelkamp, E., Garttner, J., Rock, K., Kessler, S., Orsini, L., and Weinhardt, C. Designing microgrid energy markets: A case study: The Brooklyn microgrid. *Appl. Energy* 15 (210), 870–880.

Mihaylov, M., Jurado, S., Avellana, N., Van Moffaert, K., de Abril, I. M., and Nowé, A. (2014). NRGcoin: Virtual currency for trading of renewable energy in smart grids. in *11th International conference on the European energy market (EEM14)* IEEE, 1–6.

Molle, G. (2016). How blockchain helps Brooklyn dwellers use neighbors' solar energy. National Public Radio (NPR). [Online]. Available at: http://www.npr.org/sections/Alltech/considered/2016/07/04/482958497/how-blockchain-helps-Brooklyn-dwellers-use-neighbors-solar-energy.

National Grid (2015). Short-term operating Reserve Events of default and consequences. [Online]. Available at https://www.nationalgrid.com/sites/default/files/documents/BM%20STOR%20Events%20of%20Default%20-%202015_0.pdf.

Octopus Energy (2020). Octopus energy. [Online]. Available at: https://octopus.energy (accessed July 19, 2020).

Open Utility (2021). A glimpse into the future of Britain's energyeconomy. Available at: https://piclo.energy/publications/piclo-trial-report.pdf (Accessed November 15, 2021).

Orsini, L., Kessler, S., Wei, J., and Field, H. (2019). How the Brooklyn microgrid and Trans Active Grid are paving the way to next-gen energy markets. *Energy Internet,* Woodhead 223–239. doi:10.1016/B978-0-08-102207-8.00010-2

Potter, R., SSEPD, N., Edwards, C., SSEPD, N., Leonard, T., and DNV, G. (2015). *New Thames Valley Vision*.

Quarterly Energy Prices (2019). Quarterly energy prices. [Online] Available at https://assets.publishing.service.gov.uk/government/uploads/system/uploads/attachment_data/file/853753/QEP_Q3_2019.pdf.

Shan, J., Hu, J., and Wu, J. Peer-to-peer market trading mechanism and model for virtual power plant energy management. *Power Syst. Technol.* 44 (9), 3401–3408.

Shen, Y., Ross, K. W., Panwar, S. S., and Wang, Y.Substream trading: Towards an open P2P live streaming system. In 2008 IEEE international conference on network protocols. 2008 October. Orlando, FL, USA. IEEE, 94–103.

Sönnichsen, N. (2021). Electricity prices for households in the United Kingdom (UK) 2010-2019, semi-annually. [Online]. Available at: https://www.statista.com/statistics/418126/electricity-prices-for-households-in-the-uk/.

The National Development and Reform Commission and the National Energy Administration of China (2022). Guidelines on accelerating the construction of a unified national electricity market system. Available at: https://www.ndrc.gov.cn/xxgk/zcfb/tz/202201/t20220128_1313653.html?code=&state=123 (Accessed January 18, 2022).

Torriti, J. (2017). Understanding the timing of energy demand through time use data: Time of the day dependence of social practices. *Energy Res. Soc. Sci.* 25, 37–47. doi:10.1016/j.erss.2016.12.004

Turkanović, M., Hölbl, M., Košič, K., Heričko, M., and Kamišalić, A. (2018). EduCTX: A blockchain-based higher education credit platform. *IEEE access* 6, 5112–5127. doi:10.1109/access.2018.2789929

Vranken, H. (2017). Sustainability of bitcoin and blockchains. *Curr. Opin. Environ. Sustain.* 28, 1–9. doi:10.1016/j.cosust.2017.04.011

Wang, T., Yang, B., and Chen, C. Double-layer Game based Wireless charging Scheduling for electric vehicles. In 2020 IEEE 91st Vehicular Technology Conference (VTC2020-Spring). May 2020. Antwerp, Belgium. IEEE.

Wang, X., Li, Z., Shahidehpour, M., and Jiang, C. Robust line hardening strategies for improving the resilience of distribution systems with variable renewable resources. *IEEE Trans. Sustain. Energy* 10 (1), 386–395.

Wang, X., Shahidehpour, M., Jiang, C., and Li, Z. (2019). Coordinated planning strategy for electric vehicle charging stations and coupled traffic-electric networks. *IEEE Trans. Power Syst.* 34 (1), 268–279. doi:10.1109/tpwrs.2018.2867176

Wang, X., Shahidehpour, M., Jiang, C., and Li, Z. (2019). Resilience enhancement strategies for power distribution network coupled with urban transportation system. *IEEE Trans. Smart Grid* 10 (4), 4068–4079. doi:10.1109/tsg.2018.2848970

Wu, Z., Ma, G., Yang, S., Wu, Y., and Kong, Y. Virtual powerplant operation optimization strategy based on analysis target cascading of distributed transaction model. *Power Demand Side Manag.* 24 (1), 7–13.

Xiaoling, Jin, Cuifen, Bai, Zhebo, Zhang, Shenyi, Zhao, Haoran, Wang, Zheng, Yan, et al.Blockchain-enabled transactive method in distributed systems considering security constraints. In 2019 IEEE Congress on Evolutionary Computation (CEC). Wellington, New Zealand. June 2019. IEEE, 1203–1207.

Xu, Annie (2016). German power company integrates Ethereum blockchain technology with car charging service. Available at: https://www.sohu.com/a/62418810_286863 (Accessed March 8, 2016).

Zhang, C., Wu, J., Long, C., and Cheng, M. (2017). Review of existing peer-to-peer energy trading projects. *Energy Procedia* 105, 2563–2568. doi:10.1016/j.egypro.2017.03.737

Zhang, Y., and Wen, J. (2017). The IoT electric business model: Using blockchain technology for the internet of things. *Peer. Peer. Netw. Appl.* 10 (4), 983–994. doi:10.1007/s12083-016-0456-1

Zhou, Y., Wu, J., and Long, C. (2018). Evaluation of peer-to-peer energy sharing mechanisms based on a multiagent simulation framework. *Appl. energy* 222, 993–1022. doi:10.1016/j.apenergy.2018.02.089

Zhou, Y., Wu, J., and Long, C. (2018). Evaluation of peer-to-peer energy sharing mechanisms based on a multiagent simulation framework. *Appl. energy* 222, 993–1022. doi:10.1016/j.apenergy.2018.02.089

frontiers | Frontiers in Energy Research

TYPE Methods
PUBLISHED 05 January 2023
DOI 10.3389/fenrg.2022.1032051

OPEN ACCESS

EDITED BY
Yang Li,
Hohai University, China

REVIEWED BY
Fu Shen,
Kunming University of Science and Technology, China
Han Wang,
Shanghai Jiao Tong University, China

*CORRESPONDENCE
Sun Wenyao,
iris6421@163.com

SPECIALTY SECTION
This article was submitted to Smart Grids,
a section of the journal
Frontiers in Energy Research

RECEIVED 30 August 2022
ACCEPTED 14 September 2022
PUBLISHED 05 January 2023

CITATION
Weichong L, Wenyao S, Yi Z and Mingfei B (2023), Research on market trading strategy of multi-microgrid intelligent power distribution system based on Bi-level optimization. *Front. Energy Res.* 10:1032051. doi: 10.3389/fenrg.2022.1032051

Research on market trading strategy of multi-microgrid intelligent power distribution system based on Bi-level optimization

Lei Weichong[1], Sun Wenyao[1]*, Zhao Yi[1] and Ban Mingfei[2]

[1]College of Electric Power, Shenyang Institute of Engineering, Shenyang, China, [2]School of Mechanical and Electrical Engineering, Northeast Forestry University, Harbin, China

With the continuous promotion of the "dual carbon" idea, future power generation will rely heavily on renewable energy sources. As an effective utilization form of clean power sources, it is of positive significance to study the trading strategy of microgrids in the intelligent power distribution system under the influence of carbon quota. In this research, a bi-level optimization method is used to build a trading model of the distribution-side power market, with the upper-level planning aiming to reduce the cost of distribution system operators and the lower-level planning aiming to increase the revenue of microgrids. Secondly, the genetic algorithm and sequential quadratic planning algorithm are applied to the upper and bottom models to determine the optimal clearing strategy for the microgrid and the optimal scheduling scheme for the distribution system operator, respectively. Finally, a typical day is used as an example to analyze in detail the market trading strategy of a multi-microgrid intelligent distribution system under the influence of carbon quota, and the effectiveness of the method described in this paper is verified.

KEYWORDS

microgrid, carbon quota, distribution side power market, bi-level optimization, market transactions

1 Introduction

With the continuous promotion and implementation of the concept of "carbon peaking and carbon neutral," China has implemented various carbon policies in order to effectively reduce carbon emissions, including carbon quotas, which are an important basis of the carbon trading market (Jin et al., 2021). In the form of power generation, clean power will gradually replace thermal power as the main power source in the future. The new power system needs to have greater power balancing capacity on both the power side and the customer side to undertake more clean power consumption tasks. As an effective carrier for clean power consumption, the microgrid is an important means to revitalize the power regulation potential on the user side. In the future, the intelligent power

distribution system will be more friendly to cope with multiple microgrid grid connections, and its regulation method should be based on the originally planned regulation, and build a fair and effective distribution side power market trading mechanism and method, to stimulate the initiative and flexibility of clean power supply grid connection. (State Grid Cooperation of China, 2021; Zhao et al., 2022Yi et al., 2022).

Current research by scholars in China and abroad on distribution-side electricity market trading mechanisms focuses on the following two aspects:

(1) Game theory-based market transaction mechanism

Most of the studies on market transaction mechanisms based on game theory are based on the autonomous operation of micro-networks (Du et al., 2021). For example, (Zhao et al., 2015, Min et al., 2015), used noncooperative game theory to build a general model of the trading model between multiple microgrids, and analyzed and proved the existence of Nash equilibrium of the game; (Le et al., 2016); proposed a new regional grid market-oriented operation model based on game theory to meet the demand of market-oriented reform on the distribution side in the context of high penetration distributed electric energy resources access operation; (Bai et al., 2017, Peilin et al., 2017); uses cooperative game theory to solve the problem of bidding and revenue allocation among multiple microgrids, considering the source-load duality of microgrids; (Zhao et al., 2018, Wenhui et al., 2018); constructs a three-party noncooperative game model based on Nash equilibrium for the wind-fire grid and analyzes the factors affecting the utility of each game party; while (Wang et al., 2019, Xian et al., 2019) establishes a joint game equilibrium model for multi-energy markets and uses a nonlinear complementary approach to solve the bid variance problem of microgrid participation in distribution-side electricity market transactions with uncertain power output.

(2) Optimization theory-based market transaction mechanism

At present, the research methods based on optimization theory mainly focus on two-tier optimization methods and two-stage optimization methods (He et al., 2020). In (Peng et al., 2021), a two-tier model of the optimal bidding strategy of integrated energy service providers is established for the bidding behavior of multiple integrated energy service providers in the integrated energy market, and the impact of each integrated energy service provider's bidding strategy on the integrated energy market clearing is quantitatively analyzed; (Zhao et al., 2022, Yue et al., 2022); constructs a two-tier optimization model for dynamic pricing and market clearing to study the distribution side market trading strategy taking into account multiple stakeholders. In (Liu et al., 2017), a two-layer optimization model is developed to study the distribution side market trading and bidding mechanism for multiple microgrid operators to participate in the distribution side market bidding. In (Liu et al., 2018), a two-stage robust optimization model with a min-max-min structure is developed for the uncertainty of renewable energy and load within the microgrid to find the scheduling scheme with the lowest operating cost under the worst scenario; (M. H. Moradi et al., 2016), a two-stage optimization model is developed for the power system, where the optimal distribution problem of the microgrid is solved in stage 1, and stage 2 combines Nash equilibrium theory and two-layer The second stage combines Nash equilibrium theory and two-layer planning theory to solve the optimal clearing problem in the distribution side of the electricity market. In (De Gejirifu et al., 2019), the uncertainty of wind storage plants participating in the electricity spot market bidding is considered and modeled by the two-stage optimization idea and stochastic chance constrained planning theory, and the developed model can provide a basis for the wind storage plants to participate in the electricity spot market bidding scheme and the operation plan formulation; (Fazlalipour et al., 2018); considering that the microgrid can be used as a rotating backup resource, a two-stage bidding model for microgrid participation in the joint market of day-ahead market and rotating backup market is established.

Overall, the above study considers the economic benefits of distribution networks and each microgrid operator in the electricity market. However, there is a missing consideration of the influence of carbon quotas, which are an important basis for carbon trading market, on the bidding strategy of each microgrid after the introduction of regional distribution networks.

In this paper, we study the regional distribution-side day-ahead electricity market with the participation of multiple microgrids and use two-layer planning theory to solve the optimal bidding strategy of microgrid operators and the optimal dispatching problem of distribution network operators under the consideration of carbon quotas. The upper-level planning is solved by a genetic algorithm to minimize the cost of the distribution market operator; the bottom-level planning is solved by a sequential quadratic programming algorithm to maximize the revenue of the microgrid, and finally determines the optimal clearing strategy of the microgrid and the optimal dispatching scheme of the distribution network operator. The article concludes with a detailed analysis of the trading strategy of the distribution-side electricity market under the influence of carbon quotas and the participation of multiple microgrids, taking a typical day as an example.

2 Distribution side power market model

2.1 Market structure

The structure of regional distribution-side electricity market transactions is shown in Figure 1, where market players include: distribution system operators (DSO), microgrid operators, wholesale electricity markets, and load aggregators, and the behavior of each player in the market is:

(1) The DSO is responsible for the operation and clearing of the electricity market and needs to receive the load demand for

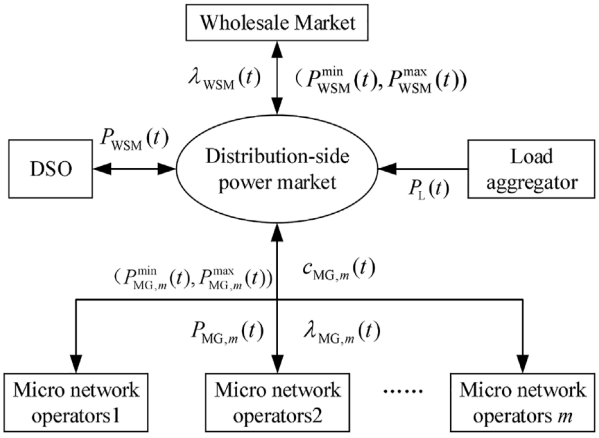

FIGURE 1
Power market construction of distribution system.

the next day and information on the offers of the parties, and the DSO can purchase electricity from the microgrid operators and wholesale markets in the region.

(2) The load aggregator, which owns the load resources in the region, is responsible for purchasing electricity from the electricity market and selling it to customers, and it needs to submit to the DSO the load demand $P_L(t)$ for each period on the second day.

(3) The wholesale power market is required to issue the next day's wholesale tariff $\lambda_{WSM}(t)$ to the DSO, and the power purchased by the DSO is required to satisfy the line operating constraint $(P_{WSM}^{min}(t), P_{WSM}^{max}(t))$, where $P_{WSM}^{max}(t)$ and $P_{WSM}^{min}(t)$ are the upper and lower limits (kW) of line transmittable power, respectively.

(4) Based on the historical data and the carbon quota issued by the Ministry of Ecology and Environment, microgrid m shall declare the power range $(P_{MG,m}^{min}(t), P_{MG,m}^{max}(t))$ and corresponding quotation for DSO to participate in the bidding for each period on the following day. The power range declared for the microgrid is explained as follows: Firstly, in the electricity market, power generation equipment can be divided into high-carbon power sources and low-carbon power sources according to carbon emissions. Taking microgrids with the same capacity and free carbon allowances, for example, the declared upper limit of microgrids with high-carbon power sources is lower than that of microgrids with low-carbon power sources. Secondly, at present, the primary purpose of accepting clean energy-based microgrids to the grid is to reduce carbon dioxide emissions, so microgrids connected to the grid should contribute to the achievement of carbon emission targets in the regional electricity market, i.e., the declared power limit is the minimum power commitment of the microgrid to meet the carbon emission target.

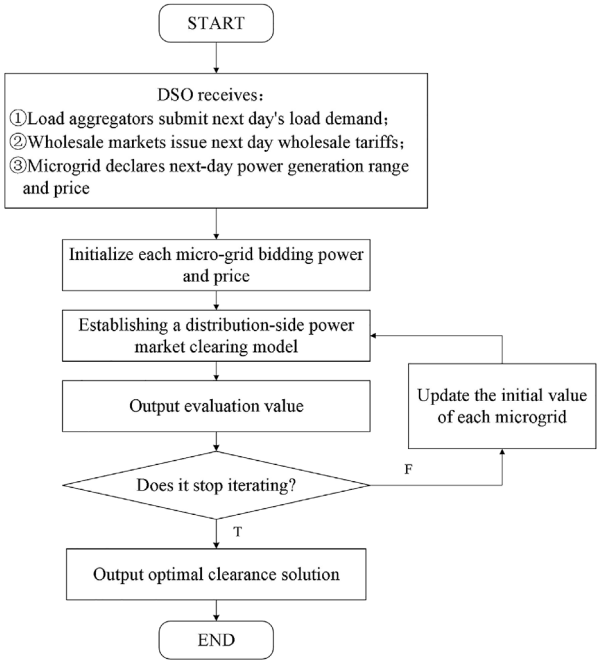

FIGURE 2
Transaction flow chart.

The trading process is shown in Figure 2.

Step 1. The load aggregators in the region forecast the load demand for each time slot of the next day and declare it to the DSO, the wholesale market issues the wholesale power price for the next day, and each micro-network operator declares the power sales range for each time slot of the next day to the DSO and offers the corresponding price.

Step 2. After receiving the information from each entity, DSO shall establish a power market clearing model to minimize power purchase cost and the constraints of load power, declare the power range of the microgrid and safety operation constraint of the system, etc., and make the dispatch plan for the region by solving the optimal solution of this model.

Step 3. DSO shall promptly announce to each microgrid and wholesale market the regional dispatch plan derived from Step 2, i.e., the winning power $P_{MG,m}(t)$ and corresponding clearing power price $\lambda_{MG,m}(t)$ of each microgrid and the power purchased by DSO from the wholesale market $P_{WSM}(t)$ on the next day.

2.2 Market model

In the electricity market bidding process, from the perspective of the DSO, the objective is to meet the next day's load demand, ensure the safety of system operation, and minimize the cost of power

purchase; from the perspective of the microgrid, the objective is to maximize its revenue through bidding. In this process, the behaviors of microgrids and DSO are independent of each other and affect each other, so this problem can be described as a two-layer planning problem. In this regard, the upper-level optimization problem aims at minimizing the cost of expenses of the distribution system operator, while the bottom-level optimization problem aims at maximizing the profit of the microgrid operator from electricity sales, and determines the market clearing scheme after considering the load power, the declared power of the microgrid, the carbon emission index and the system security constraints. The decision variables are the power purchased by the distribution system operator from each microgrid and the wholesale market and the clearing tariff of the microgrid operator m.

2.2.1 Mathematical model for distribution system operators

The core of the upper-level optimization problem lies in the DSO's comprehensive consideration of system security constraints based on the offers of all parties to achieve economic optimality. The objective is to minimize the total system power purchase cost, and the upper-level optimization model is.

$$\min \sum_{t=1}^{N_T}\left[\sum_{m=1}^{N_m} P_{\mathrm{MG},m}(t)\lambda_{\mathrm{MG},m}(t) + P_{\mathrm{WSM}}(t)\lambda_{\mathrm{WSM}}(t)\right] \quad (1)$$

$$\text{s.t.} \sum_{m=1}^{N_m} P_{\mathrm{MG},m}(t) + P_{WSM}(t) = P_L(t), \forall t \quad (2)$$

$$P_{\mathrm{MG},m}{}^{min}(t) \le P_{\mathrm{MG},m}(t) \le P_{\mathrm{MG},m}{}^{max}(t), \forall m, \forall t \quad (3)$$

$$P_{\mathrm{WSM}}{}^{min}(t) \le P_{\mathrm{WSM}}(t) \le P_{\mathrm{WSM}}{}^{max}(t), \forall t \quad (4)$$

where: N_T denotes the total number of bidding periods, generally taken as 24; N_{m} denotes the total number of microgrid operators participating in the bidding; $P_{\mathrm{MG},m}(t)$ denotes the declared power of microgrid m in time slot t (kW); $\lambda_{\mathrm{MG},m}(t)$ denotes the declared power of microgrid m in time slot t (\$/kWh); $P_{\mathrm{WSM}}(t)$ denotes the power purchased by DSO from the wholesale market in time slot t (kW); $\lambda_{\mathrm{WSM}}(t)$ denotes the wholesale power price of the wholesale market in time slot t (\$/kWh); $P_{\mathrm{L}}(t)$ denotes the load demand in the region at time slot t (kW); $P_{\mathrm{MG},m}{}^{\min}(t)$ and $P_{\mathrm{MG},m}{}^{\max}(t)$ are the lower and upper limits of the declared power of microgrid m at time slot t (kW), respectively; and Eq. 4 represents the upper and lower constraints to be satisfied by the DSO to purchase power from the wholesale market.

(2) Mathematical model of micro-network operators

The goal of micro-network operators is to maximize their interests, and the underlying optimization model is shown below.

$$\max \sum_{m=1}^{N_m}\left(P_{\mathrm{MG},m}(t)\lambda_{\mathrm{MG},m}(t) - \left(\alpha_{\mathrm{MG},m}P_{\mathrm{MG},m}^2(t) + \beta_{\mathrm{MG},m}P_{\mathrm{MG},m}(t) + \gamma_{\mathrm{MG},m}\right)\right), \forall t \quad (5)$$

$$\text{s.t. } P_{\mathrm{MG},m}(t) = \left[\lambda_{\mathrm{MG},m}(t) - \beta_{\mathrm{MG},m}\right]/2\alpha_{\mathrm{MG},m} \quad (6)$$

$$\alpha_{\mathrm{MG},m}P_{\mathrm{MG},m}^2(t) + \beta_{\mathrm{MG},m}P_{\mathrm{MG},m}(t) + \gamma_{\mathrm{MG},m} \le P_{\mathrm{MG},m}(t)\lambda_{\mathrm{MG},m}(t), \forall m, \forall t \quad (7)$$

In this paper, the quadratic function is used to approximate the generation cost of microgrid m, $\alpha_{\mathrm{MG},m}$, $\beta_{\mathrm{MG},m}$ and $\gamma_{\mathrm{MG},m}$ denote its quadratic term coefficient (\$/(kW)^{2}h), primary term coefficient (\$/kWh), and constant term (\$/h), respectively; Eq. 6 represents the relationship between the winning power bid and the clearing tariff when the microgrid operator's revenue is maximized; Eq. 7 ensures that each microgrid benefits from the competitive bidding.

3 Solution method

By analyzing the market model, we can see that any micro-network competes with other micro-networks to win the power bid through competitive bidding, and any party who offers too much or too little will damage its interests; meanwhile, DSO makes the most economical scheduling plan based on each party's offer and considering various constraints. Therefore, the upper-level optimization problem is essentially a linear programming problem with constraints; since there is competition among multiple subjects in the bottom-level optimization problem, and the introduction of constraint (7) can ensure that each micro-network is profitable in the bidding, this paper simplifies the bottom-level optimization problem to a quadratic programming problem to find the maximum profit of each micro-network. For the distribution-side electricity market model depicted in Figure 1, this paper establishes an embedded algorithm that solves the upper-level problem by genetic algorithm and the bottom-level problem by sequential quadratic programming (SQP) method.

3.1 Upper-level optimization problem

The upper-level optimization problem aims at solving the optimal offer strategy for each microgrid to achieve its economic optimum. It is assumed that the wholesale power price of the next day in the wholesale market is known. The offer price of microgrid m affects its winning power and clearing tariff, and thus its profit.

In this paper, the genetic algorithm is used to solve the upper-level optimization problem, and the offer of each micro-network and the corresponding outgoing power $(\lambda_{\mathrm{MG},m}(t), P_{\mathrm{MG},m}(t))$ are taken as the population individuals, and the optimal outgoing of micro-network m can be found through the selection of population individuals.

3.2 Lower-level optimization problem

The lower-level optimization problem aims to find the optimal amount of power cleared from each microgrid and

the optimal amount of power purchased by DSO from the wholesale market. In this paper, we assume that the microgrid cost is a quadratic function concerning the generation capacity, so this paper adopts the SQP algorithm to solve the bottom planning problem.

3.3 Approximation φ—mapping

The general form of the Bilevel Programming Problem is shown below.

$$\min F(x_u, x_l), \forall x_u \in X_U, \forall x_l \in X_L \tag{8}$$

$$\text{s.t. } x_l \in \operatorname{argmin}\left\{ \begin{matrix} f(x_u, x_l): g_j(x_u, x_l) \le 0, \\ j = 1, ..., J \end{matrix} \right\} \tag{9}$$

$$G_k(x_u, x_l) \le 0, k = 1, ..., K \tag{10}$$

where $F(x_u, x_l)$ corresponds to the upper-level objective function shown in Eq. 1; $f(x_u, x_l)$ corresponds to the bottom-level objective function shown in Eq. 5; x_u denotes the upper-level decision variable, i.e., the clearing tariff of the microgrid; x_l denotes the bottom-level decision variable, i.e., the clearing tariff of the microgrid and the wholesale market, $g_j(x_u, x_l)$ corresponds to the bottom-level constraints shown in Eqs 6, 7; Eq. 10 corresponds to the upper-level constraints shown in Eqs 2–4.

Let function $\varphi(x_u)$ be the mapping of the underlying optimal function values corresponding to any given upper-level decision variable.

$$\varphi(x_u) = \min\left\{ \begin{matrix} f(x_u, x_l): g_j(x_u, x_l) \le 0, \\ j = 1, ..., J, x_l \in X_L \end{matrix} \right\} \tag{11}$$

Bringing Eq. 11 into the model (8)-(10) transforms the Bilevel Programming Problem into a single-level form.

$$\min F(x_u, x_l), \forall x_u \in X_U, \forall x_l \in X_L \tag{12}$$

$$\text{s.t. } f(x_u, x_l) \le \varphi(x_u) \tag{13}$$

$$g_j(x_u, x_l) \le 0, j = 1, ..., J \tag{14}$$

$$G_k(x_u, x_l) \le 0, k = 1, ..., K \tag{15}$$

In general, φ - mapping is always scalar-valued regardless of the lower level variable dimension and whether or not there exist multiple lower level optimal solutions. Thus, the calculation of φ - mapping is not complicated. (Sinha et al., 2020).

In this paper, we apply the φ - mapping idea in the nested algorithm constructed in the previous section. After updating the algorithm step, the micro-network offers are fixed and a local search is performed in the single-level planning shown in Eqs 12–15 to solve for the corresponding optimal outgoing power for each micro-network offer to update the population.

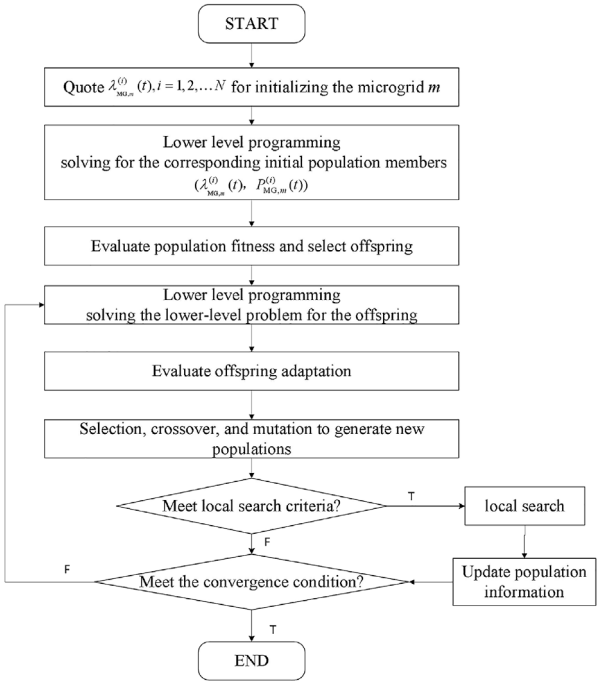

FIGURE 3
Calculation flow chart.

3.4 Bilevel programming solution method

The computational flow for solving the Bilevel Programming Problem in this paper is shown in Figure 3.

(1) Take the N-dimensional random numbers to initialize the microgrid m with the outgoing electricity price;
(2) Using the SQP algorithm in the underlying planning, find the microgrid clearing power $P_{MG,m}^{(i)}(t)$ corresponding to $\lambda_{MG,m}^{(i)}(t)$, and together with it form the initial population member $(\lambda_{MG,m}^{(i)}(t), P_{MG,m}^{(i)}(t))$;
(3) Evaluate the fitness of the population members using the objective function and constraints of the upper-level planning.
(4) Selecting the offspring members.
(5) Solve the underlying problem for each child using the SQP algorithm.
(6) Repeat step (3).
(7) Select, crossover, and mutate to generate a new population, perform a local search in its vicinity after every k generation, and update the population if there is an improvement.
(8) Check whether the termination condition is satisfied and if so, stop the iteration to output the winning power and outgoing tariff of each power seller, otherwise return to step (5).

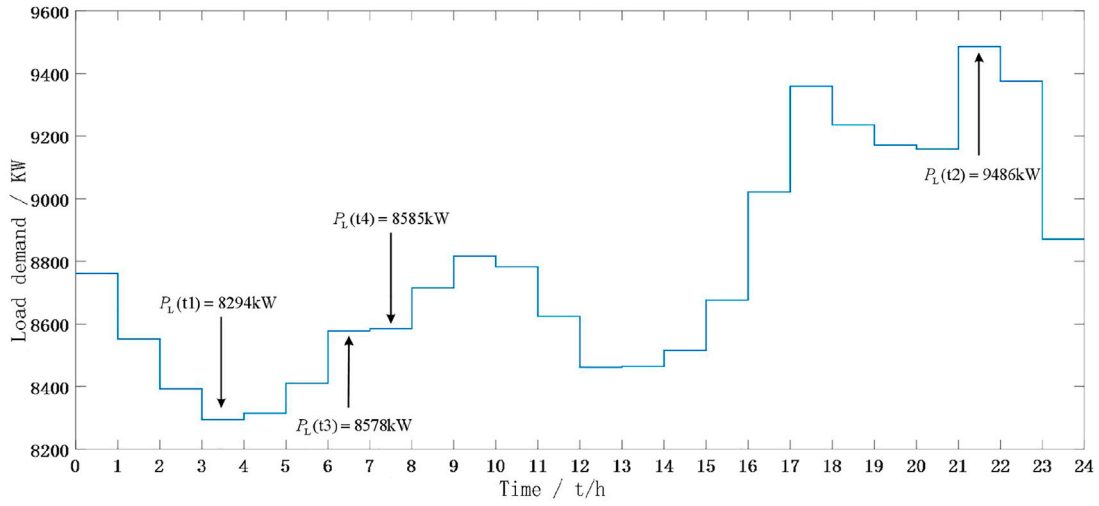

FIGURE 4
Regional daily load curve.

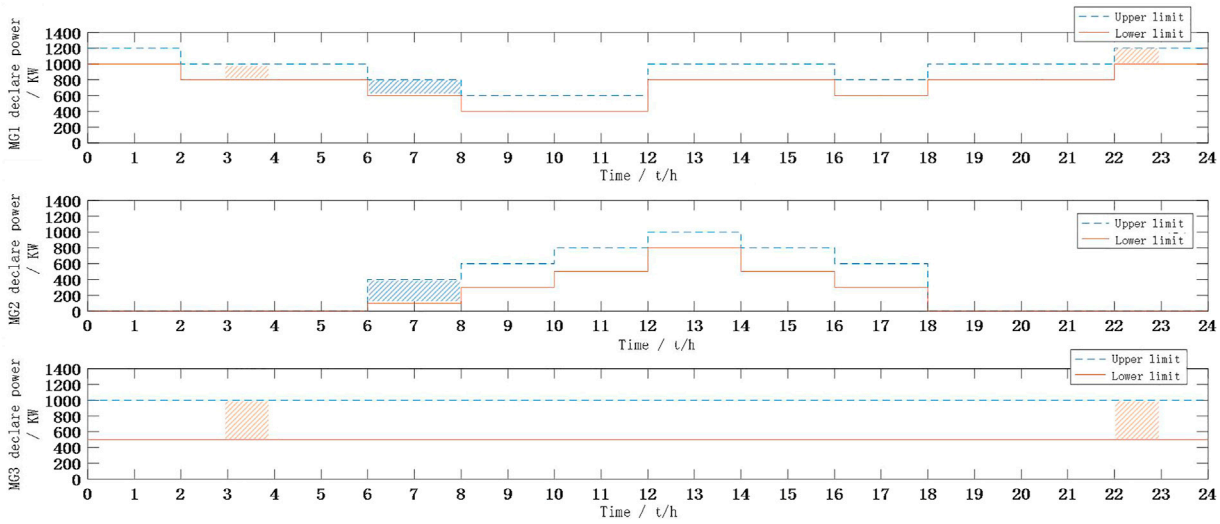

FIGURE 5
Three microgrids declare next-day power intervals.

TABLE 1 Power generation costs of three microgrids.

Microgrids	Cost factors		
	Quadratic coefficients ($/(kW)^{2}h)	Primary term coefficients ($/kWh)	Constant terms ($/h)
MG1	0.000045	0.025	5
MG2	0.000045	0.025	5
MG3	0.000085	0.025	10

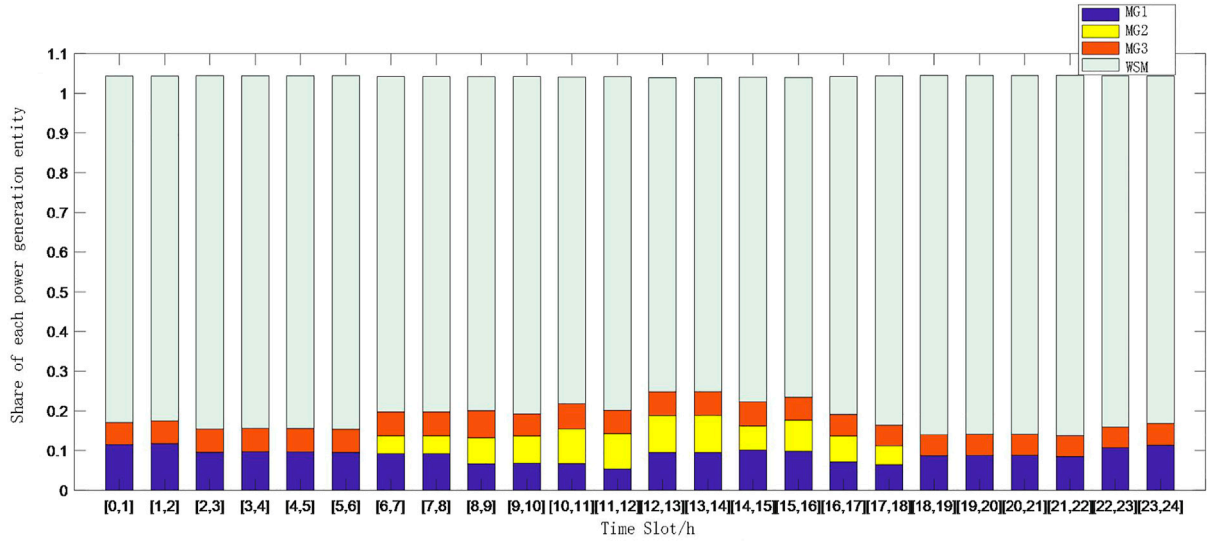

FIGURE 6
Share of electricity sold by each power seller.

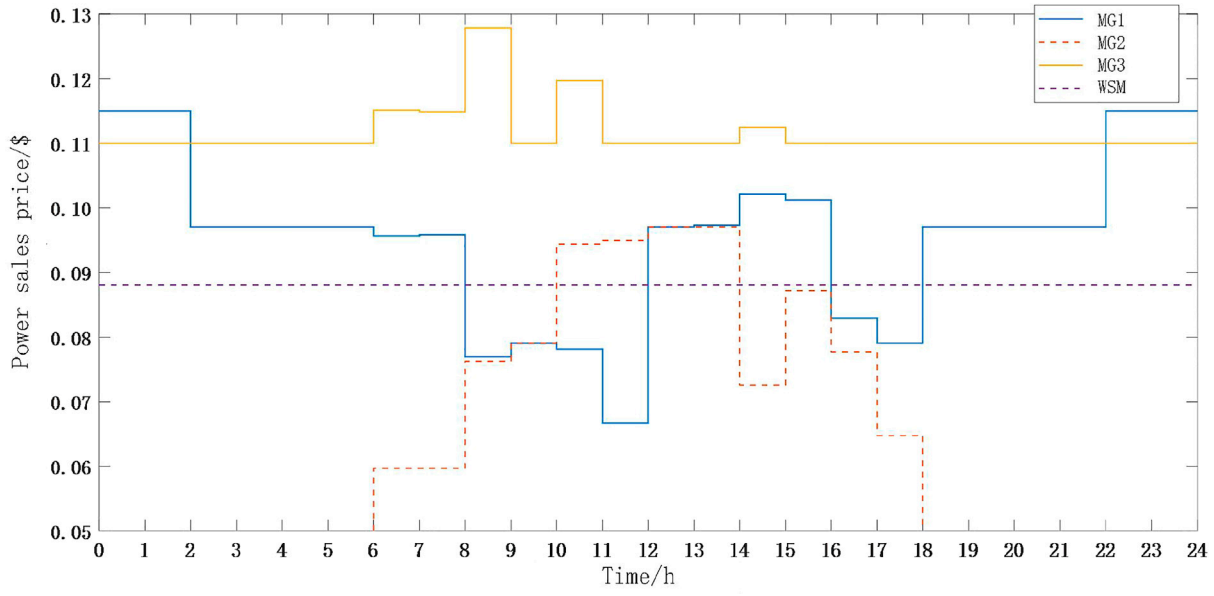

FIGURE 7
Price of electricity by each power seller.

4 Example

4.1 Simulation environment

To verify the feasibility of the proposed method, this paper builds a simulation optimization model based on Matlab + cplex, taking a two-layer iterative stopping accuracy of 0.01 and N = 100. The regional load in this paper uses simulated data of a typical day, and the daily load curve is shown in Figure 4.

It is assumed that there are three adjacent microgrids (numbered MG1, MG2, and MG3 in order) in the region, and to reflect their differences, it is set that the power generation equipment configured in

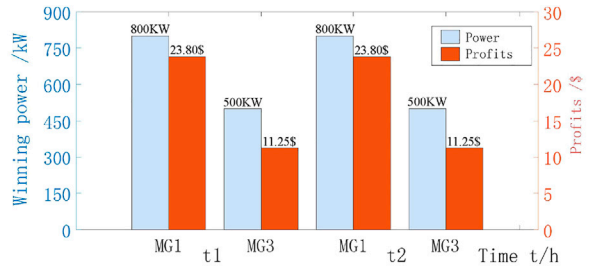

FIGURE 8
Dispatched power and profit of MG1 and MG3 under t1 and t2 scenarios.

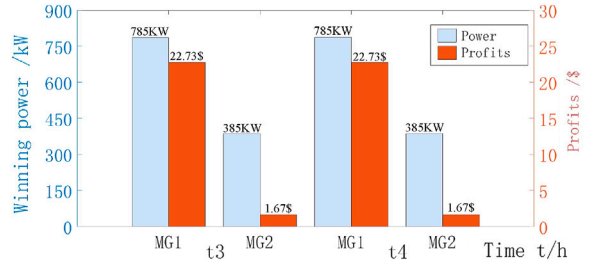

FIGURE 9
Dispatched power and profit of MG1 and MG2 under t3 and t4 scenarios.

MG1 is mainly wind power, the power generation equipment configured in MG2 is mainly photovoltaic, and the equipment that can generate stable power is configured in MG3. Given the strong coupling between new energy generation and climatic conditions, considering the climate change in a day and the carbon quota issued by the Ministry of Ecology and Environment, it is assumed that the declared power range of MG1, MG2, and MG3 in a timeshare is shown in Figure 5 (Li et al., 2009), and the generation cost is shown in Table 1. The distribution system operator purchases power from the wholesale market in the range of 0–30 MW, and the wholesale electricity price in the wholesale market is 0.088$/kWh, and the line loss rate is taken as 5%.

4.2 General analysis

The practical simulation debugging shows that the computational speed of the algorithm in this paper is moderate, and the initial value selection will affect the iteration time, but will not have a large impact on the final result. This paper will focus on the discussion of the bidding.

The simulation results are shown in Figure 6 and Figure 7. Figure 6 shows the percentage of electricity sold by each seller to the total load demand on the next day, and Figure 7 shows the price of electricity sold by each seller on the next day. Analysis shows that.

(1) the presence of line losses makes the actual power purchased by the distribution network larger than its actual power demand.
(2) The DSO uses the power interval declared by each microgrid (Figure 5) as a reference to formulate the next-day interval dispatch plan, so the general rule of the distribution-side power market to formulate the clearing power can be summarized as allocation by capacity. Therefore it is crucial that each micro-grid in the day-ahead power market can accurately predict the next day's generation.
(3) When there is sufficient power in the wholesale market, DSO can also fully respect the willingness of each microgrid to generate power, such as agreeing to the transaction price of MG3 at 0.128$/kWh, which is much higher than the price in the wholesale market, during the period [8:00,9:00] to benefit the microgrid, which can motivate the microgrid with higher generation cost to participate in the market transaction and establish a long-term partnership to cope with the lack of power in the wholesale market. This will provide an incentive for microgrids with higher generation costs to participate in the market and establish long-term partnerships to address the lack of power in the wholesale market and help achieve carbon reduction targets.

4.3 The influence of load changes on different cost microgrid bids

The clearing scheme and profit of microgrids are influenced by the cost of generation. Take the next day's electricity consumption low time t1 = [3:00,4:00] and peak time t2 = [21:00,22:00], whose load demand is 8294kW and 9486kW respectively, and the power range declared by each microgrid is the same (see Figure 5 at the red shaded mark). Since t1 and t2 are nighttime, so MG2 does not participate in the market bidding. From Figure 7, we can see that the clearing power price of MG1 is 0.097$/kW and MG3 is 0.110$/kWh in both t1 and t2 scenarios, and the winning power and profit of MG1 and MG3 are shown in Figure 8, which shows that.

(1) From the fact that MG1 has the same winning power and profit in both scenarios t1, t2, it is clear that its optimal clearing scenario is not affected by load changes when the declared power range and cost of the microgrid are constant.
(2) In the two scenarios of t1 and t2, the pay-out tariff of MG1 is at a lower level because of its lower generation cost. In the case of the market, competition leads to the fact that MG3 is always unable to raise its price and to ensure the profit of MG3 makes the winning power of MG3 smaller than that of MG1. It is obvious from Figure 8 that MG1 with its low generation cost has a clear advantage in the power market and can achieve maximum profit itself.

4.4 The influence of different declared power on micro network bidding

The generation costs of MG1 and MG2 are the same, but their declared power ranges vary with time. Take the scenarios [6:00,7:00] and [7:00,8:00] in Figure 4, where the load demand does not change much, as t3 and t4, respectively, and their load demands are 8,578 kW and 8,585 kW, respectively. The declared power ranges of MG1 are 600–800 kW and MG2 are 100–400 kW (see Figure 5 at the blue shaded mark). The declared power range of MG1 is 600–800 kW and the declared power range of MG2 is 100–400 kW (see Figure 5 at the blue shaded mark). From Figure 7, it can be seen that the clearing tariffs for MG1 and MG3 in t3 and t4 scenarios are 0.096$/kW and 0.06$/kWh, respectively. The clearing tariffs and profits for MG1 and MG2 at t3 and t4 are shown in Figure 9.

The changes in load demand in scenarios t3 and t4 are small, and the calculated microgrid clearing scheme is approximately the same with the same cost and declared power range, which shows that the algorithm used in this paper has good calculation performance and can guarantee the accuracy of the calculation results.

From Figure 9, it can be seen that the winning bids of MG1 and MG2 with the same cost but different declared power ranges are in line with the law of "capacity-based allocation". In this scenario, the declared power range of MG2 is lower, and the final price of its electricity clearance is lower than that of MG1 as shown in Eq. 6, which ultimately leads to its low profit because the internal configuration of MG2's photovoltaic power generation equipment is limited in the morning when the solar energy resources are insufficient, which leads to its insufficient allocation of carbon quotas and ultimately makes the declared power range of MG2 unable to make more profit. Therefore, the microgrid should optimize itself and declare a reasonable power interval to maximize its profit.

5 Conclusion

The day-ahead power bidding problem for a regional distribution market with multiple micro-networks is solved in this paper using a bilevel programming approach. The upper-level planning aims to reduce the cost of the distribution system operator, and the bottom-level planning aims to maximize the revenue of the micro-networks. This helps to identify the best clearing strategy for the micro-networks and the best dispatching scheme for the distribution system operator. The simulation's findings support this.

(1) The algorithm used in this paper has good computational performance and can ensure that the system can optimize the interests of each power seller and distribution system operator on the basis of economy and safety.
(2) The generation cost and declared power range of the microgrid affect the final clearing result, and the microgrid with a low generation cost and reasonable declared power range has certain advantages in the market.
(3) Under certain conditions, DSO can benefit microgrids with higher generation costs to address the scarcity of power in wholesale markets and help achieve carbon reduction targets.

This paper assumes that each microgrid can accurately predict the next day's generation interval, but in actual operation, distribution system operators should consider the situation that clean power generation is affected by weather, resulting in the actual generation capacity being different from the interval scheduling plan made before the day, and optimize the market trading rules to ensure the safe and stable operation of the regional distribution system (Fang et al., 2020).

Data availability statement

The original contributions presented in the study are included in the article/Supplementary Material, further inquiries can be directed to the corresponding author.

Author contributions

All authors listed have made a substantial, direct, and intellectual contribution to the work and approved it for publication.

Funding

This study is supported by the National Natural Science Foundation of China under Grant 52107075.

Acknowledgments

I would like to thank my supervisor for his constant encouragement and support. I could not have completed this thesis without his patient guidance.

Conflict of interest

The authors declare that the research was conducted in the absence of any commercial or financial relationships that could be construed as a potential conflict of interest.

Publisher's note

References

Bai, P, Xia, L, and He, J (2017). Design of bidding mechanism for multiple microgrids[J]. *Mod. Electr. Power* 34 (06), 22–27. doi:10.19725/j.cnki.1007-2322.2017.06.004

De, G., Tan, Z., Li, M., Yang, S., Ma, J., Tan, Q., et al. (2019). Bidding strategy of wind-storage power plant participation in electricity spot market considering uncertainty[J]. *Power Syst. Technol.* 43 (08), 2799–2807. doi:10.13335/j.1000-3673.pst.2019.0547

Du, Y., Li, F., Zandi, H., and Xue, Y. (2021). Approximating nash equilibrium in day-ahead electricity market bidding with multi-agent deep reinforcement learning[J]. *J. Modern Power Syst.Clean Ener.* 3 (9), 534–544. doi:10.35833/MPCE.2020.000502

Fang, X., and Cui, M. (2020). Analytical model of day-ahead and real-time price correlation in strategic wind power offering[J]. *J. Modern Power Syst.Clean Ener.* 5 (8), 1024–1027. doi:10.35833/MPCE.2019.000598

Fazlalipour, P., Ensan, M., and Mohammadiivatloo, B. (2018). Optimal participation of low voltage renewable micro-grids in energy and spinning reserve markets under price uncertainties. *Int. J. Electr. Power & Energy Syst.* 102, 84–96. doi:10.1016/j.ijepes.2018.04.010

He, S., Gao, H., Tian, H., Wang, L., Liu, Y., and Liu, J. (2021). A Two-stage robust optimal allocation model of distributed generation considering capacity curve and rpeal-time price based demand response[J]. *J. Modern Power Syst.Clean Ener.* 1 (9), 114–127. doi:10.35833/MPCE.2019.000174

Jin, T, Chen, M, and Chen, Y (2021). Discussion on carbon quota management of power generation enterprises based on energy consumption level[J]. *Shanghai Energy Conserv.* (01), 53–59.

Le, J, Liu, Y, Ye, X, Wu, Z, and Li, Z (2016). Market-oriented operation pattern of regional power network integration with high penetration level of distributed energy resources[J]. *Proc. CSEE* 36 (12), 3343–3354. doi:10.13334/j.0258-8013.pcsee.152844

Li, S, Li, G, Li, Z, and Wu, J (2009). *Research on typical curve prediction method of wind farm output[C]*. Haikou: Wind Farm Access to Grid Technology Symposium, 255–261.

Liu, Y, Guo, L, and Wang, C (2018). Economic dispatch of microgrid based on two-stage robust optimization[J]. *Proc. CSEE* 38 (14), 4013–4022+4307. doi:10.13334/j.0258-8013.pcsee.170500

Liu, Y, Guo, L, and Wang, C (2017). Optimal bidding strategy for microgrids in electricity distribution market[J]. *Power Syst. Technol.* 41 (08), 2439–2476. doi:10.13335/j.1000-3673.pst.2016.2989

Moradi, M. H., Abedini, M., and Hosseinian, S. M. (2016). A combination of evolutionary algorithm and game theory for optimal location and operation of DG from DG owner standpoints. *IEEE Trans. Smart Grid* 7 (2), 1–616. doi:10.1109/TSG.2015.2422995

Peng, L, Ma, X, Guo, Z, Lei, J, Yuan, Z, He, S, et al. (2021). Game strategy of integrated energy service providers based on Bi-level optimization[J]. *Power Syst. Technol.* 45 (02), 460–473. doi:10.13335/j.1000-3673.pst.2020.1013

Sinha, A, Lu, Z, Deb, K, and Malo, P (2020). Bilevel optimization based on iterative approximation of multiple mappings. *J. Heuristics* 26, 151–185. doi:10.1007/s10732-019-09426-9

State Grid Cooperation of China (2021). *State Grid Cooperation of China releases the "carbon peak, carbon neutrality" action plan[N]*. Beijing: State Grid News, 2021-03-02.

Wang, X, Zhang, Y, and Zhang, S (2019). Game analysis of multi-energy market considering microgrid bidding[J]. *Power Syst. Technol.* 43 (09), 3184–3192. doi:10.13335/j.1000-3673.pst.2019.0797

Zhao, M, Chen, S, Liu, F, and Huang, X (2015). A game-theoretic approach to analyzing power trading possibilities in multi-microgrids[J]. *Proc. CSEE* 35 (04), 848–857DOI10. doi:10.13334/j.0258-8013.pcsee.2015.04.011

Zhao, W, Yan, H, and He, W (2018). Equilibrium model of electricity market based on non-cooperative game of wind farms, thermal power plants and power grid company[J]. *Power Syst. Technol.* 42 (01), 103–111. doi:10.13335/j.1000-3673.pst.2017.1337

Zhao, Y, Chen, Y, and Sun, W (2022). Region dispatch method and market trading strategy for multi-microgrid distribution system[J]. *Power Syst. Technol.* 46 (01), 47–56. doi:10.13335/j.1000-3673.pst.2021.0245

Zhao, Y, Zhang, X, Zhao, C, Gong, C, Xiao, Y, Li, M, et al. (2022). Dynamic pricing and market clearing strategy for power distribution considering multiple stakeholders[J]. *South. Power Syst. Technol.* 16 (01), 137–144. doi:10.13648/j.cnki.issn1674-0629.2022.01.015

Frontiers in
Energy Research

Advances and innovation in sustainable, reliable and affordable energy

Explores sustainable and environmental developments in energy. It focuses on technological advances supporting Sustainable Development Goal 7: access to affordable, reliable, sustainable and modern energy for all.

Discover the latest Research Topics

See more →

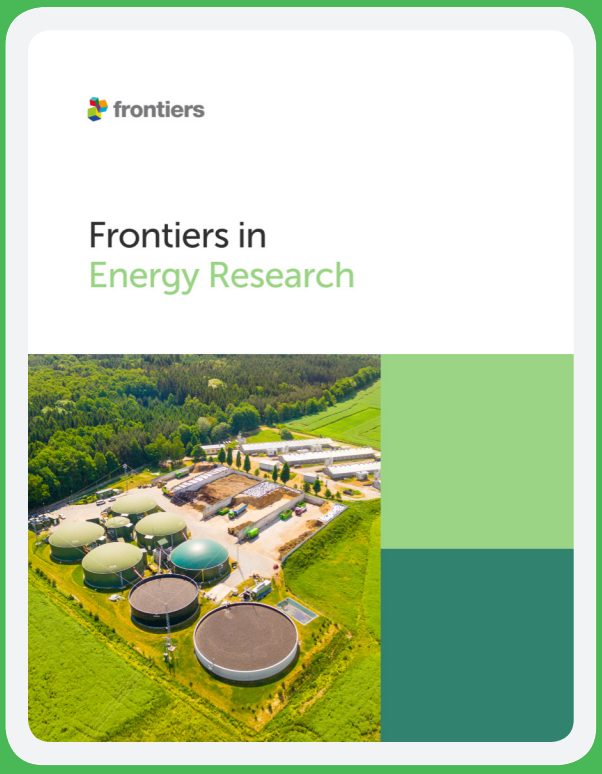

Frontiers

Avenue du Tribunal-Fédéral 34
1005 Lausanne, Switzerland
frontiersin.org

Contact us

+41 (0)21 510 17 00
frontiersin.org/about/contact